Development of a braided electrospun suture to augment tendon repairs

A dissertation submitted to the University of Oxford in partial fulfilment of the requirements for the degree of

Doctor of Philosophy



Roxanna Elizabeth Abhari

St Catherine's College

Nuffield Department of Orthopaedics, Rheumatology, and Musculoskeletal Sciences
University of Oxford
Trinity Term 2019

Supervisors: Professor Andrew Carr, Associate Professor Sarah Snelling, and Dr Pierre-Alexis Mouthuy

Declaration

I certify that this thesis is true and honest account of my own research, which was conducted ethically and the resulted obtained are genuine. Where I have drawn on the work, ideas, and results of others, this has been appropriately acknowledged in the thesis.

Attribution statement:

Jaron Kuehlcke at Herzog provided technical support for braiding the electrospun yarns used in Chapter 4.

Patrick Blott at Fibre Extrusion Technologies (Leeds, UK) fabricated the melt-extruded yarns used in Chapter 4.

Simon Davis at the Target Discovery Institute (University of Oxford, UK) ran the mass spectrometer and associated analyses in Chapter 5.

Roxanna Elizabeth Abhari

Abstract

Tendon tears are common and often require surgical repair. However, many surgical repairs fail, despite continued advances in surgical materials and techniques. Rotator cuff surgery, the clinical focus of this thesis, has particularly poor outcomes. Repair failure can be partially attributed to the inappropriate repurposing of sutures from use in other tissues, which fail to integrate with the specialised tendon tissue.

The overall aim of this study was to develop a novel polydioxanone suture that has the potential to provide both biological and mechanical support to torn tendons. It is hypothesized that electrospun submicron fibres, which mimic native tendon extra-cellular matrix (ECM), can provide biological support to tendon. Meanwhile, larger and more robust melt-extruded microscale fibres can mechanically support surgical tendon repair. It is further hypothesized that a suture containing both electrospun and extruded fibres will overcome structural limitations associated with electrospun-only sutures, while still providing biological improvements over current sutures.

This thesis describes a process to fabricate and evaluate translatable suture biomaterials deliberately designed for tendon, by engineering materials on the fibre, filament, and multifilament level. On the fibre level, annealing enables tailoring of the degradation rate of electrospun fibres, which could allow for biomaterial degradation kinetics to match new tissue deposition. On the filament level, melt-extruded materials had superior strength and stiffness to support surgical repair. Electrospun filaments had a higher surface area, porosity, and faster degradation rate, making them more suitable as biological support. On the multifilament level, industrial braiding enabled further control over suture size, porosity, and mechanical properties by altering braiding design and component ratios.

A hybrid braided suture with an electrospun sheath and melt-extruded cores was designed to meet the demands of tendon: electrospun fibres on the outside approximate ECM and will be in contact with the biological milieu, while the melt-extruded fibres in the core provide prolonged mechanical support. The hybrid suture had a similar size and tensile strength to currently used sutures, but was less stiff and more porous. It induced differential serum protein binding and promoted more favourable tendon fibroblast attachment and proliferation, when compared to currently used sutures.

This novel hybrid suture has potential to improve current treatment options for tendon repair. Future work should investigate its local surface properties, followed by a dynamic culture and *in vivo* study, to bring the device to the standard needed for pre-clinical and clinical trials. The design process and pipeline of characterisation methods developed in this thesis could be applicable and adaptable to biomaterials for other soft tissues in need of improved treatments.

Publications and presentations arising from this thesis

Journal Publications

Abhari, R.*, Nezhentsev, A.*, Baldwin, M., Carr, A, Snelling, S. (2020). Comparison of the gene expression response of tendon fibroblasts to currently used sutures and an electrospun yarn. *Manuscript in preparation.*

Abhari, R., Snelling, S., Augustyniak, E., Davis, S., Carr, A, Mouthuy, P. (2020). An electrospun-based braided suture for tendon tissue engineering. *Manuscript in preparation.*

Snelling, S., Stace, E., **Abhari, R**., Baldwin, M., Carr, A. (2020). Protein adsorption and immune cell attachment are modulated by the diameter of electrospun polydioxanone fibres. *Manuscript in preparation. Target Journal: Advanced Healthcare Materials.*

Abhari, R., Mouthuy, P., Vernet, A., Schneider, J., Brown, C. and Carr, A. (2018). Using an industrial braiding machine to upscale the production and modulate the design of electrospun medical yarns. *Polymer Testing*, 69, pp.188-198.

Abhari, R., Martins, J., Morris, H., Mouthuy, P. and Carr, A. (2017). Synthetic sutures: Clinical evaluation and future developments. *Journal of Biomaterials Applications*, 32(3), pp.410-421.

Abhari, R., Mouthuy, P., Zargar, N., Brown, C. and Carr, A. (2017). Effect of annealing on the mechanical properties and the degradation of electrospun polydioxanone filaments. *Journal of the Mechanical Behaviour of Biomedical Materials*, 67, pp.127-134.

Book chapters

Abhari, R., Carr, A. and Mouthuy, P. (2018). Multifilament electrospun devices for soft tissue reconstruction. In: *Electrofluidodynamic technologies for biomaterials and medical devices*, 1st ed. Woodhead Publishing, pp.295-328.

Selected Presentations

Abhari, R., Mouthuy, P., Brown, C., Carr, A. (2016). Development of a novel electrospun suture. Oral presentation at: *Royal Society of Medicine Orthopaedic Section, London UK.* (Award: Best Presentation).

Abhari, R., Mouthuy, P., Zargar, N., Carr, A. (2016). Development and optimization of a novel electrospun suture with potential for use in rotator cuff tendon repair. Poster presented at: *International Scientific Tendinopathy Symposium Annual Meeting, Cape Town South Africa.* (Award: Best Poster).

Acknowledgements

I am tremendously grateful to everyone that has helped shaped this thesis and made the last four years some of the best of my life.

I feel fortunate to have been part of such a fun and stimulating research group at the Botnar. Prof, thank you for the hours of support that were devoted to developing the framework of this thesis. Thank you for your encouragement at every stage of this project and for your boundless advice and help with medical school applications. Sarah, you are an absolutely brilliant scientist. Thank you for your friendship, for showing me the value of scientific collaboration, and for making cell biology seem not so bad. Pierre, thank you for your clear vision and supervision at every stage of this project, especially early on over many skype calls. Thank you to Nasim and Cameron for their early supervision and to the infamous patch girls Hayley, Tonia, and Jo for electrospinning support and regulatory chats. Thank you, Ann, for administrative help. I am tremendously grateful to everyone in the Carr group, especially Ed, Mike, Mat, Steph, Bridget, Kim, and Dom for their advice and support. Afsie, thanks for the big hug on my first day in the Botnar and for the many that came after that.

There are many people outside of the Botnar that helped shaped this work. I am grateful to the Materials department for giving me access to their equipment. Thanks to Kalin and Nick in the Engineering department for their assistance with machines and data interpretation. I am also grateful to Jim in the IBME workshop for his willingness to engage with my poorly hand-made drawings. Finally, this thesis would definitely not have been possible without the expertise and hospitality at FET and Herzog. Thank you to Patrick and Jaron for helping me achieve my targets for this work and for inspiring confidence in academic-industry collaborations.

I have made wonderful friends over the last four years, with whom I have shared many adventures and hours of stimulating and not-so-stimulating conversations. Thank you to Alex, Emily, Emma L, Emma B, Faidra, Florian, Hannah, Luca, Mikesh, and Sarah. I am especially grateful to Mark for his unwavering support and interest in my work.

My loving sisters, Sara and Claire, have been thoroughly supportive throughout. Their emotional support and willingness to read absolutely anything is greatly appreciated. I am indebted to my confidant and companion, Blake, whose love and patient support has inspired me to pursue opportunities I would not otherwise have. Last, but definitely not least, thanks to mom and dad. Thank you for your unwavering encouragement and instilling in me the value of education.

Contents

Abstract iii

Publications and presentations arising from this thesis iv

Acknowledgements v

List of Figures xii

List of Tables xvi

Abbreviations xviii

Chapter 1 1

Introduction 1

1.1 Scope of this thesis 2

1.2 Thesis objectives 4

1.3 Thesis hypotheses 4

Chapter 2 6

Background 6

2.1 The healthy shoulder 6

2.1.1 Shoulder and rotator cuff anatomy 6

2.1.2 Tendon biomechanics 8

2.1.3 Tendon structure and function 9

2.2 Rotator cuff tendinopathy 12

2.2.1 Burden of disease 13

2.2.2 Diseased tendon structure and function 13

2.3 Tendon response to injury 15

2.4 Treatment strategies and limitations 16

2.4.1 Non-surgical treatments 16

2.4.2 Surgical treatments 16

2.4.3 Emerging surgical treatments 24

2.5 Mechanisms of cell-material interactions 28

2.5.1 Biophysical and biochemical stimuli 28
2.6 Biomaterial fabrication techniques 29
2.6.1 Electrospinning 29
2.6.2 Melt-extrusion 33
2.6.3 Polydioxanone 34
2.7 Filament post-processing 36
2.7.1 Mechanical drawing 36
2.7.2 Annealing 37
2.7.3 Spin-finishing 38
2.8 Textile strategies for assembling multifilament sutures 38
2.8.1 Textile assembly methods and their use with electrospun filaments 38
2.8.2 Properties of multifilament yarns 43
2.9 Electrospun sutures currently in development 45
2.9.1 General tendon and ligament repair 45
2.9.2 Rotator cuff 47
2.9.3 Other soft tissue applications 47
2.10 Development and justification of suture specifications in this thesis 48
2.10.1 Justification for polydioxanone as the base polymer 48
2.10.2 Justification for using electrospinning to fabricate submicron fibres 51
2.10.3 Suture design criteria and their development 52
2.10.4 PDS and Vicryl as control sutures 58
2.11 Summary 59
Chapter 3 61
Fabrication of polydioxanone filaments 61
3.1 Abstract 61
3.1.1 Background 61
3.1.2 Materials and methods 61
3.1.3 Results 61
3.1.4 Conclusions 61
3.2 Introduction 62
3.3 Objectives and hypotheses 67
3.4 Materials and methods 68

3.4.1 Optimising the electrospinning process 68
3.4.2 Electrospinning filaments 71
3.4.3 Melt-extruding filaments and yarns 73
3.4.4 Scanning electron microscopy 74
3.4.5 Tensile testing 75
3.4.6 Mercury porosimetry 77
3.4.7 Differential scanning calorimetry 79
3.4.8 In vitro degradation 80
3.4.9 Statistical analyses 80
3.5 Results 82
3.5.1 Electrospun filament parameters and characteristics 82
3.5.2 Annealing effects on electrospun filament properties 84
3.5.3 Melt-extruded yarn parameters and characteristics 92
3.5.4 Comparison between electrospun filaments and melt-extruded yarns 96
3.6 Discussion 102
3.6.1 Optimisation and reproducibility of electrospun filaments 102
3.6.2 Annealing modulates mechanical properties and in vitro degradation of electrospun filaments 105
3.6.3 Production of melt-extruded multifilament yarns made up of 10μm fibres 111
3.6.4 Differences in mechanical and material properties between electrospun filaments and melt-extruded yarns 113
3.7 Conclusions 115
Chapter 4 117
Development of multifilament sutures 117
4.1 Abstract 117
4.1.1 Background 117
4.1.2 Materials and methods 117
4.1.3 Results 117
4.1.4 Conclusions 117
4.2 Introduction 118
4.3 Objectives and hypotheses 121
4.4 Materials and methods 122
4.4.1 Material fabrication and preparation 122

4.4.2 Braided suture production 122
4.4.3 Visual analysis 124
4.4.4 Mercury porosimetry 125
4.4.5 MicroCT analysis 125
4.4.6 Tensile testing 126
4.4.7 Thermal testing 127
4.4.8 Statistical analyses 127
4.5 Results 128
4.5.1 Fabrication of base materials 128
4.5.2 Electrospun braided sutures 128
4.5.3 Hybrid braided sutures 134
4.5.4 Comparison to currently used clinical sutures 137
4.6 Discussion 143
4.6.1 Industrial braiding can be used to modulate structure and improve reproducibility and production rate of electrospun sutures 143
4.6.2 Hybrid electrospun-extruded sutures meet the target design criteria for use as surgical sutures 147
4.6.3 Hybrid sutures have more similar macro-scale properties to surgical sutures and more similar micro-scale properties to electrospun sutures 149
4.7 Conclusions 156
Chapter 5 158
Exploring the bioactivity of hybrid sutures 158
5.1 Abstract 158
5.1.1 Background 158
5.1.2 Materials and methods 158
5.1.3 Results 158
5.1.4 Conclusions 158
5.2 Introduction 159
5.3 Objectives and hypotheses 162
5.4 Materials and methods 163
5.4.1 Biomaterial fabrication 163
5.4.2 Serum protein adsorption 163
5.4.3 Human tendon tissue acquisition 165

5.4.4 Tendon fibroblast isolation and expansion 165
5.4.5 Tissue culture experiments 166
5.4.6 Metabolic activity during prolonged culture 169
5.4.7 Fixation of the cell-suture constructs 169
5.4.8 Assessment of tendon fibroblast coverage by SEM 169
5.4.9 Assessment of tendon fibroblast infiltration by μCT 170
5.4.10 Statistical analyses 170
5.5 Results 172
5.5.1 Protein corona composition on hybrid suture components and surgical sutures 172
5.5.2 Cell seeding optimisation 176
5.5.3 Tendon fibroblast attachment and metabolic activity on hybrid suture components 177
5.5.4 Tendon fibroblast attachment and metabolic activity on hybrid sutures 179
5.5.5 Tendon fibroblast coverage on hybrid sutures 180
5.5.6 Tendon fibroblast infiltration into hybrid sutures 183
5.6 Discussion 184
5.6.1 All sutures adsorb a protein corona but its composition is dependent on suture type 184
5.6.2 Tendon fibroblasts preferentially bind to extruded yarns but are more metabolically active on electrospun filaments 187
5.6.3 Tendon fibroblasts preferentially bind and proliferate on hybrid sutures compared to surgical sutures 190
5.6.4 Tendon fibroblasts cover hybrid sutures but do not display distinct infiltration 191
5.6.5 Strengths and limitations of cell-material experiments 193
5.7 Conclusions 195
Chapter 6 197
Discussion 197
6.1 Overview 197
6.2 The potential for novel sutures to improve tendon repairs 198
6.2.1 Clinical need 198
6.2.2 Limitations with current sutures used for rotator cuff repair 198
6.2.3 Addressing limitations of electrospun sutures for tendon repair 199
6.3 Development of a hybrid suture to augment tendon repair 201

6.3.1 Fabrication of continuous electrospun filaments made up of submicron fibres 201
6.3.2 Melt-extruded multifilament made up of micro-scale fibres are stronger and degrade more slowly than electrospun filaments 202
6.3.3 Potential improvements of a electrospun-extruded hybrid suture 203
6.3.4 Short-term biocompatibility and bioactivity of the hybrid suture 204
6.4 Implications of this thesis 206
6.4.1 For patients 206
6.4.2 For researchers designing novel suture materials 206
6.4.3 For surgeons 207
6.4.4 For translational biomaterials research 208
6.4.5 For integrating academia and industry 210
6.4.6 For regulatory bodies 210
6.5 Limitations of this thesis 211
6.6 Future work 213
6.7 Clinical translation of a hybrid suture 215
6.7.1 Translational potential of a hybrid suture 215
6.7.2 Industrial viability of the manufacturing process 216
6.7.3 Hypothetical clinical translation pathway 219
6.8 Key findings of this thesis 223
Chapter 7 226
References 226
Chapter 8 246
Appendices 246
Appendix A: Additional information for Chapter 2 246
Appendix B: Additional information for Chapter 3 248
Appendix C: Additional information for Chapter 4 252
Appendix D: Additional information for Chapter 5 264
Appendix E: List of equipment and suppliers 268

List of Figures

Figure 2.1: Anatomical features of the right shoulder in anterior view. 6

Figure 2.2: Rotator cuff tendons and muscles of the right shoulder....7

Figure 2.3: Representative stress-strain curve for tendon loaded in tension. 8

Figure 2.4: Hierarchical architecture of tendon....11

Figure 2.5: Differences in tendon architecture and composition in healthy and tendinopathic tissue....14

Figure 2.6 Common types of rotator cuff tendon tears....18

Figure 2.7: Surgical techniques for rotator cuff repair. 19

Figure 2.8: Electrospinning apparatus. 30

Figure 2.9: Methods for collecting continuous filaments. 32

Figure 2.10: Melt-extrusion apparatus. 33

Figure 2.11: Polydioxanone chemical structure....35

Figure 2.12: Textile assembly methods for electrospun filaments....40

Figure 3.1: Textile terminology used in this chapter....66

Figure 3.2: Custom electrospinning setup with a single nozzle and a stainless-steel wire collector....68

Figure 3.3: Melt-extrusion set-up used to fabricate PDO fibres....74

Figure 3.4: Custom tensile testing set-up for yarns....76

Figure 3.5: Mercury intrusion porosimetry theory....78

Figure 3.6: SEM images of electrospun fibre morphology after annealing for 3 hours at various temperatures and subjecting to a 6-week degradation period. 86

Figure 3.7: Changes in mechanical properties of undegraded PDO electrospun filaments due to annealing treatments. 87

Figure 3.8: Changes in mechanical properties of electrospun filaments annealed for 3 hours at 65°C, 75°C, and 85°C, over a 6-week degradation period. 89

Figure 3.9: Representative Differential Scanning Calorimetry thermographs of PDO electrospun filaments annealed at different temperatures and subjected to in vitro degradation for 6 weeks. 91

Figure 3.10: Changes in crystallinity of electrospun filaments annealed at 65°C for various times and subjected to in vitro degradation for 6 weeks 92

Figure 3.11: Changes in mechanical properties of melt-extruded yarns over 12 weeks of degradation 95

Figure 3.12: Changes in thermal properties of melt-extruded yarns over 12 weeks of in vitro degradation. 96

Figure 3.13: Representative stress-strain graph comparing an electrospun filament and a melt-extruded yarn. 97

Figure 3.14: Mechanical properties of electrospun filaments and melt-extruded yarns. 98

Figure 3.15: Representative thermal data comparing PDO electrospun filaments, melt-extruded yarns, and raw resin 99

Figure 3.16: Hg porosimetry data comparing electrospun filaments and melt-extruded yarns. 100

Figure 4.1: Possible carrier configurations using the Variation Braiding Machine. 123

Figure 4.2: Fabrication of multifilament electrospun sutures using an industrial braiding machine. 129

Figure 4.3: μCT scans and SEM images of braided electrospun sutures. 131

Figure 4.4: Representative stress-strain graph of braided electrospun sutures. 133

Figure 4.5: Tensile properties of braided electrospun sutures. 134

Figure 4.6: μCT scans and SEM images of braided hybrid sutures. 136

Figure 4.7: Representative stress-strain graph of a braided hybrid suture 137

Figure 4.9: Representative pore size distribution of braided electrospun and hybrid sutures, compared to control sutures, measured by Hg porosimetry. 139

Figure 4.10: Representative stress-strain graph of braided electrospun, hybrid, and control surgical sutures. 140

Figure 4.11: Tensile properties of braided electrospun, hybrid, and control surgical sutures..... 141

Figure 4.12: Representative thermal data comparing electrospun, hybrid, and surgical PDS sutures. 142

Figure 5.1: Three different seeding set-ups for filaments. 167

Figure 5.2: Principal component analysis of protein coronas formed on electrospun filaments (Es) and melt-extruded yarns (Ext), as well as on surgical sutures PDS (PDS) and Vicryl (V). 172

Figure 5.3: Heat map of differentially expressed proteins in the coronas of PDS sutures, electrospun filaments (Es), and melt-extruded yarns (Ext). 174

Figure 5.4: Heat map of differentially expressed proteins in the coronas of electrospun filaments (Es) and melt-extruded yarns (Ext)..... 175

Figure 5.5: Optimising the cell seeding set-up and seeding density. 176

Figure 5.6: Initial attachment of tendon fibroblasts on hybrid suture components. 177

Figure 5.7: Metabolic activity of tendon fibroblasts on hybrid suture components. 178

Figure 5.8: Initial attachment of tendon fibroblasts on hybrid and control sutures. 179

Figure 5.9: Metabolic activity of tendon fibroblasts on hybrid and control sutures. 180

Figure 5.10: SEM images of healthy tendon fibroblasts seeded on hybrid and control sutures..... 182

Figure 5.11: μCT scans of hybrid, Vicryl, and PDS sutures seeded with tendon fibroblasts and cultured for 7 days. 183

Figure B.1: Influence of PDO manufacturer and concentration on electrospun filament properties. 249

Figure B.2: Changes in mechanical properties of electrospun filaments annealed for various times at 65°C, 75°C, and 85°C, over a 6-week degradation period. 250

Figure B.3: Representative thermal data comparing PDO electrospun filament, melt-extruded yarn, and raw resin. 251

Figure B.4: Representative pore size distribution of electrospun filaments and extruded yarns, measured by Hg porosimetry..... 252

Figure C.1: Pilot data comparing hand-braiding and hand-twisting electrospun filaments to surgical PDS and Vicryl sutures. 252

Figure C.2: Pull through testing of braided electrospun sutures compared to surgical sutures PDS and Vicryl. 254

Figure C.3: Mechanical pull through properties of braided electrospun sutures compared to surgical sutures PDS and Vicryl. 255

Figure C.4: Hg porosimetry data comparing the electrospun sheath, melt-extruded cores, and hybrid braided sutures. 255

Figure D.1: Principal component analysis (PC2/PC3) of protein coronas formed on electrospun filaments (Es), and melt-extruded yarns (Ext), as well as on surgical sutures PDS (PDS) and Vicryl (V). 264

Figure D.2: Functional pathways of detected proteins. 265

Figure D.3: Differential expression of binding proteins in the coronas of electrospun filaments, melt-extruded yarns, PDS, and Vicryl. 267

List of Tables

Table 2.1: Important suture mechanical properties and properties at the suture-tendon interface that are relevant to rotator cuff (RC) repair.....23

Table 2.2: Comparison of textile methods for electrospun filaments.....40

Table 2.3: Factors considered in choosing PDO for the work in this thesis.....50

Table 2.4: Advantages and disadvantages of using electrospinning as the main fibre production method for this thesis, presented in order of importance.....51

Table 2.5: Target design criteria for the bioactive suture developed in this thesis.....57

Table 3.1: Parameters modulated in electrospinning to affect fibre diameter, alignment, and topography. 63

Table 3.2: Parameters for electrospinning PDO filaments used in this thesis.....83

Table 3.3: Effect of stretching on electrospun filament characteristics.....84

Table 3.4: Electrospun filament characteristics. 84

Table 3.5: Parameters for melt-extruding PDO yarns used in this thesis. 93

Table 3.6: Melt-extruded filament and yarn characteristics. 94

Table 3.7: Melt-extruded yarn characteristics. 94

Table 3.8 Summary of electrospun filament and melt-extruded yarn characteristics. 101

Table 3.9: Chapter 3 in context..... 116

Table 4.1: Electrospun braided suture parameters and characteristics. 130

Table 4.2: μCT and Hg porosimetry data of electrospun braided sutures. 132

Table 4.3: Hybrid braided suture parameters and characteristics. 135

Table 4.4: Chapter 4 in context..... 157

Table 5.1: Chapter 5 in context..... 196

Table 6.1: Summary table of design criteria and hybrid suture properties. 225

Table A.1: USP size classification for synthetic absorbable sutures..... 246

Table B.1: PDO manufacturers and concentrations tested for optimal electrospinning. 248

Table C.1: Materials needed for usability testing. 257

Table D.1: Full list of differentially expressed proteins in the coronas of electrospun and melt-extruded yarns. 266

Abbreviations

μCT	Micro-computed tomography
3D	Three-dimensional
ACL	Anterior cruciate ligament
AFM	Atomic force microscopy
CSA	Cross-sectional area
CTGF	Connective tissue growth factor
DSC	Differential scanning calorimetry
ECM	Extra-cellular matrix
FBS	Fetal bovine serum
FDA	Food and Drug Administration
FET	Fibre-Extrusion Technology Ltd
FT-IR	Fourier transformation infra-red spectroscopy
GAG	Glycosaminoglycan
GMP	Good Manufacturing Practices (FDA)
GLP	Good Laboratory Practices (FDA)
Ha	Annealing peak
Hf	Heat of fusion
HFIP	1,1,1,3,3,3-Hexafluoro-2-propanol
Hg	Mercury
Hm	Melting peak
HMDS	Hexamethyldisilane
hMSC	Human mesenchymal stem cell
iPSC	Induced pluripotent stem cell
ISO	International Organisation for Standardization
LS-MS	Liquid chromatography-mass spectrometry
MFR	Melt flow rate
MHRA	Medicines and Healthcare products Regulatory Agency
NOC	Nuffield Department of Orthopaedics
OCT	Optimal cutting temperature compound
OsO_4	Osmium tetroxide
P/S	Penicillin/streptomycin
PCA	Principal component analysis

PCL	Polycaprolactone
PDO	Polydioxanone
PDS	Polydioxanone suture
PEG	Polyethylene-glycol
PERC	Perchloroethylene
PGA	Polyglycolic acid
PLA/PLLA	Polylactic acid
PLGA	Poly(lactic-co-glycolic acid)
PMA	Premarket Approval (FDA)
PMT	Physico-chemical, morphological, and topographical characterisation
PPI	Patient and public involvement
ppm	Parts per million
PRP	Platelet rich plasma
R&D	Research and development
SOP	Standard operating procedure
TC	Tissue culture
TCP	Tissue culture plastic
TERM	Tissue engineering and regenerative medicine
Tm	Melting point
UK	United Kingdom
US	United States of America
USP	United States Pharmacopeia
XPS	X-Ray photoelectron spectroscopy
XRD	X-Ray powder diffraction

Chapter 1

Introduction

Many surgical tendon repairs do not heal successfully. Tendon tissue has a hierarchical architecture that is specialised for its function to enable locomotion and load-bearing. In tendinopathy, this structure is disrupted, often leading to tears. Rotator cuff tears, the clinical focus of this thesis, are highly prevalent and have particularly poor surgical outcomes. More than 200,000 operations are performed in the United States (US) and 10,000 in the United Kingdom (UK) per year.[1] Despite decades of advances in surgical technique and materials, 40% of rotator cuff repairs fail within 12 months.[2] There are significant unmet challenges in restoring function and mobility in patients with tendon tears, due to the tendon's poor intrinsic healing capacity and an incompatibility between surgical materials and the tissues they seek to replace. As a result, improving rotator cuff repair outcomes is an important unmet healthcare need.

The main mode of rotator cuff failure is that sutures pull-through the tendon causing a cheese-wiring effect.[3–6] Pull through is a complex, multifactorial problem and not a specific focus of this thesis, but fundamentally stems from a lack of integration of the suture with the tissue. This is perhaps unsurprising, given that the sutures used in rotator cuff repairs are biologically inactive materials, often non-degradable, used for surgical repairs at many different anatomical sites, and are not designed for use on torn tendinopathic tissue with compromised regenerative potential. Indeed, most sutures currently used in tendon repair are not designed to biologically integrate with the tissue it seeks to repair.

Many researchers are attempting to solve the problem of tendon failure using different approaches: some focus on understanding the mechanical interactions between suture and tendon at their interface mostly through benchtop biomechanical studies. Other work

focuses on optimising the surgical construct using synthetic or biological rotator cuff patches and experimenting with different surgical constructs to reattach the torn tendon. Some, like the work in this thesis, address the lack of tendon healing, by developing degradable materials specifically designed for rotator cuff tendon cells to adhere, proliferate, and integrate with the native tissue.

1.1 Scope of this thesis

This thesis build upon previous work in the Carr group, developing degradable biomaterials using electrospinning to improve rotator cuff tendon repair. This project specifically focuses on developing a novel suture for tendon repair that can mechanically support the tissue and also contain biophysical cues to direct cell-driven tissue repair conductive to tendon healing. Because the suture-tissue interface is often the weakest point of the repair and the suture is the main implanted material in contact with torn tendon, it is a promising medium through which novel treatments can be explored. Electrospun materials are promising candidates for tendon tissue engineering, due to their ability to mimic native tendon extra-cellular matrix (ECM) structure and induce similar biophysical cues. For this thesis, electrospinning was chosen as the main biomaterial fabrication method, because of the flexibility in fabricating submicron and nanoscale fibres, ability to fabricate continuous materials that can be braided into sutures, expertise and resources in the Carr group, and substantial literature on the bioactive potential of electrospun materials for tendon regeneration.

An ideal suture to augment tendon repair needs to fulfil several mechanical and biological requirements, which will be explained in detail in Chapter 2, but are summarized here. First, the suture needs to be safe. Polydioxanone, a synthetic, semi-crystalline polymer, was

chosen mainly because of its long-term evidence of safe use in humans. The suture needs to show evidence of bioactivity compared to currently used sutures. In particular, tendon cells should adhere to the material, proliferate, and show signs of infiltration into the structure. It is hypothesized that electrospun submicron fibres can provide bio-instructive cues to promote cell adhesion and proliferation. The suture should also have comparable tensile strength and strain to currently used sutures for tendon repair. It is hypothesized that a combination of electrospun material with another, stronger melt-extruded material will be needed to achieve this requirement. The suture needs to degrade at a rate that is appropriate for tendon repair and the formation of new tissue and the degradation products must be safe. Finally, the suture needs to be have handling properties that are suitable for surgeons and compatible with surgical equipment for tendon repair.

This thesis is divided into 6 chapters. Chapter 2 provides an anatomical and clinical background of rotator cuff tendon tears, followed by a review of treatment strategies and their shortcomings. Electrospinning and melt-extrusion, the biomaterial fabrication techniques relevant to this thesis, are introduced. Chapter 3 explores the fabrication of electrospun and melt-extruded fibres using the same medical grade polymer polydioxanone. Electrospun fibres are fabricated with a target diameter of <1μm to mimic tendon fibrils, whereas melt-extruded fibres are fabricated with target micrometre diameters to provide mechanical support. Moreover, annealing is explored as a post-processing method to improve the tensile strength of electrospun materials. Chapter 4 investigates the use of an industrial braiding process to fabricate continuous sutures and enable control over their structure, reproducibility, and production volume. A hybrid suture, made up of an electrospun sheath and melt-extruded cores, is developed to specifically meet the demands of tendon. Chapter 5 explores the interactions between the novel hybrid suture and the tendon biological environment, in terms of its serum protein

adsorption and tendon fibroblast attachment and proliferation. Moreover, the novel hybrid suture is compared to currently used surgical sutures to evaluate its potential to improve existing treatment options. Chapter 6 provides an overall discussion of the contribution of this thesis to the development and translation of a novel hybrid suture to improve tendon repairs. Finally, a possible path to pre-clinical and clinical trials for the hybrid suture is proposed.

1.2 Thesis objectives

The overarching objective of this thesis is to develop a novel bioactive suture that has the potential to support the biological repair of tendon tissue. The specific thesis objectives are:

1. Generate continuous electrospun filaments made up of submicron-sized fibres, which will replicate tendon fibril fibre diameters found in native tendon ECM.
2. Generate continuous melt-extruded filaments made up of micrometre sized fibres, which will add mechanical strength to the suture.
3. Use industrial braiding to manufacture a hybrid electrospun-extruded suture that meets the design criteria developed in Chapter 2, by combining materials from Chapter 3.
4. Investigate the bioactivity of the hybrid suture, in terms of its potential to influence protein adsorption and patient-derived tendon fibroblast activity.

1.3 Thesis hypotheses

The overarching hypothesis of this thesis is that a combination device using electrospun and melt-extruded materials would be needed to achieve the mechanical and biological requirements of a suture to augment tendon. The specific thesis hypotheses are:

1. It will be possible to fabricate electrospun filaments made up of submicron fibres on a continuous wire. Post-processing methods, such as annealing, will improve the strength and tailor their degradation rate.

2. Melt-extruded multifilament yarns can be made up of 10μm fibres. Compared to electrospun material of the same overall diameter, melt-extruded materials will be stronger, stiffer, and degrade more slowly.

3. Industrial braiding will enable the flexibility to modulate suture properties and increase their rate of production. Using both electrospun and melt-extruded fibres in a hybrid device will be needed to meet the criteria for a suture suitable for tendon repair.

4. The novel hybrid suture will have a different serum adsorption profile compared to clinical sutures. There will be increased attachment, proliferation, and elongation of tendon fibroblasts along hybrid sutures compared to currently used sutures.

Chapter 2

Background

2.1 The healthy shoulder

2.1.1 Shoulder and rotator cuff anatomy

The shoulder is made up of four joints: the acromioclavicular joint, the sternoclavicular joint, the scapulothoracic joint, and the glenohumeral joint (Figure 2.1). These joints are coordinated to perform complex movements and together make the shoulder the most mobile part of the human body. The glenohumeral joint, a ball and socket joint, is the main articulating site of the shoulder and connects the head of the humerus with the glenoid fossa of the scapula. In a healthy shoulder, the humeral head is not displaced during movement, mainly due to the soft tissues that stabilize the joint. These tissues include the fibrocartilaginous labrum, the ligaments, and the muscles and tendons. The muscles and tendons that stabilise the shoulder are collectively called the rotator cuff.

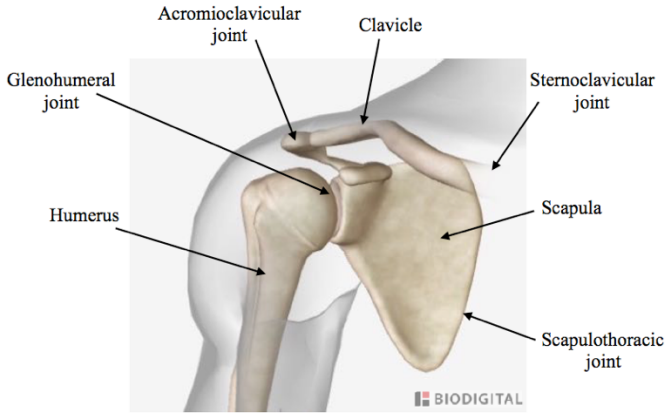


Figure 2.1: Anatomical features of the right shoulder in anterior view. The shoulder is a complex structure made up of three bones (humerus, clavicle, and scapula) and four joints (glenohumeral, acromioclavicular, sternoclavicular, and scapulothoracic). There are also a number of soft tissue supporting structures which are not shown to improve clarity of the other structures. Figure adapted with permission from BioDigital HUMAN (www.biodigital.com).[7]

The rotator cuff is comprised of four muscles and tendons: subscapularis, supraspinatus, infraspinatus, and teres minor (Figure 2.2). The supraspinatus controls abduction, the infraspinatus controls external rotation, and the subscapularis is critical to internal rotation. While their relative contributions vary, the rotator cuff muscles act together to maintain shoulder stability during motion. Because the rotator cuff is integral to shoulder stability and initiation of shoulder movement, its damage can cause significant disability.

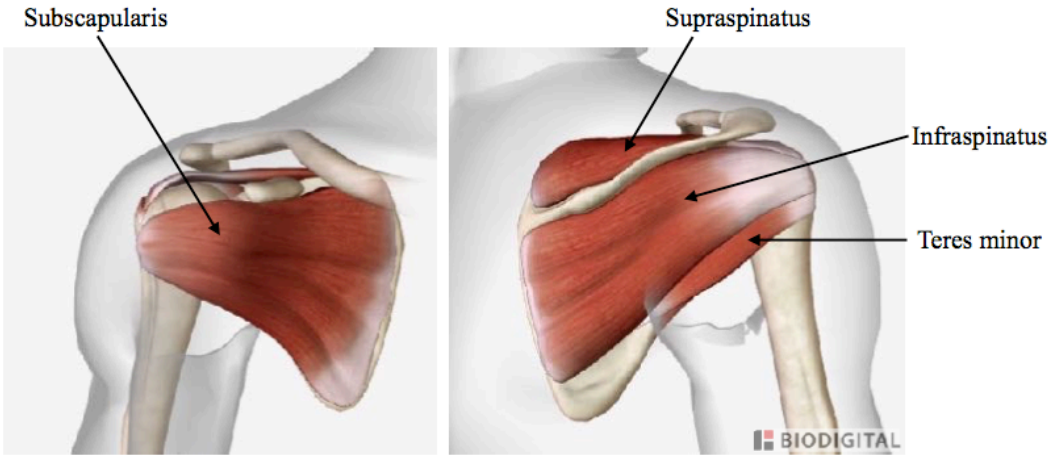


Figure 2.2: Rotator cuff tendons and muscles of the right shoulder. The left panel is the anterior view and the right panel is the posterior view. The rotator cuff is made up of four muscles and tendons: subscapularis, supraspinatus, infraspinatus, and teres minor. All structures originate from the scapula and insert into the head of the humerus. Figure adapted with permission from BioDigital HUMAN (www.biodigital.com).[7]

All of the rotator cuff tendons originate from the scapula and insert into the proximal humerus. As the tendons pass over the glenohumeral joint, they join together to form a cuff and envelope the humeral head. It is at this common point, most commonly on the supraspinatus tendon, where rotator cuff tendon tears are most likely to occur. If a tendon does tear, surgical repair is often necessary. This involves reattaching tendon to tendon or tendon to bone, depending on the type and location of the tear.[8] The enthesis refers to the tendon to bone transition and is a complex structure that effectively transfers forces from tendon to bone matrix.[9] This site is also commonly affected in rotator cuff tears.[10]

2.1.2 Tendon biomechanics

During motion, the shoulder experiences shear, torsion, compression, and tension. Shoulder tendons are most commonly loaded in tension and follow a characteristic stress-strain curve (Figure 2.3). A typical stress-strain curve has three regions: (1) The toe region corresponds with the straightening of the collagen fibre bundles. Staggered collagen molecules are configured in a crimp pattern, which is thought to minimise damage under rapid loading.[11,12] This crimp disappears under low strain (around 4%) and reappears once the stress is released; (2) The linear or elastic region is the area where the collagen fibres are straightened, but can still recoil and assume their original form. The slope of the linear region is used to calculate Young's modulus, to approximate the tissue stiffness;[13] (3) The plastic or failure region is the final region, where micro- and macroscale tearing leads to irreversible damage of the tendon tissue.

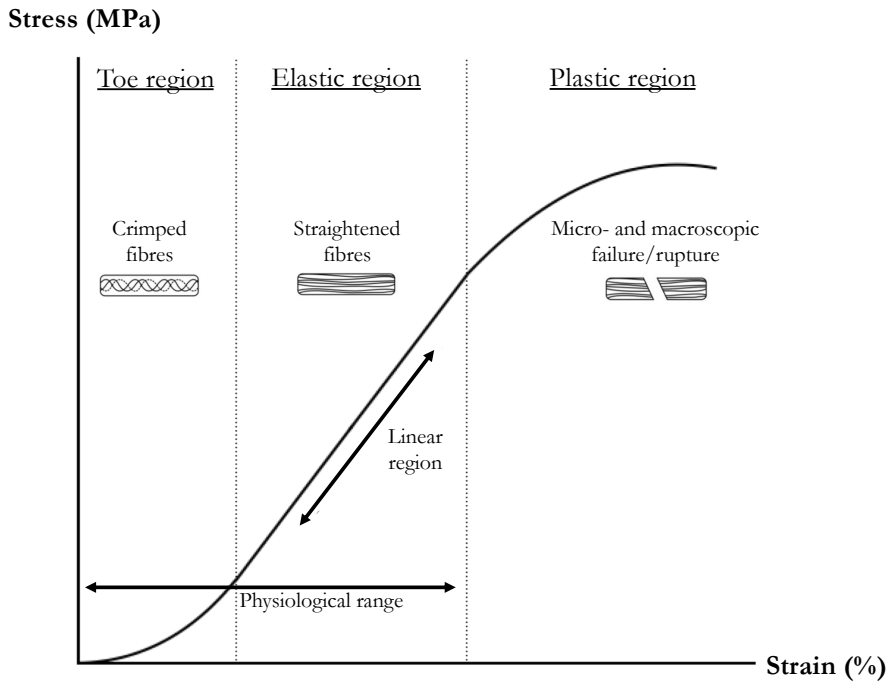


Figure 2.3: Representative stress-strain curve for tendon loaded in tension. The curve has three distinctive regions: toe, elastic, and plastic regions. In the toe region, the crimped fibres are straightened under low strain. In the elastic region, fibres are straightened, but still able to assume their original form. In the plastic region, micro- and macroscale failure leads to irreversible damage to the tendon.

Healthy tendons can withstand very high forces before they reach the point of macroscopic failure. An intact supraspinatus tendon will detach from the insertion of the humerus before the tendon itself fails, with detachment forces reported between 652-784N.[14,15] The supraspinatus is able to retain sutures up to forces of 168-228N.[14,16] These mechanical properties observed in healthy tendon are reflective of its microscale structure. The tendon's hierarchical architecture of collagen molecules, fibrils, fibres, fascicles, and tendon units, make it well suited for carrying and transferring load and is discussed in the following section.

2.1.3 Tendon structure and function

Tendon enables joint movement by permitting force transmission from muscle to bone.[17] The hierarchical architecture in tendon is complex and this structure varies along the length, width, and depth of the tendon. The cellular and non-cellular components of healthy tendon are considered in this section.

2.1.3.1 Tendon architecture

The ECM is the non-cellular component of tissues. The tendon mid-substance is ECM rich, avascular, un-innervated, and has low cellularity and limited lymphatic drainage. ECM is a dynamic structure and is constantly being degraded, remodelled, and synthesized. Importantly, ECM provides physical scaffolding for tendon cells alongside biophysical and biochemical cues, to direct cell behaviour.[18]

Tendon ECM is composed of collagen, proteoglycans and other protein structures, elastin, glycosaminoglycans, and water. All collagens make up 80% of its dry weight and collagen I accounts for 95% of all healthy tendon collagen. Figure 2.4 shows the hierarchical architecture of tendon.[17] Collagen fibrils are the smallest tendon structural units visible by electron microscope. Fibrils are formed through the initial assembly of amino acids into

an alpha-chain, where glycine occupies every third position.[17,19] Three alpha-chains coil to form the right handed triple helix of a tropocollagen molecule, which is the basic structural unit of collagen.[19] Tropocollagen molecules form cross-links to create collagen molecules, which then aggregate progressively into microfibrils and then into collagen fibrils.[17,20]

Collagen fibrils have a diameter of approximately 100nm but can range from 20-500nm in diameter depending on anatomical location and tendon function. Fibrils bundle together to form collagen fibres, which range from 1-20μm in diameter. Fibres bundle together to form a primary fibre bundle, or a subfascicle; these further collect together to form a secondary fibre bundle, or a fascicle. Secondary fibre bundles collect to form a tertiary fibre bundle. Tertiary fibre bundles bundle to form a tendon unit and tendon units group together to form a tendon.[13] The primary, secondary, and tertiary fibre bundles are bound and separated by a thin layer of connective tissue, known as the endotenon.[13] The connective tissue surrounding the tendon units and the whole tendon is called the epitenon, which contains the nervous, lymphatic, and vascular supply of the tendon.[13] Above this is a loosely connected fibrous tissue called the paratenon. In the rotator cuff, the paratenon and epitenon together form the peritendon, which reduces friction between tendons and surrounding tissues in the shoulder.

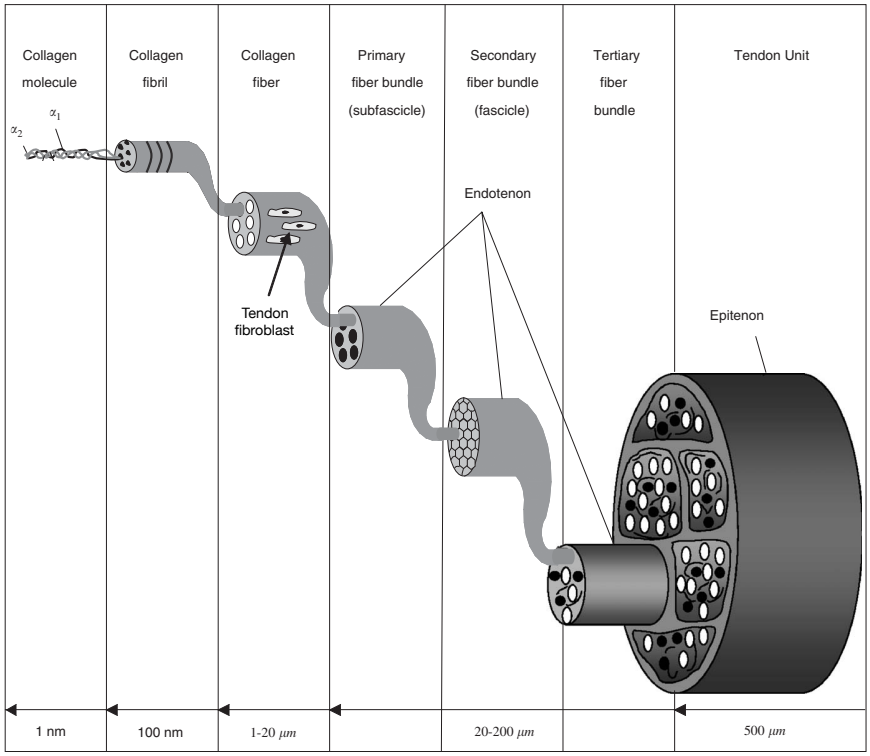


Figure 2.4: Hierarchical architecture of tendon. Tendon is a complex structure made up predominately of collagen molecules. Its hierarchical architecture of collagen molecules, fibrils, fibres, fascicles, and tendon units make it well suited to carry and transfer load from muscle to bone. Tendon fibroblasts are found interspersed in the collagen fibres. The endotenon and epitenon are connective layers that reduce friction and contain the nervous, lymphatic, and vascular supply of the tendon. Figure modified from Wang et al[13].

The non-collagenous components of the tendon ECM are predominantly proteoglycans, glycosaminoglycans, and elastin. Proteoglycans consist of a core protein with attached glycosaminoglycan (GAG) side chains.[17] GAGs trap water and give tendon its specific viscoelastic properties. This trapped water lubricates the collagen fibrils, allowing them to slide more easily past each other, and resist compression. Proteoglycans are involved in fibril formation, maturation, and in linking together collagen fibrils.[17,21] Elastin fibres are also integral to the tendon ECM and provide stability to the collagen fibres.[21]

2.1.3.2 Tendon cells

Around 90-95% of cells in the tendon matrix are tendon fibroblasts. They are present throughout the matrix and produce tendon specific ECM components, largely based on biophysical and biochemical cues in their environment.[13,21] However tendon fibroblasts are slow to divide and have low collagen turnover rates, contributing to tendon's poor intrinsic healing capacity. Tendon fibroblasts in healthy tendon have an elongated, bi-directional morphology, whereas diseased fibroblasts have a more rounded morphology.[17,22] The differences between fibroblasts in healthy and diseased tendon are discussed further in Chapter 2.2.2.

There are also a small number of macrophages residing in tendon tissue.[23] However, in the context of rotator cuff injury, the immune response is thought to be driven by recruited peripheral immune cells (such as peripheral macrophage infiltration) to the site of tendon injury. The infiltrated macrophages are postulated to drive an increase in levels of transforming growth factor-beta (TGF-β), which can drive fibrotic scar formation in the tendon.[24] The inflammatory cascade following rotator cuff injury and subsequent repair is discussed further in Chapter 2.3.

2.2 Rotator cuff tendinopathy

A tendinopathy refers to a non-rupture injury in the tendon that is exacerbated by mechanical loading, often leading to a tear.[22] As a result, in this thesis, the term tendinopathy can encompass inflammatory and fibrotic conditions of the tendon as well as torn tendon tissue. Rotator cuff tendinopathy describes pathologies which affect the rotator cuff and its surrounding structures. A rotator cuff tear is associated with macroscopic damage to the tendon and a loss of function. Tears can occur in any of the rotator cuff tendons, but most commonly occurs in the supraspinatus tendon. While the

aetiology of rotator cuff tears is complicated and not fully understood, it includes a range of factors, such as anatomic variation[25], genetic factors[26], age[27], overuse[28], and inflammation[29].

2.2.1 Burden of disease

Rotator cuff tendinopathy is very common and places a significant physical and emotional burden on patients and a financial burden on healthcare systems. Many tendinopathies progress to a full tendon tear. Rotator cuff tears affect around 50% of people over 66 years old.[30] With an ageing population, the socioeconomic burden of rotator cuff tear related disability and subsequent surgery is likely to increase.[31] Due to their inherent poor blood supply and healing potential, most tears, especially larger ones, require surgical intervention. Over 200,000 operations are performed in the US every year and 10,000 in the UK.[1,32] Surgery is performed by using sutures and suture anchors to reattach the torn tendon to bone, and sometimes synthetic scaffolds to additionally support the repair construct (further discussed in Chapter 2.4.2). Despite advanced surgical techniques and augmentation strategies, 40% of repairs fail within 12 months.[2] To compare to another common musculoskeletal condition, less than 5% of patients receiving hip replacements experience implant failure within 10 years after surgery. Improved treatments for rotator cuff tendon tears are needed.

2.2.2 Diseased tendon structure and function

There are distinct changes to tendon ECM in rotator cuff tendinopathy compared to healthy tendon (Figure 2.5). Overall, tendinopathic tissue is thicker and weaker than that of healthy tendon. The decline in both structural and material properties of diseased tendon, as well as its lack of inherent repair capacity and chronic inflammation, means that if the tendon does tear, it often does not heal.[22] The specific physical and chemical changes to tendon ECM relevant to the development of novel biomaterials are[22,33–35]:

- Loss of longitudinal alignment in the matrix
- Decrease in collagen fibril diameter, and a larger range of fibre diameters
- Reduction in collagen I content and increase in collagen III content
- Altered collagen ratios
- Increased cellularity and rounded cell morphologies
- Increase in proteoglycan and GAG content
- Increased vascularity

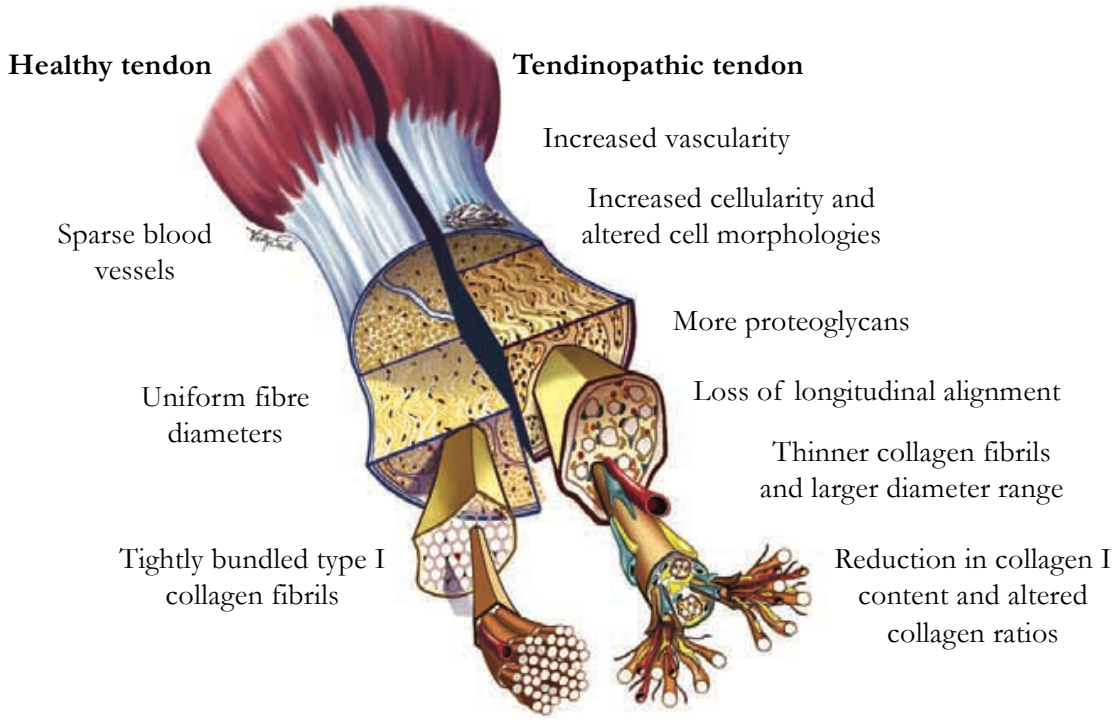


Figure 2.5: Differences in tendon architecture and composition in healthy and tendinopathic tissue. The healthy tendon, shown on the left, is composed of tightly bundled collagen fibres made up of mostly type I collagen. The tendinopathic tendon, shown on the right, is less organised. Collagen fibrils are thinner and more loosely organised. There is a reduction in type I collagen, an increase in type III collagen, and altered collagen ratios. There is an increase in cellularity and more rounded cell morphologies. There is also an increase in proteoglycans and GAG content, leading to increased swelling in the tissue. Figure modified from Brukner et al[36].

It has been widely shown that surgically repaired tendon properties are different to the properties of healthy tendon. There is evidence that repaired tendons are weaker and have

increased scar tissue, which likely contribute to the high rates of re-tearing and follow up surgeries.[37–39] However the exact pathophysiology underpinning the differences between repaired and healthy tendon have not been well characterised. Tissue engineering and regenerative medicine (TERM) and biomaterial strategies aim to develop materials that match the hierarchical architecture and properties of native tendon tissue to guide tendon to adopt a structure that more resembles healthy tissue.

2.3 Tendon response to injury

Following tendon injury, the body initiates a natural healing response to restore function. This healing cascade is divided into three overlapping stages, which are characterised by the cellular processes that occur: inflammation (day 1-7), proliferation (day 3-14), finally resulting in remodelling and resolution.

The inflammatory phase starts immediately after injury and is characterised by the release of chemotactic factors and the recruitment of acute inflammatory cells, such as neutrophils and primary monocytes, to the injury site.[13] Neutrophils and macrophages phagocytose damaged matrix and intrinsic tendon fibroblasts are recruited to the injury site and begin to synthesize various components of the ECM.[40] Moreover, angiogenic factors begin to form a vascular network.[21] The proliferative phase is characterised by the proliferation of tendon fibroblasts and an increase in immature tendon ECM, which is particularly high in collagen III and proteoglycans. This is also accompanied by an increase in vascularization, with new nerves and blood vessels connected to the existing tissue.[41] At this point the tissue has a scar-like appearance.[41,42] Controlled mechanical loading of the tendon is critical during this phase: too much loading can lead to re-injury but not enough loading can lead to scar tissue development.[12] Finally, the remodelling phase is predominately characterised by an increase in collagen I production, a decrease in collagen III, and the production of matrix metalloproteinases, which are responsible for the turnover of tendon ECM.

Although ECM components become more organised during this stage in an attempt to recreate the original tissue, the final repaired tissue does not replicate the un-injured tendon, but does afford more function than scar tissue.[40,43] This natural healing response may be sufficient for small tears, however larger tears often require surgical intervention.[2]

2.4 Treatment strategies and limitations

2.4.1 Non-surgical treatments

It is most common for patients with rotator cuff tears to initially be treated conservatively, unless the patient presents with acute traumatic tears which may benefit from surgery immediately.[44] However, most patients can reduce pain and improve function through a combination of analgesic treatments and physiotherapy. Glucocorticoid steroid injections have shown short-term benefit for pain relief, however the effects of long-term repeated injection on tendon health are controversial.[45] Numerous studies have raised concern about repeated steroid injections leading to diminished cellular proliferation, tissue degeneration, and the rupture of weight-bearing tendons.[46–48] It is important to note that currently available drug treatments provide only symptomatic relief and do not initiate or support a therapeutic healing response.

Physiotherapy is used as a non-surgical treatment option, but also used during post-operative rehabilitation. Studies investigating the outcomes of treating torn tendons with physiotherapy alone are inconclusive, often showing a range of success rates with limited follow-ups.[45,49] However, it seems that patients with tears larger than 1cm and symptoms lasting for more than 1 year do not improve from physiotherapy alone and require surgery.[49]

2.4.2 Surgical treatments

If non-surgical treatments are not sufficient to reduce pain and improve function, patients will undergo surgical treatment. The type of operation is largely dictated by the size and location of the tear and management after surgery will vary. The two most common tear types are crescent and U-shaped tears (Figure 2.6).[50] Both repair types use sutures to approximate tissue and suture anchors to approximate tissue to bone. Crescent tears typically present with the tendon pulled away from bone, but it doesn't retract far and can be repaired to bone with minimal tension.[51] Conversely, U-shaped tears extend much farther medially and require a side-to-side closure of the vertical side of the tear before the tendon-to-bone closure.[51] Over the last 100 years, the surgical practice has evolved with the introduction of arthroscopic procedures, new surgical techniques, and new surgical materials. Despite these surgical developments, 40% of repairs still fail within 12 months.[2] The repairs can fail at the anchor-bone interface, the tendon-suture interface (Type 1 failure), or from a recurrent tear, medial to the original repair (Type 2 failure). Commonly, the suture cheese-wires through the tendon, making the suture-tendon interface a vulnerable link in the repair.[3–6]

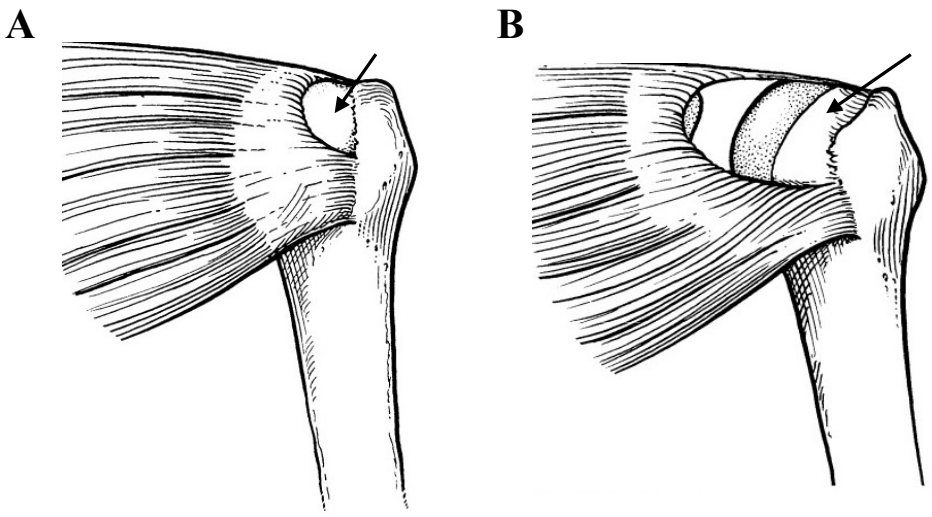


Figure 2.6 Common types of rotator cuff tendon tears. (A) Crescent shaped tears. These tears pull away from the bone but do not retract far and can be repaired directly to bone with minimal tension. (B) U-shaped tears. These tears extend much farther medially, sometimes extending to the glenoid or even medial to the glenoid. Closure of a U-shaped tear involves first side-to-side closure of the vertical sides of the tear and then tendon-to-bone closure of the transverse side. Arrows indicate tendon tears. Figure adapted from Burkhart et al.[51]

2.4.2.1 Surgical repair constructs

The goal of rotator cuff surgery is to optimize the bone to tendon connection, which can be performed either by open repair or arthroscopic surgery. Figure 2.7 demonstrates various repair constructs and the surgical materials that are used in the repair. The two main types of constructs are tendon-to-tendon repairs and tendon-to-bone repairs. Sutures, suture anchors, and occasionally scaffolds are used to surgically repair a torn rotator cuff. The suture is the most ubiquitous material in tendon repair and is of particular relevance to this thesis. A variety of suturing techniques are possible, however there is no conclusive evidence to support one technique over any other.[52] Three common techniques, single row, double row, and suture bridge techniques, are outlined in Figure 2.7. A single or double row of sutures are passed through the tendon and connected via a suture anchor into the humerus (Figure 2.7A and B). A variation of this technique uses a lateral row of suture anchors placed further outside of the tendon footprint, which is intended to

minimise damage and invasion of the footprint by sutures, as well as increasing the compression over the footprint (Figure 2.7C).[53]

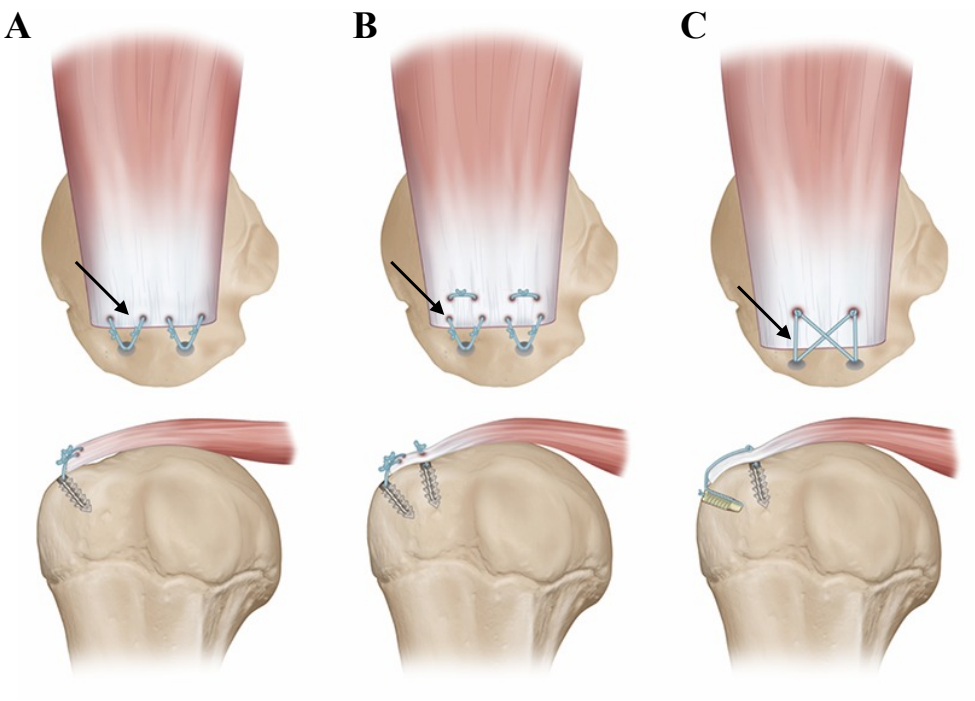


Figure 2.7: Surgical techniques for rotator cuff repair. Different surgical techniques for repairing rotator cuff are shown, with an emphasis on how sutures are used (shown with black arrows). (A) Single row repair. A single row of sutures is passed through the tendon using a bone anchor to fix and compress the tendon free edge back on the humerus; (B) Double row repair. A double row of sutures and two bone anchors are used to enable increased compression of the free tendon edge; (C) Suture bridge repair. A lateral row of sutures is placed further outside of the tendon footprint in order to increase the compression over the footprint. Figure modified from Bedeir et al.[54]

Choosing the appropriate surgical anchor is also important for a successful rotator cuff repair. Anchors can be grouped into metal screw anchors, non-metal absorbable and composite anchors, and mini-anchors. Typically, non-degradable anchors are made of metals, such as steel or titanium alloys, and polymers, such as polyethylene. Absorbable anchors may be made of polyglycolic acid (PGA), co-polymers or other polymers.[55–57] In choosing the appropriate anchor, the surgeon must have an understanding of the biology and biomechanics that affect their use – both in terms of initial fixation, but also over the lifetime of the implant and the tissue healing process. A typical suture anchor has an eyelet through which a suture is threaded and may be used to attach the soft tissue to the bone

where the anchor is inserted.[58] Because suture materials play an integral part in achieving a successful repair, choosing the right materials and performing an appropriate close technique are often of equal importance in a clinical setting.

2.4.2.2 Sutures

A suture is a strand of fibrous material used during surgery to approximate tissue.[59] The use of the suture is one of the most common practices in the medical field and is significant in influencing healing and repair.[60] Until the 1930s, catgut and silk dominated the suture market, however during and after World War II, the discovery of nonabsorbable synthetic polymers revolutionized the chemical sourcing of suture materials.[61–63] In the late 1960s, the synthetic absorbable polymer PGA was introduced to the market. Synthetic absorbable polymers changed suture production by improving the uniformity in chemical composition and more reliable strength and degradation than the previously naturally sourced materials.[63] These polymers also generally elicited a less intense immune response and tissue reaction and promoted faster wound healing and strength.[64]

Contemporary sutures are classified based on their origin (natural or synthetic), degradability, and configuration (monofilament or multifilament). Multifilament sutures have better mechanical properties and are more flexible and pliable than monofilament sutures.[65] Although multifilament sutures increase the risk of surgical site infection, compared to monofilaments, this risk is minimized by clean room manufacturing and effective sterilization methods.[66] Sutures are also classified based on their size, most commonly based on the United States Pharmacopeia (USP) standard.[59] Small suture sizes are represented by two numbers; the second number is always zero, i.e. 2-0, or 4-0. The larger the first number, the smaller the suture is. Sutures larger than 0 (1-0) are denoted with a single number, i.e. 1,2,3. The larger the number, the larger the suture is. Table A.1 in the Appendix provides USP size classification with the corresponding range of suture

diameters. For rotator cuff repairs, surgeons typically use sutures in the USP size 2-0 to 4 range. Sutures outside of this range afford poorer handling properties and are not usable with commercial suture anchors.

Sutures developed in the late 20th century were used to mechanically support tendon by transferring load from muscle to bone and providing compression to the construct. They are designated as inert or biocompatible materials, meaning that they do not induce an intended biological response. Over the years, incremental changes to sutures have been made, such as modifications to the polymer composition or the addition of an antimicrobial coating. A recent innovation is suture tape – a flat, ribbon like suture which is meant to improve the compression of tendon to bone.[67] Although there have been changes in sutures and suturing techniques, no clinically significant improvements in rotator cuff repair outcomes have been demonstrated. Because suture design is mainly industry driven, incremental changes have allowed for a steady outflow of products, while maintaining a safe regulatory position and limiting costs. Moreover, surgeons are guided by bench-top cadaveric evaluations of newly released suture materials, which poorly mimic the complex biophysical environment within which the material will perform. It is true that suture materials used today cause fewer infections. However, suture failure is still frequently caused by knot slipping or persistent tension on the sutures causing pull-through and a cheese-wiring effect.[3–6] Pull through is a complex, multifactorial problem, but fundamentally stems from a lack of integration of the suture with the tissue. This is perhaps unsurprising, given that the sutures used in rotator cuff repairs are used for surgical repairs at many different anatomical sites and are not designed for use in highly specialised tendon tissue at the limits of its capability. The inappropriate re-purposing of surgical materials is a major clinical concern and has led to recent changes for device regulation in the European Union.[68–70] Many researchers are attempting to solve the

problem of tendon failure from different angles: some focus on understanding the mechanical interactions between suture and tendon at their interface through mostly benchtop biomechanical studies. Other work focuses on optimising the surgical construct using rotator cuff patches and different surgical methods and materials. Some, like the work in this thesis, address the lack of tendon healing, by developing degradable biomaterials specifically designed for rotator cuff cells to adhere, proliferate, and integrate with the native tissue.

Although this thesis focuses on the development of bioactive materials to guide tissue repair, it is worth considering the biomechanical properties of currently used suture materials and characteristics of the suture-tendon interface during rotator cuff repair. The main purpose of currently used sutures is to mechanically approximate native tissue and to minimise a host immunological response to the foreign material. Because most synthetic sutures are made from semi-crystalline polymers, they exhibit viscoelastic behaviour.[71,72] As a result, biomechanical properties such as tensile strength, stiffness, creep, gapping, and knot slippage, are important to consider in evaluating suture properties and are summarised in Table 2.1.[63] Some characteristics are intrinsic to the suture material, such as strength and stiffness, and some characteristics are related to the suture-tendon construct, such as gap formation. It is challenging to weigh the importance of each property, however because tensile strength and breaking stress are the most frequently studied mechanical properties of suture materials, they are the ones investigated in this thesis. Because tensile stress is expressed in terms of the cross-sectional area of the material, it is normalised based on the dimension of the material and can be used to compare sutures of different chemical structures and sizes.

Table 2.1: Important suture mechanical properties and properties at the suture-tendon interface that are relevant to rotator cuff (RC) repair. Table adapted from information in [59,63,71,73]

Property	Description	Contribution to the failure of RC repairs	Range of properties of sutures used for RC repair
Stiffness	Ability of the suture to resist extension under applied tensile load.	If the suture if too stiff, it could cheese-wire through the tendon. If the stiffness is too low, it could contribute to gap formation. Gapping results in a separation between tendon and suture after repair and increases risk of re-rupture.	Stiffness: 7-34 N/mm[71,73] Gapping is more common using monofilament Prolene/PDS compared to multifilament Vicryl/Fibrewire/Ethibond[73]
Creep	Time-dependent deformation during application of constant load.	Could result in gap formation between suture and tendon.	Sutures loaded at rate of 0.5mm/s to 60N, then held at 60N for 10 min. Creep: 0.57-1.52 mm[71]
Knot security	Ability of a knot to resist slippage as a load is applied.	Some sutures require many knot throws to prevent slippage, which is a concern where there is limited amount of tendon.	Fibrewire requires the most throws to create a secure knot compared to other sutures used for RC repair.[74,75]
Porosity	Proportion of the suture that is porous, as well as the shape and diameter of the pores.	If a suture has a very low porosity, it could limit tissue integration with the material.	Overall porosity: 0-40%
Fibre diameter	The diameter of the base fibres used in multifilament sutures and the diameter of the whole suture in monofilament sutures.	Sutures with large fibre diameters (>30μm) don't mimic collagen fibrils and don't influence cell attachment through biophysical cues. Minimal cell attachment to sutures could contribute to a lack of integration between tendon and suture and contribute to cheese-wiring.	Fibre diameters of multifilament sutures: (Fibrewire, Vicryl, Ethibond) fibre diameters: 30-40μm[75]

It is tempting to extrapolate from benchtop biomechanical studies of the suture-tendon interface, such as the ones in Table 2.1, to make correlations about ideal suture to repair tendon. In reality, tendon is an understudied tissue and it has not been well characterised, compared to other soft tissues, like muscle. Almost all existing data regarding basic mechanisms of tissue physiology, or detailed investigations of tendon damage and repair stem from non-primate animal studies.[76] As a result, there is a wide spectrum of likely tendon mechanical properties across anatomical locations, ages, and progression of tendinopathy.[43,76] Only recently, studies like the Tendon Seed Network are attempting to characterise healthy tendon at different anatomical sites, like the rotator cuff, and in different parts of the tendon.[77] Until tendon has been more thoroughly characterised, it will not be clear what the biomechanical properties of a suture, such as stiffness, should be, or how that stiffness should change over time during tendon healing.

2.4.3 Emerging surgical treatments

The high failure rate associated with rotator cuff repairs have encouraged the search for new materials and methods to improve surgical repair. Assuming that an appropriate technique is employed, then surgical repairs could be improved with a combination of mechanical and biological support. Currently, regenerated tendon tissue often does not recapitulate the complex structure, organisation, or properties of native tissue (Chapter 2.2.2).[78] A potential way to improve tendon healing is through the use of an augmentation technique that encourages the regeneration and repair of existing native tendon tissue.

As mentioned, surgical sutures in tendon repair are currently used to mechanically reattach the torn tendon to the bone. The need to consider the biology of wound healing has long been recognised as important for preventing implant failure, especially in tissues with poor regenerative capacity. It is suggested that the tissue-suture interface may represent the weakest link in soft tissue repair and be the cause for some repair failures.[79,80] This has been

demonstrated in studies evaluating load to failure and modes of failure, as well as observations made at revision surgery.[55–57,74,81] Specifically, suture failure is frequently caused by a lack of tissue integration and persistent tension on the sutures, causing a pull-through effect.[3–6] As a result, new materials, which aim to biologically interact with the host environment to prevent repair failure and to promote a positive healing response, are emerging. These materials are intended to provide mechanical support to the surgical repair, but primarily act as biological support by imitating biophysical properties of native tendon ECM, which are needed to induce local cell-driven responses. Two emerging surgical materials hold tremendous potential as regenerative devices: scaffolds, also known as patches, and sutures. Sutures are the main surgical material in contact with tendon during repair. Thus, they provide a potential medium through which treatment can be improved and are the focus of this thesis. Scaffolds provide structural support to the suture-anchor repair construct and a biological scaffold upon which tissue integration can occur. Because augmentation scaffolds are intended to be used surgically over the suture-tendon construct, they are also relevant to this thesis.

2.4.3.1 Augmentation scaffolds

Scaffolds are implantable biomaterials that enable additional fixation of the tendon. The scaffold is typically placed over top of the sutured tendon, which is called the onlay technique. There are over 20 scaffolds currently available on the market, which are divided into biological, synthetic, and biosynthetic scaffolds. Biological scaffolds are most commonly used and are prepared from allograft, xenograft, or autograft tissue. Biological scaffolds have been shown to cause negative foreign body and immunological reactions. Conversely, synthetic scaffolds are mostly made from non-degradable polymers and are designed to provide mechanical support and not to influence tissue response.[82–84] Despite the variety of surgical scaffolds on the market, there are continued questions about their

clinical efficacy. Some studies suggest improvements in mechanical, vascular, or biological nature of a scaffold-augmented repair; however, there is no large, well-designed clinical trial showing the benefit of any one material.[82,85–88] Moreover, none of the scaffolds currently on the market mimic the complex biophysical cues provided by native tendon matrix.[89] Although there aren't currently any commercially available augmentation scaffolds containing biophysical cues, BioPatch[90,91] (Carr group, Oxford) and BioWick[92] (Zimmer, Biomet) are examples of emerging degradable synthetic scaffolds specifically designed for rotator cuff repair.

2.4.3.2 Augmentation sutures

Today's sutures are designed to be inert, when in reality no artificial implantable material can be classified as truly biologically inactive. At a local level, cell-material interactions influence cell adhesion, proliferation, and migration, which affect wound site healing.[93] Emphasis is now shifted towards TERM strategies to develop degradable surgical biomaterials that provide sufficient mechanical strength to connect torn tissue, but that can also augment the repair by providing an appropriate biological environment to promote healing at the implant site and replacement of the suture with newly formed tissue.[94] It is worth clarifying the terms biomaterial and medical textile in this thesis, as the terms can be used interchangeably in the literature. Medical textiles, like current sutures, are medical devices made from materials that are inert or biologically inactive, meaning that they don't generate an intended tissue response. Conversely, biomaterials are designed to intentionally induce a local, favourable biological effect.

To develop a suture that will stimulate a favourable healing response, it is necessary to consider the biological environment within which the suture will act. Resident cells within tissue, as well as inflammatory cells infiltrating after injury, sense and respond to micro-

and nanoarchitecture in the ECM and to each other.[95] There are a range of material fabrication techniques that are able to approximate native ECM components. In particular, methods to fabricate submicron fibres can be used to create a material that mimics the hierarchical architecture of the native collagen fibrils of tendon ECM, which is important in providing a biological scaffold for cells that resembles native tissue (Chapter 2.7).[96,97] There are numerous electrospun scaffolds intended to encourage endogenous tissue healing with biophysical cues in various stages of the research and development (R&D) and clinical trial pathways. Biowick (Zimmer Biomet) is the first FDA approved implant for rotator cuff disease that has an electrospun component.[92] Biowick a scaffold wick and suture anchor component specifically designed for rotator cuff surgery, although its clinical effectiveness has not been evaluated. Furthermore, Bosworth et al are developing a twisted electrospun suture for regenerating flexor tendons in the hand and use many of the same manufacturing techniques as in this thesis.[98,99] However, there is currently no commercially available suture for rotator cuff repair that uses biophysical cues to alter the activity of endogenous cells and drive tissue repair.

It is worth noting that although augmentation sutures are described as sutures, they serve a different purpose to commercially available sutures and cannot be thought of as equivalent. In contrast to currently used sutures, augmentation sutures have a biologically active component, which drives cellular activity to promote a healing response. In some way, it is more appropriate to describe them as augmentation scaffolds that are in the form of a suture for ease of use. This point will be particularly relevant in considering the design criteria for the suture developed in this thesis in Chapter 2.11, as well as the cost-effectiveness of the technology in Chapter 6.

2.4.3.3 Other treatments

Stem cells and platelet rich plasma (PRP) therapy have been explored as treatment options for rotator cuff disease. Whilst some studies have showed improved tendon healing with PRP, there has been no conclusive indication of benefit.[100,101]

2.5 Mechanisms of cell-material interactions

There is increased interest and need to develop surgical materials that favourably interact with the native tissue. Understanding cell-ECM relationships in healthy and diseased tissue can be used to develop materials with biophysical and biochemical cues which direct specific cell-material responses.

The relationship between cells and ECM is understood as an active, bi-directional, changing relationship.[102] *In vivo*, matrix biophysical cues largely control what is adsorbed from the environment and the subsequent cell responses to the adsorbed complexes. It is the aim of biomaterial research to understand and replicate these specific cell-ECM interactions.[102,103] Upon implantation, a material adsorbs a surface layer of proteins and other molecules, called the provisional matrix or protein corona. It is through this adsorbed protein layer, instead of directly to the material surface, that cells initially respond. The type, abundance, and conformation of these proteins is largely dependent on chemical and biophysical properties of the material and ultimately influences how cells interact with the material. The specific protein corona composition that will best promote tendon healing is a still emerging picture, but previous work has highlighted the importance of cell adhesion proteins, like fibronectin and vitronectin[104–106], and complement proteins driving potential effects on the initial immune response.[107]

2.5.1 Biophysical and biochemical stimuli

Biophysical and biochemical stimuli drive attachments between the cell surface integrins and the matrix receptors. These attachments are called adhesion complexes and form the basis for directing a cell response. Increased understanding of cell-matrix interactions, and the regulators of these pathways, have greatly advanced biomaterials research. The main biophysical cues that are relevant to tendon biomaterial research and to this thesis are: fibre diameter, fibre alignment, and porosity.[107,108] However, modifying surface stiffness, roughness, and topography are all tunable biophysical cues as well.[85,109–111] Moreover, material surface properties such as hydrophobicity, charge, and chemistry, can be manipulated to induce specific biochemical responses.[104,112] The flexibility researchers have in tuning these parameters is largely due to the emergence of new biomaterial fabrication techniques that enable the tuning of local fibre properties.

2.6 Biomaterial fabrication techniques

Various fabrication techniques exist to create tunable fibres, such as 3D printing, electrospinning, and melt-extrusion. Each of these methods enables the production of fibres of varying sizes and properties. Electrospinning and melt-extrusion fabrication methods are relevant to this thesis and presented here. Electrospinning was chosen as the preferred fibre production method because it has the ability to mimic the extracellular matrix components of tissues, such as tendon, and is scalable and affordable. Moreover, there was substantial expertise and resources in the Carr group for electrospinning. Finally, there is vast supportive academic literature on tendon cell interactions with electrospun submicron fibres. The justification for electrospinning as a manufacturing method in this thesis is expanded upon in Chapter 2.10.

2.6.1 Electrospinning

Over the last two decades, electrospinning has become an increasingly popular method to produce submicron or nanoscale fibres because of its simplicity and versatility. Using this

technique, fibres are drawn from a polymer fluid with an electric field towards an oppositely charged collecting surface (Figure 2.8). As the volatile solvent evaporates, polymer molecules entangle and form a long continuous fibre, which is deposited on a collecting unit. Five key components to enable a simple version of electrospinning are: a polymer solution with a volatile solvent, a pump to deliver the polymer solution to the system, a nozzle to feed the solution into the chamber with the electric field, a high voltage power unit to create the electric field, and a collecting unit where the fibres are deposited. Electrospinning is usually performed in a chamber where temperature, airflow, and humidity can be regulated. Further details of the electrospinning process are outside of the scope of this background section but is described in more detail in Appendix A2.

Electrospun fibres are currently in development, or in use, for numerous applications, such as for filtration, sensors, drug delivery, energy storage, as well as for biomedical applications.[113,114] Electrospinning shows tremendous promise for biomaterials research, as it enables the fabrication of materials that mimic native ECM, by controlling fibre diameter, morphology, and alignment.[115,116] The specific factors which can be manipulated to control the electrospinning process are discussed Chapter 3.2.

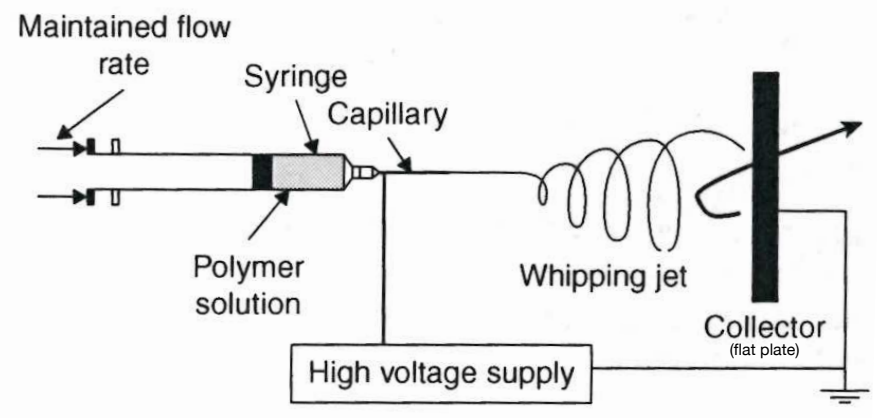


Figure 2.8: Electrospinning apparatus. A polymer solution (made up of resin and a volatile solvent) is delivered via a pump system through a syringe into an electric field. A high voltage supply creates an electric field that draws polymer fibres in a whipping jet formation towards a collector. Figure modified from Gupta et al[117].

There is particular interest in using electrospun materials to augment the surgical repair of soft tissues, such as tendons and ligaments.[98,118–120] Because of the poor outcomes associated with many soft tissue repairs, there is interest in developing electrospun materials that actively contribute to the endogenous repair process by providing physical cues for local cells to attach, proliferate, differentiate, and secrete ECM, leading to neo-tissue formation.[121,122] Aligned fibres are particularly attractive to mimic the anisotropic structure of native soft tissue ECM, which is important for approximating tendon structure and mechanical properties, but also for facilitating cell attachment and orientation along the aligned fibres.[113,118,122,123]

2.6.1.2 Electrospinning continuous filaments

So far, electrospun fibres have been predominantly collected as flat sheets by using a belt or drum collector, which restrict their ability to be processed further into structures that meet the functional demands of soft tissues. To overcome these limitations, researchers are also exploring methods to produce aligned, bundles of fibres, known as filaments. The production of filaments enables the use of textile assembly techniques to create more complex multifilament yarns. These yarns can be designed with sufficient mechanical properties to be used as sutures or scaffolds soft tissue applications, while still retaining a high porosity and large surface area to encourage cellular infiltration and cell-mediated repair.[124–127]

Several methods have been proposed to collect filaments. These are usually classified into two categories: those to collect discontinuous filaments or short strands, and those to collect continuous filaments or long, potentially uninterrupted strands. Discontinuous filaments can be collected using static or dynamic collection units, while continuous filaments are only collected using dynamic collection units. It is worth noting that static

collectors usually enable the production of meshes made of randomly oriented fibres, while dynamic collectors (such as rotating disks) can yield aligned fibres. Moreover, the production of continuous filaments implies that there is continuous uptake from the collecting unit. Various methods for collecting continuous electrospun filaments are shown in Figure 2.9.

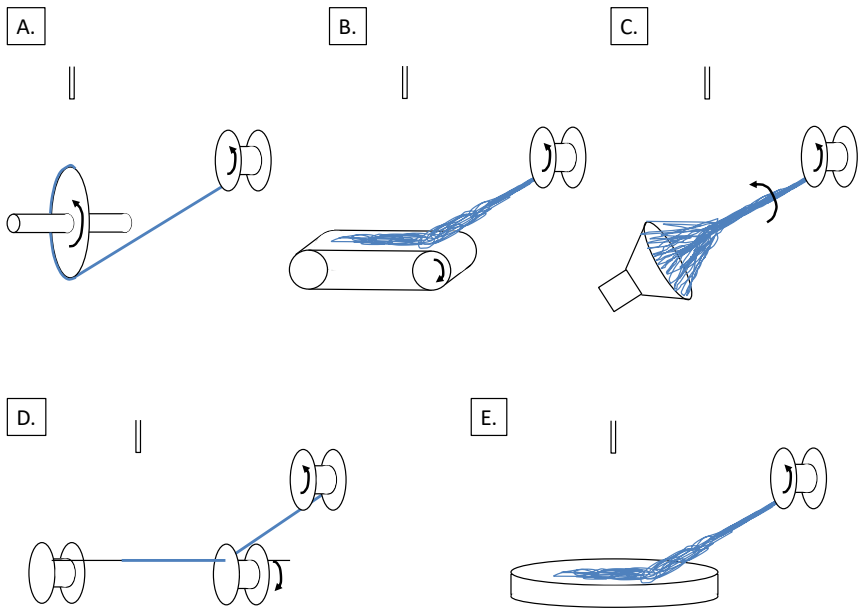


Figure 2.9: Methods for collecting continuous filaments. Uninterrupted filaments can be produced by continuously taking up the filament from the collecting surface of (A) a rotating disk or (B) a moving belt. Continuous filaments can be produced using a funnel collector, either by converging the fibres from the edge of the funnel into filaments, as shown in (C), or by converging the fibres into a filament at the base of the funnel. (D) Electrospinning on a small wire collector forces the fibres to form dense meshes that can be removed directly as a filament. (E) Meshes can also be collected on the surface of a water bath. When the bundles of fibres are lifted from the water for winding, the surface tension of the liquid bundles the fibres into continuous filaments. With permission, figure extracted from Abhari et al.[128]

The Carr group has recently developed a method for collecting continuous filaments on a moving conductive wire, as shown in Figure 2.9D.[129] This method has been used to produce unstretched filaments at a speed of about 1.6 metres/hour. Compared with filaments produced with a flat or a belt collector and subsequently rolled or twisted,

electrospinning on a small wire surface area forces the fibres to form highly interconnected meshes that can be removed directly as a filament, which is then stronger, denser, and easier to process.[130] Although this collecting method has only been optimized for one polymer, polydioxanone (PDO), so far[129], continuous filaments collected on a wire show great potential for subsequent assembly into multifilament structures using existing commercial textile machinery.

2.6.2 Melt-extrusion

Melt-extrusion is a process whereby a polymer resin is melted and the molten polymer is forced through a network of small holes (called a spinneret) at a high pressure (Figure 2.10).[131] The size of the holes influences the final diameter of the fibres. As the soft polymer emerge from the spinneret into cooler air, they harden into fibres. The fibres are collected continuously in a bundle and typically reheated as they are drawn out to create the final stretched product.

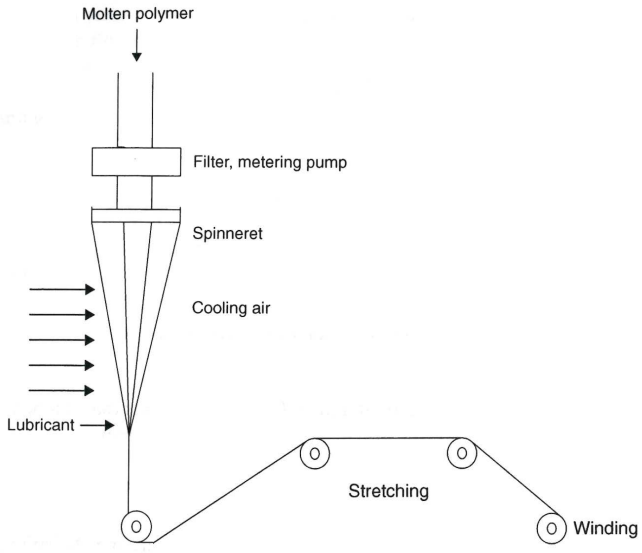


Figure 2.10: Melt-extrusion apparatus. In melt-extrusion, a raw resin is melted and forced through a spinneret under high pressure conditions. As soft fibres emerge into cooler air, they harden into fibres. A lubricant is applied in order to stretch the fibres over heated rollers before they are wound. Figure modified from Gupta et al[131].

Melt-extrusion is the primary fibre production method for commercial sutures and scaffolds. Most synthetic polymers are melt-extruded into monofilaments (a single fibre is collected through the spinneret) or multifilaments (multiple fibres are collected through the spinneret and subsequently braided or woven). Importantly for this thesis, PDO is predominantly extruded as a monofilament, due to its slow rate of crystallisation.[132] PDO has been used in surgery marketed as the suture material PDS® since 1982.[63] It is rarely used for fixation in rotator cuff, as stronger, braided sutures (such as Fibrewire and Ethibond) have become more popular. Ethicon recently released a multifilament melt-extruded PDO suture, called PDS® cord, but its structure and clinical use have not been reported to date.

In the context of developing biomaterials, melt-extrusion is less popular, compared to electrospinning. Current melt-extrusion technology is mostly not capable of producing fibres that are below 10μm, offering fewer opportunities to mimic native ECM, in particular collagen fibrils, at the nano- and microscale. However, microscale fibres offer other distinct advantages, such as their improved tensile strength, much faster production rate (on the order of 150-200 times faster), as well as being a continuous production process with fewer manual steps. Finally, there is evidence that native cells are able to attach to, and the degree of attachment, proliferation and orientation be influenced by fibres up to 10μm.[106,133,134]

2.6.3 Polydioxanone

PDO is the polymer used for both electrospinning and melt-extrusion in this thesis. The justification for choosing PDO for the work in this thesis is described in Chapter 2.10.1. PDO is a synthetic, semi-crystalline, degradable polymer made up of repeating ether-ester units, as shown in Figure 2.11. It is fabricated by the ring-opening polymerisation of the

monomer p-dioxanone and has a glass transition temperature of -10°C to 0°C and a melting point of 110°C to 115°C. These characteristics allow monofilament PDS® sutures to be manufactured via an extrusion process at the lowest possible temperature, preventing spontaneous depolymerisation.[135] This point is relevant to optimising the melt-extrusion of PDO in Chapter 4.

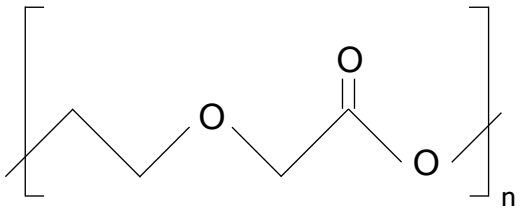


Figure 2.11: Polydioxanone chemical structure.

Degradation of PDO occurs predominantly through hydrolytic breakdown. Simply, polymer chains exist in either crystalline or amorphous states. Crystalline areas are dense, cross-linked regions, which confer strength. Amorphous areas are less organised and are the site of hydrolytic breakdown. Semi-crystalline polymers, such as PDO, consist of highly orientated folded chain crystals connected by many highly stretched tie chains in the amorphous regions separating the crystals. Hydrolytic breakdown of polymer chains disrupts these ordered sequences, leading to the break down and eventually degradation of the material.[132,136] Degradation occurs through a non-specific scission of ester bonds and PDO is either metabolised to glyoxylate and excreted through the kidneys, or is converted to glycine and then carbon dioxide and water through the citric acid cycle.[137] Its degradation rate depends largely on the porosity, crystallinity, and molecular weight of PDO.[138] Increasing the relative proportion of crystallinity in the material improves

mechanical properties and alters the degradation rate, as there are relatively fewer amorphous areas available for hydrolytic breakdown.

2.7 Filament post-processing

Although several methods have been developed to manufacture filaments, the resulting materials often lack the necessary material properties for further processing into multifilament yarns or for being used as multifilament scaffolds in tissue engineering applications (Chapter 2.10). Processing treatments, such as mechanical drawing and annealing, are often conferred as part of the filament collection process or after the filament has been spun. Drawing and annealing electrospun filaments is described, focusing on how they improve their strength, fibre alignment, degradation properties, and biocompatibility.[139–141] The use of a spin-finish is described in the context of processing melt-extruded filaments.

2.7.1 Mechanical drawing

Mechanical drawing is a processing method commonly used in textile industry whereby filaments are stretched along their longitudinal axis. Drawing electrospun filaments serves multiple purposes: it increases the strength and stiffness of the fibres, decreases the risk of plastic deformation in the stretched filament, reduces the fibre diameter, changes the pore size distribution, increases the crystallinity of the material, and aligns the fibres in the direction of the filament, which is particularly relevant in considering that degree of fibre alignment can be a biophysical cue for cells to recognise.[129,142]

Drawing techniques differ if electrospun fibres are collected as sheets or as continuous filaments. For sheets collected on a rotating device, such as a drum or disk, the mechanical drawing force can be imparted on the material as it is collected.[143,144] Optimizing the right speed at which the rotating collector will maximally draw the sheet without breaking it

requires trial and error. These drawn-out sheets are then removed from the collector and cut or rolled into filaments. Adjusting the speed of the take-up roller can change the stretch in the filament and resulting fibre alignment. As mentioned earlier, controlling fibre alignment is crucial to imitating native ECM.[119,145]

Alternatively, continuous electrospun filaments can be stretched after collection. Post-spinning stretching of electrospun filaments was first investigated by Lai et al.[146] These authors showed that stretching electrospun polyacrylonitrile filaments to between two to four times their initial lengths resulted in an improvement in filament macro-molecular orientation, crystallinity, and mechanical properties. More recently, an industrial drawing machine has been used in the Carr group to stretch the filament up to three times its initial length. In this context, industrial drawing refers to using a machine that allows for an increased scale of processing, fewer manual steps, improved consistency, and compatibility with clean room manufacturing, all of which cannot be achieved by hand drawing.

2.7.2 Annealing

Annealing, or heat treatment, is a post-spinning treatment known to change the mechanical properties of materials.[139,147,148] Heat treatment increases the crystallinity of a material by changing the relative proportion and organization of amorphous and crystalline regions. For many degradable polymers, the structural rearrangement due to annealing results in changes in fibre alignment, mechanical properties, and degradation profile.[149–153] Annealing electrospun fibres made of poly-l-lactide (PLLA)[139–141,154] and polycaprolactone (PCL)[154] led to changes in the crystalline structure and resulting improvements in their mechanical properties. However, the effects of annealing PDO have not been well characterised. Electrospun materials are commonly annealed as part of the manufacturing process; however, most existing studies have focused on the effects of annealing randomly oriented electrospun meshes.[139,144,147] Meshes are manufactured and processed differently to

continuous filaments, making their comparison difficult. The meshes are either annealed and drawn simultaneously, or drawn before heat treating, and subsequently investigated for changes in properties. More recently, annealing parameters have been explored for electrospun filaments. It is known that annealing changes the degree of crystallinity of aliphatic polyester polymer chains, which in turn affects the degradation rate of the polymer.[147] However, how annealing affects mechanical properties and degradation has not been explored for many polymers.

2.7.3 Spin-finishing

In melt-extrusion, it is common to apply a lubricant, or spin-finish, to the extruded filament after collection. This lubricant enables the mechanical drawing of the filament over heated godets, as well as controls static build up. There are oil-based and PEG-based finishes that are approved by the Food and Drug Administration (FDA) and are routinely used during suture manufacturing. Because of the proprietary nature of the medical device industry, the manufacturers do not disclose the precise formulation of their products. In preparing melt-extruded filaments for surgical suture manufacture, it is usual to remove the spin finish by scouring the sutures before terminal sterilisation. Scouring is essentially a dry-cleaning process, typically using the solvent perchloroethylene (PERC).

2.8 Textile strategies for assembling multifilament sutures

2.8.1 Textile assembly methods and their use with electrospun filaments

Textile manufacturing is an ancient human activity, with the oldest known textiles dating back to 5000 BC. Over thousands of years, textile assembly techniques, such as twisting, braiding, and weaving, have been developed and refined to make the relatively weak fibres found in nature suitable for human use. With these techniques, natural fibres (e.g., cotton) and animal fibres (e.g., wool or silk) have been processed into yarns and transformed into various items such as clothing and ropes. In the 20th century, the textile industry

underwent a major shift with the introduction of industrial machines, synthetic fibres, and the globalization of the business. In the medical market today, textile manufacturing is widely used to create dressings and wound closure devices such as sutures.

As mentioned, electrospinning is a promising biomaterial fabrication method for regenerative medicine due to its ability to fabricate submicron or nanoscale fibres that mimic native ECM. Although biologically advantageous, the submicron scale dimensions present significant mechanical and structural limitations, preventing the use of electrospun materials as surgical materials, such as sutures, stents, or drug-delivery devices. However, it is projected that textile manufacturing techniques could be used to assemble electrospun filaments into robust multifilament yarns with suitable properties for surgical use. The three most common textile techniques are shown in Figure 2.12 and their potential for use with electrospun filaments are outlined in Table 2.2. In the context of tendon repair, multifilament yarns present an exciting opportunity to design devices that can mimic the hierarchical structure and mechanical behaviour of the target tissue. In particular, tendons possess distinctly anisotropic characteristics that can be engineered by means of innovative machinery and methods.[155] In the following section, twisting, braiding, and weaving technologies are described, as they show particular promise for assembling electrospun filaments into three-dimensional multifilament yarns.

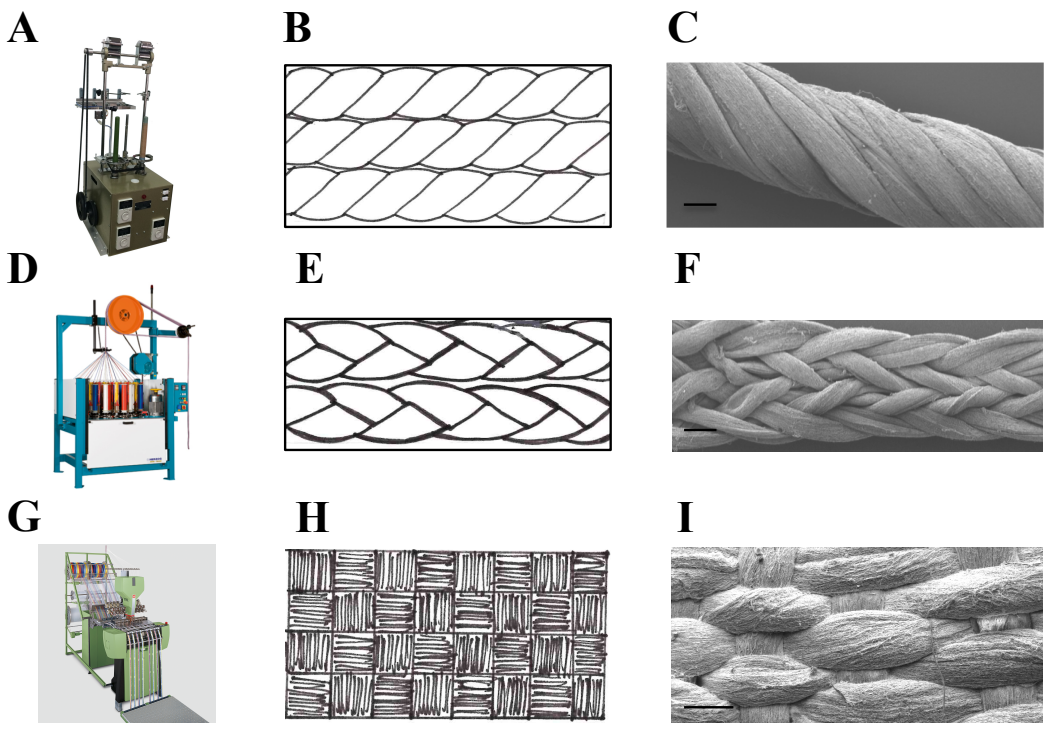


Figure 2.12: Textile assembly methods for electrospun filaments. (A) Industrial twisting machine (Mini Twister AMT 2S-Marui Textile Machinery Co. Ltd.)[156]; (B) Twist neutral yarn formed by twisting in the S and Z directions; (C) Twisted electrospun yarn; (D) Industrial braiding machine (HERZOG Braiding Machine SENG 1/32-160)[157]; (E) Braided yarn formed by intertwining three or more strands of material; (F) Braided electrospun yarn; (G) Industrial weaving machine (Narrow Fabric Loom NH2 53 4/66 - Jakob Mueller AG)[158]; (H) Woven yarn formed by interlacing two distinct sets of warps or wefts at right angles; (I) Woven electrospun yarn. Scale bars are 100μm. With permission, figure extracted from Abhari et al.[128]

Table 2.2: Comparison of textile methods for electrospun filaments. Textile assembly methods are ranked in terms of the ease of machine setup, control of structural parameters, and ability to minimize material waste during production. The scale of assembly that has been achieved with electrospun filaments is also indicated. With permission, table extracted from Abhari et al.[128]

	Ease of setup	Control of structural parameters	Ability to minimize material waste	Scale of assembly	References
Twisting	+++	+	+++	Hand-twisted/ Manual twisting machine	110,130,131
Braiding	++	+++	++	Hand-braided/ Manual braiding machine	126,133,148,161–165
Weaving	+	++	+	Manual loom	133,166,167

2.8.1.1 Twisting

Twisting is a simple way to assemble material into a yarn by combining multiple filaments twisted to the right, described as Z twist, or to the left, described as S twist. The convention is to use S twist first and then to apply a twist in the Z direction to end up with a stable, or twist neutral, yarn. For a given material there is an optimal twist level to improve mechanical properties of the yarn and limit inter-fibre friction.[168] Twisted textiles are not common in the medical textile industry, likely due to twisted yarns exhibiting more fraying and limited to less control over structural parameters, compared to braiding or weaving. For medical textiles in the research and development (R&D) phase, twisting is appealing because of its simplicity and little waste produced during production. Besides affecting the mechanical properties, twist level affects the final yarn diameter, tightness, and the orientation of the fibres. Tightness is especially important considering the yarn's regenerative potential. A yarn that is too tight (high twist number) would prevent cellular infiltration into the material, preventing the material from effectively biologically augmenting the repair. This phenomenon has been illustrated with multifilaments made from both discontinuous[160] and continuous[129,159] yarns.

2.8.1.2 Weaving

Plain weaving is a textile technique in which two distinct sets of warps or wefts are interlaced at right angles to form a fabric with controlled strength, porosity, morphology, and geometry.[169] Many woven medical textiles, such as arterial and stent grafts, usually have a plain weave structure. Weaving electrospun filaments poses some challenges, due to the difficulty in producing continuous electrospun filaments for industrial weaving machines. Furthermore, weaving machines are designed for more robust, stronger material than the relatively delicate electrospun filaments. Perhaps the most relevant use of weaving is with multifilament braided or twisted yarns for soft tissue repair.[123,133,166,167] With the

development of more sensitive weaving machines and the automated production of continuous filaments, twisted or braided electrospun yarns could be used to weave tightly bound, stronger structures with macroscale pores.

2.8.1.3 Braiding

Braids are formed by intertwining three or more strands of material, creating a long and narrow structure by zigzagging each strand through the overlapping mass of the others. While some efforts have been made to hand-braid filaments for research, it is more difficult to control braiding parameters, such as braid angle and tightness with hand-braided yarns. Industrial braiding machines allows for the production of yarn with consistent and tunable properties by adjusting the orientation of fibres, pore structure, density, and distribution of fibres, by means of number of bobbins, yarn count, braid angle, and inlay yarns.[155] Furthermore, for industrial medical device manufacturing, braiding is a reproducible and cost-effective technique with minimal material loss. Braiding offers some advantages over twisting for the development of electrospun multifilament yarns, such as reduced fraying of the final yarn, better control over porosity and pore size, and a slight improvement in mechanical strength. It is also easier to upscale the production of braided yarns, as braiding machines are already used to produce numerous medical textiles, most notably sutures and stents.

Braiding machines range in size and complexity from machines used to produce the finest surgical suture to bigger machines with hundreds of strands of material used for stent and catheter manufacturing. Despite the range of machines that are available, braiding electrospun filaments by machine is not common, as industrial textile machines require continuous uniform filaments—a target that has not been achieved with many polymers or electrospinning setups. Hu et al. produced braided electrospun yarns from filaments collected with a rotating disk.[133,165,170] While there was indication that a braiding machine

was used for yarn production, no details about the braid parameters or resulting braid characteristics were given. To date, braiding electrospun filaments into yarns been limited to short hand-braided yarns.[126,133,148,161–163] Scaling up production to an industrial braiding machine that can support electrospun filaments has not been explored yet but represents the next step in manufacturing braided electrospun yarns with tunable mechanical and structural properties for medical use.

2.8.2 Properties of multifilament yarns

2.8.2.1 Mechanical properties

Most research on multifilament electrospun yarns has focused on the influence of the electrospinning setup on certain mechanical properties, such as elastic modulus and ultimate stress, of short sections of twisted yarns, as manually twisted yarns can be easily made from both continuous and discontinuous filaments.[160,161,168,171–173] The influence of multifilament assembly, such as twist angle or yarn tightness, on the yarn's mechanical properties has not been fully explored. As with any multifilament yarn, uniform filament production, filament diameter, and yarn twist level are important factors for determining the mechanical properties of the twisted yarn.[174] However, in contrast to industrial textile yarns, it is not fully established how these three factors interact for yarns made up of filaments with submicron or nanoscale fibres.

There has been limited work characterising the effect of braiding or weaving parameters on mechanical properties of multifilament electrospun yarns. Czaplewski et al. explored the effect of braid angle on mechanical properties of hand-braided PLLA yarns with filaments collected on a rotating drum.[163] They found that braids with larger braid angles had a higher ultimate and yield stress, but a lower yield strain. The authors postulated this was because braids with larger braid angles have filaments more closely aligned with the

longitudinal axis of the braid, making the yarn stiffer in the direction of the applied force. In contrast, yarns with smaller braid angles have filaments that must move further to become aligned in the direction of applied force, increasing yield strain. Together, the results showed that mechanical properties of yarns could be altered by varying braid angle.[163]

2.8.2.2 Porosity

The porosity of electrospun multifilament yarns can be examined on three scales: the macroscopic level (1mm upward), the mesoscopic level (1mm–100μm), and the microscopic level (<100μm).[155] A common concern with aligned electrospun material is that the densely arranged architecture of fibres and microscopic pores between fibres could hinder three-dimensional cellular integration with the host tissue after implantation, which is crucial for the implant's regenerative potential.[175] In this section, the yarn's mesoscale structural elements, such as tightness of twists or braid angle, and effect on porosity and cellular attachment and infiltration, are considered.

By fabricating densely packed filaments and assembling them with textile techniques into multifilament yarns with larger mesoscopic pores, infiltration of cells too big to fit in micropores between fibres can be improved. Some groups have examined cellular infiltration in porous twisted electrospun material, however, only work with twisted monofilaments has been published so far.[98,118,176] The authors observed no cellular infiltration into the centre of the yarn, likely because the diameter of the cells was larger than the pores between the fibres. This conclusion supports the hypothesis that developing yarns with mesoscale pore sizes could improve cellular infiltration into the centre of the material. Although microscopic pores are shown to improve fibroblast adhesion[177,178], mesoscopic pores have been shown to improve the mass transport of nutrients, and

increases fibroblast proliferation, migration, and infiltration.[179–181] In previous work, the Carr group observed that the tightness of multifilament twist affected cell infiltration *in vivo* at 1 month in an ovine model, likely due to altered pore size and shape distribution with different twist ratios. Similar results have been shown by Bosworth et al. *in vitro*, albeit only with twisted monofilaments.[118]

The influence of braided or woven yarn structure on cellular infiltration has not been well explored. Czaplewski et al. hand-braided yarns with various braid angles and found that looser (more porous) braids better supported the expression of tendon- and ligament-associated markers and induced elongated cell morphology similar to tendon and ligament fibroblasts.[163] Although weaving is the most flexible textile technique to create macroscale or mesoscale pores, few studies have used electrospun filaments to create porous woven structures.[167]

2.9 Electrospun sutures currently in development

2.9.1 General tendon and ligament repair

Electrospun filaments have been used for tendon and ligament tissue engineering because of their high surface area, tunable porosity, and ability to control fibre diameter, morphology, and orientation. Filaments have been twisted, braided, and woven, to create multifilament scaffolds that mimic both the hierarchical architecture of collagen fibres and the mechanical properties of these tissues.[106,126,148,163,182] Rothrauff et al. produced braided and multilayered stacked electrospun scaffolds intended for tendon and ligament tissue regeneration.[126] While both scaffolds supported the expression of tenogenic markers, the effect was greater on braided scaffolds, confirming the importance of the macro-scale architecture in modulating nano- and microscale cues.[126]

Barber et al. fabricated PLA yarns with different braiding configurations as potential scaffolds for tendon and ligament engineering[148] The authors noted that human mesenchymal stem cells (hMSCs) adhered, proliferated, aligned parallel to the length of the fibres, and induced an upregulation in the expression of key pluripotency genes. When cultured in the presence of tenogenic growth factors and stimulated in a bioreactor with cyclic tensile strain, hMSCs differentiated into the tenogenic lineage, evidenced by the significant upregulation of Scleraxis gene expression. The authors concluded that braided PLA yarns were capable of supporting both stem cell expansion and differentiation for use as scaffolds for tendon and ligament tissue engineering applications.[148]

Finally, Czaplewski et al. fabricated braided electrospun yarns and investigated the role of fibre chemistry and braiding angle on mechanical properties and tenogenic differentiation of human-induced pluripotent stem cells (iPSCs) seeded on yarns subjected to cyclic tensile stimulation.[163] It was found that PLLA braids supported the highest adhesion, compared to PCL braids, when controlling for other properties. This result indicated that fibre chemistry played a significant role in cell adhesion, while braid angle had a larger effect on mechanical properties and regulated cell response. Larger braid angles (looser braids) supported expression of tendon- and ligament-associated markers, such as an upregulation of tenomodulin and a higher collagen I to collagen III ratio, and induced elongated cell morphologies with a similar phenotype to tendon and ligament fibroblasts. The authors concluded that loose PLLAs braids in combination with human iPSCs and cyclic strain can be used as scaffolds to support tendon and ligament tissue engineering and that braid tightness had more of an impact on human iPSC differentiation than submicron fibre chemistry.[163]

2.9.2 Rotator cuff

To improve the high failure rate associated with rotator cuff repairs, tissue engineers have explored developing electrospun sutures that provide mechanical support to the repair site and also to provide an appropriate biological environment to promote cell-directed repair.[98,126,129,148] Electrospun filaments that are twisted, braided, or woven can create a more robust and stronger suture with tunable structural properties, compared to electrospun sheets.

In recent work, Mouthuy et al fabricated twisted PDO electrospun sutures, and studied the morphology, adhesion, and proliferation of tendon fibroblasts cultured on the yarns *in vitro* and tested the safety of the material *in vivo*.[129] Tendon fibroblasts were collected from patients with chronic degenerative rotator cuff tendinopathy and partial or full thickness supraspinatus tendon tears. Compared to clinically used PDS, there was a significantly higher initial cell attachment and improved cell alignment on the electrospun yarn. A safety evaluation carried out in a rodent infraspinatus model showed that electrospun yarns improved cell proliferation and infiltration and were safe for implantation. These results are consistent with previous studies investigating monofilament twisted electrospun material.[98,118,148]

2.9.3 Other soft tissue applications

Aside from tendon and ligament applications, using electrospinning has been explored to create novel sutures and scaffolds for other specific tissue applications, most notably for cardiac[133,166] and bone[124] tissue engineering. Hu et al. published a series of studies on the development of braided drug-loaded yarns and their potential for use as a suture material.[164,183] In early work, the authors developed a method to collect PLLA filaments on a rotating disk and subsequently used a minitype braiding machine with eight carriers to fabricate a braided yarn with a diameter of 0.35mm. In order to investigate its potential as

a suture material, the authors applied a chitosan coating to smooth the surface and to minimize bacterial colonization, and performed *in vivo* tests to evaluate suture knotting and suturing properties.[165] The authors found that coating the suture with chitosan improved its blood compatibility, as well as platelet and erythrocyte aggregation.

The potential for using electrospun yarns as scaffolds has also been investigated for cardiac tissue engineering.[133,166] Wu et al. fabricated continuous electrospun filaments and created electrospun yarns using braiding and knitting.[133] The authors also integrated a multifilament woven scaffold with a hydrogel as a composite scaffold for heart valve engineering. The authors reported that human adipose-derived stem cells cultured on braided, woven, or knitted yarns aligned along fibre direction and were >90% viable over 21 days. Furthermore, the yarns supported biochemical induction of stem cell differentiation toward smooth muscle and osteogenic lineages. Using this method, the authors believe that multifilament scaffolds with anisotropic properties and an ECM-like vale has potential for heart valve tissue engineering.[133]

2.10 Development and justification of suture specifications in this thesis

The main objective of this thesis is to fabricate an augmentation suture, which can act as a biological scaffold for rotator cuff repair, but also mechanically support the construct. To enable this, decisions had to be made about the choice of polymer, fibre production method, specifications and design criteria for the suture, as well as appropriate controls for the mechanical tests and cell biology experiments. This section provides justifications for these choices made in this thesis.

2.10.1 Justification for polydioxanone as the base polymer

Polydioxanone was the polymer used for all of the electrospinning and melt-extrusion work done in this thesis. The main priorities in choosing a polymer were that is synthetic

and degradable, with a long-term clinical evidence of safety and efficacy in medical devices. There are four main polymers that fit these criteria: PCL, PGA, PDO, and PLA.

Because the aim of this thesis is to develop a suture prototype that can be tested in preclinical trials, it was decided that medical grade polymer, which is required for preclinical and clinical trials, would be used for this thesis. What classifies a polymer as medical grade does not have a strict definition, but most often means that polymers have a certification that they were tested for biocompatibility.[184] Previous experience in the Carr group developing an electrospun scaffold (BioPatch) for rotator cuff repair performed all *in vitro* and *in vivo* experiments with chemical grade PDO. Upon moving to medical grade PDO to fabricate samples for clinical trials, there were substantial changes to fibre properties and many tests had to be repeated. Further work in the Carr group compared PDO from different suppliers and noted substantial differences in conductivity and viscosity between different polymer solutions, which influenced electrospinning parameters and fibre properties.[107]

PDO was ultimately chosen because of its good safety profile for use in medical devices, its relatively prolonged absorption duration (182-238 days) compared to PCL or PLA, and importantly, the availability of medical polymer over this four year project, and experience in the Carr group of working with this polymer.[185] The Carr group has been using PDO to electrospin fibres since 2013, to fabricate two scaffolds for rotator cuff repair: BioPatch[186] and BioYarn[129]. As a result, substantial expertise and encouraging results had been collected using PDO.

The main disadvantages of using PDO were that it has a slower crystallisation rate compared to PCL or PLA, making melt-extrusion more challenging and that it is less commonly used in electrospinning compared to PCL, which made it more difficult to draw

comparisons to other research. Although PDO devices are widely used with very few adverse immunological events, there has been some concern about the effect of PDO acidic degradation products in the body.[187] However, this potential problem would be true for all of the semi-crystalline synthetic polymers considered for this work. An summary of the factors considered in choosing PDO for this thesis is given in Table 2.3.

Table 2.3: Factors considered in choosing PDO for the work in this thesis.

Factors considered in choosing PDO	Details
Safety	PDO has evidence of safety in medical devices for 40 years. There have been since been no product recalls in the FDA and a very low percentage of adverse reactions from the use of PDO implants.[185]
Degradation timeframe	PDO has a prolonged degradation timeline (182-238 days) compared to other synthetic polymers.[132] Tendon heals slowly and structural support would be needed for at least 6 months.[43]
Availability	Medical grade PDO was continuously available for this four year project.
Used for melt-extrusion and electrospinning	There are 47 different PDO medical devices which have gained FDA approval, most of which are sutures manufactured by melt-extrusion.[185] There is also substantial literature about electrospun PDO fibres,[115,188] although no electrospun PDO-based device is currently on the market.
Expertise in electrospinning PDO	PDO has been used for electrospinning in the Carr group since 2013. Two PDO-based products, BioPatch and BioYarn, have undergone years of *in vitro* and preclinical testing with no adverse outcomes.
Synthetic polymer	Synthetic polymers (like PDO), have evidence of fewer foreign body and inflammatory reactions, as well as a more uniform chemical composition, compared to natural polymers (like silk).[189,190]

2.10.2 Justification for using electrospinning to fabricate submicron fibres

There are many biomaterial fabrication methods that allow tuning of biophysical cues, such as molecular self-assembly, freeze drying, phase separation, 3D printing, and electrospinning. The main reason that electrospinning was chosen for this thesis is that this project built upon previous work in Carr group developing an electrospun suture for rotator cuff repair (BioYarn project). Moreover, in the context of biomaterials for tendon repair, there have been numerous reports in the literature showing promising results using electrospinning.[107] A detailed justification for choosing electrospinning for the work in this thesis is presented in Table 2.4, along with the advantages and disadvantages of this fabrication method.

Table 2.4: Advantages and disadvantages of using electrospinning as the main fibre production method for this thesis, presented in order of importance.

Electrospinning biomaterials	
Advantages	Disadvantages
Fibre morphology is similar and scalable over the range of ECM diameters. Fibre diameter can range from 300nm to 4000nm.[107]	Low production rate and historically difficult to upscale compared to other fibre production methods.[107]
Expertise in Carr group and Oxford University. The Carr group has been working on electrospun materials since 2013 and numerous other groups at the University of Oxford use electrospinning for research (Biomedical Engineering and Engineering departments).	Relatively poor tensile strength compared to extruded fibres.[59]
Resources in the Carr group. Available IME technologies electrospinning machine for sheet production and self-made glovebox for filament production.	Complexity and huge range of electrospun materials require a high-throughput strategy and better understanding of cell-matrix interactions to guide material development.

Fabrication of continuous filaments, which allows for easier upscaling and textile assembly.[129]	Little evidence of use in existing medical devices.[92]
Supportive literature on electrospun fibres for tendon regeneration.[98,99,148,191]	Costly and time-consuming to take novel biomaterials through regulatory process. Most electrospun biomaterials classify as high risk medical devices (further discussed in Chapter 6).
Potential for surface functionalization, pharmaceutical, or cell addition.	

2.10.3 Suture design criteria and their development

This section outlines ideal suture properties for augmenting tendon repair based on available evidence, followed by outlining the target design criteria for the suture in this thesis and the development of these criteria. These targets were developed based on best available evidence in the literature and clinical trials, as well as in consultation with bioengineers at the Nuffield Department of Orthopaedics, Rheumatology, and Musculoskeletal Sciences and shoulder surgeons at the Nuffield Orthopaedic Centre (NOC). In particular, the requirements for bioactivity, mechanical support, and degradability were developed by surveying the literature and in consultation with bioengineers with experience in developing bioactive devices for tendon. Requirements for safety and scalability were developed in consultation with regulatory advisors at the Botnar Research Centre and in compliance with regulatory and International Organisation of Standardization (ISO) standards, in particular ISO 13485.[192] Requirements for suture usability were developed in consultation with shoulder surgeons at the NOC and by surveying the literature for compatibility with surgical equipment for rotator cuff repair.

2.10.3.1 Development of target design criteria for the suture in this thesis

1. Safety

First, any implantable device must be safe. A polymer should be chosen that minimises the chance of negative foreign body or immune reaction and has a history of safe implantation in humans.

Polydioxanone, a synthetic semi-crystalline polymer will be used for electrospinning and melt-extrusion in this thesis. Polydioxanone is biocompatible polymer with a suitable degradation timeline for this application and has been used safely in medical devices for over 40 years. A detailed justification for choosing polydioxanone is described in Chapter 2.10.1.

2. Bioactivity

A bioactive suture will be biologically active compared to currently used sutures. This bioactivity will promote cell responses conductive to tendon healing, such as cell attachment, proliferation, orientation, and upregulation of key tendon ECM genes. There are many ways to influence cell activity through biophysical cues (covered in Chapter 2.5.1), but this work builds upon previous work focusing on fibre diameter as a biophysical cue to influence cell attachment and proliferation.[129] Mimicking the submicron architecture of the tendon matrix has been shown to influence protein adsorption and cell behaviour conductive to tendon healing.[98,148,163] Moreover, suture porosity is an important factor that determines the extent of cell infiltration and integration within the biomaterial. Pore size and fibre diameter are strongly correlated: reducing fibre diameter decreases the pore sizes between the fibres, which can hinder cell infiltration or migration.[193,194] Ideally, a bioactive suture would be made up of nano- or microscale fibre diameters to influence cell

attachment, differentiation, and proliferation, but with macroscale pores (>10μm) to encourage integration of the biomaterial with the host tissue.[193]

For the work in this thesis, the fibre diameter of electrospun fibres should be <1μm to mimic collagen fibril diameters. The fibre diameter of melt-extruded fibres should be 10μm, which, although not on the same scale as smaller ECM components, are potentially advantageous to use in combination with electrospun fibres because they are stronger and have larger pore sizes. The pore sizes of the suture should be greater than 10μm in order to encourage cell integration with the suture and bioactive sutures should be more porous than currently used devices. Finally, because it is hypothesized that the bioactive electrospun component of the suture will promote a stronger cell response conductive to tendon healing and degrade at a faster rate, the electrospun component should be on the outside of the suture.

3. Mechanical support

Optimising the mechanical properties of a suture for tendon repair is difficult, because healthy and diseased rotator cuff tendon tissue have not been well characterised.[76] Clinical evidence suggests that variation in rotator cuff tendon properties and surgical repair outcomes are predominantly driven by the progression of tendon disease, the age of the patient, and the size of the tear.[2,43,76] Currently used sutures are not an ideal example for mimicking mechanical properties, because they are repurposed from use in other tissues and are not designed for the highly specialised tendon matrix. An idea of mechanical properties that will support tendon can be guided by benchtop biomechanical studies, as well as looking at the properties of currently used materials for tendon repair and their successes.

In this thesis, the mechanical property targets focused on force at failure and strain at break, because they represent basic requirements needed to make an electrospun material usable as a suture. The strain at break was set between 25-40% because this represents the strain range of most currently used sutures for rotator cuff repair. The force at break target was set to 50-100N. Although this is lower than most commercially used sutures, pilot work showed that electrospun sutures that failed at forces higher than 100N were too bulky for surgical use. Moreover, early work with orthopaedic surgeons at the NOC showed that sutures that failed at lower than 50N were potentially too weak to be used surgically.

4. Degradability

Any absorbable suture should degrade at a rate that matches the formation of new tissue. In the context of tendon repair, tendons are slow healing tissues and support from the suture would be needed for at least 3-6 months and should fully degrade by 1 year.[195] Degradation products should be non-toxic to the local cell population and not induce an immune reaction themselves.

This bioactive suture should retain 70% of tensile strength after 6 weeks and should fully degrade by 1 year. It is not known how long mechanical support from the suture is needed before new tissue can support the construct, but it has been shown that there is evidence of matrix deposition and tissue formation in and around the suture as early as 6 weeks after repair.[196]

5. Usability

Usability refers to the ease of handling by surgeons and the suture's compatibility with surgical equipment for rotator cuff repair. Ease of handling will likely be related to the

diameter of the suture, the memory (ability to return to its previous shape after deformation), and the tensile strength and strain. The suture should be strong enough to knot and approximate tissue and have an appropriate strain to prevent gap formation. Usability can be quantified by interviewing rotator cuff surgeons and surveying the literature for currently used devices and their handling success.

In the context of this bioactive suture for rotator cuff repair, the suture diameter should be between 0.4-0.7mm. This represents a suture size between USP 2-0 to 4 and sutures outside of the given range have suboptimal handling properties for rotator cuff repair and are not compatible with current surgical equipment, such as the Versalok® suture anchor.[197]

6. Scalability

The suture production processes need to be scalable to meet regulatory requirements and GMP/GLP compliance, which is the quality control of product and test facility, further discussed in Chapter 6. In the context of this thesis, a scalable process refers to increasing the volume of product, decreasing production time, and decreasing manual steps in the production pipeline. Although preclinical testing for this device would be years away, adapting the production line to be as scalable as possible at this point, will prevent serious changes to production in the future.

In this thesis, there will be three steps taken to upscale the suture manufacturing process. First, electrospun filaments will be fabricated in a clean room. Clean room manufacturing will enable production in a GLP compliant facility with fewer manual steps. Second, melt-extruded fibres will be fabricated using industrial extrusion facilities. Finally, an industrial braiding machine will be used to fabricate hybrid sutures. Melt-extrusion and braiding are the most commonly used manufacturing techniques for suture production. As a result, these processes can be easily incorporated into the suture production pipeline.

Table 2.5: Target design criteria for the bioactive suture developed in this thesis.

Design criteria	Reasoning	Accepted criteria and justification
Safety	Polymer must have evidence of long-term safe implantation in humans.	Polydioxanone, a synthetic semi-crystalline polymer will be used for electrospinning and melt-extrusion. The justification for choosing PDO is described in Chapter 2.10.1.
Bioactivity	Fibre diameter and porosity are important biophysical cues to influence cell attachment and behaviour.	Fibre diameter of the electrospun fibres should be <1μm. Fibre diameter of melt-extruded fibres should be 10μm. Pore sizes should be greater than 10μm in order to facilitate cell infiltration. The bioactive electrospun component should be on the outside of the suture and in contact with the biological milieu.
Mechanical properties	Force at failure and strain at break are important material properties to evaluate if electrospun material can be used as a suture.	The force at failure should be between 50-100N, because this represents a range that is achievable with electrospun materials and high enough to be used as a suture. The strain at break between 25-40% because this represents the strain range of most currently used sutures for rotator cuff repair.
Degradability	After rotator cuff repair, patients are immobile for 6 weeks and mostly healed 6-12 months after repair.[2]	The suture should retain 70% of tensile strength after 6 weeks and should fully degrade by 1 year. It has been shown that there is evidence of matrix deposition and tissue formation in and around the suture as early as 6 weeks after repair.[196]
Usability	Suture diameter used for rotator cuff repair: USP 2-0 to 4.	Final suture diameter should be between 0.4-0.7mm. Sutures outside of the given range have suboptimal handling properties for rotator cuff repair and are not compatible with current surgical equipment, such as the Versalok suture anchor.[197]
Scalability	Suture manufacturing processes should have a high production capacity with as few manual steps as possible.	Electrospun filaments will be fabricated in a GLP compliant clean room. Melt-extruded fibres will be fabricated using industrial extrusion facilities. An industrial braiding machine will be used to fabricate hybrid sutures. Melt-extrusion and braiding are the most commonly used manufacturing techniques for suture production. As a result, these processes can be easily incorporated into the existing suture production pipeline.

2.10.4 PDS and Vicryl as control sutures

PDS® and Vicryl® are commonly used sutures and were chosen as the control materials for the mechanical tests in chapter 4 and the cell biology tests in chapter 5. PDS is a degradable monofilament made from polydioxanone, Vicryl is a degradable multifilament made from a copolymer of 90% glycolide and 10% L-lactide.[198,199] Although Fiberwire and Ethibond are the most commonly used sutures for rotator cuff repair, they were not used as controls. The main reason for this is that the suture developed in this thesis is intended to be used differently to how Fiberwire and Ethibond are used. Fiberwire and Ethibond are non-absorbable sutures, made of polyethylene and polyester, respectively, which solely act to mechanically approximate tendon tissue and minimise a host immunological response. The suture developed in this thesis has a different purpose: its main aim is to provide a biological scaffold upon which cells can adhere and proliferate. In addition, it is highly likely that this suture will be used in combination with scaffolds for rotator cuff repair, or even in combination with conventional sutures, like Fiberwire and Ethibond, to provide additional mechanical support. Because of these differences in utility, Ethibond and Fiberwire were not used as controls, but future work should consider how the mechanical properties and cell-material interactions compare between these suture types.

Because all of the material fabrication in this thesis was done using PDO, it was more scientifically interesting and relevant to compare this suture to PDS®, a polydioxanone monofilament melt-extruded suture that is already frequently used in surgery. Finally, Vicryl was used as the multifilament suture control, because it was easily available (whereas Fiberwire and Ethibond were not), less expensive, and frequently used in the literature as a control for electrospun materials.[129,200,201]

2.11 Summary

Rotator cuff tendinopathy is a significant societal and economic burden. The structure of tendon tissue is highly specialised and its hierarchical architecture is important for its function. In tendinopathy, this structure is disrupted, often leading to rotator cuff tears. There are significant unmet challenges in restoring function and mobility in patients with rotator cuff tears, due to the tendon's poor ability to heal and an incompatibility between surgical materials and the tissues they seek to replace. Currently 40% of rotator cuff repairs fail within 12 months. Better rotator cuff strategies are needed for people with tears to lead a pain free and independent life.

There is increasing interest in developing surgical materials that actively contribute to guiding tissue repair. Currently, sutures for rotator cuff tendon repair are biologically inactive materials adapted from use in other clinical applications. Low success rates indicate that this repair strategy is ineffective. The tendon does not heal through the formation of specialised ECM; instead, scar tissue is formed, which is not mechanically robust, leading to re-tear and treatment failure. Indeed, sutures cheese-wiring through tendon tissue is the most common mode of rotator cuff repair failure. One strategy being explored to improve repair outcomes focuses on tendon healing and developing biomaterials that can promote a local cell response that is conductive to tendon healing. In particular, sutures that can act as biological scaffolds for tendon tissue and also mechanically support the tissue are being considered as novel treatment options and are the focus on this thesis.

Electrospinning was introduced as a potentially reliable and reproducible method to develop sutures to augment tendon repair. These novel sutures are intended to be used instead of, or in combination with, conventional sutures in tendon repair.

Electrospun sutures, made up of submicron and nanofibres provide a microenvironment which can influence local cell behaviour. In spite of their biological potential, upscaling, structural, and mechanical limitations of electrospun fibres have been limiting factors in translating these materials for use in surgery. This chapter discussed electrospun filament post-processing and the possibility of adding supporting melt-extruded fibres as methods to overcome these limitations. While electrospun-based sutures hold promise for improving soft tissue repairs, they will also increase the regulatory burden, cost and required clinical evaluation to ensure that they are safe and effective.

Chapter 3

Fabrication of polydioxanone filaments

3.1 Abstract

3.1.1 Background

Novel electrospun-based sutures could improve tendon repair outcomes, as they are the main surgical material used to reattach torn tendons. However, the tensile strength of electrospun filaments is too low for them to be used clinically. It is hypothesized that annealing can be used to improve electrospun filament mechanical properties. It is also hypothesized that adding another, stronger material in combination with electrospun fibres will enable its utility as an augmentation suture. This chapter investigates the fabrication of filaments with target fibre diameters, using both electrospinning and melt-extrusion techniques.

3.1.2 Materials and methods

Both electrospun filaments and melt-extruded yarns were fabricated using the same medical grade PDO. Electrospun fibres were fabricated with a target <1μm diameter to replicate biophysical cues found in native ECM to favourably drive cell attachment. Annealing electrospun filaments at various times and temperatures was explored to improve their tensile strength. Systematic characterisation of melt-extrusion parameters was investigated to produce target 10μm diameter melt-extruded fibres to provide mechanical support. Electrospun and extruded materials were compared in terms of their tensile properties, porosity using Hg porosimetry, thermal properties using DSC, and *in vitro* degradation.

3.1.3 Results

Continuous electrospinning and melt-extrusion was possible and target fibre diameters of <1μm and 10μm, respectively, were met. Within the parameters tested, changing annealing temperature resulted in larger changes to filament properties than changing annealing time. Annealing at 85°C had detrimental effects on fibre properties, whereas annealing at 65°C and 75°C resulted in an increase in stress at failure at shorter annealing times. Annealing at 65°C for 3 hours minimally improved stress, but substantially slowed the degradation rate compared to not annealing. Electrospun filaments and melt-extruded yarns had similar overall diameters, but marked differences in their mechanical properties and porosity. Melt-extruded yarns were 2 times stiffer with a 11.5-fold increase in force at failure. Electrospun filaments were 20% more porous and had a faster degradation rate.

3.1.4 Conclusions

Electrospinning and melt-extrusion enables consistent fabrication of fibres with target diameters. For PDO electrospun filaments, annealing is more useful to tailor degradation rate than it is to improve mechanical properties of pristine fibres. Extruded fibres have higher tensile strength and are likely to mechanically support tendon repair. It is hoped that combining these materials to produce a hybrid device with an electrospun and extruded component, can be a method to biologically and mechanically support tendon repair.

3.2 Introduction

For torn tissues with a poor intrinsic healing capacity, it is suggested that biomaterials could be used to guide tissue repair. In particular, medical filaments made up of nano- or submicron scale fibres are of interest, due to their ability to imitate native ECM and be assembled into multifilaments to meet the demands of native tissue. Most spinning techniques for fabricating filaments are fundamentally based on the extrusion of a polymer solution that is then acted upon by shear forces to convert a solution of molten polymer to a network of fibres that are organised on the molecular, nano-, and microscale.[106] However, significant mechanical and structural limitations have prevented the implementation of spun filaments in biomedical applications. In this chapter, the polymer PDO is used to fabricate filaments with target fibre diameters using both electrospinning and melt-extrusion techniques. Electrospun and melt-extruded materials will be combined to form a hybrid suture with improved mechanical properties in Chapter 4 and with biophysical properties to influence tendon cell biology, presented in Chapter 5.

Electrospinning, a process where fibres are drawn out from a polymer solution using electrical charges, is one of the most popular biomaterial fabrication techniques, due to its easy manipulation of key biophysical parameters, such as fibre diameter and alignment.[202] The main focus in electrospinning research has been on producing nano- or submicron scale fibres, due to their semblance to building blocks of native ECM. For tendon applications, electrospun fibres are fabricated at submicron diameters to imitate collagen fibrils and promote fibroblast attachment, proliferation, and a phenotype similar to what is seen in native tissue.[122,191,203] One of the objectives of this chapter, therefore, was to fabricate continuous electrospun filaments made up of fibres with submicron diameters. A detailed description of the electrospinning process is described in Appendix A but is covered briefly here. Importantly, the balance between the electrostatic force and surface tension of the polymer is crucial for electrospinning stability. When the surface tension of

a polymer solution is balanced with an applied electrostatic force, then polymer chains can form appropriately to allow for a stable jet and continuous electrospun fibres deposited on the collector. There are many electrospinning variables that can be manipulated to change electrospinning behaviour and resulting fibre topography, alignment, and diameter. There is considerable debate in the literature on how to group electrospinning variables, but for the purposes of this thesis, they will be divided into system parameters, which cannot be changed once electrospinning has begun, and process parameters, which can be tuned during the electrospinning process (Table 3.1). More detailed information about how each parameter affects electrospinning can be found in the references in Table 3.1, but the parameters that were controlled and optimised in this thesis are bolded and further discussed in the methods section of this chapter. It is important to note that the objectives for electrospinning in this thesis were not to investigate every electrospinning parameter, but instead to focus on achieving continuous filaments with submicron fibre diameters. As a result, only factors that were thought to enable consistent electrospinning, like temperature control, or enable control of fibre diameter, like the addition of pyridine, were investigated.

Table 3.1: Parameters modulated in electrospinning to affect fibre diameter, alignment, and topography. System parameters cannot be changed once electrospinning has begun, whereas process parameters can be tuned during the electrospinning process.[204,205] Bolded parameters indicate that they were optimised in this thesis.

System parameters	Process parameters
Polymer (**type**, molecular weight, **concentration**, **storage conditions**)	**Polymer flow rate**
Nozzle (material, diameter, number)	**Voltage**
Distance from nozzle to collector	Collector motion
Solvent (type, concentration)	
Salts/**additives**	
Collector (type, material)	
Temperature	
Airflow + particulates in air	
Humidity	

Prior to the start of this thesis, a method to fabricate continuous electrospun filaments on a wire collector was developed. Compared to collecting discontinuous electrospun material on a rotating drum, this method overcame some crucial production limitations. In spite of these production improvements, electrospun filaments have a notoriously low tensile strength. Post-electrospinning treatments, such as annealing, are often needed to enhance the strength and stiffness of the fibres.[139–141] Annealing, or heat treatment, changes the properties of electrospun materials[139,147,148] and its effect on crystal structure, fibre alignment, and mechanical properties is documented in the literature for some polymers.[149–152] However the effect of annealing on electrospun PDO filament properties had not been investigated. This chapter outlines the fabrication of continuous electrospun filaments and the potential for annealing to improve their tensile strength. It has been proposed that most polymer annealing changes occur in a range below melting temperature, generally between 60°C below the melting temperature and the melting temperature.[152] While PDO has a melting temperature of about 110°C , the 65–85°C temperature range is chosen for this experiment to avoid melting of the polymer chains seen at higher temperatures.[115]

As mentioned, although biologically advantageous, electrospun filaments often lack the necessary tensile strength for biomedical applications as scaffolds, sutures, and drug-delivery devices.[127] Moreover, due to the nano- and submicron fibre sizes and their collection as a dense mesh, electrospun filaments have small pore sizes. This could restrict cellular infiltration, which is necessary for the material to integrate with the host tissue. Indeed, it has been shown that high porosity improves the mass transport of nutrients and increases fibroblast proliferation, migration, and infiltration.[206] More recently, microscale fibres (>1μm fibre diameters) are being considered as potential biomaterial candidates.

Although they are not on the same scale as the smaller ECM components, they are potentially advantageous to use in combination with submicron fibres because they are stronger and have larger pore sizes compared to electrospun filaments. Melt-extrusion is a material fabrication technique that uses heat and pressure to melt a polymer and extrude microscale fibres in a continuous process. It is the most common method used in industry to fabricate medical textiles, such as scaffolds and sutures. Synthetic scaffolds are typically made up of extruded fibres with diameters between 20-30μm, woven into a mesh, whereas multifilament sutures are often made of extruded fibres with diameters between 20-30μm braided into a yarn. While melt-extrusion is commonly used in the medical textile industry, commercially produced fibres between 20-30μm might be too large influence cell attachment.[106,133,134]

There is some evidence that cells respond by attaching to fibres in the 1-10μm range, colloquially known as "cell-sized" fibres. Because this size approximates collagen fibres, and not fibrils, fibroblasts respond to these fibres differently compared to smaller scale fibres.[106,133,134] Using melt-extrusion, it is possible to fabricate fibres that are 10μm in diameter. Thus, another aim of this chapter is to fabricate multifilament yarns made up of 10μm fibres. This work will be completed at Fibre Extrusion Technologies (FET), a melt-extrusion company in Leeds (UK) that has experience in melt-extruding PDO, but only in monofilament form. As a result, establishing the feasibility of reliably fabricating multifilament PDO yarns made of 10μm fibres requires further investigation.

Overall, this chapter explores the fabrication of both electrospun and melt-extruded fibres using the same medical grade PDO. An overarching hypothesis of this thesis is that a suture made up of both electrospun and melt-extruded fibres has the potential to provide both biological and mechanical support for tendon repair. Therefore, electrospun fibres are fabricated with a target <1μm diameter, in order to employ biomimicry; replicating the

biophysical cues found in native tissue to favourably drive cell biology. Melt-extruded fibres are fabricated with a target 10μm diameter, to provide mechanical support.

A note on terminology: fibre, filament, and yarn terminology are used interchangeably in the literature, which can create misunderstanding. For this chapter, these terms are described in Figure 3.1 to improve clarity. Fibre refers to the base unit of both electrospun (<1μm diameter) and extruded (10μm diameter) materials. Filament refers to a bundle of electrospun or extruded fibres, with diameters of around 300μm and 120μm, respectively. Extruded filaments were twisted into a multifilament yarn that was around 300μm in diameter.

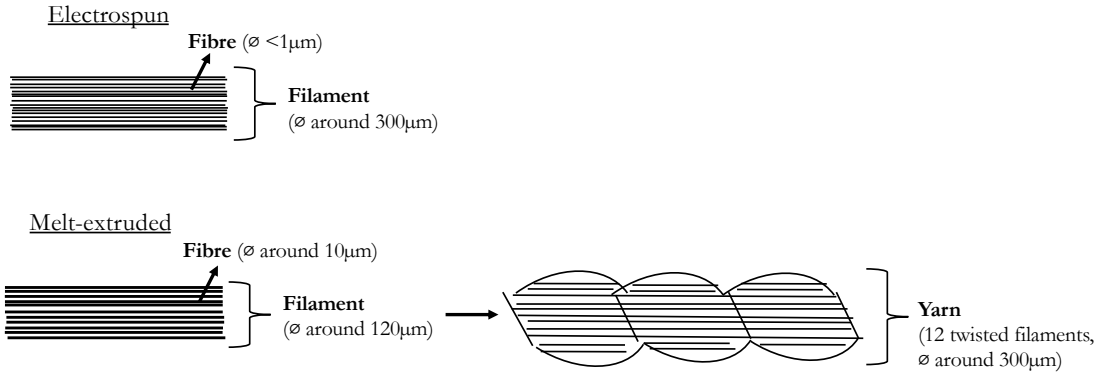


Figure 3.1: Textile terminology used in this chapter. Fibre refers to the base electrospun or melt-extruded material unit. Electrospun fibres are <1μm in diameter (⌀), whereas melt-extruded fibres are 10μm in diameter; Filament refers to the assembly or bundle of fibres, preferably aligned along the length of the filament. Electrospun filaments form a densely connected mesh of fibres that are removed directly from the collecting wire. Melt-extruded filaments are made up of 28 fibres, collected directly from the spinneret; Yarn or multifilament yarn refers to the assembly of filaments using textile technologies. In this chapter, a yarn refers to 12 melt-extruded filaments that have been twisted.

3.3 Objectives and hypotheses

The overall aim of this chapter is to produce continuous PDO fibres using both electrospinning and melt-extrusion techniques. Electrospun filaments and melt-extruded yarns with target properties are developed and their material and mechanical properties are compared.

- Objective 1: To improve the tensile strength of electrospun filaments by exploring annealing as a post-processing method.

- Objective 2: To consistently and reliably produce 10μm fibres through melt-extrusion.

- Objective 3: To characterise electrospun filaments and extruded yarns in terms of their mechanical properties, porosity, thermal properties, and degradation rate.

The overall hypothesis is that it will be possible to electrospin and melt-extrude continuous fibres. Electrospun fibres will be used in filament form, whereas melt-extruded fibres will need to be twisted into yarns to meet target criteria. Although manufactured from the same base PDO resin, the two materials will have significantly different mechanical and material properties.

- Hypothesis 1: Annealing will affect the mechanical and degradation properties of electrospun filaments.

- Hypothesis 2: Melt-extrusion will enable the production of target 10μm fibres. To reliably enable this, PDO viscosity, spinneret diameter, draw speed, and temperature will be controlled.

- Hypothesis 3: Mechanical properties, porosity, thermal properties, and degradation rate will differ between electrospun filaments and melt-extruded yarns.

3.4 Materials and methods

3.4.1 Optimising the electrospinning process

A custom electrospinning apparatus with a single nozzle and stainless-steel wire collector was developed prior to the start of this thesis and used to fabricate continuous electrospun filaments made up of aligned submicron fibre diameters, as shown in Figure 3.2.

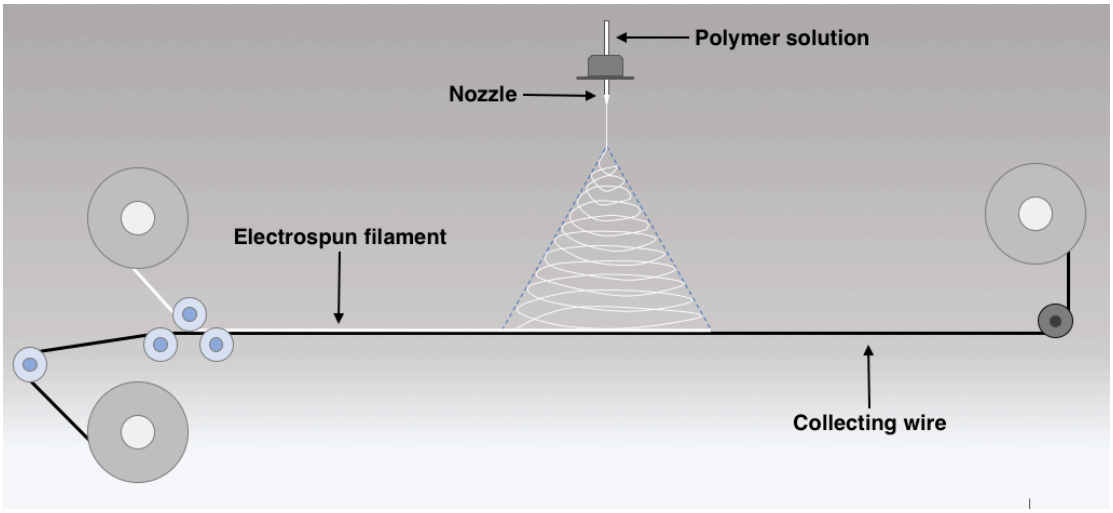


Figure 3.2: Custom electrospinning setup with a single nozzle and a stainless-steel wire collector. Electrospinning on a wire forces the fibres to form a dense, interconnected mesh that can be removed directly and continuously as a filament. Figure reproduced with permission of Ms Hayley Morris (Carr group).

There was significant optimisation work of the electrospinning process that was needed prior to starting experiments. This involved tuning system parameters, such as polymer solution and electrospinning environment, as well as tuning process parameters, such as the polymer flow rate and system voltage.

3.4.1.1 Polymer solution

PDO was the chosen polymer for this work and the justification for this choice is described in Chapter 2.10.1. Hexofluoro-2-propanol (HFIP) was the volatile solvent used to dissolve

the polymer, because it is frequently used in the literature and had been successfully used by the Carr group for eight years.[98,129,207–209] PDO from different manufacturers and at different concentrations were investigated, as described in Table B.1 in the Appendix. PDO manufacturers were chosen based on availability and concentrations chosen based on trial and error.

Previous work in the Carr group using a different electrospinning setup with a rotating drum collector had shown that the addition of pyridine, a compound that increases the polymer solution's conductivity, had a substantial influence on fibre homogeneity.[107] Because the collection surface on the wire is relatively small, compared to a plate or drum, the deposition is more sensitive to perturbations of the electrical field, such as the static charges on the walls of the chamber. The addition of pyridine to the PDO solution used for the wire electrospinning, resulted in an increase in fibre deposition length and a reduction in fibre diameter. The effect of pyridine on fibre diameter and deposition was explored by other members of the Carr group (Dr Edward Stace and Ms Antonina Lach) and has been published.[107,210]

3.4.1.2 Electrospinning environment

Electrospinning for the annealing experiment in this chapter was performed using a custom electrospinning setup, in the Botnar Research Centre (Figure 3.2). Although every effort was made to control the temperature in the electrospinning room, the laboratory was shared with many researchers, who came in and out of the room during electrospinning and made controlling the temperature difficult. The effect of temperature on the stability of the electrospinning jet was trialled by adjusting the room temperature between 20-40°C, keeping all other electrospinning parameters constant, and visually observing the stability of the Taylor cone and whipping of the electrospinning jet. It was

found that lower temperatures enabled a more stable Taylor cone, and future electrospinning was conducted at 20°C.

With the exception of the annealing experiment in this chapter, all of the electrospinning work in this thesis was performed in a clean room environment at the Harwell Science Centre (Oxfordshire, UK). The temperature, humidity, air particulates, cleaning, gowning, and biocontamination were tightly controlled according to ISO 14644-1:2015.[211] Although this meant that these variables couldn't be manipulated, it also meant that all electrospinning was performed in a GLP standard facility, which will ease the transition to pre-clinical testing (further discussed in Chapter 6).

3.4.1.3 Optimising the electrospinning process

The main process parameter that was controlled during electrospinning was the voltage. The only visible part of the electrospinning process, apart from the deposited fibres on the collector, is the shape of the Taylor cone and the electrically driven polymer jet that emerges from the Taylor cone (Figure A.1 in the Appendix outlines the electrospinning process in more detail). As a result, these were the two factors that were used to assess the stability of the electrospinning process. Increasing the voltage was the main way to change the shape of the Taylor cone and the behaviour of the polymer jet. If the voltage was too low, the polymer emerged from the nozzle as a drop and did not form a jet or deposit on the collector. Increasing the voltage led to more charge separation, whipping of the jet, and more reliable fibre deposition. Increasing the voltage above a certain threshold, however, resulted in a multi-jet sputtering, irregular fibre patterns, and fibre collections on the walls of the electrospinning chamber.

It is possible to focus on each electrospinning parameter in Table 3.1 individually, however in reality, they are all interlinked. Any small change in the electrospinning chamber environment or polymer solution conductivity would influence the voltage needed to

achieve a stable Taylor cone and jet. As a result, for each electrospinning experiment in the Botnar research centre and in the clean room at Harwell Science Centre, setting up the electrospinning process followed the same protocol:

1. The polymer solution was loaded into a syringe and left to stand vertically for 20 minutes to allow air bubbles to rise to the surface of the liquid and be squeezed out of the syringe.
2. The room temperature was set to 20°C and the electrospinning chamber was thoroughly cleaned with 70% ethanol and disposable wipes.
3. The polymer solution was loaded into the syringe pump and the moving collecting wire was turned on.
4. The electrospinning chamber was sealed shut and a low voltage was applied (around 4kV) until the polymer solution emerged at the tip of the nozzle
5. The voltage was slowly increased 0.2kV every 5 seconds, until the polymer stopped forming droplets and formed a cone with a single stable polymer jet emerging from its tip. The electrospinning setup was deemed stable when the Taylor cone didn't change shape or size and there was minimal movement of the emerging jet.
6. Electrospinning was periodically checked every 30 minutes and the voltage was adjusted if the jet was sputtering (voltage too high) or if the polymer was dripping (voltage too low).

3.4.2 Electrospinning filaments

This section describes the optimised electrospinning process.

3.4.2.1 PDO solution preparation

PDO was supplied by Sigma-Aldrich (PDO, Sigma, viscosity 1.5–2.2 dL/g; Tg -10 to -5 °C; Tm 110-115 °C, Dorset, UK) for the annealing experiment, and by Riverpoint Medical (Riverpoint, MFR 3.9-4.5g/10min at 170°C; Portland, OR, USA) for the rest of the work

in this thesis. Polymer solutions were made by dissolving PDO resin in HFIP solvent (Apollo Scientific; 1,1,1,3,3,3, -hexafluora-2-propanol) at a specified weight to volume ratio (7% for the Sigma PDO and 9% for the Riverpoint PDO) and gently rolled for 24 hours before electrospinning. For the annealing experiment, the PDO solution was prepared as described above. For the work in the rest of this thesis, pyridine (Sigma, Dorset, UK) was added to the PDO solution, at a concentration below 100ppm, prior to rolling overnight.

3.4.2.2 Electrospinning process

The collecting wire was manually wiped with 70% ethanol prior to use. A 5mL syringe pump (Harvard Apparatus, Kent, UK) delivered PDO solution at a feed rate of 1mL/hour for solutions without pyridine, and 0.8mL/hour for solutions with pyridine. The wire feed rate was 0.5mm/second and the filament was spun under an electric field of 6.5-9.5kV. The filaments were detached from the collecting wire and were manually stretched according to protocols in Chapter 3.4.2.3. The stretched filaments were then thermally annealed following Chapter 3.4.2.4 and stored at 25°C in a dessicator.

3.4.2.3 Drawing of electrospun filaments

Electrospun filaments were detached from the collecting wire and were manually stretched until resistance was felt (3.5 times their original length). Drawing electrospun filaments serves multiple purposes: it increases the strength and stiffness of the fibres, decreases the risk of plastic deformation in the final device, reduces fibre diameter, increases the crystallinity of the material, and aligns the fibres in the direction of the filament.[128,129,142]

3.4.2.4 Annealing effect on electrospun filament properties

The extent to which heat treatment can improve the mechanical properties and alter the degradation rate of electrospun filaments was explored in this chapter. Electrospun filaments were manufactured using a Sigma PDO solution, as previously described.

Filaments were thermally annealed for 3, 6, 9, 12 and 24 hours at 65°C, 75°C, or 85°C in an oven (Drying Oven UF750 plus, Memert, Germany) and subjected to degradation in phosphate buffer saline (PBS) for up to 6 weeks. This annealing and degradation time range was chosen following optimization work done at 65°C. Filaments were degraded in a falcon tube with 8mL of PBS per 1 meter of filament. The tubes were kept in a static environment in an incubator, at 37°C and 95% humidity, and removed every week for media replacement. Immediately after annealing, filaments were subjected to visual inspection, mechanical testing, and thermal testing, as well as after 4 and 6 weeks of degradation.

3.4.3 Melt-extruding filaments and yarns

3.4.3.1 Melt-extrusion process

PDO was supplied by Riverpoint Medical (Portland, OR, USA) in individual lots of 100g characterised by melt flow rate (MFR), a surrogate measurement to molecular weight. Two lots of PDO with MFRs of 3.9g/10min and 4.5g/10min at 170°C were blended at a 1:1 ratio to yield a final blend of 400g. Once blended, the resin was transferred to the feed of the extruder and kept under a blanket of dry nitrogen.

Extruded filaments were produced with a Melt-Extrusion Spinning Line (Fibre Extrusion Technologies, Leeds, UK) using a 20mm diameter extruder and a 1mL/rev melt pump, as shown in Figure 3.3. Raw PDO resin was introduced into the extruder and heated. Molten PDO was then passed through a metal spinneret with 28 holes of 0.2mm in diameter. The fibres were drawn at a ratio of 4:1, initially in the melt and then the solid phase, over a series of paired ceramic rollers to yield a bundle of fibres, called a filament. Each filament was made up of 28 fibres with a 10μm diameter. In order to draw the filament over the heated godets, it was necessary to apply a spin finish, or lubricant (Vystat 2264, Leeds, UK)

to the filament. The lubricant was a polyethylene-glycol (PEG) based, FDA approved, finish used in suture manufacturing, diluted at a ratio of 1 part Vystat: 3 parts water.

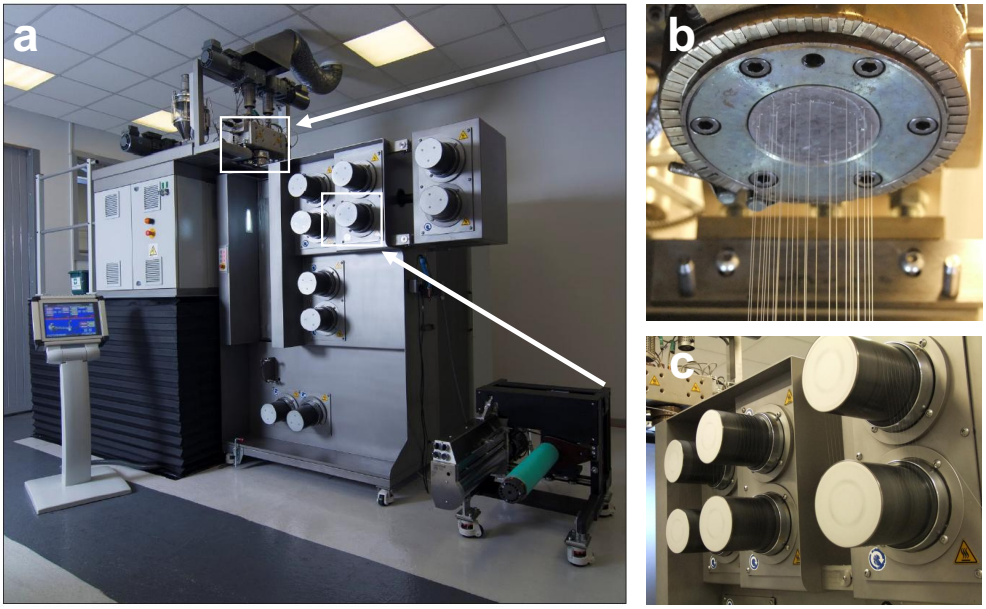


Figure 3.3: Melt-extrusion set-up used to fabricate PDO fibres. Fibres were melt-extruded at Fibre Extrusion Technologies in Leeds UK. (a) Spin-draw-wind cabinet; (b) Spinneret with 28 holes of 0.2mm in diameter. 28 fibres are continuously collected, which form a filament; (c) Filaments were drawn out at 65°C over heated godets directly after filament collection. Figures courtesy of Fibre Extrusion Technologies.

3.4.3.2 Twisting of melt-extruded filaments into yarns

To produce a stable final yarn, filaments were combined using a ring twister, first combining 4 filaments in one direction (S twist) and then combining 3 S-twisted bundles in the other direction (Z twist). This yielded a final twist-neutral yarn with a diameter of 278µm, made up of 12 filaments.

3.4.4 Scanning electron microscopy

Electrospun and melt-extruded materials measuring 2-3cm were cut and mounted on aluminium stubs (Agar Scientific, Essex, UK) using carbon tape (Agar Scientific). These stubs were coated with gold for 120 seconds using a SC7620 Mini Sputter Coater System (Quorum Technologies Ltd, Laughton, UK). Scanning electron microscope (SEM) images

were acquired using an EVO LS15 VP-SEM (Carl Zeiss, EVO LS15, Oberkochen, Germany) in high vacuum mode to examine fibre diameter and morphology of pristine fibres, as well as changes in morphology due to degradation, such as fibre fusing and breaking. Fibre diameter was measured using ImageJ software (National Institutes of Health, Bethesda, USA). For each experimental condition, five different locations on 3 samples were imaged and 10 measurements per image were captured at magnifications between 200-1000x.

3.4.5 Tensile testing

Two different tensile testing set-ups were used. Preliminary work showed that the gross mechanical properties were very different between the electrospun filaments and melt-extruded yarns and thus required tensile setups with different load cells. Electrospun filaments were tested using a 20N tensile stage (Deben Stage Tensile Compression Stage, UK). Grip-to-grip separation at the beginning of each test was 1cm and the samples were tested to failure. Ten specimens were tested for each condition and for each experimental repeat.

Melt-extruded yarns were tested using a 5kN tensile stage (Zwick Roell Group, USA). A preliminary investigation with Pincer grips (Zwick Roell Group, USA) yielded inconsistent results and yarn pull through the grip clamps. To generate more reproducible data, custom grips were designed to slide onto the existing Zwick grips, based on tensile grips used in the textile industry for yarns and ropes.[212] These grips are shown in Figure 3.4 and were also used in Chapter 4 to test multifilament sutures. Grip-to-grip separation at the beginning of each test was 1.8cm and the samples were tested to failure. Five specimens were tested for each experimental repeat.

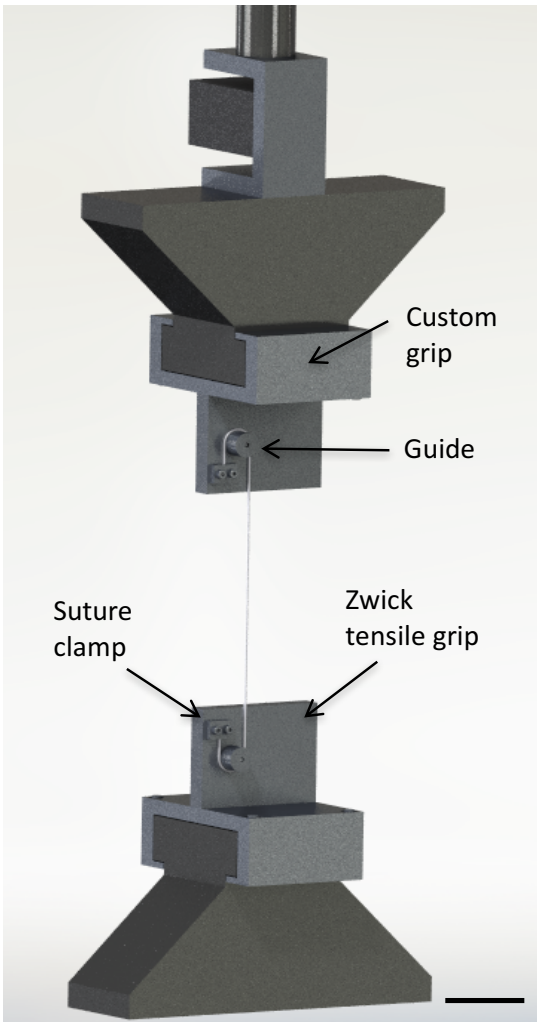


Figure 3.4: Custom tensile testing set-up for yarns. Grips were designed for this study to improve yarn grip and slide onto existing Zwick Pincer grips. Scale bar represents 5cm.

For the polymeric filaments tested in this chapter, viscoelastic, non-linear behaviour under loading was expected.[71,72] As a result, strain rate, temperature, and humidity would all have an influence on the mechanical test. In preparation for mechanical testing, electrospun filaments and melt-extruded yarns were sterilised with 70% ethanol for 2 hours, left to air dry overnight and finally sealed in a vacuum prior to testing to remove any residual liquid. All filaments were mechanically tested to failure at room temperature. Filaments were tested knotless at a crosshead speed of 50mm/min until failure. The strain rate was chosen based on similar experiments in the literature[210,213,214] and in complying with ISO standard 2062:2009.[215] Humidity was not controlled, which is a limitation of this experiment.

The force at break (N), ultimate stress (MPa), grip-to-grip breaking strain (%), and Young's modulus (MPa) were recorded. Stress was calculated using the ratio of the force at failure (N) and the cross-sectional area (CSA) (mm^2). CSA measurements were obtained by multiplying the micro-computed tomography (μCT) solid cross-sectional area by (1-overall porosity obtained from Hg porosimetry). Chapter 4.4.5 outlines μCT methods and Chapter 3.4.6 describes Hg porosimetry methods. Young's modulus was calculated from the linear region of the stress-strain curve, shown as *E* in Equation 3.1. Viscoelastic properties, such as creep or stress relaxation, were outside of the scope of this thesis and should be considered in future work using dynamic mechanical analysis (DMA) or exploring different strain rates or cyclical loading to develop a more detailed picture of the mechanical behaviour of these filaments.

$$E = (\frac{F}{A0})/(\frac{\Delta L}{L0})$$

Equation 3.1: Calculating Young's modulus from tensile testing results.
E=Young's modulus (MPa)

F= Maximum force to failure (N)

A0= Original cross-sectional surface area (mm^2)

ΔL= Change in length (mm)

L0= Original length (mm)

3.4.6 Mercury porosimetry

Mercury (Hg) porosimetry was used to measure the porosity of electrospun filaments and melt-extruded yarns, by applying controlled pressure to a sample filled with mercury. This technique is based on the principle that mercury does not wet the surface of solid biomaterials and will not spontaneously penetrate pores (Figure 3.5b).[216,217] Instead, mercury must be forced into the pores through the application of external pressure, with the required pressure being inversely proportional to the size of the pore (Figure 3.5a).

The applied pressure and volume of mercury are recorded and overall porosity and pore sizes can be deduced. Assuming that pores are cylindrical in shape, the Washburn equation (Figure 3.5c) can be used to calculate pore diameter.[218]

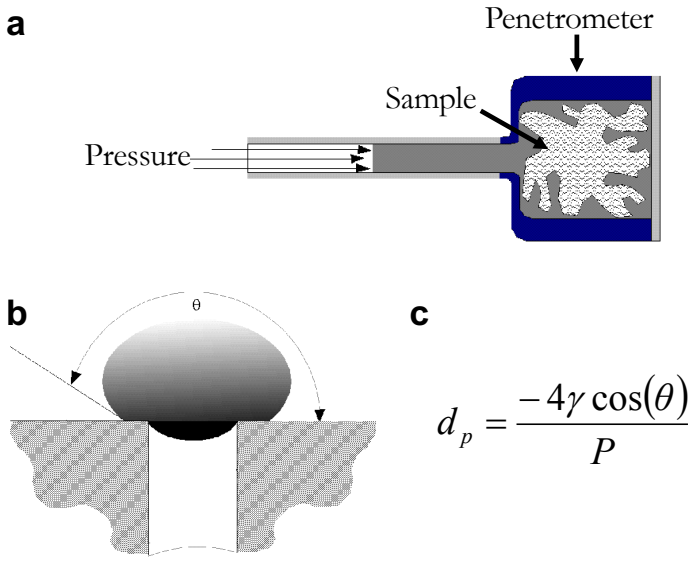


Figure 3.5: Mercury intrusion porosimetry theory. (a) Penetrometer filled with a sample material. Pressure is applied up the capillary stem to fill the sample cup with mercury; (b) Contact angle between mercury and the sample pores. Because mercury does not wet most materials and won't spontaneously penetrate pores, it must be forced into the pores through the application of pressure; (c) Washburn equation. d_p is the pore diameter, γ is the surface tension of mercury (under vacuum), θ is the contact angle between mercury and the porous material, and P is the pressure applied to mercury. The contact angle between mercury and porous solid material can be variable; a value of 130° is used in the absence of specific information.[216] Figure modified from Micromeritics Instrument Corporation.[219]

Average pore diameter and overall porosity were determined using an Autopore IV 9500 mercury porosimeter (Micromeritics Instrument Co, Norcross, GA, USA). The porosimeter had a maximum pressure range of 33,000 psia and a measurable pore size range of 360μm to 0.005μm. Electrospun filaments and extruded yarns were cut into sections weighing 70-100 mg and placed in the penetrometer fixed with a sample cup bonded to a metal-clad, glass-capillary stem (s/n = 14, 3 bulb, 0.412 stem, powder). The penetrometer was first passed through the low-pressure port where the gases were evacuated from the penetrometer and then backfilled with mercury. Then, the penetrometer was passed through the high-pressure port, where pressure on the

penetrometer increased and mercury intruded into the sample pores, beginning with the pores of the largest diameter. Samples were run with a mercury filing pressure of 0.49 psia and an equilibration time of 10 seconds. Two experimental repeats were performed for both the electrospun filaments and melt-extruded yarns.

3.4.7 Differential scanning calorimetry

Differential scanning calorimetry (DSC; TA Q2000-1275 Differential Scanning Calorimeter) was used to examine the thermal changes due to annealing electrospun filaments. It was also used to compare thermal properties between electrospun filaments, melt-extruded yarns, and raw PDO resin. DSC measures heat flow associated with material transitions as a function of time and temperature. The output can provide information about physical and chemical changes occurring within the sample. While it doesn't give a thorough mechanistic understanding, it can give a phenomenological understanding of changes in crystal sizes and morphologies and an approximation of overall crystallinity by comparing it to a 100% crystalline PDO sample. This is important because crystallinity is correlated with tensile strength and degradation rate in semi-crystalline polymers like PDO.[132,220]

PDO is a semi-crystalline polymer with a glass transition temperature of -10°C to 0°C and melting temperature of around 110°C.[115,221] For each condition, 3-4 mg of sample was cut and mounted in aluminium pans (TZero Aluminium). An empty tin was used as the reference standard. The pans were heated from 25°C to 140°C at a rate of 10°C/min in a nitrogen atmosphere. The sample was held at 140°C for 2 minutes before cooling back to 25°C at the same rate. A second heating and cooling cycle was performed using the same settings. Using the first cycle thermogram, the melting point (Tm), measured melting peak (Hm), and measured area of the annealing peak (Ha), were determined. The annealing peak is the endothermic peak found about 10–20°C below the melting temperature.[150] The heat

of fusion (Hf) was calculated, where Hf = Hm + Ha. Overall percent crystallinity was calculated as shown in Equation 3.2 below.

$$\%\ Crystallinity = \left(\frac{Hf}{Hf[100\%]}\right) * 100$$

Equation 3.2 Calculating overall crystallinity (%) from DSC thermographs.
Hf: measured heat of fusion

Hf [100%]: theoretical heat of fusion of a 100% crystalline PDO material, which is indicated as 141.2 J/g for PDO.[222]

3.4.8 *In vitro* degradation

Prior to *in vitro* degradation, electrospun filaments and extruded yarns were cut and sterilized for 2 hours in 70% ethanol. Materials were degraded in separate falcon tubes with 8mL of PBS per 1 meter of filament. The tubes were kept in a static environment in an incubator at 37°C and 95% humidity. Every week, the samples were washed and replaced with fresh PBS and the pH was monitored with a pH meter. Prior to analysing the degraded filaments, they were washed twice with deionized H_2O and dried in a vacuum for 3 hours. Electrospun filaments were mechanically tested at 3,4, and 6 weeks and thermally tested at 6 weeks. Melt-extruded yarns were mechanically tested at 2,3,4,6, and 12 weeks and thermally tested at 4,6, and 12 weeks.

3.4.9 Statistical analyses

A Kolmogorov-Smirnov test was used to determine normality for each experiment. With the exception of the Hg porosimetry testing and crystallinity calculations, the data from each experiment and each material tested was normally distributed. The number of repeats in the Hg porosimetry testing and crystallinity comparisons were too low to test for normality, so non-parametric testing was performed.

Statistical analysis was performed with GraphPad Prism version 7 software (GraphPad Software Inc, California, USA). For all analyses, statistical significance was taken at $p<0.05$.

Statistics in some figures are represented by lower and upper case letters. An upper case letter (i.e. "A") represents that the material is statistically significantly greater than every other material with the corresponding lower case letter (i.e. "a").

For testing the effect of different annealing temperatures on mechanical properties of electrospun filaments, a one-way ANOVA with Tukey's multiple comparisons testing was used. These same statistical analyses were used to test the effect of different annealing times on overall percent crystallization and to test the effect of different degradation time points on extruded filament mechanical properties.

For testing the effects of annealing on both the mechanical properties and degradation of electrospun filaments and melt-extruded yarns, a two-way ANOVA with Sidak's multiple comparisons testing was used.

To compare the statistical differences of electrospun filaments and extruded yarns, an unpaired, two-tailed t test with Welch's correction was used.

3.5 Results

3.5.1 Electrospun filament parameters and characteristics

The polymer solution protocols, electrospinning environment, and electrospinning parameters that enabled the production of continuous filaments were optimised. Preliminary polymer and electrospinning optimisation are described in Appendix B.1. Overall, it was shown that electrospinning with PDO from different suppliers resulted in differences in filament mechanical properties, when controlling for electrospinning parameters (Figure B.1 in the Appendix). It is reasonable to assume that these changes were, in part, due to variations in PDO molecular weight, although this has not been explicitly tested. It is also possible that the differences in PDO from different suppliers also affected local mechanical properties and other electrospinning characteristics that were out of the scope of this thesis. It was also shown that increased PDO concentration was directly proportional to filament mechanical strength and fibre size (Figure B.1 in the Appendix), which is supported by the literature.[223,224]

By electrospinning on a moving collection wire, it was possible to produce unstretched filaments continuously at a rate of 1.6 meters/hour. Fresh filaments were manufactured for each experiment presented in this thesis, in order to minimise the time between production and use to less than 6 weeks. Preliminary work had shown that degradation, in the form of fibre breaking, had started to occur after 6 weeks. The parameters for electrospinning filaments used in this thesis are outlined in Table 3.2.

Table 3.2: Parameters for electrospinning PDO filaments used in this thesis.

	Annealing experiment (Chapter 3.5.2)	The rest of this thesis
PDO supplier	Sigma-Aldrich	Riverpoint Medical
PDO concentration	9%	7%
Melt flow rate	n/a	3.9-4.5g/10min at 170°C
Inherent viscosity	1.5-2.2 dL/g	n/a
Pyridine concentration	0 ppm	<100 ppm
Solution Feed Rate	1mL/hour	0.8mL/hour
Wire Feed Rate	0.5mm/s	0.5mm/s
Voltage	6.9kV	7.2-9.5kV
Distance nozzle-wire	20 cm	20 cm

Due to the relatively slow speed of the wire, collected filaments had randomly oriented fibres. Through the drawing process, fibres were aligned along the length of the filament and the overall filament length increased by 3-4 times. As a result, in one hour, it was possible to collect 1.6 meters of unstretched filament, or 5-7 meters of stretched filament. Table 3.3 shows SEM images of fibre morphology and changes in filament and fibre diameter before and after stretching. Filaments had a flat cross-section and filament diameter was reduced from 359.2±10μm to 226.4±1μm after stretching. Fibre diameter was reduced from 1.3±0.3μm to 0.86±0.2μm after stretching. In the context of fibre size to support biomimicry, it is worth noting that the fibre diameter was less than a micrometre (which was the fibre diameter target) only after stretching. The final electrospun filament porosity, mechanical properties, and cross-sectional area after stretching are shown in Table 3.4.

Table 3.3: Effect of stretching on electrospun filament characteristics. SEM images of electrospun filament morphology, as well as filament and fibre diameters before and after stretching, reported as mean ± standard deviation. Magnification 1000x; scale bars represent 20μm.

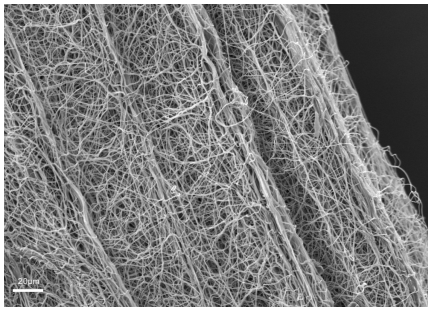
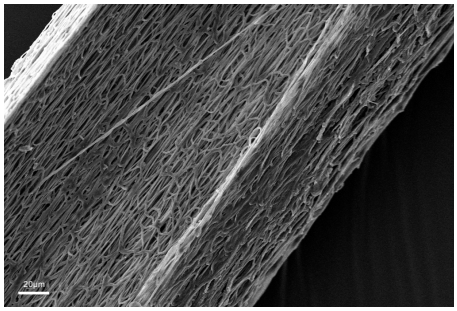
	Before stretching	After stretching
Morphology		
Filament diameter (μm)	359.2 ± 10	226.4 ± 1
Fibre diameter (μm)	1.3 ± 0.3	0.86 ± 0.2

Table 3.4: Electrospun filament characteristics.

Overall porosity (%)	79.8 ± 10.3
Average pore size (nm)	1480 ± 116
Force at break (N)	1.3 ± 0.1
Strain at break (%)	26.8 ± 2
Cross-sectional area - full (μm^2)	7089.3 ± 897
Cross-sectional area – adjusted for porosity (μm^2)	5859 ± 741

3.5.2 Annealing effects on electrospun filament properties

Annealing filaments at various temperatures (65°C, 75°C, and 85°C) and times (3,6,9,12, and 24 hours) had substantial effects on pristine filament properties and their subsequent degradation.

3.5.2.1 Fibre morphology

Filament and fibre morphology of electrospun PDO filaments after annealing for 3 hours and following 6 weeks of degradation, are shown in Figure 3.6. Annealing temperature did not affect fibre arrangement immediately after annealing, but unsurprisingly did affect the rate at which fibres lost their organisation during *in vitro* degradation. Figure 3.6a shows undegraded filaments annealed at 65˚C, Figure 3.6b shows filaments annealed at 75˚C, and Figure 3.6c shows filaments annealed at 85˚C. Samples that were annealed at 65˚C maintained a high degree of fibre alignment and there were few visible breaks in the fibres after 4 weeks (Figure 3.6d) or at 6 weeks (Figure 3.6g). Samples annealed at 75˚C maintained a high level of fibre alignment after 4 weeks of degradation (Figure 3.6e), but lost much of the linear organization by 6 weeks. These samples took on a more wavy appearance with visible breaks along the length of the filament (Figure 3.6h). Samples annealed at 85˚C exhibited these signs of degradation by 4 weeks (Figure 3.6f). By 6 weeks, the fibres had fused together, making the samples brittle and difficult to handle (Figure 3.6i). There was an increase in filament size of 50±20μm visible at this time, likely due to PBS expanding within the filament, as well as the degraded PDO expanding.

Samples annealed at 6, 9 and 12 hours showed similar patterns of degradation but are not shown here. Samples annealed at 65˚C for 24 hours already displayed signs of fibre breaking and fusing by 4 weeks of degradation. Annealing at 75˚C or 85˚C for 24 hours did not improve the mechanical properties and rendered the samples more brittle than not annealing, as shown in Figure 3.7. After 6 weeks of degradation, samples that were annealed for 24 hours at 85˚C were too brittle to mechanically test.

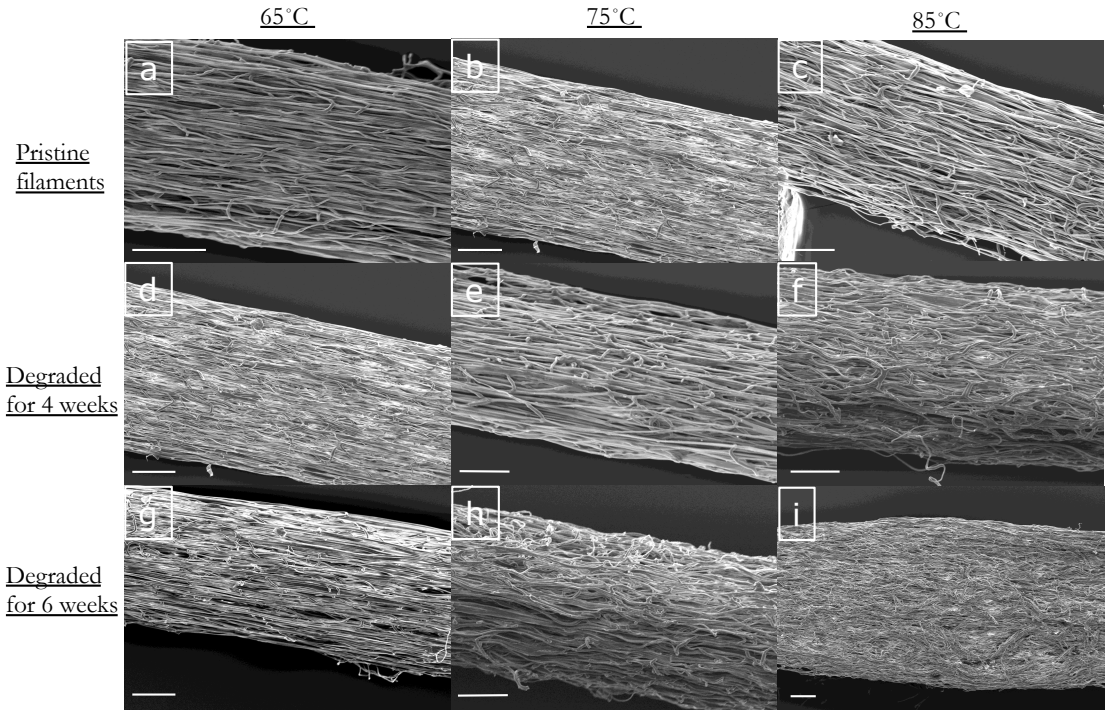


Figure 3.6: SEM images of electrospun fibre morphology after annealing for 3 hours at various temperatures and subjecting to a 6-week degradation period. (a-c) Pristine filaments. These filaments were freshly manufactured the day of or day before imaging. No visual differences in fibre alignment observed for samples annealed at different temperatures, but there is some evidence of fibre breaking after annealing at 85ºC. (d-f) Samples degraded for 4 weeks in PBS at pH 7.4. Samples annealed at (d) 65ºC and (e) 75ºC maintained a high degree of fibre alignment compared to samples annealed at (f) 85ºC. (g-i) Samples degraded for 6 weeks in PBS at pH 7.4. High degree of fibre alignment retained for samples annealed at (g) 65ºC, compared with (h) 75ºC, or (i) 85ºC. Magnification 200x for (i), 400x for (a,b,c,d,e,g), and 500x for (f,h); scale bars represent 100μm.

3.5.2.2 Mechanical analysis

Figure 3.7 shows relative changes in stress and strain at failure as a result of annealing treatments. The stress subtly increased after annealing filaments at 65˚C (Figure 3.7a) and 75˚C (Figure 3.7b) for some time points, compared to samples that weren't annealed. However, the changes were only statistically significant when annealing at 75˚C for 3 hours ($p=0.0230$). The maximal stress decreased after annealing filaments at 85ºC for 9 hours or longer ($p<0.0001$) and after annealing at 75˚C for 24 hours ($p<0.0001$), as shown in Figure 3.7c and 3.7b, respectively. The strain decreased at all annealing temperatures, compared to not annealed, and this result was significant for samples annealed at 65˚C and 75˚C for 3 hours ($p<0.001$) and at all annealing temperatures for longer than 6 hours ($p<0.0001$).

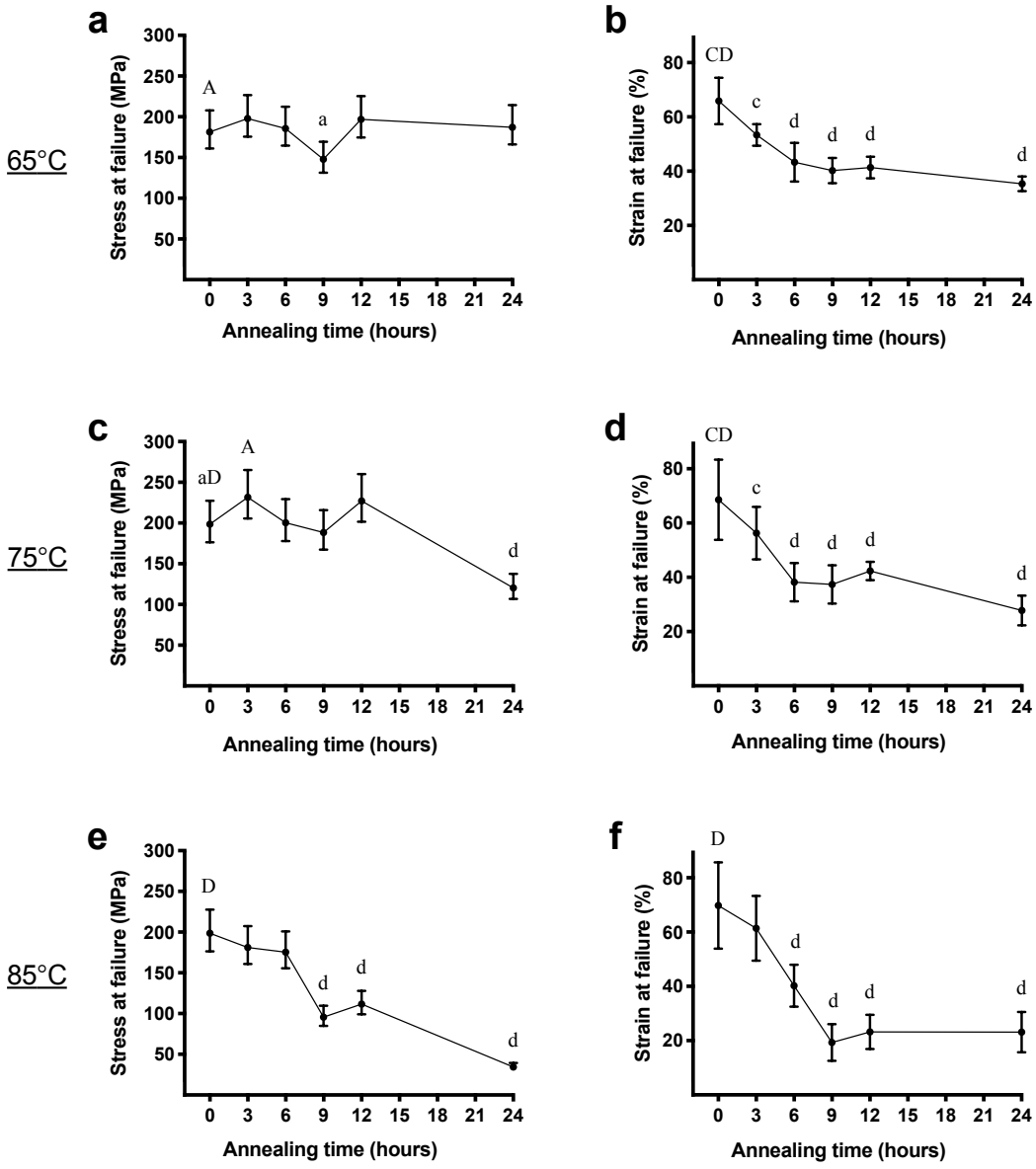


Figure 3.7: Changes in mechanical properties of undegraded PDO electrospun filaments due to annealing treatments. Relative changes in stress (MPa) and strain (%) recorded as a function of annealing time. (a,c,e) Relative changes in maximal stress at failure for samples annealed for various times at (a) 65ºC, (c) 75ºC, and (e) 85ºC compared to those not annealed. Filaments annealed at 85ºC for 9 hours or longer were weaker than those not annealed ($p<0.0001$). Annealing for 24 hours at 75ºC also resulted in a lower stress ($p<0.0001$). (b,d,f) Relative changes in strain for samples annealed for various times at (b) 65ºC, (d) 75ºC, and (f) 85ºC compared to those not annealed. Annealing at all temperatures for more than 6 hours significantly reduced the filament strain ($p<0.0001$). Annealing for 3 hours at 65ºC and 75ºC also reduced the filament strain ($p<0.001$). Statistical significance was determined at Aa=$p<0.05$, Bb=$p<0.01$, Cc=$p<0.001$, Dd=$p<0.0001$. Error bars represent standard deviations; n=10 for each condition.

Filaments annealed at lower temperatures and for shorter times better maintained their mechanical properties during *in vitro* degradation. Figure 3.8 shows the stress and strain of electrospun filaments annealed for 3 hours over a 6 week degradation period. Samples annealed at 65˚C retained a similar stress over 6 weeks (Figure 3.8a) and had a significantly lower strain at failure at 4 weeks ($p<0.0001$) and 6 weeks ($p<0.0001$). In contrast, samples annealed at 75˚C showed a lower strain at all degradation time points ($p<0.0001$). Similarly, samples annealed at 85˚C for 3 hours showed a lower stress at 3 and 4 weeks, although not significant, but showed a statistically lower stress at 6 weeks ($p<0.0001$) and a lower strain at all degradation time points ($p<0.0001$). It is worth noting the change in the size of standard deviations between filaments annealed and not annealed, as well as following degradation. For example, in comparing the strain at failure after 3 weeks of degradation, non-annealed samples had a standard deviation of 7.4%, compared to 3.1% and 3.8% for samples annealed at 65˚C and 75˚C. This difference is likely reflective of annealing inducing changes to local fibre properties and will be addressed in the discussion.

The 3 hour annealing time at 65˚C was the most promising in maintaining mechanical properties, based on the results shown in Figure 3.8. The changes in mechanical properties over the 6-week degradation period for filaments annealed for longer times, are shown in Figure B.2 in the Appendix.

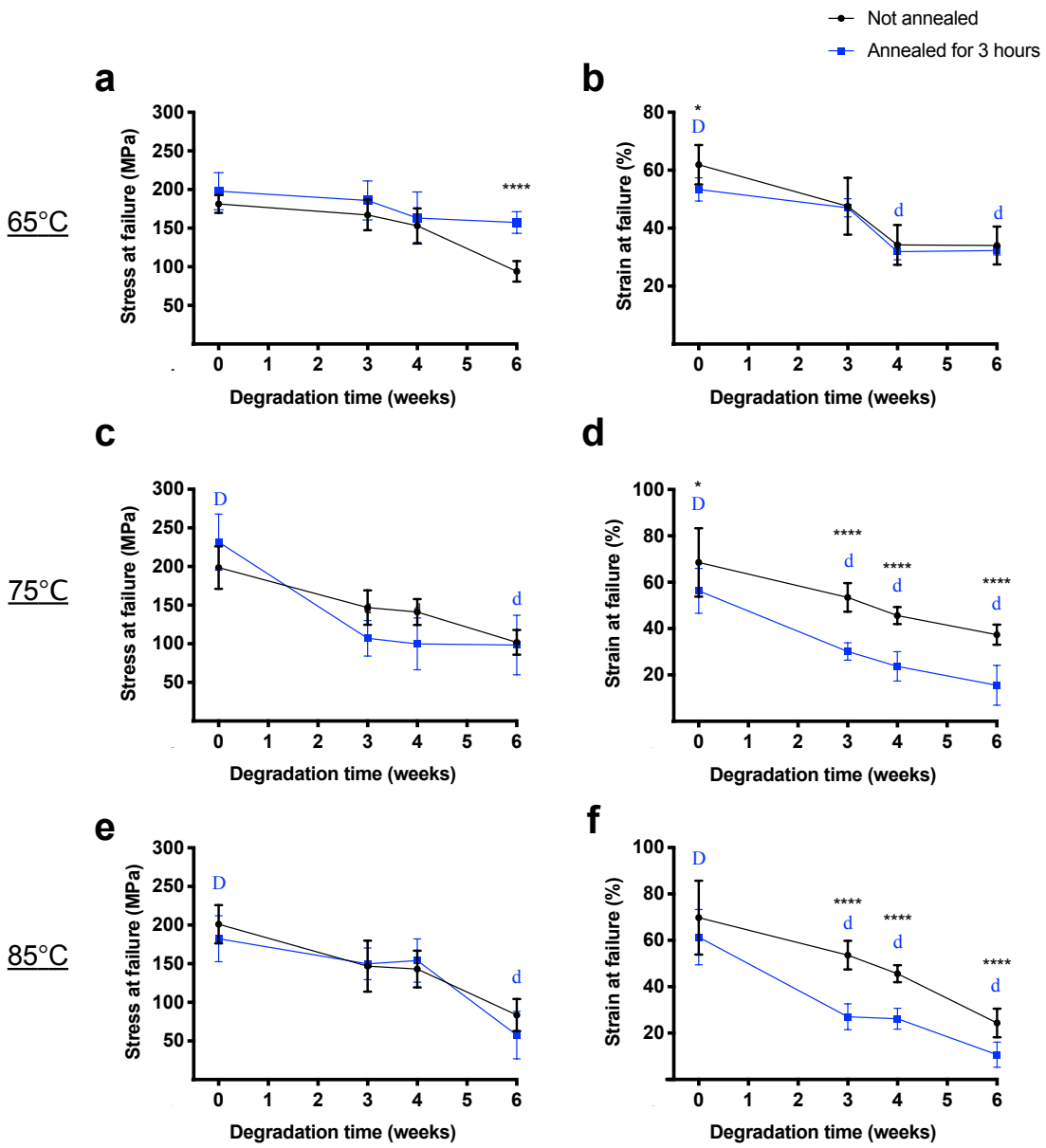


Figure 3.8: Changes in mechanical properties of electrospun filaments annealed for 3 hours at 65°C, 75°C, and 85°C, over a 6-week degradation period. Relative changes in stress and strain at failure shown as a function of degradation time, compared to filaments not annealed. (a,c,e) Relative changes in stress at failure for samples annealed for 3 hours at (a) 65°C, (b) 75°C, and (c) 85°C. (a) Samples annealed at 65°C showed a subtle decrease in stress over 6 weeks that was not significant. Compared to non-annealed samples, stress was higher at 6 weeks of degradation ($p<0.0001$); (c) Samples annealed at 75°C had a lower stress at failure at all degradation time points ($p<0.0001$); (e) Samples annealed at 85°C had lower stress at 6 weeks of degradation ($p<0.0001$). (b,d,f) Relative changes in strain at failure for samples annealed for 3 hours at (b) 65°C, (d) 75°C, and (f) 85°C. Strain at failure was statistically lower at 3 weeks of degradation for samples annealed at 75°C and 85°C ($p<0.0001$) and lower beyond 3 weeks of degradation for all annealing temperatures ($p<0.0001$) and compared to non-annealed samples at all degradation time points ($p<0.0001$). Statistical significance was determined at */Aa=$p<0.05$, **/Bb=$p<0.01$, ***/Cc=$p<0.001$, ****/Dd=$p<0.0001$. Letters are used to compare annealed samples at each degradation time point, whereas stars are used to compare

annealed samples to non-annealed samples at each degradation time point. Error bars represent standard deviations; n=10 for each condition.

3.5.2.3 Thermal analysis

Figure 3.9 shows DSC thermographs from annealing electrospun filaments at various times and temperatures. These graphs contain three characteristic regions: (1) an annealing peak (Ha), (2) a melting peak ranging from 90˚C to 110˚C (Hm) and (3) a melting point (Tm) with a maximum around 106˚C.

From the thermographs of the pristine filaments, shown in Figure 3.9a,c, and e, an increase in magnitude and a temperature shift of the annealing peak towards the melting peak were observed with both increased annealing time and temperature. This shift was most noticeable for samples annealed at 85% (Figure 3.9e). Annealing peaks appeared at 70-85˚C for samples annealed at 65˚C (Figure 3.9a) and 75˚C (Figure 3.9c), but appear at 90-100˚C for samples annealed at 85˚C (Figure 3.9e). The annealing peak was found at a lower temperature for samples annealed for 24 hours at 65˚C, compared to at 75˚C or 85˚C. Double melting peaks were observed for samples annealed at 65˚C and 75˚C, but only a single melting peak for samples annealed at 85˚C. Moreover, filaments annealed at 65˚C versus 75˚C or 85˚C had a lower melting peak. For all annealing times, there was a shift of the melting peak as annealing temperature increased. Overall crystallinity (measured by adding the melting and annealing peaks) decreased slightly with longer annealing times, although these results were not statistically significant (Figure 3.10).

From the thermographs of the samples degraded for 6 weeks, clear annealing peaks were still visible for samples annealed at 65˚C (Figure 3.9b), but were barely visible for samples annealed at 75˚C and 85˚C (Figure 3.9d and 3.9f, respectively). All degraded samples had single melting peaks. For samples annealed at 65˚C for any time period, there was a steady decrease in the melting peak compared to samples that were not annealed (Figure 3.9b). No clear changes in melting peak was observed for samples annealed at 75˚C and 85˚C.

Overall crystallinity didn't change significantly between different annealing times but had a larger standard deviation at longer annealing times, as shown in Figure 3.10. The difference in crystallinity between undegraded and degraded samples was statistically different at each annealing time point (3 hours, p=0.0039; 6 hours, p=0.0012; 9 hours, p=0.0082; 12 hours, p=0.0044; 24 hours, p=0.0024) as well as for samples not annealed (p=0.0009).

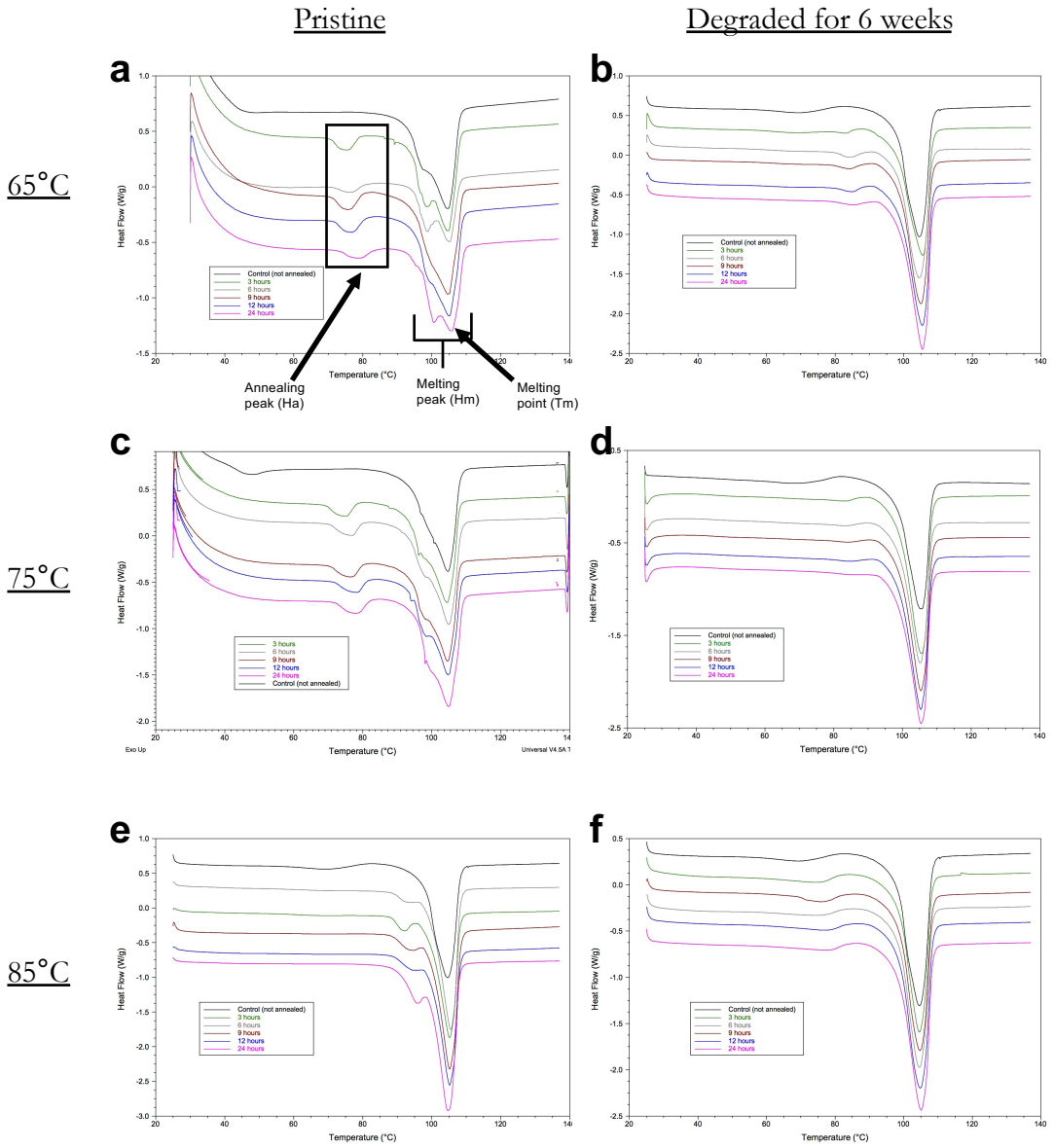


Figure 3.9: Representative Differential Scanning Calorimetry thermographs of PDO electrospun filaments annealed at different temperatures and subjected to in vitro degradation for 6 weeks. The scans contain three characteristic regions: an annealing peak (Ha), a melting peak (Hm), and a melting point (Tm). (a,c,e) Undegraded filaments annealed at (a) 65°C, (c) 75°C, (e) 85°C; (b,d,f) Filaments degraded in PBS at pH

7.4 for 6 weeks after annealing at (b) 65°C, (d) 75°C, (f) 85°C. The annealing peak appears to be shifting towards the melting peak at higher annealing times. A double melting peak can be observed for samples annealed at 65°C and 75°C, but disappears during degradation and is not visible for any samples annealed at 85°C.

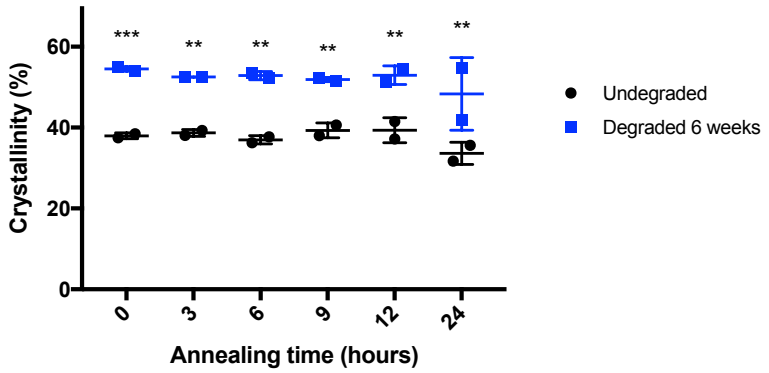


Figure 3.10: Changes in crystallinity of electrospun filaments annealed at 65°C for various times and subjected to in vitro degradation for 6 weeks. The difference in crystallinity between undegraded and degraded samples was statistically different at each annealing time point (3 hours, p=0.0039; 6 hours, p=0.0012; 9 hours, p=0.0082; 12 hours, p=0.0044; 24 hours, p=0.0024) as well as for samples not annealed (p=0.0009). Statistical significance was determined at *p<0.05, **p<0.01, ***p<0.001, ****p<0.0001. Error bars represent standard deviations; n=2 for each condition.

3.5.3 Melt-extruded yarn parameters and characteristics

3.5.3.1 Yarn morphology

Establishing material and processing conditions to yield a robust 300µm yarn made up of 10µm fibres formed the core of the processing trials at FET. Previous trials at FET using PDO had established a baseline set of conditions for producing a thicker monofilament. However, extruding PDO both as a multifilament generally, and specifically made up of 10µm fibres, had not been attempted. It was anticipated that PDO's slow crystallization rate would present challenges to achieving high strength and therefore required optimisation.

The parameters that were established over multiple trials are outlined in Table 3.5. Multiple spinneret types were investigated and it was determined that the most robust fibres meeting the required specifications could be achieved with a 28 hole spinneret with a

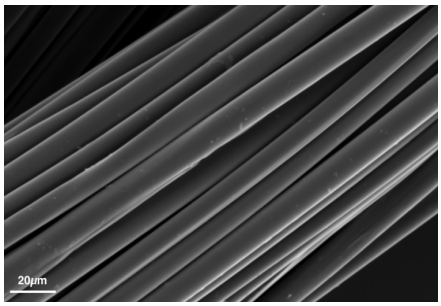
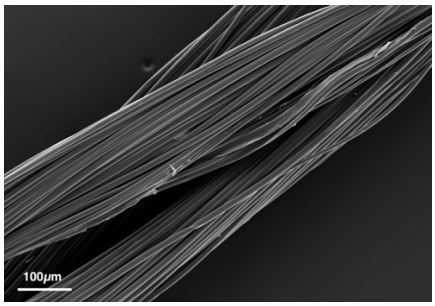
0.2mm diameter. These 28 fibres were extruded together to form a filament, which was fed over Godets heated at 65°C to apply strain and heat to induce crystallization. Then, 12 filaments were twisted to yield a final yarn with an overall diameter of 227μm, made up of 336 fibres each with a diameter of 10μm.

Table 3.5: Parameters for melt-extruding PDO yarns used in this thesis. Fibre indicates the smallest unit extruded through the spinneret; 28 fibres are extruded together to form a filament; 4 filaments were 'S' twisted, followed by 'Z' twisting 3 bundles to form a yarn with an overall diameter of around 278μm.

PDO Resin supplier	Riverpoint Medical
PDO Resin MFR	4.2g/10min @170°C
Extruder diameter	20mm
Spinneret properties	28 hole; 0.2mm in diameter, 0.8mm in length
Melt pump speed	1mL/rev
Twist parameters	4 filament 'S' twisted; 3 bundles 'Z' twisted
Total number of fibres in final twisted yarn	336

Fibre, filament, and yarn morphology and characteristics are presented in Table 3.6. The overall diameter was 9.2±1.2μm and 277±0.02μm for fibre and twisted yarn, respectively, meeting target diameters. The force at failure was 1.4±0.06N and 17.5±0.2N for the filament and twisted yarn, respectively. The filament had strain at failure of 20.2±2% compared to 25.4±0.6% for the twisted yarn. The porosity, mechanical properties, and cross-sectional area of the final yarn are shown in Table 3.7.

Table 3.6: Melt-extruded filament and yarn characteristics. Representative SEM images of fibre morphology, along with mechanical and material properties of filament and twisted yarns. Magnification 200-500x; scale bars represent 20μm for filaments and 100μm for twisted yarns.

	Filament	Twisted Yarn
Morphology		
Fibre diameter (μm)	9.2 ± 1.2	9.2 ± 1.2
Filament/yarn diameter (μm)	120.1 ± 0.5	277 ± 0.02

3.5.3.2 Mechanical analysis

Table 3.7 shows the mechanical properties and CSA of the final melt-extruded yarn. The force at failure was 17.5±0.2N and strain at break was 25.4±0.6%. The cross-sectional area measured from μCT was 74550±2934μm^2, and the CSA was 32781±756μm^2 when adjusted for porosity. Yarns were subjected to 12 weeks of degradation in PBS and changes in stress and strain were investigated. Stress at failure was statistically significantly lower at 6 weeks ($p=0.0002$) and at 12 weeks ($p<0.0001$), as shown in Figure 3.11a. Strain at failure did not significantly change over 12 weeks (Figure 3.11b).

Table 3.7: Melt-extruded yarn characteristics.

Force at failure (N)	17.5 ± 0.2
Strain at failure (%)	25.4 ± 0.6
Ultimate stress (MPa)	440.9 ± 4.6
Young's modulus	3468.67 ± 104.5
Cross-sectional area – full (μm^2)	74550 ± 2934
Cross-sectional area – adjusted for porosity (μm^2)	32781 ± 756

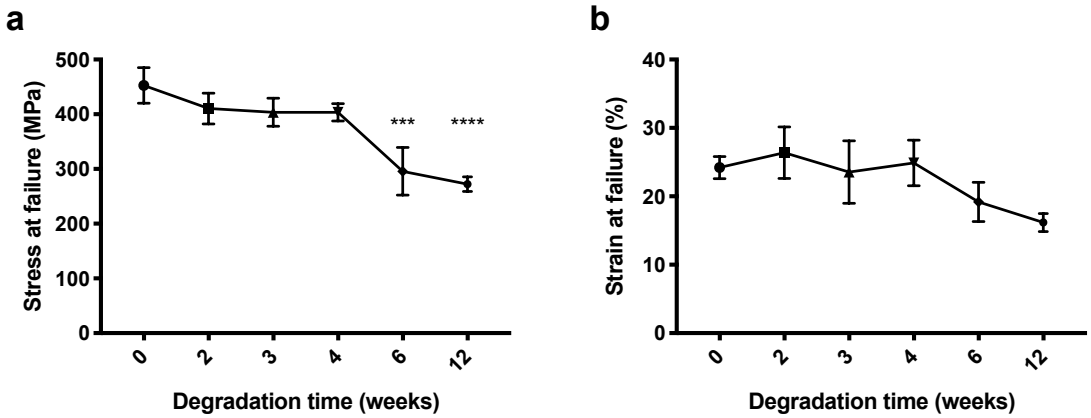


Figure 3.11: Changes in mechanical properties of melt-extruded yarns over 12 weeks of degradation. (a) Changes in stress at failure are recorded over 12 weeks of degradation in PBS at pH 7.4. Stress is significantly lower at 6 weeks ($p=0.0002$) and at 12 weeks ($p<0.0001$) compared to week 0; (b) Strain at failure did not significantly change over 12 weeks of degradation. Statistical significance was determined at $*p<0.05$, $**p<0.01$, $***p<0.001$, $****p<0.0001$. Error bars represent standard deviations; n=5 for each condition.

3.5.3.3 Thermal analysis

Prior to degradation, melt-extruded yarns had a narrow melting range with a melting point at 104˚C and weak endotherms around 10˚C and 50˚C (Figure 3.12). The overall crystallinity was 53.4%.

After *in vitro* degradation for 12 weeks, there was no change in percentage crystallinity (Figure 3.12a). There was a significant increase in the melting temperature at week 4 ($p<0.0001$), week 6 ($p<0.0001$), and week 12 ($p=0.0003$), compared to week 0 (Figure 3.12b). Figure 3.12c shows the thermal properties of extruded filaments over 12 weeks. There was a shift of the melting peak at week 4, and a narrowing and elongation of the peak at week 6 and week 12. It is worth noting that the error bars on crystallinity graph are much larger than those on the melting temperature graph. However, melting temperature is measured as a single point on the thermograph, whereas crystallinity is calculated from the addition of Hm and Ha (both of which are calculated by manually approximating the area on the thermograph).

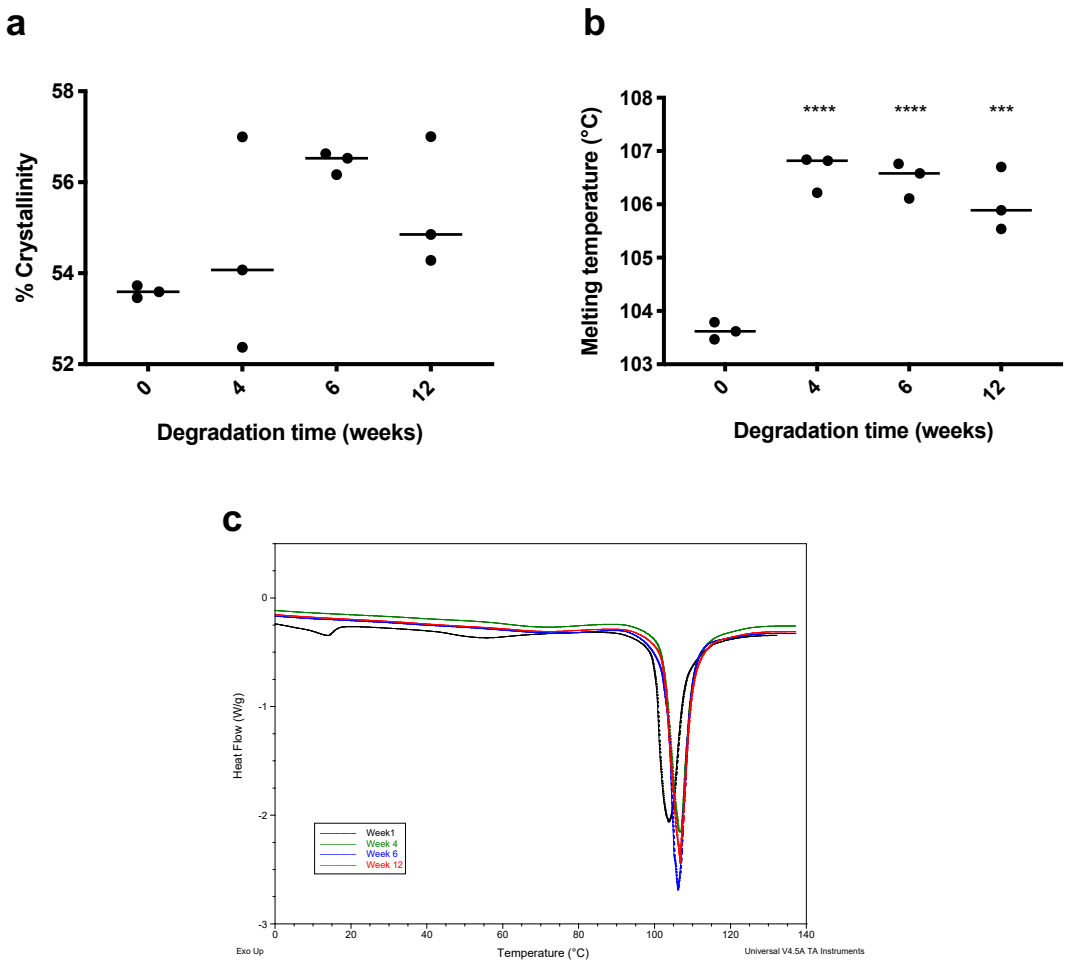


Figure 3.12: Changes in thermal properties of melt-extruded yarns over 12 weeks of in vitro degradation. (a) There were no statistically significant changes in crystallinity over 12 weeks; (b) Melting temperature was significantly higher at week 4 ($p<0.0001$), week 6 ($p<0.0001$), and week 12 ($p=0.0003$) compared to week 0; (c) DSC thermographs showed a shifting of the melting peak at week 4 and a narrowing of the melting peak at weeks 6 and 12. Statistical significance was determined at *$p<0.05$, **$p<0.01$, ***$p<0.001$, ****$p<0.0001$. Error bars represent standard deviations; n=3 for each condition.

3.5.4 Comparison between electrospun filaments and melt-extruded yarns

3.5.4.1 Mechanical properties

A representative stress-strain graph comparing electrospun filaments and melt-extruded yarns is shown in Figure 3.13. All filaments failed in the mid-substance region and electrospun filaments showed a characteristic toe, linear, and yield regions. Tensile testing was used to calculate the force at break (N), ultimate stress (MPa), breaking strain (%), and Young's modulus (MPa) (Figure 3.14). The force at failure was 11.5 fold higher for

extruded yarns ($p<0.0001$). The strain at failure was 22.7±2% and 26.8±2% for extruded yarns and electrospun filaments, respectively ($p=0.0201$). Stress at failure was 440.9±5MPa for extruded yarns and 214.4±9MPa for electrospun filaments ($p<0.0001$). The Young's modulus of extruded yarns was significantly higher than that of electrospun filaments (3468.7±121MPa compared to 1603.8±163MPa, respectively, $p<0.0001$).

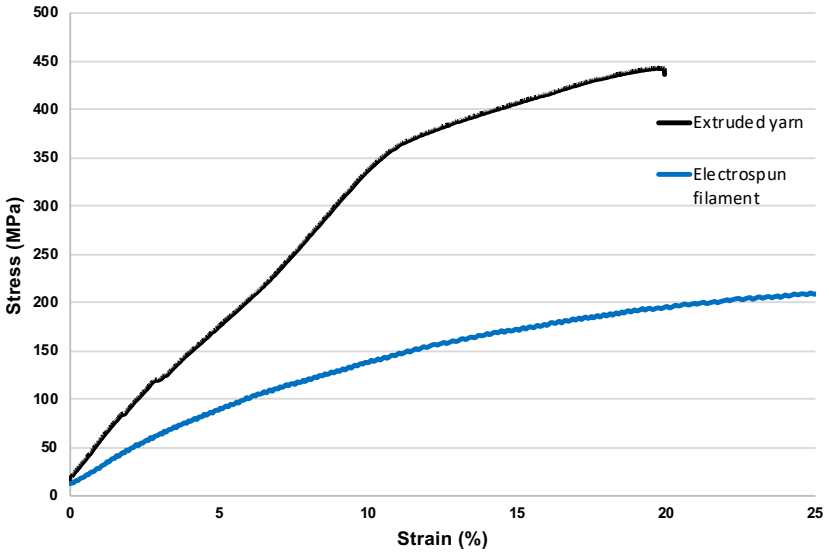


Figure 3.13: Representative stress-strain graph comparing an electrospun filament and a melt-extruded yarn.

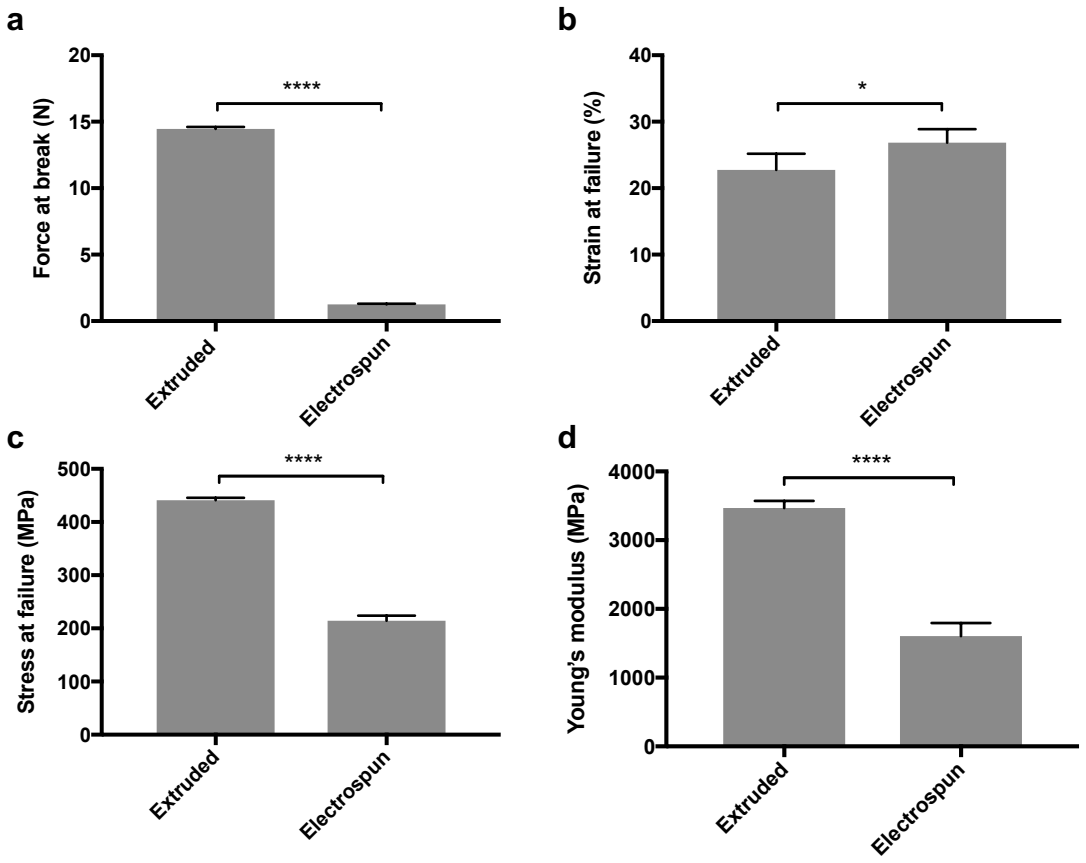


Figure 3.14: Mechanical properties of electrospun filaments and melt-extruded yarns. (a) Force at break (N) was significantly higher for extruded yarns ($p<0.0001$); (b) Strain at failure (%) was significantly higher for electrospun filaments ($p=0.0201$); (c) Stress at failure (MPa) was significantly higher for extruded yarns ($p<0.0001$); Young's modulus (MPa) was significantly higher for extruded yarns ($p<0.0001$). Statistical significance was determined at *$p<0.05$, **$p<0.01$, ***$p<0.001$, ****$p<0.0001$. Error bars represent standard deviations; n=5 for all conditions.

3.5.4.2 Thermal properties

DSC analysis showed significant differences in the thermal properties of electrospun filaments, extruded filaments, and the raw PDO resin (Figure 3.15). Electrospun filaments had a broad double melting peak with a melting point at 104.5°C. The extruded peak had a similar melting point of 104°C, but the melting peak was elongated and more narrow compared to that of the electrospun filament. The melting peak of the raw PDO resin was significantly higher at 109.6°C ($p<0.0001$) and the curve was elongated. There were also differences in crystallinity between the materials tested (Figure 3.15c). Electrospun filament had the lowest overall crystallinity of 41.1%, compared to the extruded yarn

(53.4%, p=0.0002), and the resin (55.1%, p<0.0001). Integrating the first cooling peak indicates the degree of crystallinity upon cooling. The electrospun filament exhibited a rapid recrystallisation over a narrow temperature range, the extruded yarn exhibited a broader crystallisation over a wide temperature range, and the resin exhibited a small crystallisation over the lowest temperature range. These results are presented in Figure B.3 in the Appendix and suggest that the resin is less amorphous than the electrospun filament and extruded yarn.

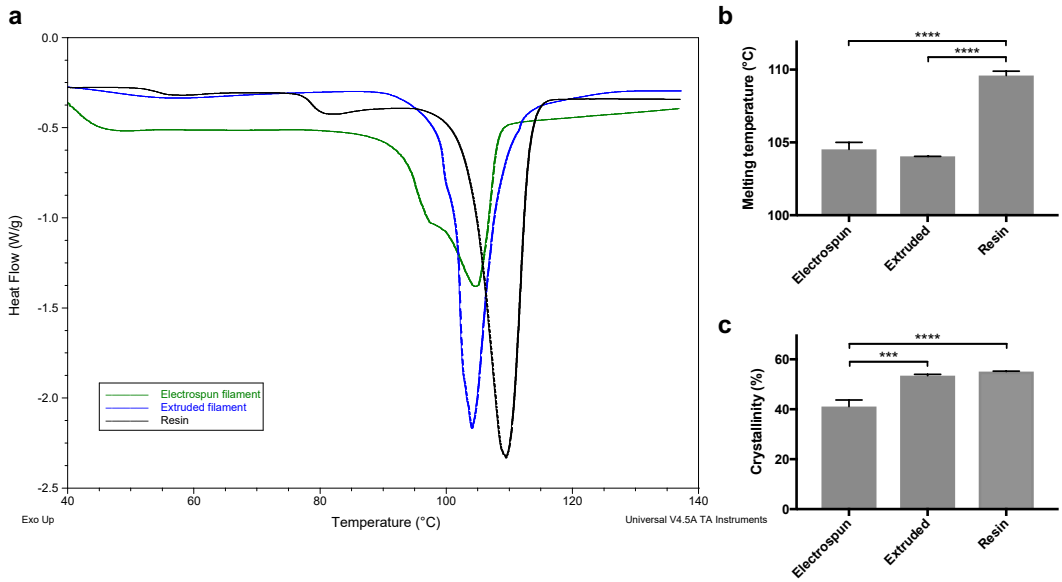


Figure 3.15: Representative thermal data comparing PDO electrospun filaments, melt-extruded yarns, and raw resin. (a) DSC thermograph. The melting peak of the resin is more narrow, elongated, and shifted to the right, compared to that of the electrospun filament or extruded yarn; (b) Melting temperature is highest for the resin compared to the extruded yarn (p<0.0001) and electrospun filament (p<0.0001); (c) Overall crystallinity (%) was significantly lower for the electrospun filament, compared to the extruded yarn (p=0.0002) or resin (p<0.0001). Statistical significance was determined at *p<0.05, **p<0.01, ***p<0.001, ****p<0.0001. Error bars represent standard deviations; n=3 for each condition.

3.5.4.3 Porosity and pore size characterisation

Comparisons in average pore diameter and overall porosity between electrospun filament and melt-extruded yarn are presented in Figure 3.16. The overall porosity was 79.8±10.3% for electrospun filaments and 56.3±1.6% for extruded filaments. The average pore diameter was significantly higher for electrospun filaments (1480.2±116nm), compared to

extruded yarns (537.4±7.6nm), p=0.0076. The most frequent pore diameters, which are represented by the local maxima on the mercury porosimetry intrusion curves (Figure B4 in the Appendix), were approximately 1μm and 80μm for the electrospun filament and 7μm and 80μm for the melt-extruded yarns.

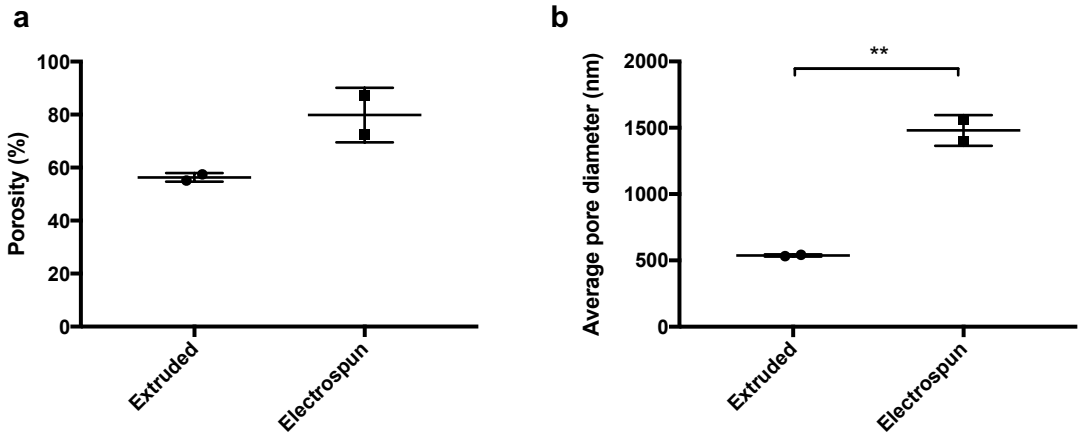


Figure 3.16: Hg porosimetry data comparing electrospun filaments and melt-extruded yarns. (a) Overall porosity (%) was not significantly different between the materials; (b) Average pore diameter (nm) was significant higher in electrospun filaments compared to extruded yarns (p=0.0076). Statistical significance was determined at *p<0.05, **p<0.01, ***p<0.001, ****p<0.0001. Error bars represent standard deviations; n=2 for all conditions.

3.5.4.4 Summary of electrospun filaments and melt-extruded yarn characteristics

Table 3.8 Summary of electrospun filament and melt-extruded yarn characteristics.

	Electrospun filament	Melt-extruded yarn
Diameter (μm)	226.4 ± 1	278 ± 0.02
Cross-sectional area – full (μm^2)	7089 ± 897	74550 ± 2934
Cross-sectional area – adjusted for porosity (μm^2)	5859 ± 741	32781 ± 756
Diameter of base fibre (μm)	0.86 ± 0.2	9.2 ± 1.2
Stress (MPa)	214.4 ± 9	440.9 ± 5
Strain (%)	26.8 ± 2	22.7 ± 2
Young's Modulus (MPa)	1603.8 ± 163	3468.7 ± 46
Crystallinity (%)	41.12	53.42
Melting temperature (°C)	104.50	104.04
Porosity (%)	79.80 ± 10.3	56.33 ± 1.6
Most frequent pore diameters (μm)	1μm and 80μm	7μm and 80μm
Degradation time to 75% of maximal stress	~ 6 weeks	< 6 weeks
Degradation time to 75% of strain at failure	< 4 weeks	< 8 weeks

3.6 Discussion

The aims of this chapter were threefold: to explore annealing as a method to improve the tensile strength of electrospun filaments, to develop methods to reliably melt-extrude yarns made up of 10μm fibres, and finally, to compare the properties of electrospun and extruded materials. The first part of this discussion focuses on the production of electrospinning filaments and the potential for annealing to improve filament properties. The second section addresses the production and characterisation of melt-extruded filaments and yarns. Finally, electrospun and extruded properties are compared in the context of their intended use in supporting tendon repair. In each section, the limitations of the experiments and results are considered.

3.6.1 Optimisation and reproducibility of electrospun filaments

Electrospun filaments were exclusively fabricated on a self-built electrospinning set up that was developed prior to the start of this thesis. Early exploratory electrospinning work and the annealing experiment was performed with chemical grade PDO resin from Sigma Aldrich, because it was readily available and a constant supply of polymer was needed. HFIP was chosen as the solvent for its easy dissolution and its fast evaporation in electrospinning conditions.[225] Although measuring residual HFIP solvent should be investigated more in the near future, previous *in vitro* and *in vivo* work has shown no adverse effect of using this type and concentration of HFIP.[128,165]

It was necessary to spin Sigma PDO at a 9% weight/volume ratio to avoid irregular fibre formation. However, even at a 9% concentration, there were significant variations in filament properties and fibres exceeded 1μm in diameter. It was hypothesized that more homogenous filament production could be achieved by controlling electrospinning parameters, PDO supplier, and storage conditions. While it is assumed that PDO from

different suppliers would be slightly different, the effects of different suppliers on fibre production highlighted the importance of the polymer's molecular properties on the robustness and reproducibility of filaments with homogeneous fibre diameters. One challenge in ensuring consistency between polymer solutions is that manufacturers don't provide information about crucial polymer properties, such as its molecular weight. Moreover, depending on manufacturer, PDO resin can be supplied in aliquots or in a single larger batch. Sometimes the resin is characterised in terms of its viscosity and MFR, but not always. It is possible that the changes in fibre diameter and mechanical properties due to different PDO resin properties could also be affecting local fibre properties, which were outside of the scope of this thesis. In light of these solution variables, and to ensure homogeneity for the work in this thesis, all electrospinning was performed using polymer batches with similar MFRs. Moreover, large volumes of high concentration stock solutions of PDO in HFIP were used to minimise hydrolytic degradation.

Because the long-term goal for this work is to translate a safe, implantable device, this thesis moved towards exclusively using a medical grade polymer from Riverpoint medical, which is compliant with regulatory standards to facilitate clinical translation of the device. Moreover, pyridine was added to improve the conductivity of the solution, thereby reducing fibre diameter and improving filament homogeneity.[107,210] From 2016 onwards, Riverpoint PDO at a 7% weight/volume ratio with the addition of a pyridine concentration below 100ppm was used for electrospinning.

Collecting electrospun filaments on a conductive wire offers some distinct advantages over other collection surfaces, which are covered in Chapter 2.6.1.2. The use of a small contact area for collection means that the setup is particularly sensitive to differences between polymer solutions or perturbations of the electric field, such as a build-up of static charges on the walls of the spinning hood. Empirically, it was seen that the deposition length (the length of the wire where fibres were initially deposited) influenced the quality of filament

produced. Larger deposit lengths correlated with improved filament mechanical properties and smaller fibre diameters. It was hypothesized that the deposition length is related to the conductivity of the solution and this relationship was later systematically investigated and confirmed by a member of the Carr group.[210] Pyridine was added to increase the solution's conductivity, which, as expected, resulted in more homogenous, robust filaments with smaller fibre diameters. Although collecting electrospun filaments on a wire has only been optimised for PDO so far, further work is investigating this setup to electrospin polycaprolactone (PCL) filaments to use as scaffolds for ACL repair.

Because electrospun filaments are too weak to process into multifilament yarns, mechanical drawing is commonly employed to improve fibre alignment, induce crystallisation, and reduce strain. Moreover, to imitate native tendon ECM, the synthetic fibres must be highly aligned. In clean room manufacturing environments, industrial drawing machines are commonly used to stretch filaments either during or after the filament collection process. In this thesis, filaments were hand-stretched. Although this method has the potential to introduce more variability between stretched samples, there was limited access to the industrial drawing machine. Stretching lengthened the filament between 3-4 times its initial length and aligned the fibres along the direction of the filament and reduced the fibre diameter to $0.86 \pm 0.2 \mu m$, meeting the submicron fibre target. While stretching was sufficient to align fibres and reduce fibre size (Table 3.3 in the results section), further processing was needed to improve its tensile strength. It was thought that annealing could be employed to further reduce strain and improve strength, which is explored in the following section.

3.6.2 Annealing modulates mechanical properties and *in vitro* degradation of electrospun filaments

Semi crystalline polymers, such as PDO, consist of highly orientated folded chain crystals connected by many highly stretched tie chains in the amorphous regions separating the crystals. Annealing changes the microstructure adopted by the polymer chains and these changes strongly influence the mechanical properties of fibres.[132] This study explored a large range of annealing time and temperature points, which had not previously been explored for electrospun PDO. It was found that annealing at 65˚C marginally improved the strength of the filament, but had a more pronounced influence on reducing the strain to failure. Controlling the strain of the material has important implications for its intended future use as a suture. For example, for its use as a bridging device, it needs to stretch enough to allow for physiological movement, but not so much as to lead to a gap formation between the tissue.

Filaments annealed at low temperatures (65˚C) for any length of time were stronger and less brittle than filaments annealed at high temperatures (75˚C/85˚C), which implies there was more of a temperature than a time effect on mechanical properties within the parameters tested. The minimal, and in many cases detrimental, effect of annealing on mechanical properties of PDO were unexpected. In contrast, studies exploring annealing electrospun PLLA found that annealing substantially increased the tensile strength.[139,141,226] Tan et al found that annealing electrospun PLLA at 75˚C resulted in a 150% increase in the Young's modulus and a 10% decrease in fibre diameter (melting temperature of as-spun PLLA fibres: 182˚C).[139] They also chose a long annealing time of 24 hours to ensure all rearrangements of polymer chains were complete.[139] Weir et al annealed compression-moulded and extruded PLLA fibres at a higher temperature of 120˚C for 4 hours, and observed a slight increase in Young's modulus from 620 MPa to 658 MPa, but a decrease in tensile strength, extension at maximum, and stress at yield for annealed PLLA.[141] This

experiment used a different polymer, processing technique, and annealing parameters compared to that from Tan & Lim (2006) and Weir et al (2004) making the results difficult to compare. Nevertheless, the results of both studies indicate there are optimal annealing parameters to influence the fibre mechanical properties for a specific polymer and processing method. While there haven't been many studies specifically exploring the annealing temperature-time relationship on electrospun fibre properties of a given polymer, it is hypothesized that there is more of a temperature than time effect of annealing on fibre properties.[140] Annealing PDO for longer than 9 hours had detrimental effects to the fibre properties. In contrast, it had been previously shown that annealing PLLA for longer than 24 hours improved fibre properties.[139,140] As a result, it is highly likely that the annealing temperature in this experiment had not been optimised and annealing at a lower temperature would enable longer annealing times without compromising mechanical properties.

Thermal analysis showed changes in location and size of annealing peaks, which are associated with changes occurring in the amorphous phase of the material.[150] The increase in the heat of fusion with higher annealing temperature and time is correlated with increased crystallinity, assuming proportionality to the heat of fusion of 100% crystalline PDO.[141,154] Overall, the measured increase in crystallinity and shifting of annealing peaks points to changes in crystal sizes and morphologies due to rearrangements of the polymer chains in the amorphous regions.[132,139] Since the mobility of polymer chains increases with temperature, more annealing may lead to rearrangement of the polymer chains in the amorphous regions, ultimately resulting in bigger crystalline structures. Bonnet et al summarized five proposed models explaining how changes to the endothermic annealing peak reflect crystal morphologies, crystal sizes, and melting-recrystallization behaviours.[150] Two major challenges in developing these models and interpreting annealing results stemmed from a lack of standardized methods to explain annealing changes; additionally,

many annealing-related changes are dependent on factors internal to the material, such as prior thermal history, physical state, chemical structure and composition.[152,227]

Due to the large surface area to volume ratio of electrospun materials, controlling the timeline and by-products of degradation are critical. Controlling the timeline of degradation means that the device provides initial mechanical support and that the degradation kinetics match the growth rate of new tissue. Controlling the by-products of degradation means that the device needs to be safe to implant and safe over the lifetime of the implant. Because hydrolytic degradation happens through the selected cleaving of amorphous regions[132,154], and annealing changes the organisation of these amorphous structures, the effect of annealing on the degradation of PDO filaments was also of interest here. In the current study, it was found that annealing at high temperatures caused faster degradation and a rapid loss of mechanical properties, however, annealing closer at 65˚C seemed to make the amorphous regions less susceptible to degradation. Annealing at 65˚C showed a significant improvement compared to non-annealed filaments over 6 weeks of degradation, indicating that under the same conditions, annealing at 65˚C can reduce the risk of filament failure over time. Annealing could be used to tailor the degradation rate by extending the strength retention and maintaining fibre alignment for at least 6 weeks, which is the critical period after surgery where effective healing is needed.[228]

Thermal analysis showed that double melting peaks disappeared at 6 weeks of degradation and that there was a gradual increase in the melting peak temperature with degradation time for samples annealed at all times and temperatures. These results suggest structural changes in the material, potentially similar to what Ooi et al observed studying the degradation of commercial PDSII sutures.[132] They proposed that during degradation, hydrolytic scissioning of chain segments in the amorphous region led to a higher mobility of chain regions and a lack of unity between amorphous and crystalline regions, resulting in a loss of tensile strength.[132] In the current study, annealing at high temperatures caused

faster degradation and a rapid loss of mechanical properties, however annealing at 65°C made the amorphous domains less susceptible to degradation. The ability to modulate the degradation profile with annealing may become useful to tune the properties of biomaterials without altering the base polymer. This might help better match the degradation of the suture and gradual loss of mechanical properties with the new matrix deposition within the structure.

It is important to critically evaluate the magnitude of the change in filament properties due to annealing. Three changes in filament properties were observed after annealing. First, annealing did not substantially change the tensile strength of filaments, but had a detrimental effect on tensile strength at high annealing temperatures. Second, strain at failure of filaments decreased at every annealing time and temperature. Thirdly, fibre degradation (measured by visual inspection and tensile testing) was slower when annealed at low temperatures and unchanged or faster when annealed at high temperatures. The original objective of this chapter was to investigate whether annealing could be a method to increase the tensile strength of electrospun filaments. Based on these observations, it is not believed that annealing has a substantial impact on the tensile strength of electrospun PDO filaments. Indeed, it was shown that annealing at high temperatures or for longer times can be detrimental to filament properties. It is not recommended to anneal electrospun filaments without substantial optimisation to ensure that the heat treatment is not damaging the fibres.

However, although annealing didn't increase the tensile strength of the filaments, all annealing conditions resulted in a reduction in the strain at break, compared to non-annealed samples. Conventional sutures fail at 20-40% strain, whereas non-annealed filaments fail at 60-70% strain. Annealing, regardless of time or temperature, resulted in a decrease in the strain at failure, which could be important for its application as a suture to

prevent gap formation between the tendon and suture. Moreover, annealing at most conditions reduced the standard deviation of the mechanical test and none of the annealing conditions increased the standard deviation of the tests. For these two reasons, annealing electrospun filaments at 65˚C for 3 hours continues to be part of the manufacturing process for this suture and other PDO electrospun materials developed in the Carr group.

Finally, it is worth considering why annealing did not have a greater effect on improving filament properties. There are many studies that found that annealing increases the tensile strength and young's modulus of electrospun fibres made from a range of semi-crystalline synthetic polymers. While it is not clear how much optimisation was needed to achieve the final parameters reported in the publications, the overwhelming positive effect of annealing on tensile properties call into question why the same effects were not observed here. When this study was conducted in 2016, there were no studies found that explored the effect of annealing electrospun PDO. In 2019, Zhang et al explored the effect of annealing on the mechanical properties and degradation of raw PDO that had been injection moulded.[229] They annealed PDO at 50˚C and 80˚C for 8 hours and investigated the mechanical and thermal properties and changes due to degradation in PBS using the same methods as the current study. Annealing at 50°C for 8 hours improved the yield strength by 31%, and annealing at 80°C for 8 hours enhanced yield strength by 38.3% compared with those without annealing. In contrast, this study compared 65°C to 85°C and found minimal change in tensile strength at 65°C and detrimental changes at 85°C. The detrimental changes in filaments properties were substantial after annealing in a relatively small temperature window, which is not consistent with other studies. It is possible, therefore, that the changes observed were more influenced by variations in fibre crystalline structure prior to annealing than due to changes from annealing. Future work should employ wide angle X-Ray Powder Diffraction (XPS) or another characterisation

technique for a mechanistic understanding of the crystallinity of PDO electrospun filaments prior to annealing.

It is believed that annealing PDO electrospun filaments could improve their tensile strength more than was found in this study. However, in the absence of a more detailed structural characterisation of the filaments and optimisation of annealing parameters, other ways to improve the strength of filaments, such as increasing the concentration of the polymer solution for electrospinning, would be more reliable.

There are several strengths and limitations to be considered. First, the largest improvement in filament properties due to annealing was observed using the lowest time and temperature, suggesting further improvements may be possible. Further work investigating the structural homogeneity of electrospun filaments and annealing at lower temperatures are needed to optimize processing parameters. However, it has been shown that within the parameters tested, annealing can improve strength retention and fibre alignment after *in vitro* degradation. This has not been previously reported and has important implications for the potential clinical use of electrospun materials to support and guide tissue regrowth. This study showed that annealing can be used to tailor the degradation rate by extending strength retention and maintaining fibre alignment for at least 6 weeks, which is the critical period after surgery where effective healing is needed.[228] Moreover, this study focused on a phenomenological exploration of annealing time and temperature effects on mechanical performance. Future work aiming at a mechanistic understanding of the observed changes should adopt more detailed analysis of structure, such as XRD or Fourier Transformation Infrared Spectroscopy (FT-IR), to determine how changes in proportion and organisation of amorphous and crystalline regions affect the mechanical properties.

3.6.3 Production of melt-extruded multifilament yarns made up of 10μm fibres

The main aim of this work was to consistently fabricate multifilament yarns with a target diameter of 300μm, made up of fibres with a 10μm diameter. It was important that the base fibres did not exceed the 10μm diameter target, as there is some evidence that larger fibres are too big relative to native cellular ECM, contributing to reduced cell attachment and proliferation.[106,133,134]

The fundamental requirement to achieving a high tenacity filament was to maximise molecular organisation and alignment in the filament, which is mainly dependent on the processing conditions used for spinning and drawing of the fibres. As for electrospinning, there are a large number of material and processing variables in melt-extrusion and investigating and optimising these variables was at the core of the trials at FET. Fortunately, it was possible to achieve the yarn, filament, and fibre targets with the same medical grade Riverpoint PDO that was used for electrospinning.

The rationale for specifically exploring melt-extrusion as a technique was because it is the most common industrial method to fabricate medical textiles and many melt-extruded monofilament PDO sutures are on the market.[132,230] Moreover, FET, an experienced fibre extrusion company was eager to work together to achieve the targets in this chapter. Previous trials at FET using PDO had established a baseline set of conditions for monofilament production of PDO; however, multifilament production of a different, medical grade PDO resin required extensive further investigation.

It is unlikely that fabricating melt-extruded multifilament PDO made up of 10μm fibres had previously been attempted. Because of the slow crystallization rate of PDO, historically other similar polymers presented fewer potential hurdles during the melt-extrusion process. Further, achieving a 10μm fibre target is on the lower range of the capabilities of melt-extrusion instrumentation. Most melt-extruded sutures and scaffolds

on the market are made up of 20-30μm fibres, which requires substantially different processing parameters.[185] Suture grade PGA, another absorbable polyester, is extruded at FET as a multifilament yarn on a regular basis, typically using a 24-hole spinneret. Such a yarn has individual filaments with a diameter of around 16μm and a yarn diameter of around 100μm. Using the know-how developed from extruding multifilament PGA, it was hypothesised that a bulkier yarn with diameter closer to 300μm and a filament diameter of 10μm, could be achieved by combining several bundles of twisted filaments ensure a stable final yarn. Establishing baseline processing conditions were done with FET sourced PDO, but it was found that Riverpoint PDO behaved substantially differently. Melt-extruding Riverpoint medical grade PDO proved initially challenging because of the lack of processing information that was available from the manufacturers. Riverpoint provided PDO resin in small 100g pouches with reported MFR values, which ranged from 1.2-5.9g/10min. Because 400g of resin was needed for the extrusion trials, it was hypothesized that a mixture of resin pouches with similar MFRs would enable the fabrication of a more robust filament. As a result, two lots of PDO with MFRs of 3.9g/10min and 4.5g/10min at 170°C were blended at a 1:1 ratio to yield a final blend of 400g, which enabled the production of more robust and reproducible fibres.

Changes in mechanical and thermal properties following 12 weeks of degradation showed that the yarn retained its mechanical integrity (measured by changes in stress and strain) up to 6 weeks, which is a crucial period after implantation where mechanical support is needed in order for healing to take place.[228] Thermal analysis showed a stable overall crystallinity, but a shifting of the melting peaks at all degradation time points and a narrowing of the melting peak at higher degradation time points. This might reflect the preferential hydrolytic degradation of the amorphous regions of the polymer after the first 4 weeks, leading to a relative increase in crystallinity. Overall, these results suggest similar

structural changes occurring due to degradation, similar to what was seen during the degradation of PDO electrospun filaments, as well as the degradation of commercial PDS melt-extruded sutures.[132]

3.6.4 Differences in mechanical and material properties between electrospun filaments and melt-extruded yarns

In this section, the properties of electrospun filaments and melt-extruded yarns were compared. Because they are intended to be used together as a combination device in Chapter 4, understanding how each material behaves individually is important in determining how they should be combined. The melt-extruded yarn is intended to provide structural and mechanical support and the electrospun filament to provide biological augmentation using biophysical cues. As a result, the properties of electrospun filaments and melt-extruded yarns were compared in terms of their mechanical properties, thermal properties, and overall porosity. The force at break was 11.5 fold higher for the melt-extruded yarns, which was an expected result due to its 10 times larger fibre diameter compared to electrospun fibres. The stress at failure and Young's modulus were both around 2 times larger for the melt-extruded yarns compared to electrospun filaments. This may be due to the much larger fibre diameter and lower porosity of melt-extruded compared to electrospun filaments. While this represents a large difference in stiffness, it is not clear how stiff a suture for soft tissue repair should be and how its stiffness should change as it degrades over time.

Thermal analysis showed similar melting temperatures for melt-extruded yarns and electrospun filaments, but changes in peak size and location (and a higher crystallinity) for melt-extruded filaments. This is likely due to substantial processing differences. Melt-extruded filaments undergo various heat-cool cycles throughout the fabrication process. The raw resin is completed melted, then cooled as it's drawn out through the spinneret. It

is then heated again close to its crystallization temperature as it's passed over heated godets to induce chain elongation and stretch the fibres to their final morphology. The first reheat cycle, measured by DSC, indicated the degree of crystallinity upon cooling. Melt-extruded filaments demonstrated a wider melting range and a broader crystallisation over a wider temperature range, indicating a larger range of crystal morphologies. Conversely, electrospun filaments exhibited a rapid recrystallisation over a narrow temperature range, indicating a more narrow range of crystal morphologies. However, a larger re-crystallisation is usually consistent with increased chain mobility, as the relative amorphous and crystalline regions reorganise in response to heating and cooling. Melt-extruded yarns, despite their more mobile polymer chains, had a slower degradation rate. It is likely that the larger fibre size and smaller filament porosity resulted in slower degradation, compared to electrospun filaments which have smaller sized fibres and are more porous. It is not thought that the differences in melting temperatures are meaningful for their intended use as a combination device. However, the differences in degradation rate could allow for a stepwise degradation process that prolongs the structure support afforded by the suture and spreads out the acidic by-products of degradation over a longer time.

Finally, Hg porosimetry showed around 20% higher overall porosity for electrospun filaments. In terms of pore diameter, both electrospun and extruded yarns had pores that were 80μm in diameter and electrospun filaments additionally had pores that were 1μm in diameter, reflecting the smaller pores between fibres.

3.7 Conclusions

The overall aim of this work was to produce continuous PDO fibres using both electrospinning and melt-extrusion techniques. Using electrospinning, it was possible to fabricate filaments with an overall diameter of 226μm, made of <1μm fibres. Using melt-extrusion, it was possible to fabricate multifilaments with an overall diameter of 278μm, made up of 10μm fibres.

Annealing was explored as a post-processing method to increase the tensile strength of electrospun filaments. It was determined that annealing at 65°C for 3 hours resulted in a marginal increase in tensile strength, but had a more substantial effect on maintaining fibre alignment and failure stress after *in vitro* degradation. As a result, for PDO electrospun filaments, annealing appears to be more useful as a method to tailor degradation rate than to increase the tensile strength of pristine fibres.

Electrospun filaments and extruded multifilament yarns, despite having a similar overall diameter, had substantial differences in their mechanical properties, thermal behaviour, and overall porosity. Melt-extruded yarns were 2 times stiffer with a 11.5 fold increase in force at failure, compared to electrospun filaments. Both materials had a similar melting temperature, but melt-extruded yarns had a higher crystallinity and slower degradation rate. Electrospun filaments were around 20% more porous overall and exhibited a larger pore diameter. Future work should develop a more mechanistic understanding of the underlying structural changes to optimise the crystallinity and tensile strength of PDO filaments.

Table 3.9: Chapter 3 in context.

Evidence before this work	Added value of this work	Implications of this work
Annealing has traditionally been used a treatment to improve the strength and stiffness of electrospun materials.	For PDO electrospun filaments, annealing was better able to tailor degradation rate than improve mechanical properties of pristine fibres. Annealing could be used to extend strength retention and maintain fibre alignment for at least 6 weeks, which is the critical period after surgery where effective healing is needed. Annealing at high temperatures had detrimental effects on filament properties.	Modulating the degradation profile with annealing may be useful to tune the properties of a biomaterial without altering the base polymer used. Electrospun PDO filaments should only be annealed when fibre structure is characterised and annealing parameters are optimised to ensure that annealing is not harmful to fibre properties.
Most current surgical sutures use 20-30μm sized melt-extruded fibres. Extruding multifilament yarns made up of smaller fibres had not been explored for PDO.	It is possible to melt-extrude PDO multifilament yarns made up of 'cell-sized' 10μm fibres.	The ability to melt-extrude 10μm fibres enables future investigation of the influence of micrometre scale fibre diameters on cell biology. Melt-extruded fibres have similar mechanical and handling properties to existing sutures, making them clinically useful.
Many electrospun devices in development, such as augmentation sutures and scaffolds, are intended to replace the inert, melt-extruded sutures that are currently surgically used. However, electrospun and melt-extruded materials have not been directly compared.	Melt-extruded yarns are more likely to mechanically support surgical repair. They have a 11.5 times higher force at failure and are 2 times stiffer. Electrospun filaments are more likely to biologically support surgical repair. They are 20% more porous, have a larger pore diameter, and a faster degradation rate.	This thorough characterisation of electrospun and melt-extruded materials could influence the range of potential clinical applications. This can be done by adjusting the ratio of electrospun to melt-extruded fibres to the structural, biological, and mechanical requirements of the specific target tissue.

Chapter 4

Development of multifilament sutures

4.1 Abstract

4.1.1 Background

Electrospun sutures have shown initial biological promise for soft tissue repair. However, their development has been restricted to short hand-braided yarns, which are too mechanically weak and bulky for surgical use. An ideal augmentation suture will be porous, reproducible, degradable, have a high tensile strength, and be usable by surgeons. This chapter investigated using a scalable, industrial braiding process to fabricate multifilament yarns. Further, this chapter hypothesized that a hybrid suture, made up of an electrospun filament sheath and melt-extruded cores, can meet targets for use as an augmentation suture. Finally, electrospun and hybrid sutures were compared to each other and to currently used surgical sutures.

4.1.2 Materials and methods

Industrial braiding was used to fabricate four electrospun sutures with a range of sizes, mechanical properties, and porosities, by changing the number and orientation of electrospun filaments. Hybrid sutures were developed by adding melt-extruded yarns through the centre of the electrospun suture to create core-sheath yarns. The electrospun and hybrid sutures were compared to surgical sutures PDS and Vicryl, in terms of their tensile properties, porosity using Hg porosimetry and microCT, as well as thermal properties using DSC.

4.1.3 Results

Industrial braiding improved the reproducibility and production rate of electrospun sutures, compared to hand-braiding or twisting. It was possible to control porosity through changing filament orientation and improve the tensile strength by increasing the filament number. Hybrid sutures, with an electrospun sheath and melt-extruded core, were fabricated. Both electrospun and hybrid sutures were less stiff and more porous than surgical sutures. A hybrid suture made up of a 12 filament electrospun sheath with 4 melt-extruded yarn cores met the target suture criteria.

4.1.4 Conclusions

Incorporating electrospun filaments into existing industrial braiding production lines improves the control over structural properties, the reproducibility of the product, and the overall production volume. This is important for both fundamental studies on material properties and cell-material interactions, as well for developing sutures that meet quality control standards and are scalable for clinical trials. A hybrid suture made up of a 12 filament electrospun sheath and 4 melt-extruded yarns in the core was designed to meet the demands of tendon: electrospun fibres on the outside approximate ECM properties and will be in initial contact with biological fluids, while the melt-extruded fibres in the core provide prolonged mechanical support. This combination makes it the most promising prototype to take forward for biological characterisation in Chapter 5.

4.2 Introduction

There is growing interest in using electrospun materials to augment the surgical repair of soft tissues, such as tendons and ligaments. Electrospinning continuous filaments has the potential to overcome upscaling, structural, and mechanical limitations of electrospun discontinuous sheets. Similar to sheets, continuous filaments are made up of submicron or nanoscale fibres, but additionally, they can be upscaled with industrial textile machinery into multifilament yarns. These multifilament yarns could be used as bioactive sutures that employ biomimicry on two levels: through its submicron fibres mimicking tendon fibrils and through its hierarchical architecture similar to that of native ECM.[126,128,133,148,161–165] As a result of its similar structure to native tissue, multifilament yarns would display similar mechanical behaviour during physiological loading. Moreover, tuning its composition could enable its degradation kinetics to match the formation of new tissue.

Textile manufacturing is widely used in the medical market to create medical yarns, such as sutures. Sutures are mostly produced by braiding, which offers some advantages over other textile methods, including reduced fraying of the yarn, slight improvement in mechanical strength, and better control over structural properties such as porosity and pore size.[126] To date, braided sutures are predominantly made by melt-extruding fibres from synthetic polymers and their development is largely driven by industry. It is becoming apparent that although sutures are marketed as inert or biocompatible, no implanted material is truly biologically inactive. Indeed, there is evidence that the suture-tendon interface represents the weakest link in the repair and could be the cause for some repair failures.[55–57,74,81] Braiding electrospun filaments into multifilament yarns for use as sutures, has shown initial promise for soft tissue applications. Braided electrospun sutures support tenogenic differentiation of hMSCs and display similar mechanical behaviour to native tendons.[148,162,163] However, to date, braided electrospun sutures have only been handmade

into short sections, which limits the control over structural properties, the reproducibility of the product, and the overall production volume.[126,133,148,161–163]

The delay in upscaling hand-made sutures can be partially attributed to the sensitivity of the electrospinning process and the difficulty in producing continuous filaments. Moreover, electrospun fibres are delicate and sensitive to mechanical damage and environmental degradation, limiting its use with current textile machinery. Together, these challenges have limited the commercialization and clinical translation of many promising electrospun products.

Prior to the start of this thesis, the Carr group developed a technique to produce continuous electrospun filaments. However the possibility of using industrial textile machinery to process the filaments into sutures had remained unexplored.[129,153] The use of an industrial braiding machine would allow for a higher degree of control over the suture's structural properties than can be achieved through hand-braiding. As well, a wider variety of braiding designs can be explored by adjusting the orientation and distribution of fibres and the possibility of adding inlay yarns. Moreover, the use of an industrial machine can increase the rate of production to meet the demand for clinical trials and later commercialisation.[155]

Prior to investigating the use of an industrial braiding machine, pilot work explored hand-twisting and hand-braiding. This work showed that electrospun sutures had much lower tensile strength compared to surgical sutures (Figure C.1 in the Appendix). To improve their tensile strength would require adding additional electrospun filaments, rendering the suture too bulky for use with surgical equipment and too difficult to handle by surgeons. It was hypothesized that a combination of electrospun material with another, stronger, material in a core-sheath configuration might improve the yarn's mechanical properties while still retaining a size comparable to current sutures on the market. In Chapter 3, melt-extruded yarns with improved mechanical properties were developed. A hybrid suture,

combining electrospun filaments with supportive, robust, melt-extruded yarns could potentially improve the mechanical properties while retaining biophysical cues, porosity, and surface area necessary to encourage cell-mediated repair.[124–128]

One aim of this thesis is to offer a translatable design process that is applied to the development of a novel suture for rotator cuff repair. This is done by defining the design requirements for a suture to augment tendon repair, followed by developing specific target criteria for this thesis. The relevant criteria that guide the experiments in this chapter are outlined in detail in Chapter 2.10.3 and Table 2.5.

The criteria from Table 2.5 that are relevant for this chapter are repeated below:

- The suture diameter should be between 0.4-0.7mm to be usable by surgeons and compatible with surgical equipment for rotator cuff repair.
- The electrospun component should be on the outside of the hybrid suture.
- The suture should have a high porosity (>50%) and have pore sizes greater than 10μm .
- The force at failure should be 50-100N and strain at break should be between 25-40%.

Various electrospun and hybrid (electrospun/melt-extruded) braided suture prototypes are explored based on these criteria and compared to existing surgical sutures. Finally, one suture candidate that meets target criteria will be taken forward for further biological characterisation in Chapter 5. One main research challenge in this chapter was to fabricate homogenous and continuous electrospun filaments that were sufficiently long and robust enough to explore if braiding was possible. Moreover, because there was limited access to the braiding machine in Germany, it was a challenge to anticipate the braid structure and ratio of electrospun and extruded filaments that would meet the target design criteria.

4.3 Objectives and hypotheses

The overall objective of this chapter is to develop a multifilament yarn that meets the criteria for use as a suture for tendon repair.

- Objective 1: To manufacture electrospun sutures with a range of structural and mechanical properties.

- Objective 2: To combine an electrospun sheath with melt-extruded cores into a hybrid suture with improved tensile strength.

- Objective 3: To compare electrospun and hybrid braided sutures to existing surgical sutures used for tendon repair.

- Objective 4: To select a promising suture candidate, based on target criteria, to take forward for further testing.

The overall hypothesis is that industrial braiding will enable more flexibility in manufacturing electrospun and hybrid sutures to meet the target criteria. Hybrid sutures are expected to have more similar properties to currently used surgical sutures.

- Hypothesis 1: Using a braiding machine will enable the modulation of suture properties and increase the rate of production of multifilament yarns.

- Hypothesis 2: A combination of electrospun filaments and melt-extruded yarns will improve structural and mechanical properties of sutures.

- Hypothesis 3: Compared to currently used surgical sutures, the electrospun sutures will be larger and weaker. Hybrid sutures will have gross tensile strength more closely matching surgical sutures, but be less porous than electrospun sutures.

- Hypothesis 4: A hybrid suture will meet the target criteria for tendon repair and be taken forward for further testing.

4.4 Materials and methods

4.4.1 Material fabrication and preparation

4.4.1.1 Electrospun filament production

Electrospun filaments were fabricated using a custom setup with a wire collector as described in Chapter 3.4.1. Collected filaments were manually drawn and annealed at 65°C for 3 hours, before being stored in a desiccator prior to use.

4.4.1.2 Melt-extruded yarn production

Melt-extruded yarns were fabricated according to the methods outlined in Chapter 3.4.3. Yarns were kept in a desiccator prior to use.

4.4.2 Braided suture production

4.4.2.1 Electrospun braided sutures

The rationale for the braid designs were based, to some extent, on the availability of braiding machines. Three companies were considered for this work: Cobra braiding machinery[231] based in the UK, MB Medical braider[232] based in China, and Herzog[233] based in Germany. These companies were considered because, based on their website, they had substantial experience in braiding sutures for medical applications. Ultimately, Herzog was chosen because of the company's proximity to the UK, willingness to engage in an R&D capacity with Oxford, and availability of equipment. Although Herzog had never braided electrospun filaments before, they had years of experience of working with Ethicon on developing multifilament sutures. Moreover, Herzog, unlike other braiding companies, owned a Variation Braiding Machine (VF 1/(4–32)-140, Herzog Braiding Machine, Oldenburg, Germany), a new technology that allows for manually changeable carriers to produce braids between 4 and 32 carriers. This was important for this project, as the optimal braid pattern and number of filaments that would be needed to meet the design

targets was not known. Although the Variation braider allows for much more flexibility than one with a fixed number of carriers, the setup was limited to 7 braid configurations arranged in a square, rectangle, or circular configuration, using 8, 12, 16, 20, 24, 28, or 32 carriers (Figure 4.1). Based on the configuration of the carriers, it was anticipated that the 8 and 32 carrier configuration would result in a square braid, the 12 and 16 configuration would result in a rectangle braid, and the 20, 24, and 28 braid would result in a rounded braid with a hollow core.

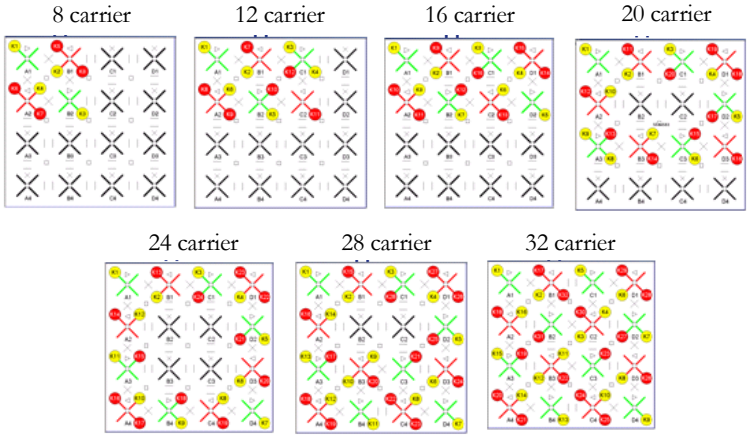


Figure 4.1: Possible carrier configurations using the Variation Braiding Machine. There were 7 possible configurations using 8, 12, 16, 20, 24, 28, or 32 carriers. Based on the configuration of the carriers, it was anticipated that the 8 and 32 carrier configuration would result in a square braid, the 12 and 16 configuration would result in a rectangle braid, and the 20, 24, and 28 braid would result in a rounded braid with a hollow core. Figure modified from Herzog.[233]

Electrospun filament was brought to Herzog in Germany in order to develop the braiding protocols. Based on pilot work in the company using melt-extruded filament of a similar diameter to the electrospun filament (200-300μm), it was determined that the 28 and 32 carrier configuration would yield braids outside of the 0.4-0.7mm target range. The project was limited by the volume of electrospun filament (1000 meters) and because the projected ribbon structure of the 12 and 16 carrier configuration was similar, only the 12 carrier braid was chosen. It was also known based on hand-braiding sutures, that a 8 filament braid would fail at less than 10N and be too weak for use as a suture. It was decided that 2

filaments per carrier would be used in the 8 carrier configuration, to yield a rounded 16 filament braid.

As a result, four different braids composed of 12, 16, 20, and 24 filaments were made using 12, 8, 20, and 24 fine yarn carrier configurations (carrier type AFDh 80, Herzog, Oldenburg, Germany), respectively. These configurations were chosen based on compatibility with the Variation Braiding Machine and falling in the desired suture diameter range of 0.4-0.7mm.

4.4.2.2 Hybrid braided suture

Two hybrid braided sutures prototypes were fabricated. One had a 12 filament sheath with a core of 4 melt-extruded yarns and the other had a 20 filament sheath with a core of 4 melt-extruded yarns. The Variation Braiding Machine (VF 1/(4–32)-140, Herzog Braiding Machine, Oldenburg, Germany) was set up with 12 or 20 fine yarn carriers with electrospun filaments. Additionally, 4 fine yarn carriers were positioned under the braiding machine, so that 4 melt-extruded yarns could be fed through the centre of the electrospun filament carriers continuously as the cores.

4.4.3 Visual analysis

An optical micrometre (Keyence LS-7010MR laser with Keyence LS-7601 monitor, Milton Keynes, UK) was used to measure suture diameter by averaging 5 measurements, which was then converted to USP suture sizing standardisation (Appendix A.1). A Plugable Optical Digital Microscope (Plugable USB2-micro-250X, Redmond, WA, USA) was used to obtain images of the final sutures. SEM images were taken following methods outlined in Chapter 3.4.3.

4.4.4 Mercury porosimetry

Overall porosity and pore size distribution was determined by Hg porosimetry, following methods in Chapter 3.4.6. Two experimental repeats were performed for all electrospun, hybrid, and control surgical sutures. Unless stated otherwise, the control surgical sutures were size 2-0 PDS and size 0 Vicryl. Moreover, this method was used to measure the porosity of the hybrid suture components separately, namely the electrospun sheath and melt-extruded cores.

4.4.5 MicroCT analysis

Braided sutures were scanned over a length of 1mm using micro-computed tomography (μCT). The sutures were placed in a tube that was mounted vertically on the μCT scanner (SkyScan 1172, SkyScan, Kontich, Belgium). The samples were scanned at an isotropic pixel size between 1-3μm. The scan parameters were set at a voltage of 40 kV; a current of 250 mA without filter and 900 projections were used. The images were reconstructed using NRecon software (SkyScan 1172, SkyScan, Kontich, Belgium) using the Feldkamp algorithm with a beam-hardening correction of 40% and a smoothing of 4. CTAn software version 1.12 (Bruker microCT, Kontich, Belgium) was used for processing and stacking the reconstructions into a tubular structure. ImageJ software version 1.52a (National Institute of Health, Bethesda, MD, USA) was used to measure the suture's CSA, diameter, and overall porosity. The CSA calculations for stress measurements were obtained by multiplying the μCT solid CSA by the percentage of solid area obtained from Hg porosimetry (Equation 4.1).

$$CSA = \text{solid CSA by } \mu CT \times (1 - \text{porosity by Hg porosimetry})$$

Equation 4.1: Cross-sectional area calculation for multifilament sutures.

CSA = cross-sectional area

μCT = micro-computed tomography (microCT)

Hg porosimetry = mercury intrusion porosimetry

4.4.6 Tensile testing

Electrospun and hybrid sutures were sterilised with 70% ethanol for 2 hours, left to air dry overnight, then annealed at 65°C for 3 hours, and finally vacuum dried prior to testing to remove any residual liquid. All sutures were mechanically tested to failure at room temperature. Sutures were cut into 20cm sections for testing. Braided sutures were tested knotless at a crosshead speed of 50mm/min with a 5kN load cell until failure, using a Zwick tensile testing machine (Zwick Roell Group, USA) and the custom grips used in Chapter 3 (Figure 3.4). The strain rate and specimen length were chosen based on similar experiments in the literature[210,213,214] and in complying with ISO standard 2062:2009[215].

The force at break (N), ultimate stress (MPa), grip-to-grip breaking strain (%), and Young's modulus (MPa) were recorded, Five experimental repeats were performed for all electrospun, hybrid, and control sutures. Viscoelastic properties, such as creep or stress relaxation, were outside of the scope of this thesis and should be considered in future work using dynamic mechanical analysis (DMA) or testing different strain rates or cycling loading to develop a more complete picture of the mechanical behaviour of multifilament sutures.

4.4.7 Thermal testing

Thermal testing was performed using a DSC, following the protocol in Chapter 3.4.7. Three experimental repeats were performed for all electrospun, hybrid, and control sutures.

4.4.8 Statistical analyses

A Kolmogorov-Smirnov test was used to determine normality for each experiment. With the exception of the Hg porosimetry testing, the data from each experiment and each material tested was normally distributed. The number of repeats in the Hg porosimetry testing was too low to test for normality, so non-parametric testing was performed.

For all quantitative analyses, data are presented as mean ± standard deviation. GraphPad Prism version 7 software (GraphPad Software Inc., La Jolla, CA, USA) was used for all statistical analyses and statistical significance was determined at $p<0.05$. In some figures, uppercase and lowercase letters represent statistics. An uppercase letter (i.e., "A") designates that material as significantly greater than every other material with the corresponding lowercase letter (i.e., "a").

For testing the effect of different braiding carrier configurations on the resulting mechanical properties of braided sutures, a one-way ANOVA with Tukey's multiple comparisons testing was used. This statistical test was also used to measure the porosity differences between the electrospun sheath, melt-extruded cores, and resulting hybrid suture.

For testing the effect of suture properties on porosity, a one-way ANOVA with Tukey's multiple comparisons was used. This same test was also used to compare the mechanical and thermal properties between different suture types.

4.5 Results

4.5.1 Fabrication of base materials

Around 1000 meters of electrospun filament was fabricated at a production speed of 5 meters of stretched filament per hour. Electrospun filament was fabricated in a clean room environment with a low particulate and microbial environment, suitable for manufacturing materials for clinical trials. The clean room was equipped with two custom electrospinning machines and purpose built collection units (Godet Rolls, Retech, Switzerland) which could be run overnight. Compared to the electrospun filament production in Chapter 3, the clean room production line was more industrial, requiring fewer manual steps. Over 24 hours, it was possible to spin 240 meters of continuous filament in the clean room set-up, compared to 40 meters in the research laboratory set-up used in Chapter 3.

4.5.2 Electrospun braided sutures

4.5.2.1 Braiding parameters and braid characteristics

Braided sutures were manufactured from continuous electrospun filaments using the Variation Braiding Machine, shown in Figure 4.2a and 4.2b. The filaments were under substantial tension as they passed through yarn carriers and any sections that were not fully hand stretched were drawn out at that point. The braiding speed was about 1–3 meters per minute depending on machine input parameters. Based on pilot hand-braiding data (Figure C.1 in the Appendix), the use of this machine represented an increase in production speed of about 500%. The various arrangements of carriers used and optical microscope pictures of the final suture morphology are shown in Figure 4.2c. It can be noted that the 8 carrier arrangement formed a closed square, the 12 carrier braid formed a more flat, ribbon-like structure, whereas the 20 and 24 carrier arrangements formed an open structure with a hollow centre. Table 4.1 shows the braiding machine parameters, braid size, and braid angle for all suture configurations. The four braid configurations yielded sutures with

diameters between 0.5-1mm. Braiding with 8 carriers and 2 filaments/carrier produced a yarn with a diameter of 0.5±0.1mm, which corresponds to USP size 2, whereas braiding with 24 carriers and 1 filament/carrier produced a yarn with a diameter of 1.0±0.1mm, which corresponding to USP size 8. The 8 carrier braid had 16 filaments as it was projected that one filament per carrier would not yield a strong enough suture.

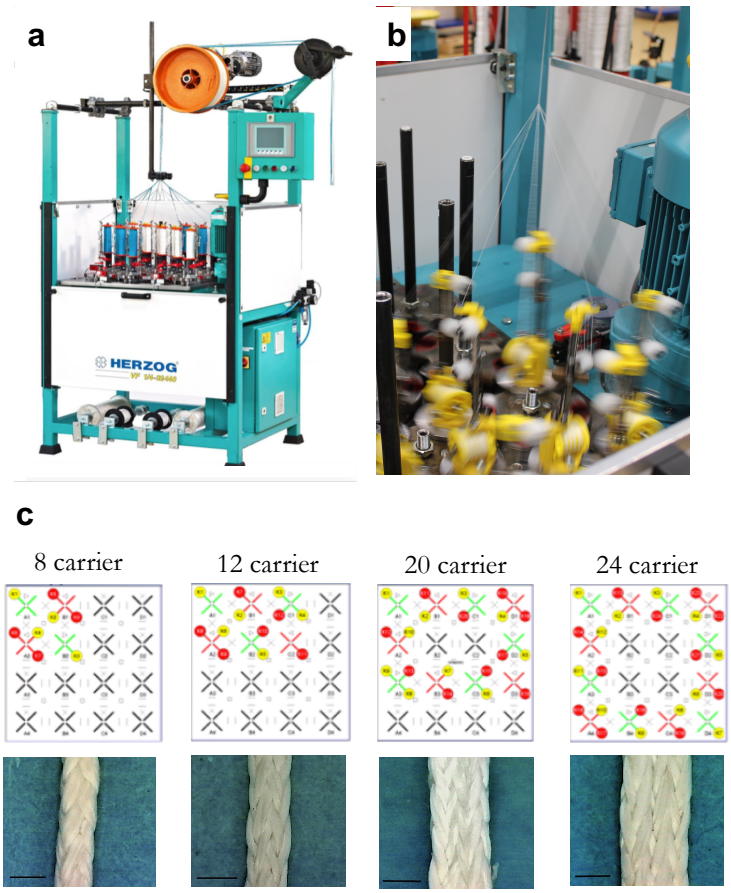


Figure 4.2: Fabrication of multifilament electrospun sutures using an industrial braiding machine. (a) Variation Braiding Machine, with manually changeable crossings, was used to fabricate braided sutures; (b) Electrospun filaments are braided into a continuous suture; (c) The different carrier arrangements used for braiding are shown above and optical microscope pictures of the final sutures are shown below. It can be noted that the 8 and 12 carrier arrangement form a relatively closed structure, whereas the 20 and 24 carrier arrangement form an open structure with a hollow centre. Scale bars are 500µm. Figure modified from Herzog.[233]

Table 4.1: Electrospun braided suture parameters and characteristics.

Nr. of carriers	Nr. of filaments	Nr. of filaments/carrier	Braid size (mm)	Braid size (USP)	Braid angle (°)	Hollow centre
12	12	1	0.6 (± 0.1)	1	68 (± 2)	No
8	16	2	0.5 (± 0.1)	0	52 (± 2)	No
20	20	1	0.8 (± 0.1)	4	70 (± 2)	Yes
24	24	1	1.0 (± 0.1)	6	74 (± 1)	Yes

4.5.2.2 Porosity

Figure 4.3 shows μCT cross-sectional and longitudinal scans and SEM images of the electrospun sutures. As anticipated, the 8 carrier configuration resulted in a tight square structure, whereas the 12, 20, and 24 carrier arrangements resulted in more flat structures. The hollow centre of the suture can be seen in the μCT images of the 20 and 24 carrier braids (Figure 4.3g and 4.3j, respectively). Braiding with 8,12, 20, and 24 carriers resulted in yarns with braid angles of 52±2°, 68±2°, 70±2°, and 74±1°, respectively. Braid characteristics obtained from μCT scans and Hg porosimetry results are given in Table 4.2. The overall porosity measured from μCT cross sections was 60±7%, 50±2%, 60±0%, and 66±2% for sutures braided with 12, 8, 20, and 24 carriers, respectively. The 12 filament suture had the smallest CSA of 0.3±0.1mm^2, whereas the 24 filament braid had the largest CSA of 1.0±0.1mm^2 . Overall porosity measured from Hg porosimetry was 67±3%, 60±1%, 65±3%, and 76±2% for sutures braided with 12, 8, 20, and 24 carriers, respectively. The average pore diameter was 386±86nm, 302±80nm, 722±96nm, and 1040±122nm for sutures braided with 12, 8, 20, and 24 carriers, respectively.

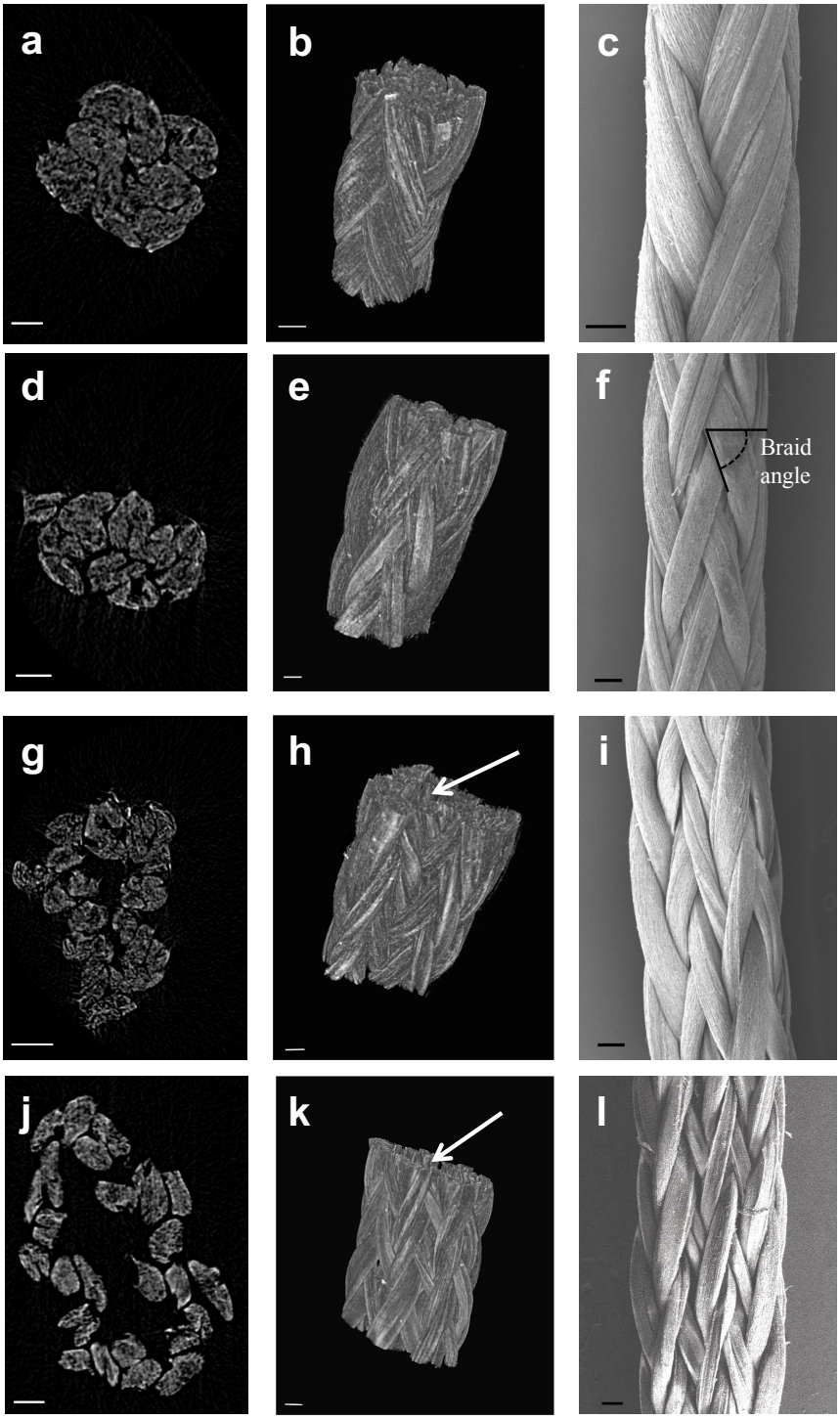


Figure 4.3: μCT scans and SEM images of braided electrospun sutures. A cross-sectional scan taken by μCT is shown in (a), (d), (g), and (j), for the 8, 12, 20, and 24 carrier braids, respectively. A longitudinal scan taken by μCT is shown in (b), (e), (h), and (k) for the 8, 12, 20, and 24 carrier braids, respectively. The hollow centre of the suture can be seen in the images of the 20 and 24 carrier braids, (g) and (j), respectively, which are also indicated by white arrows. SEM images were taken to determine suture morphology and used to measure braid angle, as shown in (c), (f), (i), and (l), for the 8, 12, 20, and 24 carrier braids, respectively. Scale bars are 100μm for μCT scans and 200μm for SEM images.

Table 4.2: μCT and Hg porosimetry data of electrospun braided sutures.

Number of carriers (nr. of filaments)	μCT		Hg porosimetry	
	Porosity (%)	CSA (mm^2)	Porosity (%)	Average pore diameter (nm)
12(12)	60 ± 7	0.3 ± 0.1	67 ± 3	386.5 ± 86
8(16)	50 ± 2	0.4 ± 0.1	60 ± 1	302.1 ± 80
20(20)	60 ± 0	0.7 ± 0.1	65 ± 3	722.4 ± 96
24(24)	66 ± 2	1.0 ± 0.1	76 ± 2	1039.9 ± 122

4.5.2.3 Tensile testing

A representative stress-strain graph of the electrospun sutures is shown in Figure 4.4a with an emphasis on the toe region in Figure 4.4b. All sutures failed in the mid-substance region and showed characteristic toe, linear, and yield regions. The nonlinear mechanical behaviour of the toe region at 0%–3% of the strain, shown in Figure 4.4b, was likely due to the reorganisation of filaments during early stages of loading. The linear region formed at around 3% of strain, at which point most fibres were engaged. The materials yielded from 12% strain with classic post yield softening.

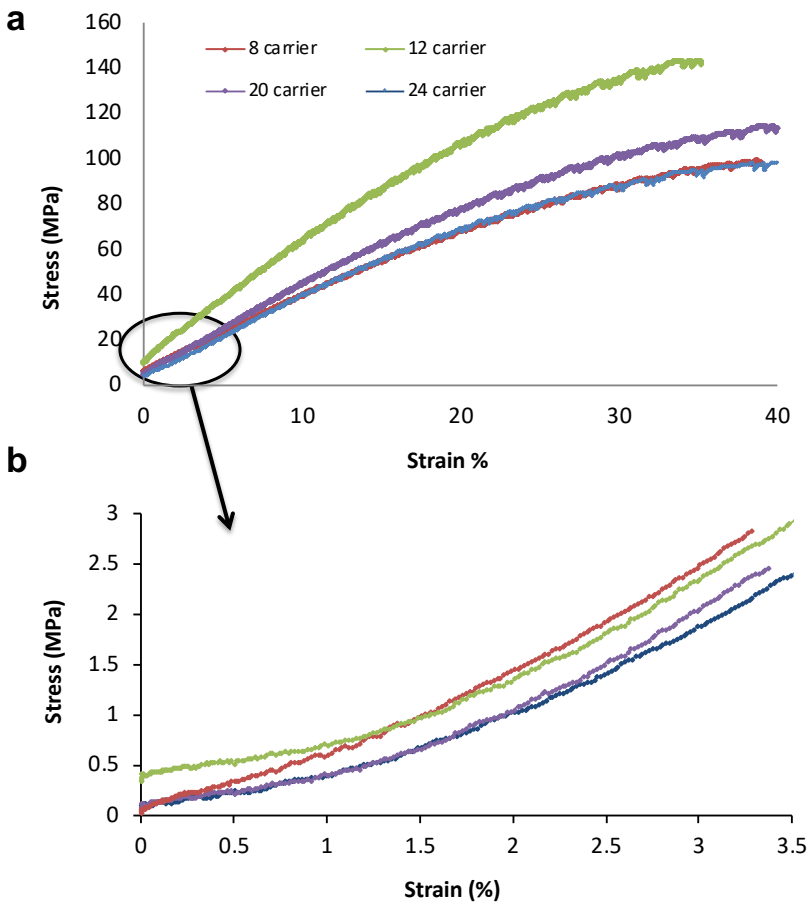


Figure 4.4: Representative stress-strain graph of braided electrospun sutures. (a) Tensile testing of 8,12,20, and 24 carrier braids showing characteristic toe, linear, and yield regions; (b) Emphasis on the toe region at 0–3% of strain shows nonlinear mechanical behaviour due to reorganization of filaments during early stages of loading.

Tensile testing of the electrospun sutures until failure was used to calculate the force at break (N), ultimate stress (MPa), breaking strain (%), as well as Young's modulus (MPa) (Figure 4.5). The average force at break was significantly different between all braids, and higher for braids made with 20 filaments (21±1N) and 24 filaments (25±1N), compared with 16 filaments (15±1N) and 12 filaments (13±1N), as shown in Figure 4.5a. The ultimate stress was significantly higher for the 12 filament braid (190±32MPa), compared with that of the 16 filament (128±17MPa, $p=0.0008$), 20 filament (132±11MPa, $p=0.0016$), and 24 filament braids (114±9MPa, $p<0.0001$), as shown in Figure 4.5c. The Young's modulus was significantly higher for the 12 filament braid (747±8MPa), compared

with that of the 16 filament (475±25MPa, p<0.0001) and 24 filament braid (490±38MPa, p<0.0001), as shown in Figure 4.5d.

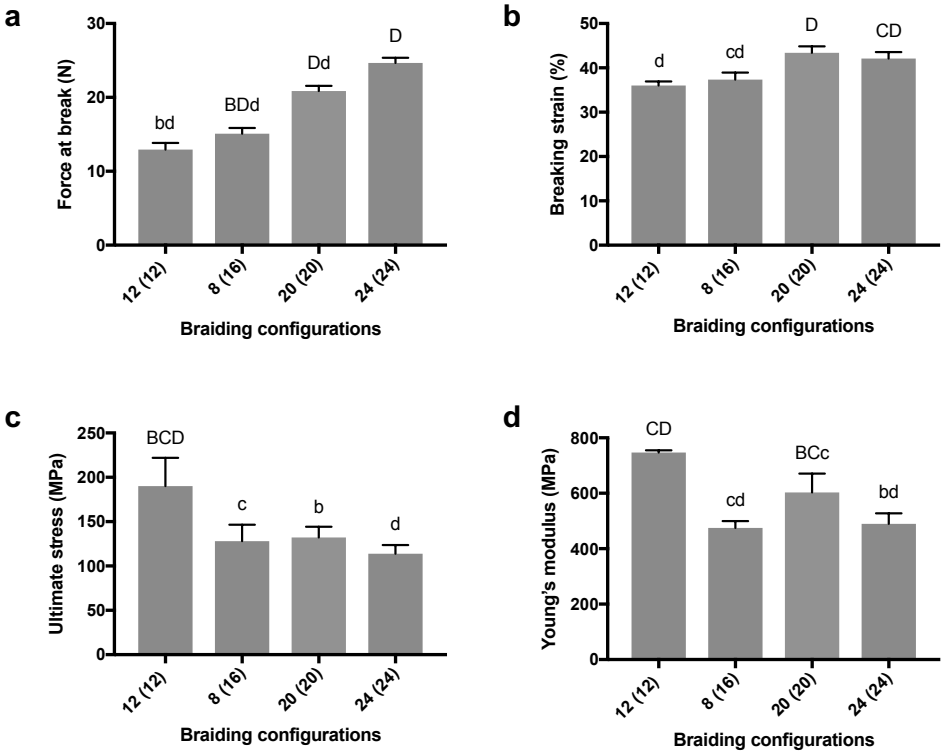


Figure 4.5: Tensile properties of braided electrospun sutures. Braiding configuration is described as: number of braiding carriers(number of filaments), i.e. 8(16). (a) Force at break (N) was highest for the 24 filament braid compared to all other configurations (p<0.0001); (b) Breaking strain (%) was higher for 20 and 24 filament braids to 12 and 16 filament braids (p<0.001); (c) Ultimate stress (MPa) was highest for 12 filament braid, compared to the 16 (p=0.0008), 20 (p=0.0016), and 24 filament braids (p=0.0001); (d) Young's modulus (MPa) was highest for the 12 and 20 filament braid compared to the 16 and 24 filament braid (p<0.01). Statistical significance was determined at Aa=p<0.05, Bb=p<0.01, Cc=p<0.001, Dd=p<0.0001. Error bars represent standard deviations; n=5 for each condition.

4.5.3 Hybrid braided sutures

4.5.3.1 Braiding parameters and braid characteristics

Hybrid braided sutures were manufactured with continuous electrospun filaments and melt-extruded cores, using the Variation Braiding Machine. Based on the results of

braiding electrospun sutures (Chapter 4.5.2), it was determined that the 8 carrier braid was too weak and tight to add cores to improve its tensile strength. The 24 carrier braid exceeded the target suture diameter. As a result, the 12 and 20 carriers were used to make hybrid sutures. Table 4.3 shows the braiding configuration, braid size, and braid angle of the hybrid sutures. The smaller suture was made up of a 12 filament electrospun sheath with 4 melt-extruded cores, denoted as a 12(4). The larger suture was made up of a 20 filament sheath with 4 melt-extruded cores, denoted as 20(4). The resulting braid size was 0.69±0.02mm for 12(4) and 0.84±0.02 for 20(4). Figure 4.6 shows a μCT cross-section and an SEM image of the 12(4) and 20(4) hybrid braided sutures. The extruded cores can be seen in the centre of the μCT scan of the 12(4) suture and are also visible on the surface of the sutures, as seen on SEM. This same observation is not true for the 20(4), where only the electrospun filaments are visible on the surface of the suture.

Table 4.3: Hybrid braided suture parameters and characteristics.

Nr. of electrospun filaments in the sheath	Nr. of melt-extruded yarns used in the core	Braid size (mm)	Braid size (USP)	Braid angle (°)
12	4	0.69 ± 0.02	4	56.3 ± 3
20	4	0.84 ± 0.02	6	66.2 ± 4

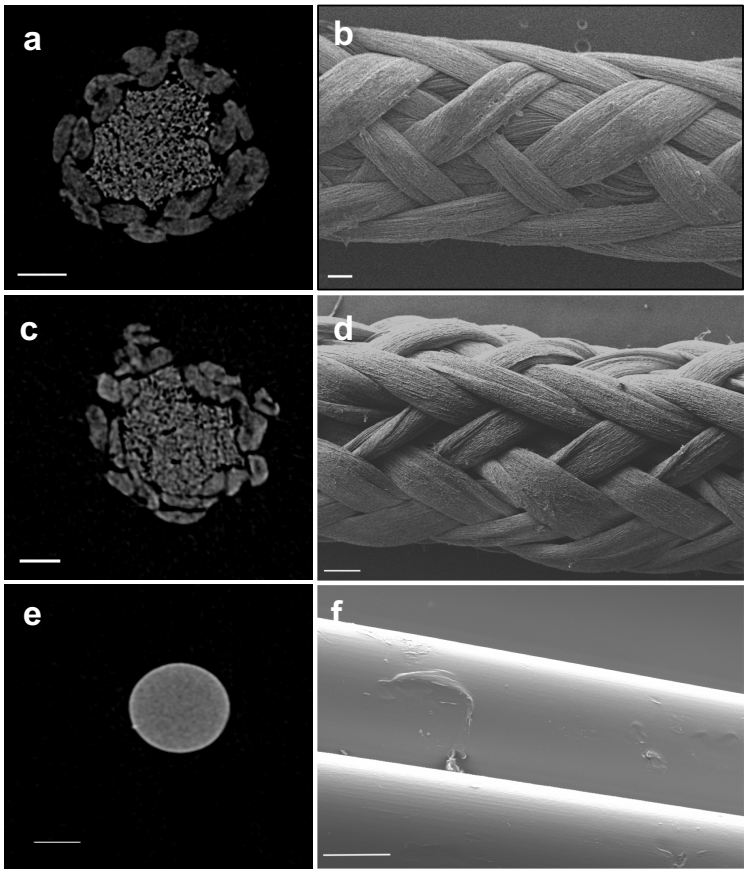


Figure 4.6: μCT scans and SEM images of braided hybrid sutures. (a) Cross-sectional μCT scan showing the 12 filament electrospun sheath with 4 melt-extruded cores; (b) SEM image showing suture morphology with both electrospun and melt-extruded fibres visible on the surface; (c) Cross-sectional μCT scan showing the 20 filament electrospun sheath with 4 melt-extruded cores; (d) SEM image showing the suture surface with no visible melt-extruded fibres; (e and f) PDS suture extruded control. Scale bars are 200μm.

Based on these tests, the 20(4) suture fell outside of the target 0.4-0.7mm size range. As a result, the 12(4) suture was taken forward for further testing. From this point onward, electrospun suture refers to a 12 electrospun filament braid and hybrid suture refers to a braided suture made up of a 12 electrospun filament sheath with 4 melt-extruded yarns in the core.

4.5.3.2 Mechanical testing

Uniaxial tensile testing of the braided hybrid suture until failure was used to determine its mechanical behaviour and properties (Figure 4.7). The force at break was 71±0.3N,

ultimate stress was 229±1MPa, breaking strain was 34±1%, and Young's modulus was 773±32MPa.

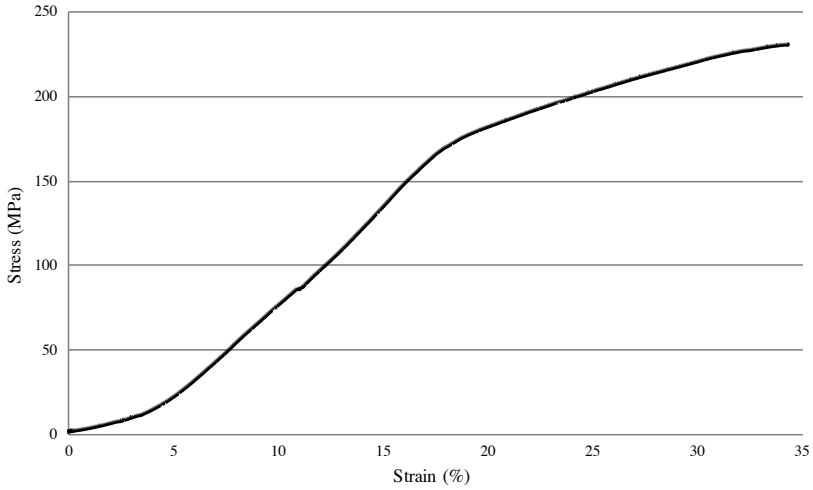


Figure 4.7: Representative stress-strain graph of a braided hybrid suture. Representative stress-strain graph of a hybrid suture made up of a 12 filament electrospun sheath and 4 melt-extruded yarn cores. The suture had characteristic toe, linear, and yield regions. The toe region shows nonlinear mechanical behaviour due to reorganisation of filaments during early stages of loading.

4.5.4 Comparison to currently used clinical sutures

4.5.4.1 Porosity

Porosity differences between the hybrid and control sutures, were measured by Hg porosimetry (Figure 4.8). The overall porosity was 60±7% for the electrospun suture, which was higher than that of the hybrid suture (40±4%, $p=0.0018$) and that of Vicryl (27±3%, $p<0.0001$). The overall porosity of the hybrid suture was also higher than Vicryl, $p=0.028$. The average pore diameter was 386±86nm for the electrospun suture, which was higher than that of the hybrid suture (198±17nm, $p=0.0079$) and that of Vicryl (141±51nm, $p=0.0015$). The PDS suture displayed no intrusion. Porosity differences between the electrospun sheath, melt-extruded cores, and final hybrid suture are presented in Figure C.2 in the Appendix.

A representative intrusion curve comparing the pore size distribution between the

electrospun, hybrid, and control sutures is presented in Figure 4.9. There were two local maxima of the electrospun suture intrusion curve, which represents the most frequent pore diameter: one around 0.5-5μm and the other between 50-100μm. The intrusion curve from the hybrid suture showed a similar range of pore sizes, but with less intrusion. The Vicryl curve showed minimal intrusion, with a peak between 20μm and 50μm, and the PDS curve displayed no intrusion. The local maximum of the curve, which represents the most frequent pore diameter, was around 1μm for the electrospun suture and 30μm for the Vicryl suture.

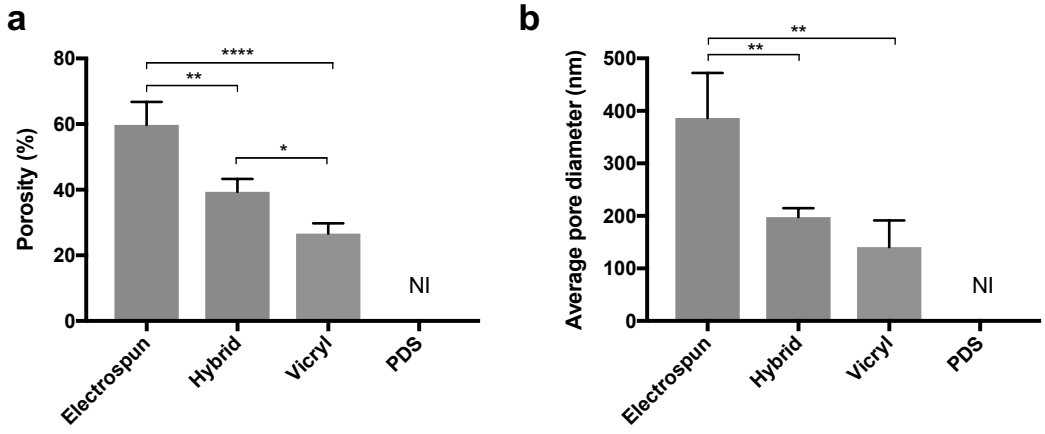


Figure 4.8: Hg porosimetry data comparing electrospun, hybrid, and control surgical sutures. (a) Overall porosity (%) was significantly higher for the electrospun suture compared to the hybrid suture ($p=0.0018$) and compared to Vicryl ($p<0.0001$); (b) Average pore diameter (nm) was significant higher for electrospun suture compared to the hybrid suture ($p=0.0079$) and compared to Vicryl ($p=0.0015$). NI = no intrusion. Statistical significance was determined at *$p<0.05$, **$p<0.01$, ***$p<0.001$, ****$p<0.0001$. Error bars represent standard deviations; n=3 for all conditions.

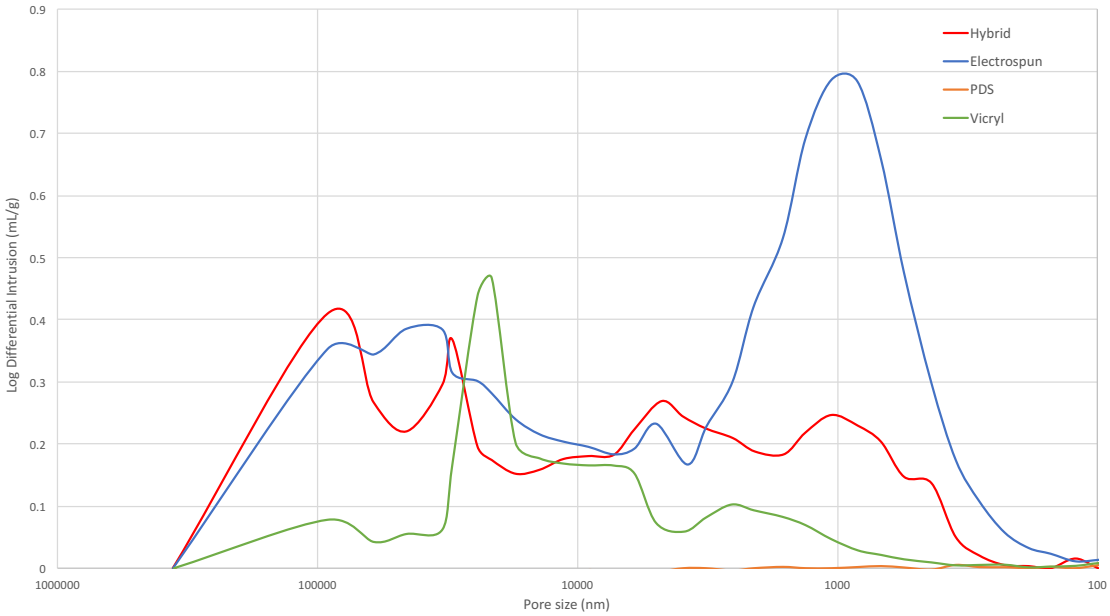


Figure 4.9: Representative pore size distribution of braided electrospun and hybrid sutures, compared to control sutures, measured by Hg porosimetry. A representative intrusion curve comparing the electrospun, hybrid, and surgical sutures PDS and Vicryl. The local maxima of the curves represent the most frequent pore diameters. The electrospun suture intrusion curve showed two broad peaks: one around 0.5-5μm and the other between 50-100μm. The intrusion curve from the hybrid suture showed a similar range of pore sizes, but with less intrusion. The Vicryl curve showed minimal intrusion, with a peak between 20μm and 50μm, and the PDS curve displayed no intrusion.

4.5.5.2 Tensile properties

There were significant differences in mechanical properties and behaviour between electrospun, hybrid, and control sutures. A representative stress-strain graph is shown in Figure 4.10. All sutures failed in the mid-substance region and all multifilament sutures showed characteristic toe, linear, and yield regions. The nonlinear mechanical behaviour of the toe region, at 0–5% of the strain, was due to the reorganisation of filaments during early stages of loading and was visible for the multifilament hybrid, electrospun, and Vicryl sutures. The linear region formed at around 5-15% of strain, at which point most fibres were engaged. The sutures yielded from 15% strain with classic post yield softening.

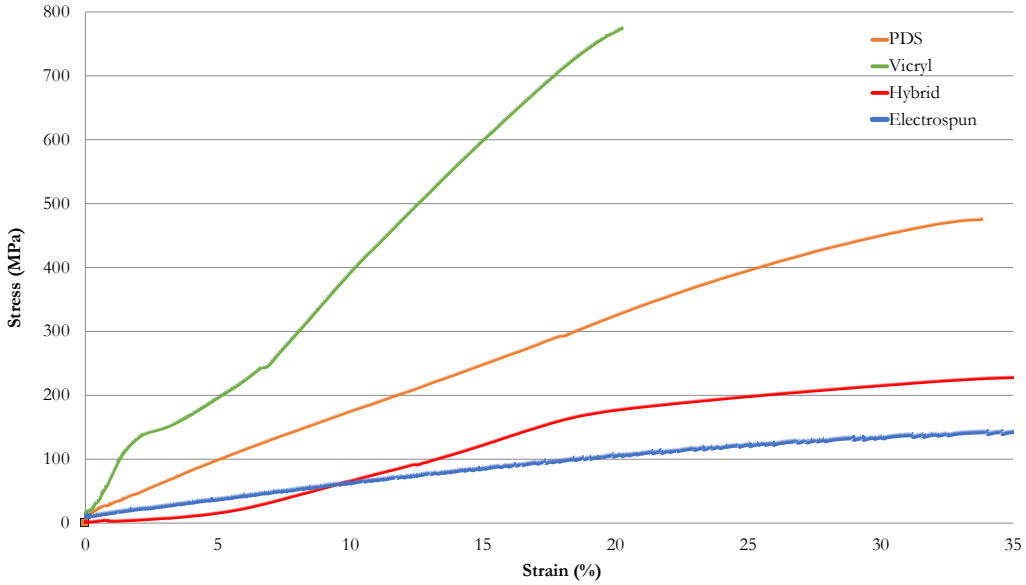


Figure 4.10: Representative stress-strain graph of braided electrospun, hybrid, and control surgical sutures. Braided electrospun and hybrid sutures were compared to control sutures PDS and Vicryl. Multifilament sutures displayed nonlinear mechanical behaviour during early stages of loading, due to the reorganisation of filaments.

Uniaxial tensile testing of the sutures until failure was used to calculate the force at break (N), breaking strain (%), ultimate stress (MPa), and Young's modulus (MPa), as shown in Figure 4.11. The force to failure was 12.9±1N for the electrospun suture, 70.1±0.3N for the hybrid suture, 46.2±0.6N for PDS, and 93.6±0.8N for Vicryl, were all significantly different from each other ($p<0.0001$). The breaking strain of Vicryl was 19.8±1%, which was lower than that of the electrospun suture (36±1%), the hybrid suture (33.7±1%), and PDS (38±2%), $p<0.0001$. The average ultimate stress was 190.2±32MPa for the electrospun suture, which was lower than the hybrid suture (229.3±1MPa, $p=0.008$), PDS (451.7±4MPa, $p<0.0001$), and Vicryl (773.3±6MPa, $p<0.0001$). These results were all statistically different from each other. The Young's modulus was 747.1±8MPa for the electrospun suture and 772.6±32MPa for the hybrid suture, which were lower than that of PDS (1693.0±69MPa) and of Vicryl (3838.0±132MPa), $p<0.0001$.

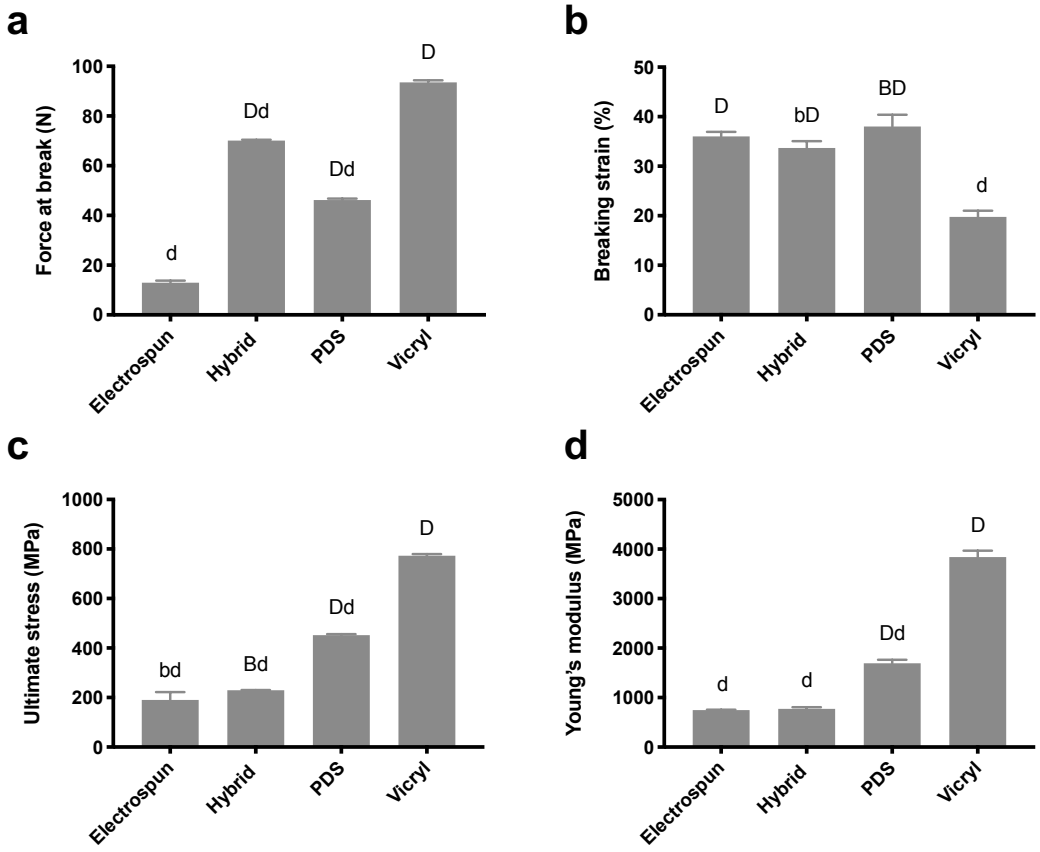


Figure 4.11: Tensile properties of braided electrospun, hybrid, and control surgical sutures. (a) Force at break (N) was lowest for the electrospun suture and highest for Vicryl, but all significantly different from each other ($p<0.0001$); (b) Breaking strain (%) was lowest for Vicryl compared to all sutures ($p<0.0001$); (c) Ultimate stress (MPa) of the electrospun suture was lower than the hybrid ($p=0.008$), PDS ($p<0.0001$), and Vicryl ($p<0.0001$) sutures; (d) Young's modulus (MPa) was lower for electrospun and hybrid compared to both surgical sutures ($p<0.0001$). Statistical significance was determined at Aa=$p<0.05$, Bb=$p<0.01$, Cc=$p<0.001$, Dd=$p<0.0001$. Error bars represent standard deviations; n=5 for each condition.

4.5.5.3 Thermal properties

DSC analysis showed differences in thermal properties between the electrospun, hybrid, and PDS sutures (Figure 4.12). Vicryl was not included in the thermal analysis, as polyglycolide-L-lactide has vastly different chemical properties requiring a different thermal testing protocol. Hybrid sutures displayed two small annealing peaks between 0-20°C and 40-70°C, whereas electrospun sutures displayed a small broad annealing peak between 35-70°C. PDS exhibited a narrower annealing peak just prior to the main melting peak between 90-100°C. It also indicated a shoulder on the return heat flow signal. The

melting peak looked similar between the polydioxanone sutures (around 105°C), but the melting temperature was lowest for the PDS suture compared to the electrospun ($p=0.0016$) or hybrid sutures ($p=0.0268$), (Figure 4.12b). Overall percent crystallinity was 66.9±0.5% for the PDS suture, which was significantly higher than the crystallinity of the electrospun (50.3±1%, $p<0.0001$) or hybrid suture (51.4±0.8%, $p<0.0001$).

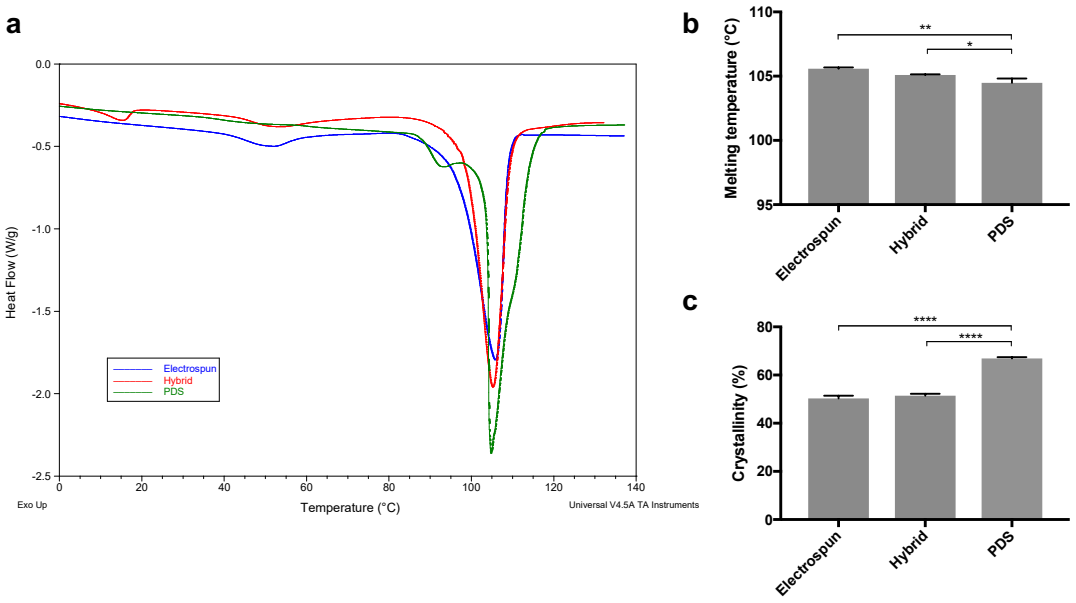


Figure 4.12: Representative thermal data comparing electrospun, hybrid, and surgical PDS sutures. (a) DSC thermograph. The PDS melting peak is broader compared to that of the electrospun or hybrid sutures. Hybrid sutures displayed two small annealing peaks between 0-20°C and 40-70°C. Electrospun sutures had a small broad annealing peak between 35-70°C. PDS had a more narrow annealing peak prior to the main melting peak between 90-100°C; (b) Melting temperature is lowest for the PDS suture compared to the electrospun ($p=0.0016$) or hybrid sutures ($p=0.0268$); (c) Overall percent crystallinity was significantly higher for the PDS suture compared to the electrospun ($p<0.0001$) or hybrid sutures ($p<0.0001$). Statistical significance was determined at *$p<0.05$, **$p<0.01$, ***$p<0.001$, ****$p<0.0001$. Error bars represent standard deviations; n=3 for each condition.

4.6 Discussion

The overall objective of this chapter was to develop a multifilament yarn that meets target design criteria for use as a suture for tendon repair. The specific aims were to:

- Explore industrial braiding to manufacture a range of electrospun sutures
- Combine electrospun filaments and melt-extruded yarns into a hybrid suture with improved mechanical properties
- Compare the properties of electrospun and hybrid sutures to currently used sutures

This discussion is divided into three sections. The first discusses the feasibility of using an industrial braiding machine with electrospun filaments. The second section discusses the production and characterisation of hybrid sutures. Finally, the hybrid suture is compared to the electrospun and surgical sutures. The limitations of the experiments and results are considered in each section.

4.6.1 Industrial braiding can be used to modulate structure and improve reproducibility and production rate of electrospun sutures

It has been indicated that many electrospun materials have neither the required mechanical nor handling properties for use in clinical applications.[234–236] To improve their utility, fabricating multifilament electrospun sutures using hand-twisting and braiding has been explored. However, these devices are not reproducible nor can they be upscaled for eventual clinical application.

As a result, this chapter investigated the feasibility in using continuous electrospun filaments with an industrial braiding machine to create multifilament braided electrospun sutures. Target criteria were set in Chapter 2 to guide the development of a multifilament yarn suitable for use as a suture for tendon repair. By adjusting the carrier number, arrangement, and filament number, it was possible to manufacture four multifilament

sutures with various structural and mechanical properties. In support of our hypothesis, it was possible to control the properties and increase the rate of production of multifilament electrospun sutures.

Using an industrial braiding machine substantially improved the reproducibility of suture properties compared to previous studies using hand-braiding. The standard deviation of Young's moduli for braided sutures ranged between 1-11%, compared to 15-86% from previous studies hand-braiding yarns.[126,162] This reduction in variability has implications for improving the reproducibility of cell-material studies. Moreover, fabricating reproducible sutures facilitates the clinical translation pathway, by enabling upscaling of manufacturing steps and adherence to manufacturing standards and clinical tolerances.

Some limited work has used mini-type braiding machines with electrospun material, however these machines were restricted to a fixed number of carriers.[164,165,169] The versatility of the Variation Braiding Machine used here is necessary for designing sutures that meet the demands of the specific target tissue. Once the tension in the carriers was optimised, it was fairly straightforward to use electrospun filaments with the braiding carrier springs. By varying the filament number and carrier arrangement, four sutures were fabricated that met the suture diameter criteria of 0.4-0.7mm. These results showed that the 8 carrier suture was tighter and more narrow, the 12 carrier suture was flat and ribbon-like, and the 20 and 24 carrier sutures were looser with a hollow centre and larger braid angles. The relationship between braid angle on mechanical properties and cellular response has been noted before.[163] Czaplewski et al. hand-braided multifilament yarns with the same number of filaments but with varying braid angles.[163] The authors found that looser braids with larger braid angles were more porous and better supported the expression of tendon and ligament associated markers and induced elongated cell morphology similar to tendon and ligament fibroblasts.[163] Notably, the braid angle range

explored by Czaplewski et al. (47°–67°) was slightly narrower than the range of the braiding angles measured here (52°–74°), however the direct relationship between braid angle and porosity was also observed within the parameters tested here.

Tensile testing revealed that the mechanical behaviour, indicated by size and length of the toe, linear, and yield regions, depended on the number of filaments. Smaller braids with 12 and 16 filaments displayed a longer toe region, whereas the larger, looser braids with 20 and 24 filaments, displayed the longest yield regions and lowest stiffness. This difference in mechanical behaviour is likely attributed to differences in filament arrangement affecting fibre repositioning during mechanical loading, which is consistent with findings from other work.[148,162,163] However it is also worth noting that because the electrospun sutures were all made with different filament numbers, it was difficult to discern mechanical differences due to filament arrangement alone.

There were also differences in tensile properties observed between electrospun sutures. While no previous work has specifically investigated electrospun multifilament PDO sutures to serve as a comparison, a number of studies have explored the effect of filament number on mechanical properties.[148,162,163] In contrast to the current study, Czaplewski et al. found that looser PCL and PLLA braids showed the highest modulus and strength.[163] In the current study, the opposite trend was observed: looser braids with larger braid angles displayed increased strain and decreased modulus and stress. Such a discrepancy could be explained by the fact that changing the filament number in the current study outweighed the potential mechanical difference due to filament organisation. Barber et al. fabricated PLLA yarns made of 3, 4, or 5 filaments and observed variable stiffnesses within the initial 10% of deformation, on a similar scale to the differences observed in the current study.[148] The stiffnesses observed in the current study, and by Barber et al, fell within the range of cyclic uniaxial tension commonly used for *in vitro* culture of tendon and ligament tissue

engineering scaffolds.[237,238] In the context of multifilament yarns for suture use, the versatile fabrication method could produce yarns that accommodate for the range of stiffnesses and mechanical strengths displayed by soft tissues *in vivo*. However, this study used mechanical characterisation methods that could not recapitulate the complex, cyclical loading of an *in vivo* environment upon implantation. While these findings reflect the suture's mechanical properties and behaviour upon implantation, their properties will change under repeated loading and when in contact with physiological fluids. Finally, in developing a suture to support tendon tissue integration, it is important to consider the problem of suture pull through. There have been numerous accounts of suture pull through at rotator cuff revision surgery.[55–57,74,81] The problem of pull through is complicated and is likely multi-factorial: due to the surgical construct creating stress concentrations, the properties of diseased tissue, which is poorly understood and highly variable between patients, and finally, the material compatibility between the suture and the tissue. Until there is a well-designed clinical trial looking at tissue-suture compatibility, changes to suture design to minimize pull through will be hypothesis driven. As a result, the suture in this thesis was not developed to address this problem.

Porosity is an important design factor for biomaterials, as it is closely linked to its degradation and can influence the cellular material response.[239–241] However, porosity is notoriously difficult to study as there are no accurate methods to measure the porosity of submicron fibres, no clear targets as to how porous a suture should be, and how the requirements of the tissue will change over time. Porosity is also difficult to study in a static environment, as the pore shapes and sizes within the structure would likely change under mechanical loading. Most methods to measure material porosity are not sensitive enough for nano- and microfibres.[216] Both μCT[98] and Hg porosimetry[241] are methods that are routinely used for measuring the porosity of electrospun materials. The rationale for

investigating porosity in this study was both to compare μCT and Hg porosimetry methods, as well as to measure the porosity and pore sizes between the braided electrospun sutures. This chapter showed that variation braiding offers the possibility of tuning porosity and pore size and that overall porosity was estimated to be 10% lower using μCT compared to Hg porosimetry. The μCT machine used here was limited to measuring pore sizes greater than 0.9μm, rendering it not sensitive enough to accurately measure the porosity of filaments made up of nano- or microscale pores. It seems that μCT is useful for a gross calculation of pore size and the detection of large pore shapes, especially in the centre of the material. In contrast, the Hg porosimeter machine had a resolution of 0.005μm and revealed that electrospun sutures were more porous and showed a wider range of pore sizes. However Hg porosimetry is not without its own limitations; there is concern that the high pressure applied to the material during testing can distort the true fibre structure.[216,242] It is possible that the true porosity lies somewhere between the two estimations made here.

4.6.2 Hybrid electrospun-extruded sutures meet the target design criteria for use as surgical sutures

In considering the electrospun sutures from the previous section, only the 12 and 20 carrier braids were suitable for hybrid suture production. Pilot work showed that the 8 carrier braid was too tight to introduce cores and the 24 carrier braid with cores exceeded the target size range for this suture. Initial experiments explored using both the 12 and 20 carrier set up for the electrospun sheath and added 4 melt-extruded filament yarns as cores through the centre of the suture. In support of our hypothesis, combining an electrospun sheath with melt-extruded cores created a hybrid braid with improved structural and mechanical properties. Braiding 12 electrospun filaments had produced a narrow ribbon, whereas adding the cores expanded the structure to a more oval shape.

μCT and SEM results showed that melt-extruded filaments were clearly visible on the surface of the yarn. This was an unanticipated result; the potential effects of cells being in initial contact with both electrospun filaments and extruded yarns are addressed in Chapter 5. Hg porosimetry revealed that hybrid braids had a significantly different pore distribution compared to the electrospun sheath or melt-extruded cores on their own. This was likely due to a more tightened structure resulting from braiding the electrospun filament directly around the cores. Braiding 20 filaments with cores resulted in a round shape. However, it is worth noting that the cores did not take up the whole centre of the suture, as noted by microCT. This could be appealing in terms of its potential to promote cell infiltration, but also mean that the structure is more susceptible to changing its conformation and porosity under mechanical loading.

This was the first study to combine electrospun filaments and melt-extruded yarns to fabricate a core-sheath suture. Previous studies have explored electrospinning as a method to develop core-sheath monofilaments, most notably for use as sacrificial fibres or drug eluting sutures.[164,183,243,244] Most commonly, two compounds were spun into a composite fibre with a core layer encapsulated inside a shell. Drugs could then be enclosed within the polymer shell to form a reservoir-type drug delivery device. The potential for the core and sheath to have different degradation or pore properties, as was shown here, or even drug eluting properties, demonstrates the breadth of potential clinical applications for this hybrid device.

The 20 carrier hybrid suture produced a uniformly round structure, but the suture diameter was too large for use with surgical equipment and exceeded the targets for this work. As a result, braiding with 12 carriers with electrospun filaments as the sheath and 4 melt-extruded yarns as the core, was the chosen hybrid configuration to achieve both the size and mechanical property requirements. It was anticipated that the hybrid yarns would

show superior performance compared to the electrospun only sutures. The hybrid yarns had a more similar stress-strain curve to native tendon, due to the melt-extruded component and had a tensile strength that was closer to the target criteria for this suture. In terms of comparing the different hybrid braided structures, it was anticipated that the 20 filament braid would show superior performance because it had a larger number of filaments (higher tensile strength), a larger core (higher porosity) and more rounded morphology. However, it wasn't anticipated that the melt-extruded component of the 20 filament braid wouldn't fit the core. This is not ideal for its intended use as a suture, because the core and sheath could slide past each other during movement, causing damage to the fibres and failure of the device.[63,155,245,246] Additionally, the 20 filament braid fell outside of the target diameter criteria and was therefore excluded from future work.

The chosen 12 filament hybrid device was compared to the 12 filament electrospun suture (without the core), as well as the surgical sutures PDS and Vicryl in the next section.

4.6.3 Hybrid sutures have more similar macro-scale properties to surgical sutures and more similar micro-scale properties to electrospun sutures

A popular tissue engineering design hypothesis is that a regenerative device should balance mechanical strength with porosity to allow for cellular infiltration, providing a sequential transition in which the regenerated tissue assumes function as the material degrades.[247] This balance often presents conflicting design requirements, as matching tissue strength usually requires a denser material whereas a more porous material is seen as favourable for tissue integration.[248,249] Here, the hybrid suture prototype was compared to an electrospun suture and surgical sutures PDS and Vicryl. In support of our hypothesis, hybrid sutures were less porous but stronger than electrospun sutures. Compared to surgical sutures, hybrid sutures had a similar force at break, but were more porous and had a lower stiffness

and stress. While some studies have assessed some of the structural aspects of braided electrospun yarns, no study has compared the properties of electrospun-based sutures directly to those of commercial sutures. The porosity, mechanical and thermal differences are considered in more detail below.

4.6.3.1 Porosity

In comparing the pore size distributions using Hg porosimetry, hybrid, electrospun, PDS, and Vicryl sutures all displayed different intrusion curves. The electrospun intrusion curve showed two main peaks, reminiscent of two pore sizes: small pores in between submicron fibres (around 1μm) and larger pores measured both in the open spaces between filaments and in the hollow core (around 10-100μm). The initial broad peak was likely due to interstitial filling when most of the open spaces between the filaments are filled by mercury. The second more narrow main peak is genuine intrusion of filling in between the fibres. Compared to the electrospun suture, the hybrid suture showed a similar range of intrusion, but lower overall peaks. This result is likely due to the fact that braiding around a core created a tighter structure with less pronounced intrusion. This is confirmed by the average pore diameter, which was significantly higher for the electrospun compared with hybrid suture. The braided Vicryl intrusion graph showed some interstitial filling with one peak around 20-50μm, indicating minimal space between the braided bundles of fibres. As anticipated, the monofilament PDS intrusion graph showed no intrusion. In the context of developing medical sutures intended to encourage cellular activity, the microporous architecture of electrospun and 10μm melt-extruded fibres is critical to encourage cellular attachment and infiltration. Previous work has focused on twisted monofilaments[98,118,176] made from sheets of densely aligned fibres, however many studies found a lack of cellular infiltration into the yarn, which could have detrimental consequences to the long-term success of the implant.[98,126] The influence of the suture porosity on cellular infiltration is

explored further in Chapter 5.

4.6.3.2 Mechanical testing

Tensile testing results revealed that the electrospun and hybrid sutures had substantially different mechanical properties compared to PDS and Vicryl. Because sutures are often used as bridging devices for the torn tissue, they often bear a large proportion of the load, especially during early phases of healing.[250] As a result, the maximum force at failure is an important parameter to investigate. Compared to the surgical sutures, the force at failure of electrospun sutures was 3 times lower than PDS and 7 times lower than Vicryl. This result was expected; unlike electrospinning, there is no dilution of the polymer for the fabrication of melt-extruded fibres, explaining the vastly different force at break measured between PDS, Vicryl, and hybrid sutures compared to electrospun sutures. The differences in ultimate stress and Young's modulus between the hybrid and electrospun sutures compared with PDS is possibly due to variations in surface area. The electrospun and hybrid sutures are made up of a higher density of fibres with smaller diameters, leading to a much larger overall surface area. Moreover, the ultimate stress and Young's modulus of Vicryl was significantly higher than any other material tested. This was unexpected, as previous work has shown PDS to be stiffer than Vicryl and braided sutures to be generally more flexible than monofilament sutures, regardless of the chemical constituents.[251] These result can be potentially explained by the relatively larger size of the Vicryl suture (size 0 USP) compared to the PDS suture (size 2-0 USP).

None of the sutures matched the force at failure of native tissue. Previous work in the Carr group measured the maximum force at failure of supraspinatus tendon in a cadaveric specimen to be 311±41N, with previous reported values ranging between 80-652N.[14,252] It is not clear what the physiological range of the supraspinatus tendon is, although it will vary between healthy and diseased tendon. Previous work measured the Young's modulus

of supraspinatus tendon to be between 1000-2000 MPa[89], which is close to the stiffness of the electrospun, hybrid, and PDS sutures (all under 2000 MPa), but is much lower than that of the Vicryl suture (around 4000 MPa). While it's important for the sutures repairing a torn tendon to be stiff enough to effectively transfer forces, if it is too stiff, it could increase the chance of re-tearing the tendon by causing pull through. Moreover, the mechanical properties required of a suture to augment tendon repair will change over time, as native tissue begins to replace the degraded suture. However, it is not clear how stiff the suture should be and how that stiffness should change over its lifetime, to promote the optimal repair. Future work characterising both the macro- and micro-mechanical properties of healthy and diseased tendon would help inform better matching of surgical materials to the requirements of the tissue. Micro-mechanical properties were investigated using Atomic Force Microscopy (AFM) in this study, however measuring fibre stiffness proved to be technically challenging. AFM was attempted on two different machines at the University of Oxford, but yielded unreliable results. There is evidence to suggest that micro-mechanical properties, such as fibre stiffness and roughness, can influence cell behaviour[253,254], however it is not well studied in the context of rotator cuff repair and warrants further investigation. Moreover, biomechanical and biocompatibility tests are needed that focus on the tendon-suture interface; both during the initial 6 weeks after surgery when the joint is relatively immobilized, and after 6 weeks, when the construct is undergoing physiological movement.

It is also worth reiterating that the hybrid and electrospun sutures are intended to act primarily as biological scaffolds, but also to provide mechanical support. Because of their intended biological function, these devices are unlike any surgical suture currently on the market, but more closely mirror the structure and function of scaffolds. Synthetic and biological scaffolds are currently used surgically as bridging devices (although they are not

licensed to do so), to mechanically and biologically support rotator cuff tendon repair.[89] Their clinical efficacy is disputed[82,86,88]; previous work suggested that this is because no scaffolds adequately approximate tendon on the macro- and microscale.[85,89] Synthetic scaffolds are made up of 30μm fibre bundles and have a high tensile strength for surgical repair. Conversely, biological scaffolds better approximate the microscale properties of native tendon (such as its local stiffness), but have macro-mechanical properties that are considered to be unsuitable for surgical repair. Moreover, biological patches are more prone to immune responses and have a higher risk of failure.[206,255] With this in mind, a strength of this work is the incorporation of electrospun fibres, which approximate submicron fibres in native tissue, with melt-extruded fibres, which provide mechanical strength, to create a hybrid device which incorporates some of the benefits seen with both biological and synthetic scaffolds.

4.6.3.3 Thermal testing

Thermal analysis showed changes in annealing and melting peak sizes of electrospun, hybrid, and PDS sutures. Both electrospun and hybrid sutures displayed annealing peaks at temperatures below the melting peak, and similar melt profiles at higher temperatures. Conversely, PDS displayed an annealing peak just prior to the main melting peak along with a shoulder upon the result heat flow signal. A wider melting range is typical of different crystallites present with different melting transitions and larger recrystallization. Electrospun and hybrid sutures displayed a lower crystallinity compared to PDS, suggesting that PDS may have a slower degradation rate. It is very possible that because both electrospun and hybrid sutures are made up of fibres smaller than 10μm, they would degrade more quickly compared to a monofilament suture of the same overall diameter (like PDS). The optimal degradation kinetics of a suture during tendon healing is not known; however, it will be necessary for a suture to provide initial mechanical support to

the tissue, especially in the first 6 weeks, and then degrade as the tissue is healing. The results in Chapter 3 found that the raw electrospun and melt-extruded filaments retained at least 70% of their mechanical properties after 6 weeks. In order to develop a more mechanistic understanding of electrospun and melt-extruded filament changes during degradation, a structural analysis technique, such as XRD should be investigated.

4.6.3.4 Summary

The overall aim of this chapter was to design a multifilament yarn that meets criteria for use as a suture for tendon repair. The target criteria for this device were based on the suture meeting certain diameter, structural properties, porosity, and tensile property requirements, some of which were similar or compatible with currently used surgical sutures. This work also developed fabrication and characterisation methods that were tunable in order to alter suture design or validate it in the future. It was shown that a hybrid suture made up of a sheath of 12 electrospun filaments with a core of 4 melt-extruded yarns met the design targets. This prototype will be taken forward for biological characterisation in Chapter 5. The properties of the hybrid suture were compared to a 12 filament electrospun suture and to Vicryl and PDS, two sutures in current clinical use. The hybrid suture properties, in the context of the design targets, are summarized below:

- **Suture diameter**: The hybrid suture has a diameter of 0.69mm. It is small enough to be handled by surgeons performing fine technical operations and also compatible with suture anchors used for rotator cuff repair. Future work should evaluate its handling properties and usability for rotator cuff surgery. A pilot usability study has been developed and can be found in Appendix C.4.
- **Porosity**: The hybrid suture has an overall porosity of around 40%, which is slightly lower than the target and lower than electrospun sutures, but higher than

surgical sutures. Hybrid sutures have larger pore sizes (between 10-100μm) and a more open structure compared to surgical sutures. The difficulty in striking a balance between a porous, open structure with one that is robust and strong enough for clinical applications will be further discussed in the context of cell material interactions in the next chapter.[209,256,257]

- **Tensile strength**: The hybrid suture has a force at failure of 70N and strain at break of 35%, which are compared to surgical sutures of the same size. Moreover, the hybrid suture displays mechanical behaviour that is similar to native tissue, indicated by toe, linear, and yield regions. The hybrid suture has a 2 fold lower stress and Young's modulus than PDS and a 3.4 fold lower stress and 5.3 fold lower modulus than Vicryl. It is possible that a lower stiffness (compared to currently used sutures) could reduce cheese-wiring of sutures through tendon, however more work is needed to understand the requirements of native tendon and how these requirements change over the course of healing and repair.
- **Biophysical cues**: The hybrid suture is made up a sheath of electrospun submicron fibres, which could provide a scaffold for tendon cells to attach and proliferate. Adding melt-extruded cores opened the electrospun braid, resulting in melt-extruded fibres visible on the surface of the hybrid suture. The influence of melt-extruded fibres on cell behaviour will be explored in Chapter 5.

4.7 Conclusions

Braiding continuous electrospun filaments with an industrial braiding machine enabled the fabrication of more reproducible multifilament sutures than could be achieved hand-braiding or hand-twisting. It was also possible to control suture porosity through the orientation of the filaments and control the mechanical strength by adjusting the filament number. Braided electrospun sutures were porous, but too bulky and weak for use in tendon repair. Combining an electrospun braided sheath with melt-extruded cores resulted in a hybrid suture that had a smaller diameter and improved tensile strength more closely matching existing sutures, while still retaining a higher porosity. The structure of the hybrid suture is designed to meet the demands of tendon: electrospun fibres on the outside of the suture approximate ECM properties and are in initial contact with biological fluids, while the melt-extruded fibres in the core provide prolonged mechanical support. A hybrid suture prototype made up of a 12 filament electrospun sheath with 4 melt-extruded yarns in the core met the target design criteria and will be taken forward for biological characterisation in Chapter 5.

Table 4.4: Chapter 4 in context.

Evidence before this work	Added value of this work	Implications of this work
Braided electrospun sutures have shown initial biological promise for soft tissue repair. However, to date, braided electrospun sutures have only been handmade into short sections.	Industrial braiding resulted in more reproducible electrospun sutures, indicated by lower standard deviations, and an increase in production rate of 500%. Suture tensile strength and porosity were controlled by adjusting the number, orientation, and distribution of filaments.	Industrial braiding overcomes limitations with controlling structure, reproducibility, and production volume. This has implications for engineering devices that have tissue-specific requirements and for meeting standards for clinical trials and later commercialisation.
Electrospun braided or twisted sutures have a low tensile strength and are too bulky to be used by surgeons and are not compatible with surgical equipment.	Melt-extruded yarns were introduced as cores into the braiding production line to fabricate hybrid core-sheath sutures. Hybrid sutures were made of an electrospun filament sheath with melt-extruded cores. Compared to electrospun only sutures of the same size, hybrid sutures were 5 times stronger with a larger overall surface area, but slightly lower porosity.	The structure of the hybrid suture is specifically designed to meet the demands of native tendon: electrospun fibres on the outside of the suture approximate the ECM properties and are in initial contact with the biological milieu, while the melt-extruded fibres in the core provide prolonged mechanical support.
Previous work observed that, while biologically advantageous, electrospun sutures are mechanically weaker than currently used surgical sutures, casting doubt on their potential to be used clinically. No work had directly compared the properties of electrospun or hybrid sutures to those of surgical sutures.	Electrospun sutures were more porous, but had a substantially lower tensile strength compared to surgical sutures PDS and Vicryl. Hybrid sutures had a force at failure and strain similar to surgical sutures. In addition, hybrid sutures had a larger surface area, higher porosity, and a lower stress and stiffness compared to PDS and Vicryl.	The potential for hybrid sutures to be incorporated into existing surgical suture production lines and have tensile properties similar to surgical sutures will ease the translation process and adoption by surgeons. Other structural properties, such as its higher porosity, increased surface area, and lower stress and stiffness, are tunable and may improve its biocompatibility over currently used sutures.

Chapter 5

Exploring the bioactivity of hybrid sutures

5.1 Abstract

5.1.1 Background

Immediately upon implantation, a layer of proteins from the tendon biological milieu are adsorbed to the surface of biomaterials. These proteins mediate the subsequent response of cells, such as tendon fibroblasts, at the surgical site. Characterising the interactions between the hybrid suture and the tendon biological environment is key to discern its potential as an augmentation device. This chapter has two main aims. First, it investigates whether protein adsorption from serum differs between the hybrid suture components. Second, it explores how the hybrid suture components and the final hybrid suture influence healthy tendon fibroblast behaviour. In both experiments, the hybrid suture is compared to currently used surgical sutures to evaluate its potential to improve current treatment options.

5.1.2 Materials and methods

To investigate the serum proteins that adsorb to each suture type, the hybrid suture components (electrospun filaments and melt-extruded yarns) and control surgical sutures (PDS and Vicryl) were incubated in human serum. Proteins were isolated and analysed by mass spectrometry. The cell-material interaction experiments were performed in two parts. First, the tendon fibroblast response to the hybrid suture components was investigated in terms of cell attachment and proliferation up to 14 days. Then, the tendon fibroblast response to the final hybrid suture was compared to control surgical sutures, in terms of cell attachment and proliferation up to 7 days, cell coverage using SEM, and cell infiltration using μCT.

5.1.3 Results

The adsorbed coronas were significantly different between all materials tested. Electrospun filaments and melt-extruded yarns had the most similar adsorption profiles. Melt-extruded yarns best supported fibroblast attachment, whereas electrospun filaments best supported fibroblast proliferation over 14 days. Compared to surgical sutures PDS and Vicryl, hybrid sutures promoted increased fibroblast attachment, proliferation, and coverage over 7 days. While μCT was a useful tool for scanning and visualising the whole cell-suture construct, no visible infiltration was observed.

5.1.4 Conclusions

These results suggest that fibre properties and macroscale architecture play an important role in regulating protein adsorption, as well as fibroblast adhesion and behaviour. The response of fibroblasts to electrospun and melt-extruded fibres is markedly different, but cells attach to, and proliferate on, the composite hybrid suture. Surgical sutures used routinely in tendon surgery adsorb a different protein corona compared to the hybrid suture components, and they do not promote fibroblast attachment or proliferation. How protein adsorption may be driving the cell-material interactions could help to identify a protein niche that drives favourable cell responses. Overall, hybrid sutures showed improved cell-material interactions compared to currently used surgical sutures, making them promising new surgical candidates to augment tendon repairs.

5.2 Introduction

Biophysical and biochemical material properties can guide cell behaviour. In the context of developing a novel suture to augment tendon repair, understanding how the suture interacts with its host biological environment can be used to deliberately harness cell responses involved in tendon healing.

Upon surgical implantation, materials are immediately coated with a layer of proteins and other molecules from the blood and interstitial fluid, called the protein corona, or provisional matrix. Adsorbed proteins enable cell attachment to biomaterials via focal adhesion kinases and integrins on the cell surface.[104,258] It is postulated that the identity and abundance of adsorbed proteins can modulate chemotactic cues as well as attachment motifs therefore influencing both the type of cell that is recruited to the biomaterial and the strength of the cellular attachment.[259,260] Additionally, adsorbed proteins can influence cell signalling behaviour and shape through providing bio-modulatory cues to cell surface receptors.[259,261,262] As a result, cells respond to these adsorbed proteins, rather than by direct contact to the material surface. Despite the importance of the protein corona in modulating immune cell and fibroblast interaction with implanted materials, they have not historically been considered in the assessment of electrospun biomaterials. In the context of biomaterials for tendon repair, adsorbed proteins are crucial in driving the immune cell and tendon fibroblast response to the biomaterial.

Tendon fibroblasts were the major focus of this chapter as they play a key role in tendon healing by laying down new ECM needed for tendon remodelling and through modulating behaviour of immune cells. Previous work from the Carr group (by Dr Edward Stace) has shown that changing the protein corona on electrospun meshes alters gene expression and metabolic activity of tendon fibroblasts.[107] The work in this thesis builds upon Edward's work by illustrating how incubating different materials with serum alters the

adsorbed protein corona composition and can help explain observed differences in tendon fibroblast attachment and proliferation. While the work in this chapter focuses on the properties of the whole protein corona, future work future work will isolate specific proteins to identify those driving cell-material interactions.

It has been widely demonstrated that biomaterial surface properties such as hydrophobicity[263,264], charge[265,266], and local stiffness[110,267] influence protein binding, protein conformation, and fibroblast attachment. Chapter 3 described how electrospinning and melt-extrusion could be used to fabricate materials with different fibre diameters, porosities, and tensile strength and strains from the same polymer. One aim of this chapter was therefore to investigate whether the composition of the adsorbed protein corona varied between the electrospun filaments and melt-extruded yarns developed in Chapter 3, and how this composition differed compared to currently used surgical sutures PDS and Vicryl.

Tendon fibroblasts are the most abundant cell type in tendon and will be in contact with any implanted biomaterial used for tendon repair. Moreover, cell growth and behaviour is, in part, regulated the cell's ability to attach to materials and to adopt an appropriate morphology.[268–270] It is well documented that tendon fibroblasts are sensitive to electrospun submicron and nanoscale biophysical cues, specifically to fibre size, fibre alignment, and local mechanical properties, such as stiffness.[107,108,271–273] In particular, modulation of these properties have been shown to affect fibroblast attachment, morphology, and proliferation, all of which are important for matrix deposition and tissue remodelling.[108,272,273] While submicron electrospun fibres are biologically advantageous, they present significant mechanical and structural limitations, which has prevented their translation of as-spun fibres for clinical applications. In Chapter 3, micron-sized fibres were developed using melt-extrusion to provide additional strength to electrospun sutures.

Previous work has investigated the effect of nano- vs microscale fibres on cell behaviour.[108,274,275] In the context of tendon repair, the work in this area remains limited; however, it was found that fibre diameter influences tenogenic differentiation.[275] Characterising the extent to which tendon fibroblasts attach, proliferate, and adopt a morphology similar to cells in native tissue, is necessary to assess the material's potential to integrate with tendon tissue. A further aim of this chapter is therefore to explore tendon fibroblast response to the components of the hybrid suture developed in this thesis, namely the electrospun filaments and melt-extruded yarns developed in Chapter 3.

Besides the nano- and microscale properties, macroscale properties are crucial to the success of an implanted biomaterial. In Chapter 4, braiding was used to fabricate multifilament sutures. There is emerging work on exploring the influence of macroscale architecture on mediating cellular attachment and behaviour. To do this, materials with similar nano- and microscale cues, but a different macroscale organisation, are compared. Differences in macroscale architecture leads to variations in porosity and exposed surface area, which in turn, influence cell behaviour and expression. A better understanding of how patient-derived tendon fibroblasts interact with both existing surgical sutures for tendon repair and new sutures under development is needed. The final aim of this chapter is to evaluate the response of tendon fibroblasts to the hybrid suture prototype developed in Chapter 4 as well as to currently used surgical sutures.

5.3 Objectives and hypotheses

The overall objective of this chapter is to explore the bioactivity of the materials developed in Chapter 3 and Chapter 4. The first part of this chapter focuses on investigating differences in adsorbed protein composition between surgical sutures and the components of the hybrid suture. Then, the response of patient-derived tendon fibroblasts to the same components of the hybrid sutures are investigated. Finally, the response of tendon fibroblasts to the final hybrid suture is explored in terms of initial cell attachment, proliferation, coverage, and infiltration.

Objective 1: To characterise the composition of adsorbed protein coronas on the components of the hybrid suture, compared to on surgically used sutures.

Objective 2: To characterise the attachment and proliferation of tendon fibroblasts to the components of the hybrid suture.

Objective 3: To compare the response of tendon fibroblasts between hybrid, electrospun, and surgical sutures, in terms of cell attachment and activity.

The overall hypothesis is that the sutures developed in this thesis and sutures in current clinical use will induce differential protein adsorption profiles and tendon fibroblast responses. When in contact with human serum, it is expected that electrospun filaments and melt-extruded yarns will have protein corona compositions that are the most similar. It is expected that tendon fibroblasts will preferentially bind to, and proliferate on, electrospun fibres.

Hypothesis 1: Proteins will adsorb to all surfaces but there will be different protein binding between all materials, with coronas on electrospun filaments and melt-extruded yarns being most similar.

Hypothesis 2: Fibroblasts will preferentially bind to melt-extruded yarns, but proliferate more on electrospun filaments.

Hypothesis 3: Fibroblasts will preferentially bind to, and proliferate more on, hybrid sutures compared to surgical sutures.

5.4 Materials and methods

5.4.1 Biomaterial fabrication

5.4.1.1 Electrospun filaments, melt-extruded yarns, and hybrid sutures

Electrospun filaments and melt-extruded yarns were produced and characterised following the protocols outlined in Chapter 3.4.2 and Chapter 3.4.3, respectively, and stored in a dessicator prior to use. Hybrid sutures, made up of a braided 12 filament electrospun sheath and 4 melt-extruded yarn cores, were produced and characterised following the protocols outlined in Chapter 4.4.2 and stored in a dessicator prior to use.

5.4.1.2 Control sutures

Vicryl size 0 and PDS size 2-0 were used as control surgical sutures. Vicryl (Ethicon Inc, USA) is a synthetic, absorbable, multifilament suture. It is made up of a 90:10 ratio of glycolic to L-lactic acid and coated with 2–10% of a 50:50 mixture of polyglactin 370 and calcium stearate.[63] PDS (Johnson & Johnson Inc, USA) is a synthetic, absorbable, monofilament suture made of polydioxanone. Electrospun sutures (12 filament braided suture without cores) were also used a control.

5.4.2 Serum protein adsorption

5.4.2.1 Material preparation

To characterise the composition of the adsorbed protein corona on electrospun filaments, melt-extruded filaments, and control sutures were mounted on cell crowns (24-well plate size, Scaffdex, Tampere, Finland), following protocols in Chapter 5.4.5.3. Cell crowns were sterilized for 2 hours in 70% ethanol, then washed 3 times with PBS and left to air dry overnight.

5.4.2.2 Material functionalisation with human serum

Serum was collected with appropriate ethical approval (REC11/H0711/7). Blood was collected from donors and left at room temperature to clot for 30 minutes. The blood samples were centrifuged at 1300g for 15 minutes, then the serum was lifted off and aliquoted to 500μL. Crowns (n=3 per filament or suture type) were soaked in 200μL of healthy human serum (n=4, 2 males, 2 females, average age 27) followed by incubation for 1 hour at 37°C.

5.4.2.3 Mass spectrometry of adsorbed protein corona

Following serum adsorption, the material was removed from crowns and placed in 2mL of PBS on a plate shaker with gentle agitation for 5 minutes. This washing step was repeated two more times to fully remove any serum or loosely bound protein. The material was then clasped in a Lo Bind Eppendorf tube (Eppendorf AG, Hamburg, Germany) before brief centrifugation to remove any remaining PBS and unbound protein from the material. Bound protein was removed and digested from the washed scaffolds using 500ng trypsin (Promega, Southampton, UK) in 50mM ammonium bicarbonate at 37°C overnight.

Samples were then processed by research staff at the Target Discovery Institute (University of Oxford, UK) using adapted in house protocols. Proteins were digested directly from washed materials by the addition of 1 μg of trypsin (Promega) in 50 mM ammonium bicarbonate overnight at 37°C. The resulting peptides were purified using SOLA C18 HRP (Thermo) desalting cartridges. Eluted peptides were dried, re-suspended in 2% acetonitrile, 0.1% trifluoroacetic acid and stored at – 20°C prior to analysis.

Peptides were detected by nano-UPLC-MS/MS over a 60 minute gradient of 0.1% formic acid in 5% DMSO to 0.1% formic acid to 35% acetonitrile in 5% DMSO using a Dionex

Ultimate 3000 nano-UPLC with an EASY-Spray column (75μm x 500μm, 2μm particle size, ThermoFisher Scientific, Waltham, MA, USA) coupled to a Q-Exactive Mass Spectrometer (ThermoFisher Scientific, Waltham, MA, USA). MS1 spectra were acquired between 375-1500m/z with a resolution of 70,000. MS2 spectra of HCD fragmented precursors were acquired with a resolution of 17,500. Selected precursors were excluded from repeated analysis for 27 seconds.

5.4.3 Human tendon tissue acquisition

Biopsies of hamstring tendons were acquired from healthy donors with informed donor consent under ethics from the Oxford Musculoskeletal Biobank (REC 09/H0606/11) and in agreement with Institutional and National ethical requirements. During surgery, hamstring biopsies were taken from residual healthy tendon from patients undergoing ACL repair. These biopsies were transferred from the patient to sterile tubes containing culture media and transported to the laboratory for fibroblast isolation and expansion.

5.4.4 Tendon fibroblast isolation and expansion

Tendon fibroblasts were extracted by cutting the tissue biopsies into small pieces, approximately 2mm × 2mm before transferring to 6-well plates (Corning Inc., Corning, NY, USA). Explants were initially cultured in supplemented media made up of DMEM/F12 media (Lonza, Slough, UK), supplemented with 50% Fetal Bovine Serum (FBS, Labtech, Lonza, Slough, UK) and 1% penicillin-streptomycin (P/S, ThermoFisher Scientific, Waltham, MA, USA). This media was replaced every three days with D10 media used once outgrowth from explants was observed. Once the cell had reached confluence, indicated by tendon fibroblasts migrating from the tendon onto the 6-well plate, they were scraped and transferred to 10cm Petri dishes (Greiner, Frickenhausen, Germany). Cells were expanded until 80-90% confluent and were used at passage 3 to avoid the phenotypic drift observed at higher passages.[276]

5.4.5 Tissue culture experiments

5.4.5.1 Preparation for tissue culture

The day before cell seeding, materials were sterilised in 70% ethanol for two hours and then air dried overnight. On the morning of cell seeding, materials were washed three times in Phosphate Buffered Saline (PBS, Sigma-Aldrich, Dorset, UK) and then submerged in 1mL of culture media for 1 hour at 37°C to facilitate serum protein adsorption. Unless stated otherwise, culture media consisted of D10 (Nutrient Mixture F-12, DMEM/F12, Lonza, Slough, UK) supplemented with 10% Fetal Bovine Serum (FBS, Labtech, Uckfield, UK) and 1% penicillin-streptomycin (P/S, ThermoFisher Scientific, Waltham, MA, USA). Materials were transferred from culture media to a 12-well plate for cell seeding.

5.4.5.2 Cell seeding optimisation

Both the optimal seeding set-up and seeding density was explored. To determine the optimal seeding set-up, a fixed density of 80,000 cells/crown in 200µL were seeded on the three seeding set-ups outlined in Figure 5.1. Filaments were either mounted as a mat, by melting together three filaments ends. The mat was in contact with tissue culture plastic (TCP) (Figure 5.1b). Figure 5.1c shows the second set up, where the filaments were mounted in a cell crown (24-well plate size, Scaffdex, Tampere, Finland) in direct contact with TCP. Or three filaments were mounted in a cell crown that was sitting on top of a crown tip, such that the crown was suspended above TCP (Figure 5.1d).

Once seeded, the samples were incubated for 2 hours at 37°C. After incubation, the samples were transferred to a 24-well plate with 2mL of culture media and incubated at 37°C for another 22 hours. After the 24 hour attachment period, filaments were removed from the cell crown and initial cell attachment to filaments was measured as described in Chapter 5.4.5.4. After measuring initial attachment, filaments were incubated and culture

media was changed every 2 days. Cell number was also measured at day 4 and day 7 as described in Chapter 5.4.6. To determine the optimal seeding density, a range of cell densities were seeded on cell crowns in contact with TCP in a 12-well plate. Between 20,000-80,000 cells/crown were seeded and left for 24 hours to attach in a 37°C incubator. Initial attachment to the filaments was measured at 24 hours using the methods in Chapter 5.4.5.4.

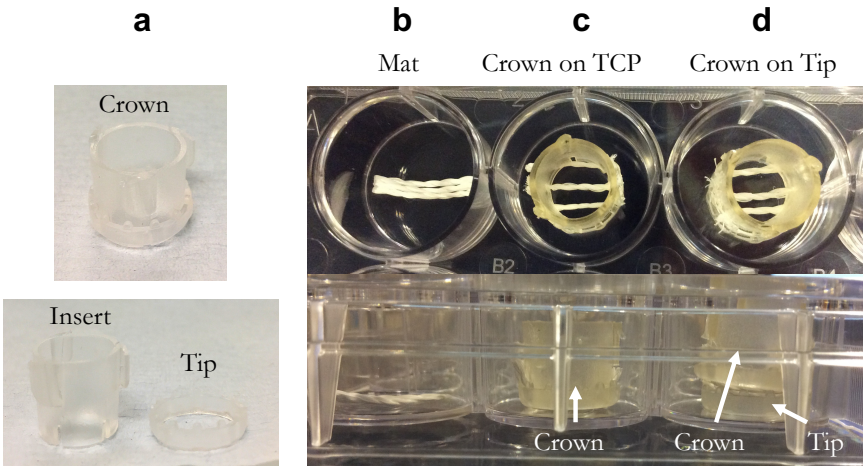


Figure 5.1: Three different seeding set-ups for filaments. (a) The top image shows an assembled cell crown. The bottom image shows a disassembled crown made up of an insert and a tip. Filaments (melt-extruded filaments shown here) were either mounted by (b) melting together three filament ends to create a mat that fit in the bottom of the well; by (c) mounting three filaments in cell crowns placed at the bottoms of the well; or by (d) mounting three filaments in cell crowns placed on a crown tip so that the filaments were suspended above TCP.

5.4.5.3 Optimised tendon fibroblast seeding and culture

For all tissue culture experiments, cells were seeded in 12-well plates at a density of 80,000 cells/crown in 200µL in a static environment. Both filaments and sutures were mounted in cell crowns in contact with TCP for seeding. Three pieces of 4cm section of electrospun filament or melt-extruded yarn were mounted per cell crown (24-well plate size, Scaffdex, Tampere, Finland). Care was taken so that separate filaments weren't twisted, overstretched, or in contact with each other, which could alter fibre properties presented

to the cells. Mounting sutures (electrospun, hybrid, and controls) on cell crowns followed the same protocol with the exception that only two pieces of 4cm suture were mounted on each cell crown, as it was too challenging to fit more than two sections per crown.

Care was taken to ensure that the same density of cells were exposed to the same surface area of filament by slowly dripping the 200μL of cells over the whole visible surface of filament. Once seeded, the plates were placed in a 37°C incubator for 2 hours. Then, crowns were moved to a 24-well plate with 2mL of culture media, so they were suspended above TCP and only the cells attached to the filaments were accounted for. At 24 hours after seeding, samples were removed from the crowns for measuring initial attachment and kept in culture media (without crowns) for prolonged culture. Unless stated otherwise, each experiment was performed with 3 biological repeats and 3 experimental repeats.

5.4.5.4 Initial attachment of tendon fibroblasts

Initial cell attachment was determined at 24 hours after seeding. At the 24 hour time point, filaments/sutures were carefully removed from the cell crowns and transferred into a new well containing 2mL of a solution of 10% Prestoblue (Invitrogen, Paisley, UK) and 90% culture media and incubated for 2 hours. A calibration curve was generated by seeding cells at the following densities in a 24-well plate (Corning Inc., Corning, NY, USA): $5x10^3$, $1x10^4$, $2x10^4$, $4x10^4$, $6x10^4$, $8x10^4$, and $1x10^5$. The calibration curve was used to approximate initial cell number attached, as represented by Prestoblue initial attachment measurements. After incubation, the fluorescence of each solution was measured in triplicates on a FluoStar Optima microplate reader (BMG Labtech, Ortenberg, Germany) with an excitation of 485nm and an emission of 520nm. Filaments/sutures were then maintained in culture media without crowns for the duration of the experiment.

5.4.6 Metabolic activity during prolonged culture

A Prestoblue assay was performed using the same protocol from Chapter 5.4.5.4 at days 7 and 14 after seeding for electrospun filaments and melt-extruded yarns, and at days 4 and 7 after seeding for hybrid and control sutures. A calibration curve was generated by seeding cells at the following densities in a 24-well plate (Corning Inc., Corning, NY, USA): $5x10^3$, $1x10^4$, $2x10^4$, $4x10^4$, $6x10^4$, $8x10^4$, and $1x10^5$. The calibration curve was used to approximate cell number as represented by Prestoblue metabolic activity measurements, throughout the experiment.

5.4.7 Fixation of the cell-suture constructs

Sutures were fixed and washed prior to imaging using SEM or μCT. After tissue culture, cell crowns were transferred to a new 24-well plate filled with 2mL of 2.5% glutaraldehyde for 1 hour in a fume hood. Crowns were then washed three times in PBS and stored in PBS in a 24 well plate covered tightly with paraffin plastic and aluminium foil to shield them from light. Plates were stored in a fridge prior to imaging.

5.4.8 Assessment of tendon fibroblast coverage by SEM

Fibroblast coverage was investigated on hybrid and control sutures after seeding fibroblasts on the sutures for up to 7 days. The day before imaging, 2cm fixed suture pieces were rinsed in deionised water before undergoing a graded ethanol series: 40%, 70%, 90%, 95% and 100%, each for 10 minutes (Sigma-Aldrich, Dorset, UK). Next, 30μL of HMDS (Alfa Aesar, Ward Hill, MA, USA) was added to each suture and left to evaporate overnight. Fixed, dried sutures were mounted on aluminium stubs (Agar Scientific, Essex, UK) using carbon tape (Agar Scientific). The stubs were gold coated for 120 seconds using a SC7620 Mini Sputter Coater System (Quorum Technologies Ltd, Laughton, UK) and images were taken at 100-1000x magnification at multiple sites using an Evo LS15 Variable Pressure Scanning Electron Microscope (Carl Zeiss AG, Oberkochen, Germany). Fibre

and cell diameters were determined using ImageJ (National Institute of Health, Bethesda, MD, USA).

5.4.9 Assessment of tendon fibroblast infiltration by μCT

Cell infiltration was investigated using μCT. Cells were cultured on the sutures for 7 days and then fixed and stored in PBS until use, following methods in Chapter 5.4.7. To prepare yarns for μCT, sutures were washed 3 times in deionized water and then submerged in 300μL of 4% osmium tetroxide (OsO_4, Sigma-Aldrich, Dorset, UK) for 2 hours. After staining, sutures were rinsed 3 times with PBS before undergoing a graded ethanol series: 40%, 70%, 90%, 95%, and 100%, each for 10 minutes (Sigma-Aldrich, Dorset, UK). Finally, 300μL of HMDS was added to each suture and left to evaporate overnight.

Sutures were scanned following μCT protocols outlined in Chapter 4.4.5. For each scan, a stained suture with cells was mounted alongside a control suture (stained with OsO_4, but without cells). The samples were scanned at an isotropic pixel size of 5μm. The images were reconstructed using NRecon software (SkyScan 1172, SkyScan, Kontich, Belgium) using the Feldkamp algorithm with a beam-hardening correction of 40% and a smoothing of 4. CTAn software version 1.12 (Bruker microCT, Kontich, Belgium) was used for processing and stacking the reconstructions into a tubular structure.

5.4.10 Statistical analyses

Post-processing evaluation, principal component analyses and statistical analyses of the mass spectrometry data were performed in Perseus[277] and R (R Core Team 2018). Raw MS data files were analysed using Progenesis QI for Proteomics (Waters) using default settings. MS2 spectra were searched against the human Uniprot reference proteome using MASCOT (Matrix Science) with the following parameters: 10 ppm precursor mass tolerance, 0.05 Da fragment mass tolerance, Oxidation (M) and Deamidation (N,Q) were set as variable modifications, two missed cleavage sites were allowed and peptides were

filtered to a 1% false discovery rate threshold. The PANTHER Classification System[278,279] was used to determine pathways that detected proteins were involved in.

Statistical analyses of the tendon fibroblast experiments were performed using GraphPad Prism version 7 software (GraphPad Software Inc., La Jolla, CA, USA). A Kolmogorov-Smirnov test was used to determine normality for each experiment. The data from each experiment and each material tested was normally distributed. For all analyses, statistical significance was taken at $p<0.05$. Statistics in some figures are represented by lower and upper case letters. An upper case letter (i.e. "A") represents that the material is statistically significantly greater than every other material with the corresponding lower case letter (i.e. "a").

For testing the effect of seeding set up on change in metabolic activity between set ups at each time point and the change in metabolic activity over a 7 day culture, a two-way ANOVA with Tukey's multiple comparisons test was used. This same test was used to test the effect of suture type on both the change in cell number at any time point and the change in cell number for each suture type over a 7 or 14-day culture.

For testing the effect of seeding density on initial attachment, a one-way ANOVA with Tukey's test was used. This same test was used to test the effect of filament type on initial cell attachment.

5.5 Results

5.5.1 Protein corona composition on hybrid suture components and surgical sutures

Protein adsorption to biomaterials plays a part in mediating cell attachment and behaviour. The adsorbed protein corona of serum-incubated hybrid suture components (electrospun filaments and melt-extruded yarns) and surgical sutures PDS and Vicryl were investigated. All materials adsorbed proteins and there were 750 proteins that were differentially expressed. The protein corona composition varied between materials, as shown by principal component analysis (PCA).

The PCA graph showed a clear separation between electrospun filaments and melt-extruded yarns, compared to PDS and Vicryl sutures (Figure 5.2). There is also relative separation of PDS and Vicryl. Interestingly, when adding the third component (PC3), the control sutures cluster together and there is a separation between electrospun filaments and melt-extruded yarns (Figure D.1 in the Appendix).

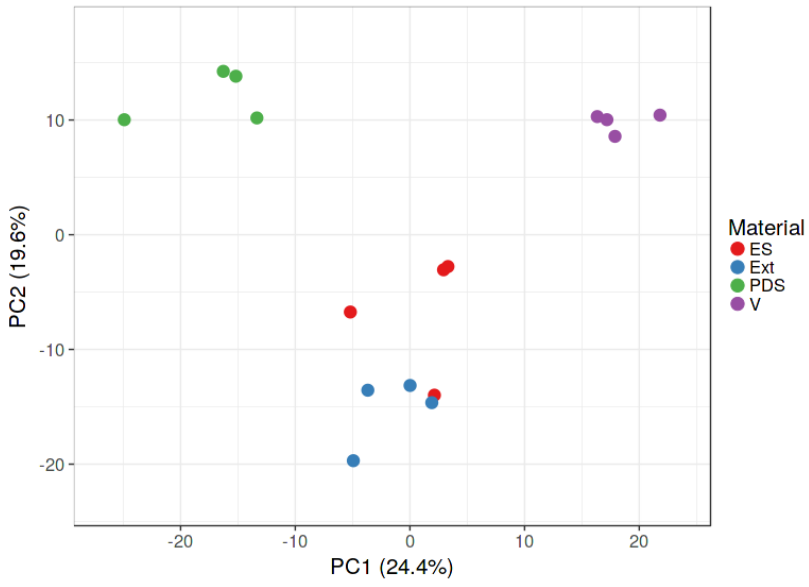


Figure 5.2: Principal component analysis of protein coronas formed on electrospun filaments (Es) and melt-extruded yarns (Ext), as well as on surgical sutures PDS (PDS) and Vicryl (V). The four materials were incubated in human serum for 1 hour before undergoing mass spectrometry to analyse the adsorbed protein coronas. PCA

separates the coronas based on material type. There is less separation between electrospun filaments and melt-extruded yarns than compared to, and between, PDS and Vicryl.

The heat map of proteins that were expressed in the coronas of PDS, electrospun filaments, and melt-extruded yarns are compared in Figure 5.3. Vicryl has very different physical and chemical properties compared to the other three materials and was excluded from this analysis to better discern differences between samples made of the same polymer PDO.

Overall, there were 338 proteins that were statistically significantly different from each other. These proteins formed 5 main clusters, as shown in Figure 5.3. The most significant differences were seen in the PDS suture corona compared to that of the other two materials. Cluster 1 and 5 are represent the largest groups of proteins that were differentially expressed (105 and 126 proteins, respectively). Cluster 1 is enriched with electrospun filaments and extruded yarns, whereas cluster 5 is enriched with PDS. For all three materials, the protein changes are largely consistent between serums tested, except for some variation in coronas from electrospun filaments, which is also reflected in the PCA graph. Both cluster 1 and 5 were driven by binding proteins and catalytic activity proteins, which has potential implications for the initial cell attachment and immune cell response. For each cluster, the pathways that the proteins are involved in are given in Appendix Figure D.2a. Figure D.3 in the Appendix compares the abundance of binding proteins between the materials tested with a focus on binding proteins that are deemed especially important for fibroblast attachment in Appendix Figure D2b. Interestingly, the dominant mass spectrometry signal from the extruded samples were polyethylene glycol (PEG) monomers. This was unexpected and will be addressed in the discussion.

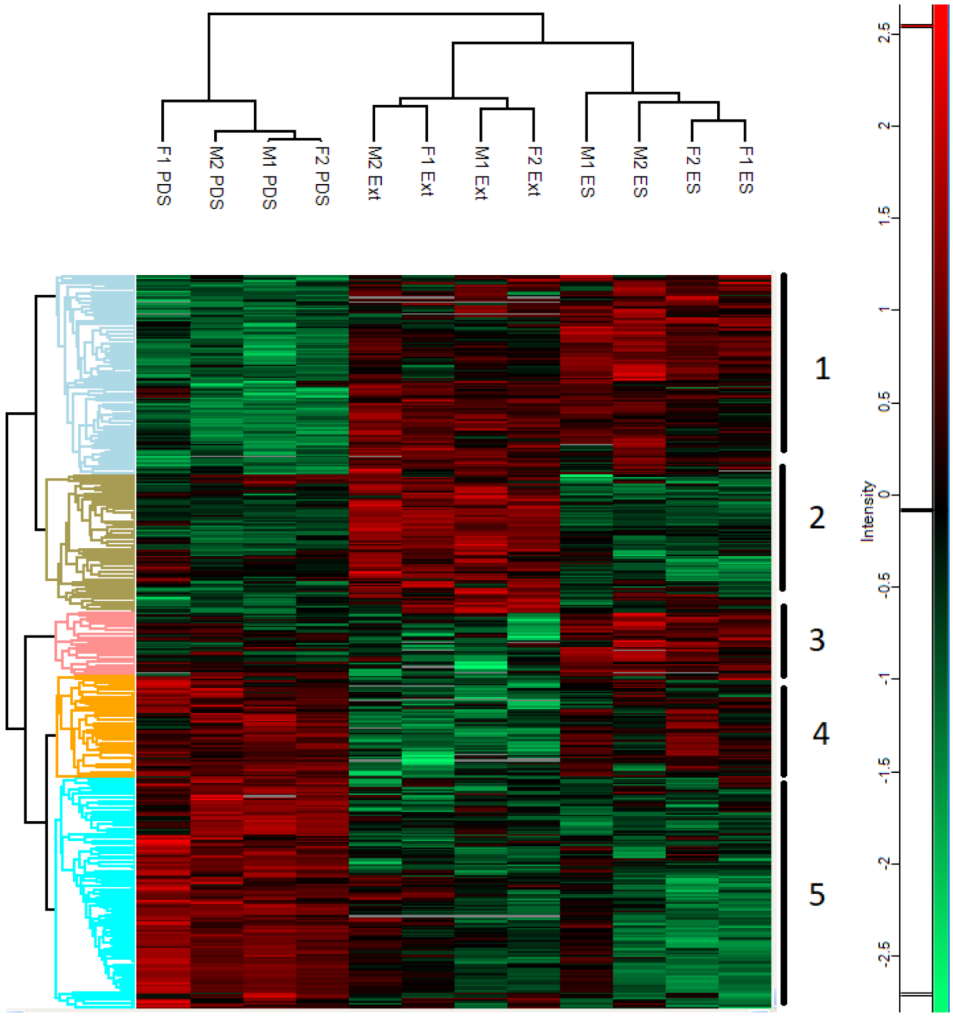


Figure 5.3: Heat map of differentially expressed proteins in the coronas of PDS sutures, electrospun filaments (Es), and melt-extruded yarns (Ext). These three materials were incubated in four serum samples (M1, M2, F1, F2) for 1 hour prior to mass spectrometry analysis of bound proteins. There were five main clusters of bound proteins detected, totalling 338 differentially expressed proteins. Cluster 1 increased in intensity with electrospun filaments and melt-extruded yarns; cluster 2 increased in intensity with extruded filaments only; cluster 3 increased with electrospun filaments only; cluster 4 increased with electrospun and PDS sutures; and finally, cluster 5 increased with PDS sutures only. There was little variation between the four serums tested. Log10 scale; red represents increasing intensity and green represents decreasing intensity.

The heat map of the proteins that were differentially expressed in the coronas of electrospun filaments and melt-extruded yarns are compared in Figure 5.4. Overall there were 102 proteins with significantly different intensities. These proteins formed 2 main clusters of proteins; 41 proteins were enriched with electrospun filaments (top cluster) and

61 proteins were enriched with extruded yarns (bottom cluster). Both electrospun and extruded protein groups were driven by binding proteins and catalytic activity proteins. Evidence that these observations were not due to chance is that the patterns are highly conserved across the 4 serums used. The full list of differentially expressed proteins are given in Appendix Table D1 and the pathways that the proteins are involved in are given in Appendix Figure D.2b.

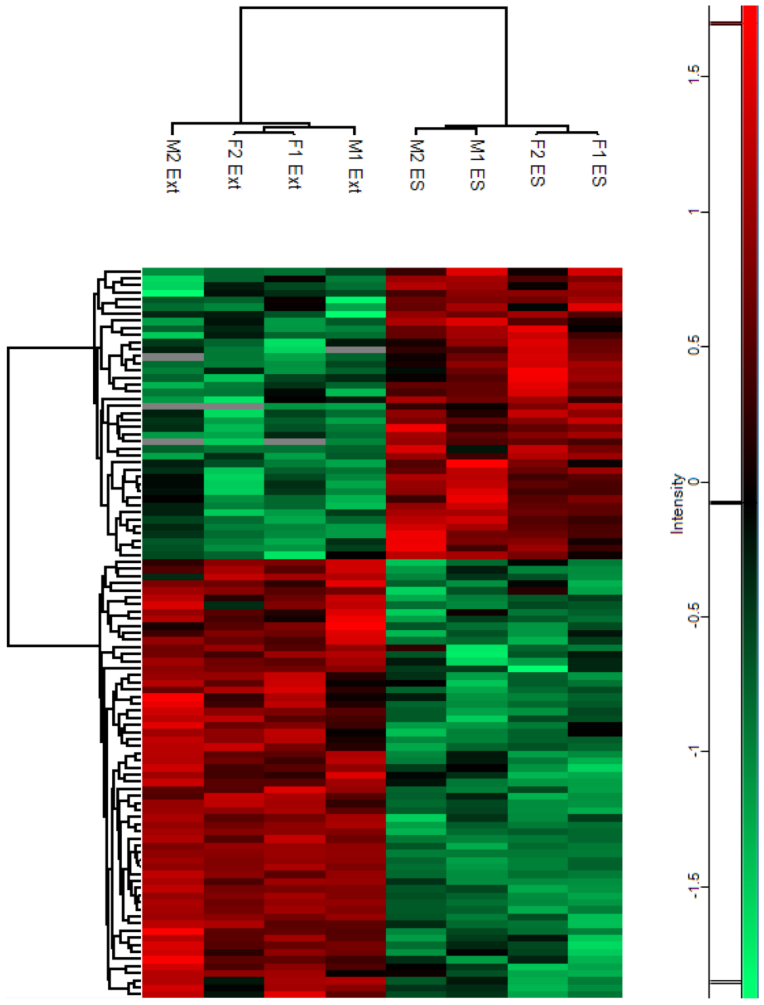


Figure 5.4: Heat map of differentially expressed proteins in the coronas of electrospun filaments (Es) and melt-extruded yarns (Ext). Electrospun filaments and extruded yarns were incubated in four serum samples (M1, M2, F1, F2) for 1 hour prior to mass spectrometry analysis of bound proteins. There were two different clusters of bound proteins detected, totalling 102 different proteins. 41 proteins were enriched with electrospun filaments (top cluster) and 61 proteins were enriched with extruded yarns (bottom cluster). There was very little variation between the four serums tested. Log10 scale; red represents increasing intensity and green represents decreasing intensity.

5.5.2 Cell seeding optimisation

This experiment aimed to optimise the seeding set up and density to promote the highest initial cell attachment. This was needed to further investigate cell-material interactions such as metabolic rate, growth, and infiltration. It was found that a higher number of cells attached to filaments that were mounted in direct contact with TCP, at day 1, 4, and 7, as shown in Figure 5.5a ($p<0.0001$). In optimising the seeding density, it was found that crowns that were seeded with 80,000 cells had a statistically higher attachment compared to crowns seeded with 20,000 cells ($p=0.0125$). Crowns seeded with 40,000 cells, 60,000 cells, or 80,000 cells were not statistically significant from each other. For all subsequent experiments, it was determined to seed at a density of 80,000 cells/crown in 200µL and to seed in a 12-well plate with the crown in contact with TCP.

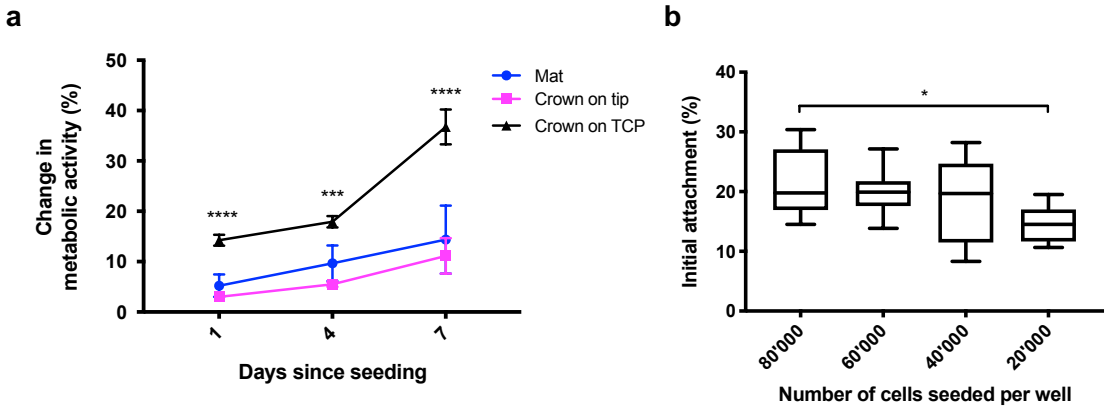


Figure 5.5: Optimising the cell seeding set-up and seeding density. (a) Filaments were seeded at 80,000 cells/crown in 200µL to test three different filament set-ups: filament ends were melted together to create a mat on TCP, filaments were mounted in cell crowns resting on a crown tip (not in contact with TCP), or filaments were mounted in cells crowns in contact with TCP. On day 1, a higher proportion of tendon fibroblasts attached to filaments mounted in crowns on TCP, compared to the crowns on tips ($p<0.0001$) and the mat ($p<0.0001$). On day 4, there was a higher cell number on crowns on TCP, compared to on tips ($p<0.0001$) and on mats ($p=0.0001$). On day 7, cell number for crowns on TCP was higher than the other two conditions ($p<0.0001$ for both). (b) Various seeding densities (between 20,000-80,000 cells/crown in 200µL) were compared by measuring cell attachment at 24 hours after seeding. The highest attachment was seen on crowns that were seeded with 80,000 cells, but the result was only statistically significant compared to sutures seeded with 20,000 cells ($p=0.0125$). Statistical significance was determined at *$p<0.05$, **$p<0.01$, ***$p<0.001$, ****$p<0.0001$. Error bars represent

standard deviations; n=3 for each condition.

5.5.3 Tendon fibroblast attachment and metabolic activity on hybrid suture components

The initial attachment of tendon fibroblasts on electrospun filaments and melt-extruded yarns, compared to on TCP, is shown in Figure 5.6. Attachment was 68±5% on melt-extruded yarns and 37±12% on electrospun filaments. Significantly more cells attached to TCP, compared to both electrospun filaments ($p<0.0001$) and melt-extruded yarns ($p<0.0001$). The attachment was also significantly higher on the melt-extruded yarns compared to on electrospun filaments ($p<0.0001$).

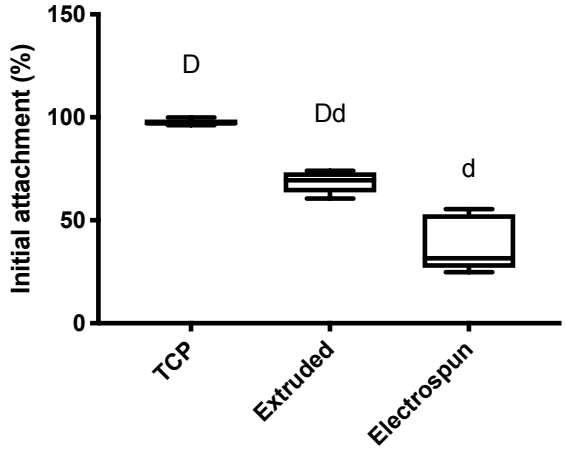


Figure 5.6: Initial attachment of tendon fibroblasts on hybrid suture components. Hybrid suture components (electrospun filaments and melt-extruded yarns) were compared to each other and to TCP. (a) Attachment was higher on melt-extruded yarns (68±5%) compared to on electrospun filaments (37±12%, $p<0.0001$), but notably lower compared to attachment on TCP, $p<0.0001$. Statistical significance was determined at Aa=$p<0.05$, Bb=$p<0.01$, Cc=$p<0.001$, Dd=$p<0.0001$. Error bars represent standard deviations; n=3 for each condition.

Prestoblue was used to quantify changes in cell metabolic viability by measuring cell numbers (a surrogate for cell proliferation) over 14 days. Figure 5.7a compares cell number measured on electrospun filaments, melt-extruded yarns, and TCP over 14 days. On day 7, there was a higher cell number on TCP, compared to electrospun and melt-extruded

materials ($p<0.0001$ for both). There was also a higher cell number on melt-extruded yarns compared to on electrospun filaments ($p<0.0001$). On day 14, there were more cells on TCP compared to on electrospun filaments ($p<0.0001$) and melt-extruded yarns ($p=0.0017$). There was also a higher number of cells on melt-extruded yarns compared to electrospun filaments ($p=0.0001$). Figure 5.7b shows the change in cell number measured relative to day 1 for each material. On day 7 and 14, there was an increase in cell number on electrospun filaments ($p<0.0001$ for both days). There was no statistically significant differences in the change in cell number between melt-extruded yarns and TCP at any time point.

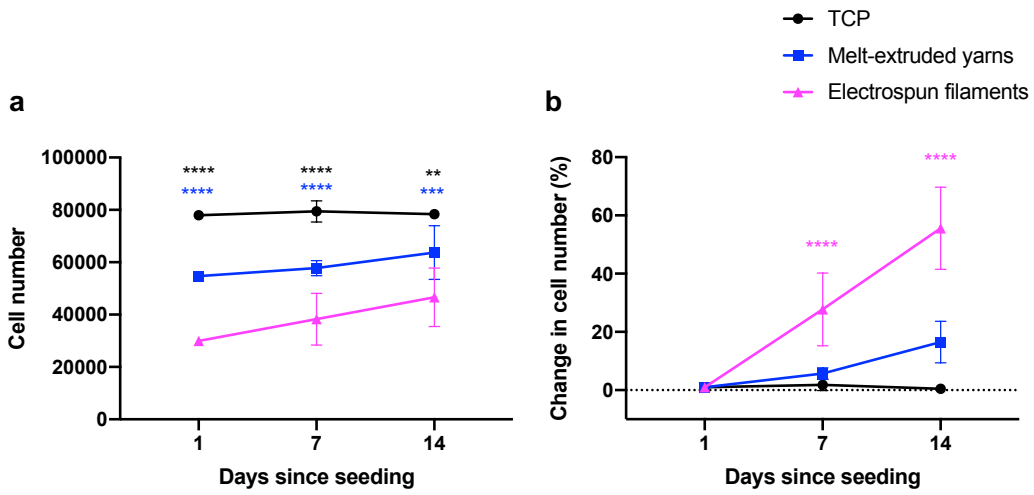


Figure 5.7: Metabolic activity of tendon fibroblasts on hybrid suture components. Hybrid suture components (electrospun filaments and melt-extruded yarns) were compared to each other and to TCP both in terms of cell number and change in cell number over 14 days. (a) On day 7, there was a higher cell number on TCP, compared to on electrospun and melt-extruded materials ($p<0.0001$ for both). There was also a higher cell number on melt-extruded yarns compared to on electrospun filaments ($p<0.0001$). On day 14, there were more cells on TCP compared to on electrospun filaments ($p<0.0001$) and melt-extruded yarns ($p=0.0017$). There was also a higher number of cells on melt-extruded yarns compared to electrospun filaments ($p=0.0001$); (b) For each material, the change in cell number was measured relative to day 1. On day 7 and 14, there was an increase in cell number on electrospun filaments ($p<0.0001$ for both days). There was no statistically significant differences in the change in cell number between melt-extruded yarns and TCP at any time point. Statistical significance was determined at *=$p<0.05$, **=$p<0.01$, ***=$p<0.001$, ****=$p<0.0001$. Error bars represent standard deviations; n=3 for each condition.

5.5.4 Tendon fibroblast attachment and metabolic activity on hybrid sutures

The initial attachment of tendon fibroblasts on hybrid sutures compared to on control sutures is shown in Figure 5.8. At 24 hours after seeding, there was 28±7% attachment to hybrid sutures, 24±7% to electrospun sutures, 10±5% to Vicryl, and 2±0.1% to PDS. The attachment on electrospun and hybrid sutures was significantly higher than on Vicryl and PDS, $p<0.0001$. There was also a significantly higher attachment on Vicryl compared to on PDS, $p=0.002$.

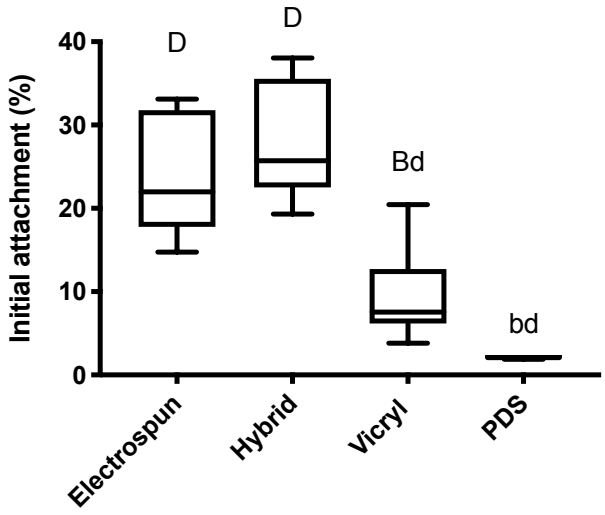


Figure 5.8: Initial attachment of tendon fibroblasts on hybrid and control sutures. Attachment was higher on hybrid (28±7%) and electrospun sutures (24±7%), compared to on Vicryl (10±5%) and PDS (2±0.1%), $p<0.0001$. Vicryl also had a significantly higher initial attachment compared to PDS ($p=0.002$). Aa=$p<0.05$, B=$p<0.01$, Cc=$p<0.001$, Dd=$p<0.0001$. Error bars represent standard deviations; n=3 for each condition.

Prestoblue was used to quantify changes in cell metabolic viability by measuring the change in cell number (a surrogate for cell proliferation). Figure 5.9a compares cell number measured on hybrid and control sutures over 7 days. On day 3 and 7, the cell number was higher for hybrid and electrospun sutures, compared to on Vicryl and PDS ($p<0.0001$ for all comparisons). There was no significant difference between electrospun and hybrid

sutures or between Vicryl and PDS sutures on day 3 or 7. Figure 5.9b shows the change in cell number measured relative to day 1 for each material. On day 3, there was an increase in cell number on hybrid sutures (p=0.0247) and electrospun sutures (p=0.0003) and a decrease on PDS sutures (p=0.0082). On day 7, there was an increase in cell number on hybrid and electrospun sutures (p<0.0001 for both), PDS sutures (p=0.0364), and Vicryl sutures (p=0.0007).

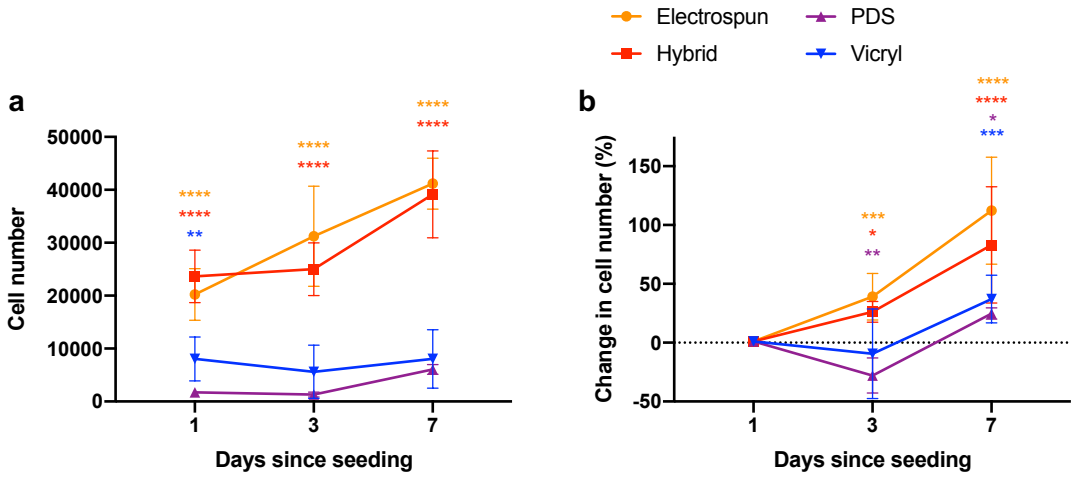


Figure 5.9: Metabolic activity of tendon fibroblasts on hybrid and control sutures. (a) The number of cells on hybrid and control sutures were compared at day 1, 3, and 7. On day 3 and 7, there were more cells attached to the hybrid and electrospun suture than to PDS and Vicryl (p<0.0001). There was no significant difference between electrospun and hybrid sutures or between Vicryl and PDS sutures on day 3 or 7; (b) For each material, the change in cell number was measured relative to day 1. On day 3, there was an increase in cell number on hybrid sutures (p=0.0247) and electrospun sutures (p=0.0003) and a decrease on PDS sutures (p=0.0082). On day 7, there was an increase in cell number on hybrid and electrospun sutures (p<0.0001 for both), PDS sutures (p=0.0364), and Vicryl sutures (p=0.0007). Statistical significance was determined at *=p<0.05, **=p<0.01, ***=p<0.001, ****=p<0.0001. Error bars represent standard deviations; n=3 for each condition.

5.5.5 Tendon fibroblast coverage on hybrid sutures

There were significant differences in cell coverage on hybrid sutures compared to on control sutures. Figure 5.10 shows the four suture types without cells (left column), cultured with tendon fibroblasts with 4 days (middle column), and cultured for 7 days

(right column). On day 4, there was cell coverage on the hybrid suture but it was localised to the electrospun component (Figure 5.10B). Conversely, there was minimal cell coverage on PDS (Figure 5.10H) or Vicryl (Figure 5.10K). On day 7, tendon fibroblasts elongated along electrospun filaments resembling the morphology seen in healthy human tendons (Figure 5.10C and F). There was some attachment of tendon fibroblasts on melt-extruded fibres in the hybrid suture, as shown in Figure 5.10F, but there was visibly reduced coverage on these fibres compared to on electrospun sutures (Figure 5.10C). The cell density was higher on electrospun sutures but some bridging of cells between fibres was apparent on melt-extruded fibres. Overall, fibroblasts seemed to conform to fibre geometry on electrospun sutures, but not as much on hybrid sutures. Cells did not visibly attach on PDS sutures (Figure 5.10I). It is worth noting that on all sutures, cells seemed to cluster together and form confluent, patchy areas of cells that did not extend throughout the length of the suture. Due to the cells forming confluent aggregates, it was difficult to discern cell shape. There was some attachment on Vicryl sutures, however these cells took on a more textured and rounded shape with no preferential direction (Figure 5.10L). Because of the coating on Vicryl sutures, it was more difficult to discern cell shape (Figures 5.10K and L).

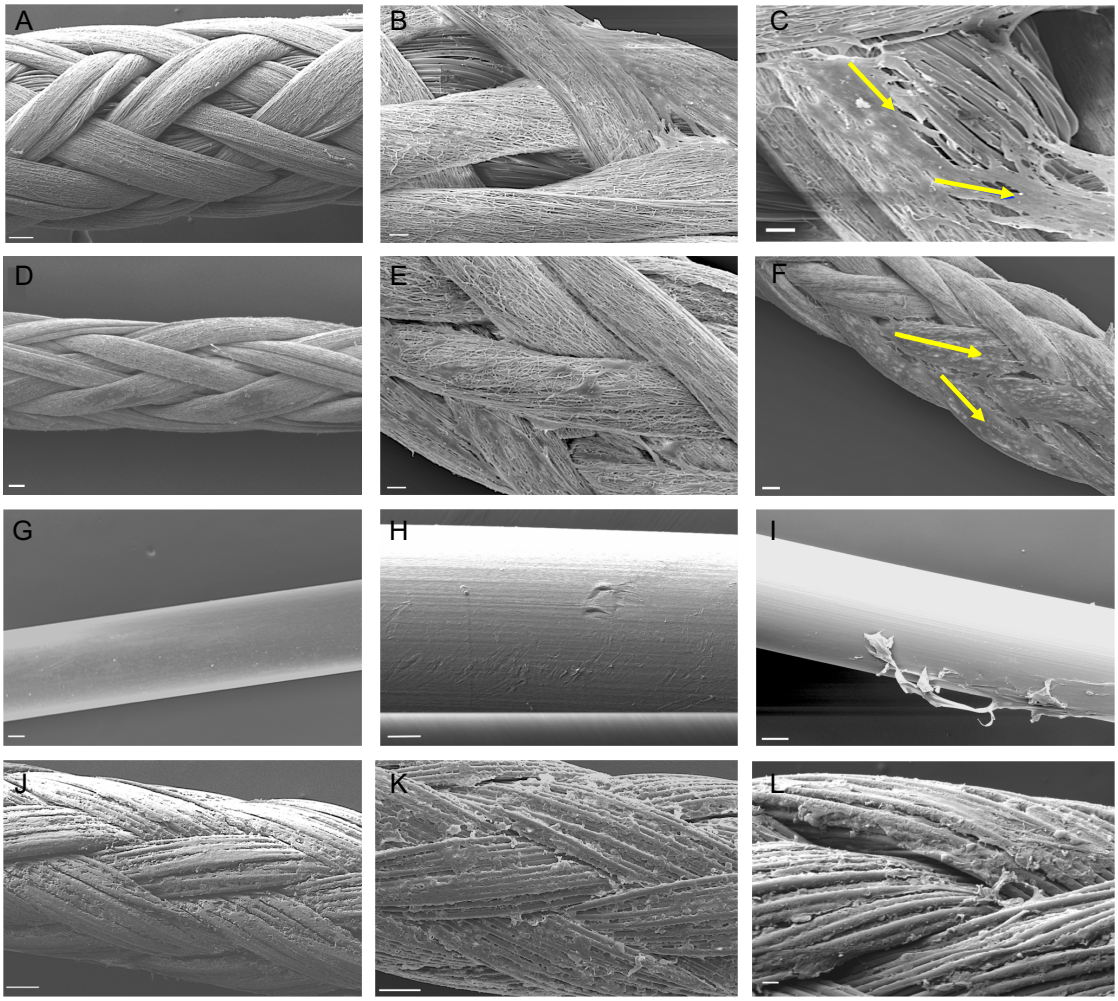


Figure 5.10: SEM images of healthy tendon fibroblasts seeded on hybrid and control sutures. The left column shows the unseeded sutures; the middle column shows the sutures cultured for 4 days; the right column shows the cells cultured for 7 days. (A,B,C) Hybrid sutures. (A) Hybrid sutures without cells; (B) Cells show preferential attachment to electrospun over melt-extruded fibres at 4 days; (C) Cells are growing and migrating to attach to the melt-extruded fibres at 7 days, however their morphology is not as clear as on electrospun fibres. (D,E,F) Electrospun control suture. (D) Electrospun suture without cells; (E) Cell attachment to electrospun fibres with individual cells visible; (F) Significant cell attachment and elongation (shown with yellow arrows) along fibres at 7 days. (G,H,I) PDS control suture. (G) PDS sutures without cells; (H) No visible cells at 4 days; (I) Some marking on the suture at 7 days, but unclear if these are cells. (J,K,L) Vicryl control suture. (J) Vicryl sutures without cells; (K) Some cells potentially attached at 4 days, but difficult to distinguish from the suture coating; (L) Some potential cell coverage at 7 days, with cells exhibiting a rounded morphology. Scale bars are 50μm for A-E and G-K and 20μm for F and L.

5.5.6 Tendon fibroblast infiltration into hybrid sutures

Hybrid sutures were seeded with tendon fibroblasts for 7 days and cell attachment and infiltration was assessed using μCT. The control sutures PDS and Vicryl were also scanned using this method. Figure 5.11A shows the scanned hybrid suture without cells on the left panel and a clear increase in signal on the suture seeded with cells on the right panel. The bottom two images show a cross-sectional scan of a suture without cells (on the left) and seeded with cells (on the right). There was clear adhesion of cells around the surface of the suture, but there was no clear indication of cells infiltrating into the centre of the suture when comparing to the signal of unseeded sutures. The same layout is used for Vicryl (Figure 5.11B) and for PBS (Figure 5.11C).

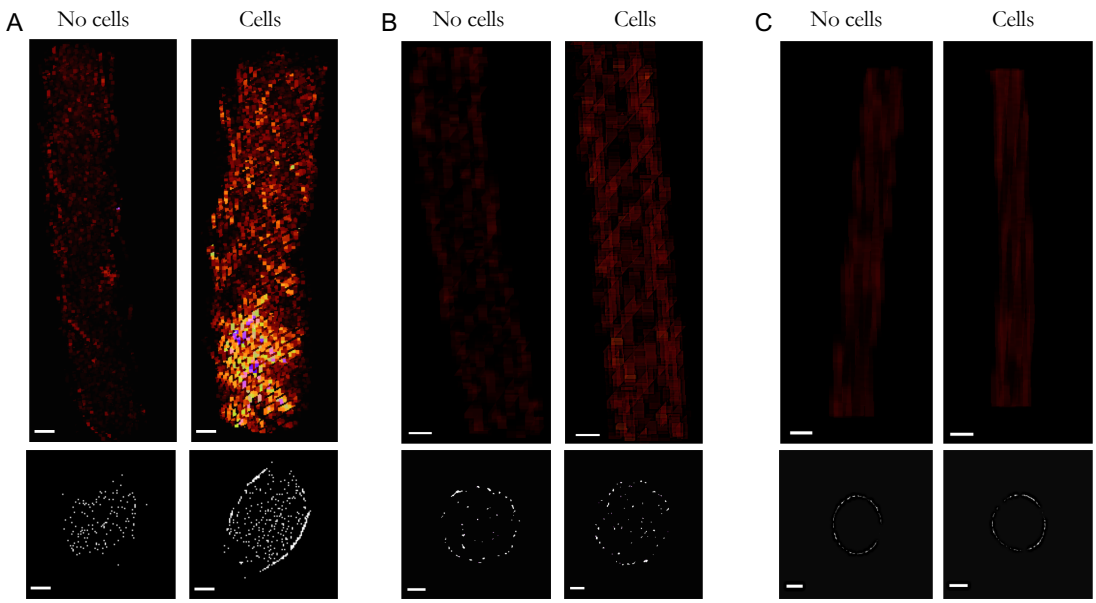


Figure 5.11: μCT scans of hybrid, Vicryl, and PDS sutures seeded with tendon fibroblasts and cultured for 7 days. For each suture type, the acellular sutures are on the left panel and sutures seeded with cells are on the right panel. Both sutures with and without cells were stained with OsO_4 to help visualize cellular attachment and infiltration. (A) Hybrid suture with cells show a clear, nonuniform signal that is absent from the acellular yarn. The cross-section of the hybrid suture (bottom two images) shows that there isn't any clear indication of infiltration into the centre of the suture; (B) Vicryl suture with cells has a slightly brighter signal compared to the acellular yarn, but no visible infiltration can be detected; (C) PDS with cells does not have a visibly different signal compared to the acellular yarn. Scale bars represent 100μm.

5.6 Discussion

The overall aim of this chapter was to investigate the short-term bioactivity of hybrid sutures compared to electrospun sutures and sutures currently in surgical use for tendon repair. To do this, this work investigated how the adsorbed protein composition changed in response to serum-incubated suture components and also how tendon fibroblasts interacted with the different suture materials. It was shown that electrospun and hybrid sutures promoted a biological response: proteins adsorbed and fibroblasts attached, survived, grew along the sutures, and adopted appropriate morphologies. There were three secondary findings from this work. Firstly, there were significant differences in the adsorbed protein coronas between all materials, with electrospun filaments and melt-extruded yarns being the most similar. Second, there was a higher initial cell attachment on hybrid sutures, but the cells on electrospun sutures were more metabolically active. Finally, electrospun fibres most supported cell growth that mirrored fibroblasts behaviour in native tissue. This discussion outlines differences in the adsorbed protein corona on electrospun filaments, melt-extruded yarns, PDS, and Vicryl. Then, fibroblast attachment and metabolic activity on the suture components, as well as hybrid and control sutures, are discussed. Finally, cell coverage and infiltration on the hybrid and control sutures are reviewed. In each section, the limitations of the experiments and results are considered.

5.6.1 All sutures adsorb a protein corona but its composition is dependent on suture type

Cell-material interactions are mediated by an adsorbed protein layer, which is formed on the material surface upon initial contact with serum and precedes the attachment of immune and stromal cells.[258,259] It is through this adsorbed layer that cells initially respond. The aim of this work was to explore whether electrospun filaments and melt-extruded yarns, as well as PDS and Vicryl, showed differential protein binding upon contact with serum. It was found that all four materials adsorbed proteins and had significantly different

adsorbed coronas from each other. Electrospun filaments and extruded yarns had more similar adsorption profiles compared to Vicryl and PDS. Exposing electrospun filaments and extruded yarns to serum led to 102 differentially expressed proteins, whereas adding PDS led to 338 proteins that were differentially expressed.

As mentioned, protein adsorption is a key determinant of cell response to material surfaces.[258] How adsorbed proteins mediate cell-material interactions are determined both by the protein adsorption profile (which proteins attach, as measured by mass spectrometry in this study) and the protein functionality (which conformation or orientation the proteins take).[258,280–282] Unfortunately, mass spectrometry as was used here, is unable to detect the functionality of adsorbed proteins. The type, abundance, and orientation of proteins is largely dependent on chemical and physical properties of the material and ultimately influences how cells interact with the material. The four materials tested here had very different physical and chemical properties. In terms of gross chemical differences, electrospun filaments, melt-extruded yarns, and PDS sutures are all made of PDO, whereas Vicryl is made of poly-L-lactate. In considering physical differences, electrospun filaments and melt-extruded yarns are made up of 1μm and 10μm sized fibres, respectively, whereas PDS and Vicryl are made up of larger fibres (on the order of 3-30 times larger). PCA analysis in the first two components revealed that most of the variation existed between surgical sutures and the hybrid suture components. However, when adding the third component, the sutures cluster together and there was a clear separation between electrospun filaments and extruded yarns. This indicates that most of the variation between samples can be explained in the first three components. This result was expected; although electrospun filaments and extruded yarns are more similar than PDS and Vicryl, differences in biophysical characteristics (such as fibre size), may lead to variations in local surface properties. In particular, local surface properties, such as surface hydrophobicity[263,283], charge[283], and chemistry[111,282] have been shown to be key determinants

in altering protein binding and fibroblast behaviour.[258,280–282] As mentioned previously in this thesis, measuring surface properties of electrospun fibres is challenging, despite their importance in mediating cell-material interactions and downstream integration of the material with the host tissue. Some studies have altered surface charge to deliberately manipulate protein orientation to mediate cell binding ability.[284,285] Future work should further explore surface characterisation methods, such as XPS and AFM, to characterise chemical elements at the surface and how they influence protein adsorption. It would also be informative to characterise pristine material surface properties using AFM and investigate how these surfaces change after protein binding.

In mass spectrometry, the removal of abundant proteins allows the detection of less abundant ones. Because the four materials tested here were so different from each other, less abundant proteins attached to any of the materials might have been missed in the protein quantification. However, this potential bias does not influence the comparison of detected proteins on different materials. Vicryl is a braided suture, made up of melt-extruded, 30μm sized, poly-L-lactide fibres, and had different chemical and physical properties from the other materials tested. On mass spectrometry, this resulted in a very different peptide population detected, which might have potentially reduced the sensitivity of the protein quantification. Moreover, the dominant signal from the melt-extruded filaments was PEG, which was not anticipated on the extruded filaments and thought to be a surface or component in the extrusion process. This is because a PEG-based finish was applied after melt-extruding PDO filaments at FET (Chapter 3.4.3), in order to control static build up and to draw the yarn over heated godets without breaking. This spin finish remained on the surface of the yarn, and is likely to have influenced the protein adsorption and quantification. Although the detection of PEG was not included in any comparisons, it could have potentially reduced the sensitivity of the protein quantification by masking the detection of less abundant proteins. Although this spin finish is commonly used in

industry, the PEG signal was not detected on Vicryl or PDS. In industry, it is usual to remove the spin finish in a dry-cleaning process (known as "scouring") using the solvent perchloroethylene (PERC). Unfortunately, the proprietary nature of many suture processing techniques in industry makes it difficult to determine their precise impact on biocompatibility. It is clear that the various steps in the suture manufacturing process alter the surface properties and likely the resulting adsorbed protein corona.[286,287] It also means that there is potential to deliberately manipulate protein-material interactions to promote a specific protein composition and conformation. The potential to incubate sutures in specialised biological fluids prior to implantation would be a potentially safe and effective way to functionalise the suture protein corona prior to implantation, such that it encourages specific material-protein-cell interactions and activation of pathways to improve tissue healing. Future work should explore scouring the melt-extruded yarns to investigate protein adsorption on clean melt-extruded yarns.

5.6.2 Tendon fibroblasts preferentially bind to extruded yarns but are more metabolically active on electrospun filaments

A successful augmentation material for tendon repair will require tendon fibroblasts to attach to the material surface in order to proliferate and differentiate.[288,289] Electrospun fibres have long been known to confer contact guidance cues to support cell attachment.[290,291] Before undergoing cell experiments, both the seeding set-up and density were optimised to promote the highest initial attachment. Unsurprisingly, there was a higher initial cell attachment to filaments that were in direct contact with TCP, a material designed to promote cell attachment. Although the filaments in a mat were also in direct contact with TCP, there was a lower attachment compared to filaments that were mounted in a crown. It is possible that there was more exposed surface area for cell attachment in the crown, where filaments weren't in contact with each other and, in theory, cells could attach on top and on the side of filaments. The seeding density experiment showed that

there wasn't much difference between the three highest seeding densities, suggesting a potential optimum above the densities tested here. It was determined to seed at a density of 80,000 cells/crown and to seed in a 12-well plate with the crown in contact with TCP.

In light of the absorbed protein coronas differing between electrospun filaments and melt-extruded yarns, the tendon fibroblast response to the same materials was evaluated. At 24 hours after seeding, a higher fraction of seeded cells attached on melt-extruded yarns compared to on electrospun filaments. This result was unexpected, as there is lots of evidence to suggest that the submicron size of electrospun fibres supports cellular adhesion.[292,293] However, it is possible that the loosely twisted structure of the melt-extruded yarn exposed more effective surface area for attachment, allowing cells to attach above and within the yarn. Conversely, the densely packed electrospun fibre mesh might have provided less open area for attachment. The possibility that densely packed fibres are impeding cellular attachment and activity has been noted before.[175,242] Additionally, the seeding method and set-up only allowed for one timepoint for the cells to attach to the material. This means that the larger effective surface area of melt-extruded fibres probably increased the chance that cells attached to them over electrospun fibres. Overall less than 40% of cells attached to the electrospun filaments and less than 70% attached to the melt-extruded yarns, suggesting the rest of the cells must either be found on the cell crown or in the bottom of the TCP well. Future work should further improve the seeding method to allow for more than one contact timepoint for the cells to attach to the material. Moreover, characterising the differences between fibroblasts that did and didn't attach to filaments could reveal information about fibroblast sub populations. However, it is possible that the attached fibroblasts would be the ones that attach *in vivo* and the interesting ones to study.

There are other factors which may have influenced cell attachment, such as local material properties influencing adsorbed protein composition and their integrin binding domains. Measuring surface stiffness of electrospun filaments and melt-extruded yarns using AFM was attempted, but did not yield reliable results (data not shown). Previous work has shown that fibroblasts preferentially respond to stiffer surfaces, by increasing their own stiffness[294], upregulating ECM genes, and increasing attachment.[109] It is possible that altered adsorbed protein composition influenced cellular attachment to the material. In order to imitate this adsorbed layer in an *in vitro* environment, sutures were preconditioned with culture media (supplemented with FBS) prior to cell seeding. The proteomics work earlier in this chapter showed that the protein adsorption between different serum batches was quite similar. Because the same FBS batch was used to precondition all samples, it is probable that the FBS-induced corona would be even more consistent. However, it is likely that the matrix formed from culture media would be different to the matrix formed from human serum and could influence the resulting cell response.

Although the largest initial cell attachment was observed on melt-extruded yarns, electrospun filaments promoted the largest increase in cell number over a 14 day culture period. This result is supported by previous studies, which suggested that an increase in surface area available for cellular attachment is not always correlated with increased cell proliferation.[295,296] It might be that electrospun fibres, or the proteins attached to them, have more cues that drive proliferation. It might also be that the higher cell density attached to melt-extruded yarns inhibited proliferation, although this is not supported by the SEM results. Finally, it is also possible that melt-extruded fibres had an adsorbed protein layer that was potentially influenced by the PEG coating and was not conductive to proliferation.

5.6.3 Tendon fibroblasts preferentially bind and proliferate on hybrid sutures compared to surgical sutures

In comparing different sutures, the initial cell attachment was higher on hybrid sutures compared to on surgically used PDS and Vicryl sutures. These results were expected; while no studies could be found that directly compared electrospun or melt-extruded materials directly to surgical sutures, there have been many accounts of poor cell attachment to surgical sutures *in vitro*[191] and *in vivo*.[196,297,298] Although proteins did adsorb to the PDS and Vicryl surface, the cell-material results suggest that they might not be the ones providing cues for attachment.

Tendon fibroblasts grown on hybrid sutures exhibited an increase in metabolic activity after 7 days of culture, whilst those grown on PDS and Vicryl exhibited a decrease in metabolic activity over the same time period. The 7 day time point was used for imaging cells on sutures with SEM and μCT, as pilot work had shown that electrospun sutures were completely covered in cells at 14 days. As mentioned, there have been numerous studies that reported poor cell survival and integration on surgical sutures.[196,297,298] Wong et al investigated the cellular activity of the tendon-suture interface in a rabbit and mouse model and found a well-demarcated acellular zone around the Prolene suture (a non-absorbable synthetic suture) as soon as 24 hours after implantation.[297] A similar acellular zone was observed by Rashid et al, between tendon tissue and a PDS suture in an ovine model.[196] In the context of developing sutures to augment rotator cuff tendon repair, it is important to establish whether the attached, proliferating cells can migrate along the suture surface, adopt a morphology that is similar to fibroblasts in native tissue, and infiltrate into the centre of the material. Unfortunately, there are not many well-established, *in vitro*, tests that reliably track cell movement along electrospun fibres.[271] Better *in vitro* models to measure cell movement after attachment would be useful to inform design requirements

that encourage cellular integration with the material. This will be discussed further in the following section.

5.6.4 Tendon fibroblasts cover hybrid sutures but do not display distinct infiltration

There was a marked difference in cell coverage between the various sutures tested at 4 and 7 days of cell culture. The fibroblasts on electrospun sutures had an elongated morphology and resembled fibroblast shapes in native tendon.[19] These cells formed patchy areas that were orientated along the direction of the fibres, indicating that the fibre structure was conferring contact guidance cues to the cells. This result is consistent with other studies looking at tendon fibroblast adhesion and shape on electrospun fibres.[299,300] It is tempting to speculate that these submicron fibres, which are capable of influencing tendon fibroblast behaviour, could improve tendon healing. However no study has yet investigated whether these cell-material interactions can modify the cellular lineage of the repairing tissue.[206] When looking at growth along hybrid sutures, there was similar growth on the electrospun fibre component. At day 4 and 7 after seeding, there were noticeably fewer fibroblasts on the melt-extruded fibre component and they had a less pronounced shape and extended in different directions. It is possible that because melt-extruded fibres were in the core of the suture, they were deeper than the electrospun fibres and not in direct contact with the cells upon seeding. Because Vicryl is coated with polyglactin 310 and calcium stearate to decrease tissue drag and bacterial adherence[63,301], it was difficult to discern where cells had attached or if the coating influenced the cell response. Future work should employ a method to stain and image cells directly on the material, such as an actin/phalloidin stain with confocal imaging. It might also be possible to quantify cell coverage to use as a proxy for growth in the future. Overall, these results suggest that the more textured micro- and nanofibrous surface of the hybrid suture better supported cell adhesion and coverage compared to the surface of the purely extruded PDS and Vicryl

sutures. These results are consistent with previous work which showed improved adhesion of cells and alignment along the direction of submicron and microscale fibres.[106,118,133,134,221,300,302,303] This work additionally adds a direct comparison to currently used sutures and shows that composite structures also enable alignment and growth of cells along filaments.

Cellular infiltration into implanted biomaterials is necessary for integrating the material with the host tissue.[242,304] Without cell ingrowth into the material, the repair could fail mechanically due to a void being left within the tissue following suture degradation.[196,297,298] Moreover, cellular infiltration into biomaterials is necessary for vascularisation, migration and proliferation of cells, and nutrient and waste diffusion.[242,305–307] In this chapter, SEM demonstrated that the exterior surface of hybrid and electrospun sutures was coated with tendon fibroblasts, but it couldn't be determined whether cells had migrated into the core of the material. Measuring cell infiltration is notoriously difficult. Numerous material fabrication methods have been developed to increase overall porosity or pore size, however whether larger pores translate to driving cells to infiltrate deeper into the scaffold is largely speculative.[175,308,309]

This chapter showed that staining cell-seeded sutures with OsO_4 and scanning with μCT proved to be a good method for visualizing cell attachment and location on and within the porous structure. It was found that most cells were observed on the surface of the suture in patchy areas, however no distinct infiltration could be detected. Bosworth et al found similar results by scanning electrospun yarns seeded with hMSCs.[98] Similarly, they didn't measure much infiltration but found a layer of cells attached to the periphery of the yarn. It has been suggested that nanoscale fibres can prevent cellular infiltration, due to the grooves between fibres being smaller than the size of a cell. In order for cell infiltration to occur, it is thought that the pore size should be at least the size of a cell, approximately

10μm.[242] Chapter 4 showed that the most abundant pore sizes in electrospun sutures were 0.5-5μm, whereas the most abundant pores in the hybrid suture were between 50-100μm.[242]

Further work quantifying the intensity of the cell signal at different locations and depths of the suture was outside of the scope of this thesis, but provides exciting opportunities for future work. This method could be further developed by investigating how cell infiltration changes with suture design and in particular, the porosity and pore sizes of the structure. However, OsO_4 is a non-specific lipid stain, so future work might need to develop other staining methods to selectively target which cell types infiltrated. Attempts to embed sutures in both wax and optimal cutting temperature compound (OCT) were unsuccessful; it was challenging to section OCT embedded samples and challenging to stain and image sutures with wax embedded samples. It is possible that the poor cellular infiltration reported in numerous *in vitro* tests is more reflective of poor amenability of existing *in vitro* models rather than biomaterials requiring design improvements.

Characterising cell-material interactions and evaluating their importance for downstream integration of the material with the native tissue should be evaluated in models relevant for the intended clinical application. After tendon surgery, there will be mechanical movement of the suture and shifting of the fibres, as well as accelerated degradation of the suture, leading to a loosening of the structure and allowing cells to migrate into the material. Moreover, shear stresses and tensile forces during movement can also stimulate cell growth. Thus, future work will need to perform a dynamic culture study, followed by an *in vivo* study to determine infiltration in a more clinically relevant environment.

5.6.5 Strengths and limitations of cell-material experiments

There are several strengths and limitations of the cell experiments presented in this chapter. Firstly, although this thesis aims to develop a suture to augment diseased tendon,

only fibroblasts from healthy tissue were available. This is a limitation, as the response of fibroblasts from healthy and diseased tissue would likely be different.[107,271,310] Previous work investigating the response of both healthy and diseased tendon fibroblasts to electrospun fibres showed that diseased cells retain the ability that healthy cells have in responding to biophysical cues, albeit at a different rate.[271] Moreover, these experiments only used cells from a small number of patients (n=3), however a benefit of this work is the use of human primary cells. This work only studied one cell type in isolation, however it is likely that native tendon fibroblasts and other cell types, such as immune cell populations, determine the initial host response. Future work should consider how the immune signature is influenced by the adsorbed protein corona and how immune cells regulate the recruitment of fibroblasts.[23,311] Finally, prior to the cell culture experiments, sutures were incubated in fetal bovine serum. Future work should incubate sutures in the same media as was used for the proteomic analyses.

Electrospun and hybrid sutures were braided with an industrial machine and there was low variability between samples. This implies that materials were produced in a reproducible way and observed cell-material interactions were due to underlying biophysical and chemical differences rather than due to sample variation. Finally, these experiments also have regulatory implications. Establishing the importance of chemical and biophysical properties in modulating the material-protein-cell response could influence the regulatory environment surrounding biomaterials in development. Most sutures are classified as class II inert medical devices. However, this work showed that, by adsorbing serum proteins, no material can be classified as truly inert and the guidelines for classification and pre-clinical testing requirements should reflect this. This point will be discussed further in the general thesis discussion.

5.7 Conclusions

Overall, this chapter demonstrated differences in the adsorbed protein corona and tendon fibroblast response between the hybrid suture and its components, compared to currently used surgical sutures PDS and Vicryl. There were significant differences in the adsorbed protein coronas between all materials tested. The hybrid suture components (electrospun filaments and melt-extruded yarns) had more similar protein adsorption profiles, which were strikingly different compared to those of Vicryl and PDS.

Investigating the tendon fibroblast response to the hybrid suture components revealed that melt-extruded yarns, made up of 10μm fibres, best supported fibroblast attachment. Electrospun filaments, made up of submicron fibres, best supported fibroblast metabolic activity.

Hybrid sutures promoted increased fibroblast attachment and cell coverage, likely due to their larger effective surface area, compared to PDS and Vicryl. While μCT was a useful tool for scanning and visualising the whole cell-suture construct, no visible infiltration was observed. Together, these results suggest that fibre properties and macroscale architecture play an important role in regulating protein adsorption, as well as cell adhesion and proliferation. Investigating local surface properties could help characterise and functionalise nano- and micro-scale surface cues in the future. Moreover, how different protein adsorption profiles may be driving the cell-material interactions observed in this chapter could help to identify a protein niche that drives favourable cell responses.

Table 5.1: Chapter 5 in context.

Evidence before this work	Added value of this work	Implications of this work
Upon implantation, biomaterials adsorb a layer of proteins. The composition of these adsorbed coronas is proposed to influence cell attachment and behaviour.	The proteins adsorbed by the components of the novel hybrid suture were similar to each other, and significantly different to the proteins adsorbed by surgical sutures in current clinical use.	Material properties can influence adsorbed protein coronas from the same serum. Adsorbed proteins could be investigated as a marker or modifiable parameter for future biomaterials. This could be used to encourage specific material-protein-cell interactions and activation of pathways to improve tissue healing.
Healthy tendon fibroblasts are responsive to submicron, nano-, and microscale biophysical cues. *In vivo* studies investigating the tendon-suture interface have shown poor cell survival and integration on currently used surgical sutures.	Melt-extruded yarns, made up of 10μm sized fibres, also influence fibroblast behaviour. A hybrid device, made up of submicron and micro-scale fibres can support fibroblast attachment and proliferation similar to electrospun-only devices. Currently used sutures promote minimal fibroblast attachment and proliferation.	The differential fibroblast response between electrospun and melt-extruded fibres has implications for designing functional biomaterials to promote a desired cell response. Surgical sutures promote minimal fibroblast activity, suggesting that the adsorbed proteins might not be the ones driving cell binding. The lack of fibroblast attachment on surgical sutures suggests that the cell-material incompatibility could be a contributing factor to their failure.

Chapter 6

Discussion

6.1 Overview

The overarching aim of this thesis was to develop a suture that has the potential to support the biological repair of tendon tissue and that can be used surgically. It was hypothesized that a combination device using two types of materials would be needed to achieve the mechanical and biological requirements of such a suture. Both electrospinning and melt-extrusion were explored to fabricate continuous and reproducible fibres with target diameters. Electrospun fibres were developed with submicron fibres to provide biophysical cues to influence cell response and melt-extruded fibres were fabricated to improve the tensile strength of the suture for clinical use. These materials were combined to create a hybrid suture with melt-extruded fibres in the core and electrospun fibres on the outside as the sheath. The hybrid suture has a similar tensile strength to that of currently used surgical sutures, but is less stiff, more porous, and has a hierarchical architecture more similar to native tendon tissue. Finally, the hybrid suture was compared to current surgical sutures in terms of its potential to influence protein adsorption and patient-derived tendon fibroblast response.

This discussion begins by reviewing the limitations with current sutures and the potential for novel sutures to improve tendon repairs. The contribution of this thesis to the development and translation of a novel hybrid suture is then described. Finally, a path to translation for the hybrid suture is proposed.

6.2 The potential for novel sutures to improve tendon repairs

6.2.1 Clinical need

Many surgical tendon repairs do not heal successfully. This inability to heal is often attributed to the tendon's poor intrinsic healing capacity and the inappropriate use of surgical materials. Rotator cuff repairs, the clinical focus of this thesis, cause significant disability, with 2-4% of visits to General practice (GP) attributed to rotator cuff pain. Surgical intervention is often necessary, but is resource intensive and has poor outcomes. The burden of rotator cuff tears significantly affects patients' quality of life and also places a financial strain on healthcare systems. Despite advances in surgical technique and improved understanding of tendon pathophysiology, there has been little improvement in reducing the rate of re-tears following surgery. In 2015, a large, multi-centre randomised trial (the UKUFF trial) reported a mean failure rate of 40% at 12 months after surgery, with both open and arthroscopic rotator cuff repairs.[2] This high failure rate has encouraged the search for novel treatment strategies to improve the outcomes of tendon repair.

6.2.2 Limitations with current sutures used for rotator cuff repair

Currently, in rotator cuff repair, synthetic absorbable sutures are the main means of connecting the tendon to bone or the tendon to tendon, depending on the type and location of the tear. However, both *in vivo* studies and observations made at revision surgery note that suture pull through is the main mode of failure. Indeed, the tissue-suture interface may represent the weakest link in tendon repair and be the cause for many repair failures.[79,80] The mechanism of pull through is poorly understood and likely multi-factorial. There are three likely contributing factors that are relevant to this thesis. First, tendon has a highly specialised hierarchical architecture and a poor intrinsic healing potential due to its low innervation, hypovascularity, and hypocellularity. Second, surgical sutures currently

in use are marketed as inert materials that only provide mechanical support to the torn tissue. In reality, no synthetic implantable material can really be classified as truly biologically inactive; at a local level, cells interact with the material, affecting wound healing. Finally, surgical sutures for tendon repair have been repurposed from materials used for other tissue types and clinical uses. As a result, sutures for rotator cuff surgery are used without consideration for the biology of wound healing, the local response of tendon to the implanted material, or the specific requirements of repairing highly diseased tendon tissue. Unsurprisingly, even if the repair does not fail outright, "regenerated" tendon tissue often does not recapitulate the complex structure of healthy tendon and is often weaker, making it more prone to failure. This mismatch between the properties of healthy tendon and the surgical materials available to repair diseased tendon, is reflected in the high failure rates and poor outcomes despite decades of incremental changes to both surgical sutures and techniques.

Because the suture is the main foreign material in contact with torn tendon during surgical repair, it is a promising medium through which novel treatments can be explored and implemented. One potential way to improve tendon healing is by encouraging the repair of existing native tendon tissue through provision of biophysical cues, whilst providing mechanical support during the early repair process. This thesis explored this option by using electrospinning to develop a degradable suture which can provide a scaffold for tendon tissue integration and also mechanically support rotator cuff repair.

6.2.3 Addressing limitations of electrospun sutures for tendon repair

Electrospun fibres are promising candidates for tendon tissue engineering, due to their potential to mimic native tendon ECM structure and induce similar biophysical cues. Despite their biological promise, fabrication, structural, and mechanical limitations have beem hurdles prevented the translation and implementation of electrospun fibres in

devices for tendon regeneration. This thesis deepens the understanding of the potential for electrospun materials to augment tendon repair. Specifically, this thesis addresses three major limitations of translating electrospun fibres for potential clinical use:

- Most electrospun fibres have been historically fabricated in the form of discontinuous sheets, which restrict their ability to be upscaled and processed into multifilament structures that can meet the demands of tendon. Here, by using an in-house method of electrospinning on a continuous wire and through access to a clean room, the reproducibility and scalability of electrospun filaments was improved.
- Although biologically advantageous, submicron scale fibres present significant mechanical and usability limitations for use in surgical applications. In this thesis, annealing was shown to be a method to tune the degradation rate of electrospun fibres.
- The poor tensile strength of electrospun submicron fibres have raised concerns about their suitability for clinical use and withstanding the physiological forces of tendon tissue. To address this, a hybrid electrospun suture with a stronger melt-extruded fibre component was developed. A braiding machine was able to tune the size and porosity of sutures, while increasing the production rate and reducing manual steps, compared to previous work.

The next section addresses specific ways in which this thesis has used these advances to develop a hybrid suture.

6.3 Development of a hybrid suture to augment tendon repair

For tendon repair, an ideal augmentation suture will be safe, bioactive, be able to mechanically support tendon tissue, degrade at a rate that is suitable for tendon healing, be usable by surgeons, and have a scalable manufacturing process. How this thesis contributes to developing sutures that meet these complex requirements is considered in this section.

6.3.1 Fabrication of continuous electrospun filaments made up of submicron fibres

The first aim of this thesis was to fabricate continuous electrospun filaments made up of submicron fibres. The continuous aspect of the fabrication process was especially important for its downstream intended use as a suture. Until now, most electrospun filaments have been limited to short sections, collected on a rotating drum, preventing their assembly into larger structures that would meet the demands of native tissue.[128] By electrospinning on a continuous wire and optimising polymer concentration, supplier, concentration, and solution, this work showed that it is possible to fabricate hundreds of metres of electrospun filament continuously. Homogeneity and production rate have long been limiting factors in upscaling electrospinning technology. This thesis presents a method to upscale this technology that is closer to meeting standards for clinical trials.

The wire collection method was already established before the start of the thesis, however there was significant heterogeneity between filaments, they had a low tensile strength, and the electrospinning variables had not been controlled or optimised. Hand-twisting filaments into yarns showed that in order to create a yarn strong enough to use as a surgical suture, the number of filaments would exceed what is usable with surgical equipment and the suture would be difficult to handle. As a result, annealing was explored as a post-processing method, as previous studies showed that heat treatment had a pronounced influence on the mechanical properties of pristine electrospun fibres made of other

synthetic polymers.[139–141,154] This work found that annealing marginally improved the tensile strength, but had a more significant effect on modulating the degradation rate. The ability to modulate the degradation profile with annealing may be useful to tune the properties of a biomaterial without altering the base material or fabrication method. An additional benefit of changing properties after fabrication is that electrospinning is a challenging process to control due to its many related parameters, such as voltage, humidity, and temperature, all of which affect fibre properties and reproducibility of the filament. The findings from the annealing study have been incorporated into production pipelines in the Carr group and have been published.[153]

6.3.2 Melt-extruded multifilament made up of micro-scale fibres are stronger and degrade more slowly than electrospun filaments

In industry, it is common to melt-extrude monofilaments using PDO.[220] There is some evidence of extruded multifilament PDO sutures on the market, but they are made up of 30μm fibres. Vicryl is also made up of 30μm, a diameter this work has shown to be likely be too big to influence cell behaviour through biophysical cues.[185,230] It is worth reiterating that fibre diameter is one of many biophysical properties that are important in influencing cell behaviour; indeed, there is evidence that fibre stiffness and degree of fibre alignment are also important in driving changes in cell behaviour.[107,178,312] However, because the effects of fibre diameter on tendon fibroblast properties have been more thoroughly characterised, it is a good starting point for characterising cell-material interactions.

A robust production method to fabricate melt-extruded yarns made up of 10μm fibres was demonstrated in this work. In comparing the same overall diameter of electrospun and melt-extruded materials, it was found that melt-extruded materials were stiffer, had a 11.5 times higher force at failure, a 20% lower overall porosity, and a slower degradation rate. This difference in tensile strength was expected, as melt-extruded fibres have a 10 times larger diameter compared to individual electrospun fibres. The slower degradation rate was

expected, as the larger fibre size and smaller filament porosity likely presented less surface area for hydrolytic degradation. Moreover, this finding was supported by thermal analysis, which showed that melt-extruded yarns had a higher crystallinity, suggesting that electrospun filaments were more susceptible to hydrolytic cleavage in the amorphous regions. This is the first study that directly compares electrospun and melt-extruded fibres that were fabricated from the same polymer. Future work should focus on characterising local mechanical properties to help characterise some of the potential drivers of cell attachment and proliferation found in Chapter 5.

The purpose of fabricating melt-extruded yarns was to provide mechanical support to electrospun fibres in a combination device. However, it was also important to consider the biocompatibility of melt-extruded fibres as not to inadvertently induce an adverse biological response. In terms of controlling cell-material response via biophysical cues, it is widely known that fibre alignment is important. Tendon cells cultured on aligned and randomly oriented submicron fibres show preferential cell morphology, attachment, and higher levels of tenogenic markers on aligned fibres.[107,118] The optimal fibre diameter of bioactive materials is less clear. Nano-, submicron, and microscale fibres have all been shown to provide biophysical cues to cells and differentially influence cell behaviour.[313] Here, 10μm sized melt-extruded fibres were developed, as they represented the lower size range that melt-extrusion technology can fabricate reproducibly, whilst being on a scale cells can attach to. In chapter 5, it was shown that in an *in vitro* environment, tendon fibroblasts attached to, and proliferated on, melt-extruded fibres. Indeed, a higher proportion of cells initially bound to melt-extruded compared to electrospun fibres, suggesting that melt-extruded fibres could influence cell response.

6.3.3 Potential improvements of a electrospun-extruded hybrid suture

A hypothesis of this thesis was that a combination of electrospun and melt-extruded materials would be needed to meet the target criteria for use as a suture. Indeed, it was shown that electrospun braided sutures had a 7 times lower force at failure compared to Vicryl and a 3.5 times lower force at failure compared to PDS sutures of the same size. A hybrid suture made up of an electrospun sheath and melt-extruded cores resulted in tensile properties that more closely matched current surgical sutures and the design requirements for this work. Compared to an electrospun only twisted suture developed in the Carr group, the hybrid suture had a 30% smaller diameter and 43% increase in force at failure, making it easier to handle by surgeons and compatible with surgical equipment. The core-sheath design was deliberately designed for its intended clinical function. Electrospun submicron fibres on the outside of the suture will be in initial contact with biological fluids upon implantation and can direct the initial material-protein-cell response through biophysical cues. Melt-extruded fibres in the core degrade more slowly and provide prolonged mechanical support and stabilization to the surgical construct.

No core-sheath structure combining electrospun and melt-extruded materials currently exists on the market. The combination of electrospun and melt-extruded materials results in additional complexity in manufacturing, however the potential performance improvements as a surgical device, compared to an electrospun-only device, are substantial. Although this is still an early prototype, the hybrid suture overcomes some issues with handling, mechanical properties, and upscaling seen with other current electrospun devices in development.

6.3.4 Short-term biocompatibility and bioactivity of the hybrid suture

Current clinical sutures are marketed as inert or biocompatible, meaning that they are not meant to intentionally induce a tissue response. However, it has been demonstrated that surgical sutures can influence the biology of the surrounding tissue by inducing foreign

body reactions.[190,196] Indeed, it is increasingly understood that no implanted material is truly biologically inactive. Materials used in tendon repair interact with the surrounding tissue, but are not deliberately designed to enhance tendon repair, which is consistent with the findings in this thesis. As a result, currently used sutures cannot be deemed truly inert or biocompatible. Conversely, emerging augmentation materials are intended to deliberately induce a targeted biological reaction. At the heart of the success of an augmentation suture is the ability to control and tune cell behaviour to direct cells to assemble and maintain new functional tissue. The findings in this thesis were consistent with previous literature, suggesting that electrospun fibres affect tendon biology: they adsorbed proteins and influenced native tendon fibroblast behaviour. On the other hand, the augmentation potential of melt-extruded fibres is less clear. They adsorbed proteins and promoted high rates of fibroblast attachment, but less proliferation and migration compared to on electrospun fibres. However, these findings could have also been influenced by the PEG contamination on the surface of the melt-extruded fibres. It seems that melt-extruded fibres are biocompatible, but more work is needed to determined their bioactive potential. All serum-incubated sutures adsorbed proteins. The protein types and their abundance varied significantly between sutures, but adsorption on electrospun and melt-extruded materials were the most similar. These findings showed that the protein corona can be manipulated through changing biomaterial properties (as was shown here) or potentially through treating materials with specialised biological fluids prior to implantation. Previous work showed that coronas formed on electrospun scaffolds incubated in serum, plasma, blood, and synovial fluid influenced fibroblast activity more than changes in biophysical cues like fibre dimeter.[107]

The response of tendon fibroblasts to the novel hybrid suture and to current surgical sutures contributes new information to the literature. There haven't been any previous studies comparing cell-material interactions between electrospun-based sutures and

currently available sutures. Previous *in vitro* and *in vivo* studies have shown minimal, and in some cases detrimental, cell-suture interactions and a lack of integration of the synthetic suture with native tissue.[55,58,74,81,196] This study only investigated tendon fibroblasts in isolation and therefore can't draw conclusions about the potential for this device to drive tissue repair. However, the biochemical and biophysical cues imparted by the electrospun fibres and to a lesser extent, the melt-extruded fibres, drove cell attachment and proliferation, whereas the cues offered by surgical sutures did not. These results show the potential for more in depth studies investigating cell-material interactions using all cell types involved in tendon healing, especially immune cell populations, and testing in an environment that is more physiologically representative of rotator cuff healing after surgery.

6.4 Implications of this thesis

6.4.1 For patients

This thesis addresses the clinical problem of poor rotator cuff surgical repair and proposes the use of a biological augmentation suture to improve patient outcomes. This solution has the potential to improve outcomes for the 10,000 people suffering from rotator cuff pain that receive surgery per year in the UK and 200,000 people in the US.[1] Moreover, with an ageing population, the number of people that would benefit from improved rotator cuff repair outcomes are sure to increase.

6.4.2 For researchers designing novel suture materials

While this work focused on rotator cuff tendon repair, it has implications for developing augmentation sutures for other applications.

This thesis demonstrated the ability to fabricate continuous fibres through electrospinning and melt-extrusion and control their properties on the polymer and fibre level. This finding contributes to the growing body of work about tuning electrospun fibres to be suitable as a device for a specific clinical application.

An important contribution of this thesis for suture design is also the successful development of a hybrid suture. While there are a number of hybrid core-sheath sutures on the market, no hybrid sutures exist that provide high tensile strength and biophysical cues to promote a biological response. Moreover, its flexible design enables modifying the device for different applications by adjusting the proportion and number of electrospun and melt-extruded fibres, in order to meet the physiological demands of the repaired tissue. It has also been shown that the macro-scale architecture, in particular tensile strength and porosity, can be tuned by altering braiding design and component ratios. A further area of exploration with this fabrication method and technology is the potential of making a multi-phasic yarn to support a multi-phasic tissue, like the tendon enthesis. The enthesis has multiple specialised zones, each with a specific structure and function. Variation braiding could be used to develop multi-phasic braids, with each zone having its own size, porosity, and tensile properties.

6.4.3 For surgeons

There are numerous ways in which the findings in this thesis may influence surgical practice. Firstly, they highlight how important it is for surgeons to consider tissue biology when performing surgical repairs. Medical device companies regularly release new suture models for surgeons by marketing them as "stronger".[314,315] However there is no evidence to show that stronger and, in many cases stiffer, sutures will improve repairs. This thesis challenges surgeons to pragmatically think about the biological and mechanical requirements of the tissue that they are repairing.

Moreover, most augmentative strategies for rotator cuff repair focus on the development of scaffolds. For scaffolds to be used in surgical repair, changes in procedure and additional devices are needed. The benefit of a suture as an augmentation strategy is that its use won't necessarily change the surgical procedure. Surgeons already know how to deploy and attach sutures for rotator cuff repair. A stepwise progression from inert to augmentation sutures might be encouraged by upcoming clinical trials and will help to disseminate these sutures for widespread clinical use. Of course, it is also possible that an augmentation suture and scaffold could be used in combination to provide additional support to repairs. For rotator cuff surgery, the proportion of electrospun and extruded fibres in the hybrid suture and the possibility of adding scaffold augmentation could be informed by the type of tear, stage of disease, and prognosis for recovery.

Finally, in order to develop the target design criteria in Chapter 2, surgeons were consulted about the usability requirements for performing rotator cuff surgery and the appropriate handling properties needed (see Appendix C.4). This highlights the ways in which surgeons play an important role in all stages of the translational research process.

6.4.4 For translational biomaterials research

Developing a suture that meets the requirements for tendon repair is challenging, in part because there aren't any accepted *in vitro* or *in vivo* criteria to measure its performance. Complicating this, because the biology of healthy tendon and the pathophysiology of diseased tendon are poorly understood, it is challenging to characterise the stage of disease, to determine the requirements to support repair, and to determine how these requirements might change over time. As a result, establishing which properties were important for an augmentation suture and the design criteria that would guide the experiments in this thesis, was challenging. In order to overcome these challenges, the design criteria were based on requirements that were known and easier to characterise: the suture should meet certain

size requirements, as well as have appropriate degradability, porosity, mechanical properties, and biophysical cues that were similar to, or a perceived improvement upon, currently used sutures. Moreover, in the development of the design criteria, biological, engineering, and clinical expertise were sought out concurrently. A limitation of these design criteria is that they were based on what we already know about tendon, which is limited, and the surgical sutures that are currently used, which were not specifically designed for tendon. However, they provide a starting point to gather more information that would help develop more specific criteria in the future.

The needs-driven design process used in this thesis is well-established for the development of novel biomedical technologies.[317] However, implementing this strategy in an academic environment for rotator cuff repair is rare. Indeed, this approach has since been increasingly implemented in the Carr group to develop improved therapies for anterior cruciate ligament (ACL) repair. Similar to rotator cuff tendon, the ACL's limited vascular network prevents it from healing completely after rupture, creating a need for grafts to augment its reconstruction.[162,241,318] However, the use of autografts and allografts is associated with a number of drawbacks, such as donor site morbidity and risk of bacterial infection or disease transmission.[148] Through consulting with ACL surgeons, it has become clear that certain ACL repairs could benefit from a similar augmentation device to what has been developed in this thesis. Prototypes have been developed by adapting polymer, type of filament, post-processing method, and braiding design, to suit the physiological requirements of the ACL.

Finally, it is also important to remember the importance that patients play in every part of the translational research pathway. Patient and public involvement (PPI) sessions were led alongside this research to understand patient experience after surgery and to convey the potential for biomaterials to improve their condition. These PPI sessions are also

important to help seek and recruit patients who are willing and a good fit for future clinical trials for this device.[316]

6.4.5 For integrating academia and industry

There is thought that many medical devices in development fail to communicate with industry early enough in product development.[319] The melt-extrusion company FET and the braiding company Herzog are both industrial textile companies that have long standing R&D relationships with medical device companies, such as Ethicon and Johnson & Johnson. Both companies have sold machinery or fibres to academic institutions, but have never worked in an R&D capacity with academia. However, these companies had a tremendous amount of experience, resources, and interest in working with academic institutions. From the experience on this project, the industrial centres have very specific and valuable textile know-how and access to more resources, whereas academic centres foster a more interdisciplinary and innovative environment and have more ready access to valuable patient tissue. These findings support and encourage more engagement between academic, clinical, and industrial centres to achieve a faster route to clinic for promising biomaterials.

6.4.6 For regulatory bodies

Since suture design and development is industry driven, incremental modifications have allowed for a steady outflow of products while maintaining a safe regulatory position and limiting costs. As a result, the suture materials used today are cause fewer infections.[190] However, although they are marketed as inert materials, the findings from this thesis show that they are not biologically inactive as they adsorbed hundreds of different serum proteins. Given the downstream effect of the adsorbed proteins on the suture's biological

activity, this raises regulatory questions. It calls to reconsider the regulatory requirements to market a material as inert or biocompatible.

A recent report showed that 48 PDO-based implants have gained regulatory approval since 1981 and they all have the same predicate.[185] In this regulatory landscape, the electrospun and melt-extruded filaments would probably fit the criteria for equivalency-based translation (under the FDA). This is based on the fact that electrospun and melt-extruded materials were made of PDO, which is used for many sutures on the market, and melt-extruded materials were made using a similar fabrication process to many sutures on the market. However, these findings in this thesis showed that these materials are not equivalent at all. Indeed, between the electrospun, extruded, and PDS suture, they had different mechanical and thermal properties, protein adsorption profiles, and cell responses. These findings call into question the efficacy and validity of the equivalency-based translation process in maximising patient safety.

6.5 Limitations of this thesis

While the specific limitations for each experiment have been considered in the experimental chapters, there are overall limitations that should to be considered.

The main limitation of this thesis is that with the current understanding of rotator cuff tendon pathobiology and the mechanical and cellular environment of tendon ECM, as well as a lack of validated characteristics of successful repair, it wasn't possible to establish very specific suture design targets. As a result, the design targets that guided the material development in this thesis were made conservatively and the manufacturing methods were intentionally ones that allow for design refinement and modification in the future. For example, melt-extrusion and electrospinning allow for easy tuning of fibre diameter to elicit more favourable cell responses and the Variation Braiding Machine allows for flexibility in altering the size or structure of the suture. These methods enable

modifications to improve the mechanics and handling of the final suture, by adjusting the ratio of electrospun and melt-extruded fibres, and to improve the cell response, by adjusting the porosity by braid design.

Moreover, because the melt-extrusion and braiding was done with external companies, it wasn't possible to fabricate fresh material for every experiment. The material characterisation and degradation studies were performed right after material production; however, the cell culture and protein adsorption experiments were performed a few months after material fabrication. While every effort was made to seal the materials in a low humidity environment, it is likely that some degradation occurred and influenced the results.

Finally, this work only studied tendon fibroblasts in isolation in a static environment. In reality, any implanted material will be exposed to many cell types which are influenced by biophysical properties and by each other. *In vivo,* there is significant cross-talk between tendon fibroblasts, macrophages, and endothelial cells, meaning that the local response to a hybrid suture needs to be considered in a coordinated manner, ideally in a dynamic environment. Moreover, tendon fibroblasts from healthy tissue were isolated, because of limited access to diseased tissue. However, the use of diseased cells has its limitations. Diseased cells from patients are categorized based on the size of the tear (small, medium, large, or massive), which does not capture the true biological variation in tendinopathy. A model that induces targeted changes from healthy tendon phenotypes might be a more homogenous and useful cell population for evaluating cell-material interactions in the future. Finally, an implanted bioactive suture will be exposed to a dynamic biological and physical environment, over a long period of time, which could not be replicated by this *in vitro* study.

6.6 Future work

Developing a novel suture to improve rotator cuff repair requires interdisciplinary collaboration at all stages of the research process. These studies have progressed the development of a hybrid suture, however more work is needed to determine its bioactive potential before bringing the device to the stardard needed for pre-clinical and clinical trials.

Firstly, it is recommended to acquire a Variation Braiding Machine. This work explored different braiding design options based on information available at the time. It is likely that these design criteria might change with further understanding of desirable cell-material interactions, mechanical, and handling properties. Moreover, acquiring an industrial braiding machine also enables the flexibility to explore the use of other polymers and the potential for other clinical applications, as has already been done in the context of ACL repair.

An important area of future work is the development of more relevant *in vitro* tests that can be used to predict potential *in vivo* outcomes. Animal models, in particular a rat infraspinatus model, is the most frequently used model to demonstrate safety of implanted biomaterials for rotator cuff repair.[320] No adequate animal model for age related tendon disease exists to demonstrate efficacy.[274] Most lab animals are quadrupeds and subject their tendon to different magnitudes of loading compared to humans. Additionally, differences in the pathophysiology of tendon healing confound the ability to make direct comparisons to humans.[320] In the absence of relevant animal models, static *in vitro* tests, as were done here, are limited in their potential to predict *in vivo* outcomes. Future work could focus on investigating dynamic loading during culture by subjecting the sutures to a loading regime that would be more representative of the physiological environment after surgery. A bioreactor that can accurately imitate the anatomy and forces experienced by a repaired

rotator cuff would help to determine more appropriate design targets for a suture. In addition, these dynamic systems should focus on incubating sutures with human serum and seeding with diseased rotator cuff cells (preferably from large or massive tears) to more accurately model the environment after surgery. Cells from large and massive tears are important to study, as they are the most common to fail and thus are in most need of improved augmentation strategies.

Additionally, future work will need to study more than just tendon fibroblasts in isolation. Other cell populations are influenced by biophysical properties, and by each other, which contribute to long-term repair and regeneration. It will be particularly important to study the cells that infiltrate following surgical injury, as well as endogenous immune and stromal cells.

Although cell-material interactions help to understand the influence of material properties on cell behaviour, it is often unclear what a desired response should be, or how that response should change over time. Future work should use more advanced biological characterisation methods, such as Next Generation Sequencing, to compare novel biomaterials in development to existing materials in use. The responses can be evaluated by comparing key genes and pathways known to be important and potentially dysregulated in tendon disease and repair. Moreover, the material responses should be evaluated against the healthy tendon environment to identify which cell types, gene expression, and mechanical properties should be targeted. RNA extraction and sequencing was performed on the novel hybrid suture developed in this thesis and compared to existing devices on the market. These results are currently being analysed using the in-house expertise in the Carr group but were outside of the scope of this thesis.

Another necessary area of future work is in developing accurate and reproducible methods to characterise surface properties. It is difficult to interpret the cell biology and protein adsorption results in this thesis without an understanding the biochemical and biophysical

surface properties that are integral in driving these responses. Local stiffness, hydrophobicity, and local porosity are all properties which likely influence the way in which cells interact with the material. XPS and AFM are currently being explored to determine surface chemical groups and mechanical properties, respectively, of healthy tendon and the materials developed in this thesis to hopefully functionalise these surfaces in the future. Finally, it will be necessary to do a more formal evaluation of the usability of the hybrid suture developed in this thesis. This will likely involve surgeons qualitatively assessing the suture's handling properties and performing mock operations using synthetic rotator cuff models. A potential usability design protocol to enable this is available in Appendix C.4.

6.7 Clinical translation of a hybrid suture

6.7.1 Translational potential of a hybrid suture

To date, none of the promising multifilament electrospun sutures or scaffolds intended for soft tissue repair have been tested beyond pre-clinical trials. This delay can be mainly attributed to current limitations in filament manufacturing and multifilament assembly, as well as production limitations in clean rooms meeting the standards for clinical trials.

The potential for the hybrid suture to translate into clinical use is quite high. Since 2013, the Carr group has been developing tunable electrospinning filaments and scaffolds from a range of synthetic degradable polymers. These results have been encouraging and have led to two initial devices: the BioPatch[91] and BioYarn[129]. BioPatch is a multi-layered polydioxanone patch and BioYarn is a twisted multifilament polydioxanone suture. Both devices are designed for rotator cuff tendon repair and are currently in preparation for clinical trials, expected to start in 2020. Although neither device is licensed for use yet, and their translation may be many years away, the invaluable experience and know-how

developed over the last 6 years will aid in the translational process of bringing this hybrid suture to market. Specifically, because the hybrid suture uses materials and production methods that overlap with those of BioYarn and current surgical sutures, pre-clinical and clinical testing pipelines have been partially established. Moreover, it is possible that the hybrid suture could pass through the equivalency-based 510(k) route in the US without the need of a clinical trial to prove efficacy. However, the regulatory landscape surrounding this is changing and it is likely that the evaluation of medical devices will be closer to the pharmaceutical pathway in the future.[321,322] Finally, the Carr group is situated in a department with a strong translational focus and experience in clinical trial design which will aid in the pre-clinical and clinical trial development stages of the hybrid suture.

6.7.2 Industrial viability of the manufacturing process

6.7.2.1 Upscaling

It has been mentioned earlier in this thesis that the fabrication of continuous electrospun filaments at a high production rate is the biggest hurdle in the manufacturing process of hybrid sutures.

There are two aspects to upscaling electrospun filaments: the speed of electrospinning and filament collection, as well as upscaling the post-processing of filaments in preparation for braiding. It was not possible to substantially increase the speed of electrospinning due to limits in the manufacturing setup. As a result, the filament could only be produced at 5 meters of stretched filament per hour and required intermittent monitoring. However, the speed of filament collection was still upscaled by moving to a clean room environment, with a low particulate environment and consistent temperature and humidity, which allowed for a more stable environment to electrospin for longer times. In the clean room, there were also two electrospinning set-ups which could be run concurrently, a polymer

solution pump which could hold syringes up to 100mL (compared to 5mL in the laboratory set-up), and an automatic collection spool which could be run overnight. Over 24 hours, it was possible to spin 240 meters of continuous filament in the clean room set-up, compared to 40 meters in the research laboratory set-up used in Chapter 3. Provided there is no material waste, 240 meters of filament amounts to 20 meters of braided suture (using a 12 carrier braiding machine). A single standard suture is packaged in 70cm section; this means that in 24 hours, enough electrospun filament can be manufactured to yield 28.5 braided sutures. In reality, the post-processing steps and braiding will result in material waste, however, the process would still be sufficiently scaled up for pre-clinical and clinical trials, where hundreds of units would be needed.

In the context of upscaling filament post-processing, there is room for further automation and upscaling. Currently, post-processing of the filament involves removing the filament from the wire, drawing the filament, annealing, washing, and then drying. Each step is either semi-automated (with help of a machine, but still requiring manual steps) or done completely manually. In terms of the whole manufacturing process, the current post-processing is the least time-efficient part of the manufacturing process and has the highest potential for introducing human error. In theory, it is possible for the whole process to be automated in a similar way to how melt-extruded fibres are manufactured: the filament is collected and drawn over hot rollers to simultaneously stretch and anneal the fibres, then the filament is passed through a washing bath and then left to air dry or in a vacuum.

It is worth noting that most of the efforts to upscale the electrospinning process were developed to prepare BioPatch and BioYarn for pre-clinical and clinical trials. There are two additional resources needed for the hybrid yarn: the braiding equipment and the melt-extruded component. However, the current clean room facility has a weaving loom which is used for the BioPatch product and two full time employees who are proficient in

operating textile machinery. The Carr group has recently purchased the Variation Braiding Machine used in this thesis and these employees are now being trained to operate the braiding machine independently. This will enable more efficient upscaling of the hybrid suture to continue this project as well as for developing a scaffold for ACL repair. Moreover, melt-extruded yarns are needed for the fabrication of the hybrid suture. Melt-extrusion is a scaled up process that has been used by hundreds of medical device companies to fabricate sutures for the last 50 years and doesn't face the same upscaling and reproducibility challenges that electrospinning does.

6.7.2.2 Cost-effectiveness of electrospinning

Because no purely electrospun medical products are available on the market, it is difficult to judge the cost-effectiveness of electrospinning as a manufacturing method. However, there are numerous commercially viable companies that sell electrospun materials or electrospinning equipment for medical and non-medical applications. For example, The Electrospinning Company[323] sell tailored electrospun scaffolds to clients for research and industry applications. IME Medical Electrospinning[324] is another company that sells electrospinning machines. Part of what makes electrospinning potentially cost-effective is that it is a relatively cheap and simple method to produces fibres that have applications for a range of industries, such as filtration systems, electronics and batteries, and fabrics/textiles.[325] Indeed, electrospun fibres are currently bulk produced for many non-medical applications. The limitation in biomedical research is that electrospun materials have more stringent fibre requirements, such as a narrow range of fibre diameters, which would lower the potential yield of product. The true cost-effectiveness of electrospinning for biomedical applications is still to be determined, however, significant upscaling progress and success in other industries makes it a commercially promising technique.

6.7.2.3 Perceived cost-effectiveness of the hybrid yarn

PDS® sutures are currently priced at around £4 per piece, surgical patches (such as GraftJacket and X-repair) are usually priced between £500-1500, and stem cell and growth factor therapies are many thousands more. As mentioned earlier, the hybrid suture is not equivalent to a suture and has a more similar function to a surgical patch. It will be priced more similarly to a patch, and marketed as a bioactive device that is in the form of a suture for ease of use. It is also worth highlighting that the hybrid suture is meant to be used in combination with an augmentation patch, such as BioPatch, and potentially conventional sutures for additional stability.

The largest cost of a rotator cuff operation is the cost of the theatre. Currently, 40% of rotator cuff surgeries fail, which means that the operation did not have a therapeutic benefit or potentially even caused harm. In light of the costs of the surgery and the rate of failure and revision surgery, if the hybrid suture technology can reduce the rate of re-tear and the need for revision surgery, then it will be extremely cost-effective and minimise the wastage of hospital resources for failed operations and improve patient's quality of life by only needing one operation.

6.7.3 Hypothetical clinical translation pathway

Currently, the majority of electrospun-based biomaterials in development would be classified as medical devices. Medical devices are regulated under the EU 2017/745 in the European Union and the Pre-Market Notification 510(k) and Pre-Market Approval (PMA) pathways by the FDA in the United States. In this section, the EU pathway is used as a framework to describe the route to clinical translation, although the FDA PMA pathway mirrors this process in many ways.

The pathway to translation can be roughly divided into R&D, pre-clinical, and clinical phases. The work in this thesis forms part of the R&D phase, which is preparing the device for more rigorous pre-clinical testing.

Further laboratory testing is needed, with more thorough *in vitro* testing and modifications to the device design (see Chapter 6.6 Future work). For example, future work on the hybrid suture will focus on how porous the suture should be to enable for cell infiltration (continuation of the work in Chapter 5.5.6). The design of the braided suture may need to be modified based on these results. Finalising the device design is termed "design freeze" and the design or composition of the device cannot be changed after this point. This is the version of the device that is intended for use as the final product. For the hybrid suture, this could be years away, however recent progress, like purchasing the Variation braiding machine, could shorten the reiterative design process.

Once design freeze has been achieved, the next step is to develop manufacturing processes that comply with the ISO 13485 standard.[192] Good Manufacturing Practices (GMP) standard is the US equivalent of ISO 13485, however the two terms of often used interchangeably to mean the standards that are needed to ensure the quality and consistency of the product,

To comply with GMP/ISO13485, established protocols must be designed to ensure safe, repeatable production of the hybrid yarn, with compliant equipment and facilities. Staff must also be trained to produce a finalized, sterilized, and packaged product before a device can move toward approval. Moreover, it needs to be demonstrated that the production process can be upscaled to generate hundreds of samples required for pre-clinical testing, although this has been achieved for electrospinning filament production

(see Chapter 6.7.2.1). Upscaling is often challenging for laboratory groups because of the additional equipment and staff needed, as well as access to a clean room.

Although this hybrid suture may not reach this stage of production for years, the Carr group is well equipped for this stage of the translational process. There are four full-time staff members trained to work in the clean room, that are responsible for the developing GMP manufacturing standards and pre-clinical testing of the electrospun devices BioPatch and BioYarn. There is also a further full-time staff member who operates textile machinery. As a result, the Carr group is equipped with most of the manufacturing equipment for the hybrid yarn as well as staff to operate the machinery and help with the documentation needed to bring the process to GMP standards.

Pre-clinical testing will involve validating the production processes and evaluating the biocompatibility of medical devices, following ISO 10993 standards. Specifically, this includes genotoxicity testing, *in vitro* cytotoxicity testing, as well as evaluating sterilisation residuals and degradation products. It is necessary that the pre-clinical tests are performed to a Good Laboratory Practices (GLP) standard, which is a universal standard of the quality of the test facility where pre-clinical testing occurs. Chemical analysis of the device and residuals will also be performed. For this hybrid suture, this could involve testing for residual HFIP in the electrospun material or contact of equipment with materials leaving residual compounds. *In vivo* tests will be performed to test safety and efficacy by evaluating local tissue response and systemic toxicity over time. These tests would most likely be performed in an ovine model, although there aren't really any appropriate animal models for rotator cuff disease. Finally, physico-chemical, morphological, and topographical (PMT) characterisation will be needed to evaluate if the material properties are suitable for implantation and usable by surgeons.

The pre-clinical tests will be compiled for review by the relevant authority, determined based on geographic location. In the UK, the relevant authority is the Medicines and Healthcare products Regulatory Agency (MHRA). The MHRA will examine material reliability, process repeatability, mechanical testing, cytotoxicity, genotoxicity, residual chemical data, and other relevant evidence of device safety and performance.[325] This testing must occur on the design frozen product with appropriate repetition at multiple time points and must follow strict protocols on testing and data reporting to comply with the appropriate standards. At this point, a risk analysis is also performed in conjunction with an examination of the intended clinical trial plan and ethics approval, with higher risk medical devices, subject to further requirements.

Based on this review, the MHRA can issue "no objections" which means that a clinical trial can be performed. The first in-man trial will recruit a small number (minimum 5) of carefully selected patients. The aim of the trial will be to see if the hybrid suture is safe, non-toxic, and capable of being used surgically in rotator cuff repair. Systemic, local, and cellular response will be assessed at an appropriate time point. Because the suture is made of medical grade PDO, which has been used in surgery as melt-extruded fibres for over 30 years, it is unlikely that electrospinning will alter its safety profile from a systemic toxicity standpoint. Because electrospun fibres are intended to modify cellular behaviour, additional testing will be needed to investigate unknown safety concerns regarding its bioactivity.

Larger clinical trials are then needed to definitely demonstrate the superiority of the hybrid suture over what is currently available to surgeons. However, after an initial successful in-man clinical trial, which does not have to be a randomised control trial, it is possible to apply for a CE mark in Europe and FDA approval in the United States. Theoretically, this hybrid suture will be classified as a class 3 device under the FDA, although few biomaterials

targeting cell behaviour through biophysical cues have sought regulatory approval yet to pave the path for other devices. Class 3 designates a higher risk and more complex route to market, however certain combination devices have gained FDA approval and CE marked status over the last decade, such as sub-dermal contraceptive implants[326], antibiotic bone cement[327], and drug-eluting stents.[328] Using the same medical grade PDO for both electrospun and melt-extruded materials will ease these regulatory hurdles in bringing a combination device to market. Applying for a CE mark involves submitting documentation to a notifying body, including standard operating procedures (SOPs) and data collected over the years of design history. Early input and expertise from people familiar with the entire route to market will ensure that the hybrid suture is meeting compliance and regulatory standards. This expertise will come from various people involved in the BioYarn and BioPatch product development since 2013, and include laboratory researchers, engineers, material scientists, cell biologists, certified clean room staff, clinicians, clinical trial staff, business managers, lawyers and others.

6.8 Key findings of this thesis

Many surgical tendon repairs fail despite advances in surgical materials and techniques. Repair failure can be partially attributed to the tendon's poor intrinsic healing capacity and the inappropriate repurposing of sutures from use in other tissues. Current sutures fail to meet the demands of tendon tissue. In rotator cuff tendon repair, suture pull through is the main mode of failure, with 40% of repairs failing within a year. It is thought that sutures that are designed to integrate with tendon tissue can lead to better patient outcomes. The overall aim of this thesis was to develop a novel polydioxanone suture that can provide a biological scaffold for tendon cells to grow and can mechanically support tendon repair. It was hypothesized that a hybrid suture, made up of electrospun submicron fibres, which

mimic native tendon ECM, and robust melt-extruded 10μm sized fibres, could achieve the biological and mechanical requirements of a suture to augment tendon repair.

This thesis offered a design process for developing sutures for rotator cuff repair by engineering the material on the fibre, filament, and multifilament level. On the fibre level, it was found that annealing was useful to tailor the degradation rate of electrospun fibres, which could enable matching the biomaterial degradation kinetics with new tissue deposition. On the filament level, it was found that melt-extruded materials had superior strength and stiffness compared to electrospun filaments and are more likely to mechanically support a repair. Electrospun filaments had a higher surface area, porosity, and faster degradation rate, making them more suitable to support cellular attachment and activity. On the multifilament level, industrial braiding enabled control over suture size, porosity, and mechanical properties by altering braiding design and component ratios. Moreover, industrial braiding substantially improved the reproducibility and scalability of the sutures, which have been limiting factors for many electrospun devices in development.

A hybrid suture with an electrospun sheath and melt-extruded cores was designed to meet the demands of tendon repair: electrospun fibres on the outside approximate ECM and will be in contact with the biological milieu, while the melt-extruded fibres in the core provide prolonged mechanical support. The specific ways in which this novel suture met the design targets in Chapter 2 are outlined in Table 6.1. The hybrid suture had a similar size and tensile strength to currently used sutures, but was less stiff and more porous. It promoted differential serum protein binding and tendon fibroblast attachment and proliferation, mostly due to the biomimetic electrospun component, and to a lesser extent, the melt-extruded component. Currently used sutures did not promote fibroblast responses conductive to tendon healing. This novel hybrid suture has potential to improve current treatment options for tendon repair.

Table 6.1: Summary table of design criteria and hybrid suture properties.

Design criteria	Hybrid suture
Structure to match its intended function	The hybrid suture is specifically designed to meet the demands of native tendon: electrospun fibres on the outside of the suture approximate the ECM properties and are in initial contact with the biological milieu, while the melt-extruded fibres in the core provide prolonged mechanical support.
Safety	The same polymer PDO is used for both suture components. It is FDA approved and has been used in surgery for over 40 years with no adverse outcomes.
Short-term bioactivity	The hybrid suture promoted differential serum protein binding and tendon fibroblast attachment and proliferation, mostly due to the biomimetic electrospun component, and to a lesser extent, the melt-extruded component. Currently used sutures did not promote fibroblast responses conductive to tendon healing.
Mechanical properties	The hybrid suture has a force at failure of 70N and strain at break of 35%, which is similar to surgical sutures of the same size. The hybrid suture is less stiff compared to current devices.
Degradation to match its clinical need	Both electrospun and melt-extruded components retain 70% of their tensile strength at 6 weeks, which is a critical period after surgery when support is needed. Annealing can be used to further tailor its degradation rate.
Porosity	The hybrid suture is more porous with larger pore diameters compared to currently used surgical sutures.
Usability	The suture diameter is 0.69mm, which is usable for surgeons and compatible with suture anchors for rotator cuff repair.
Scalability and reproducibility	Electrospinning on a continuous wire in a clean room environment and the use of an industrial machine substantially increased production volume and reproducibility of electrospun yarns.

Chapter 7

References

1. Judge A, Murphy RJ, Maxwell R, Arden NK, Carr AJ. Temporal trends and geographical variation in the use of subacromial decompression and rotator cuff repair of the shoulder in England. *Bone Joint J*. 2014;96-B(1):70-74. doi:10.1302/0301-620X.96B1.32556
2. Carr AJ, Cooper CD, Campbell MK, et al. Clinical effectiveness and cost-effectiveness of open and arthroscopic rotator cuff repair [the UK Rotator Cuff Surgery (UKUFF) randomised trial]. *Health Technol Assess*. 2015;19(80):1-218. doi:10.3310/hta19800
3. Taylor FW. SURGICAL KNOTS. *Ann Surg*. 1938;107(3):458-468. doi:10.1097/00000658-193803000-00011
4. Höer J, Fischer L, Schachtrupp A. Laparotomy closure and incisional hernia prevention - what are the surgical requirements? *Zentralblatt für Chir*. 2011;136(1):42-49. doi:10.1055/s-0030-1262682
5. Lambrechts M, Nazari B, Dini A, et al. Comparison of the cheese-wiring effects among three sutures used in rotator cuff repair. *Int J Shoulder Surg*. 2014;8(3):81-85. doi:10.4103/0973-6042.140115
6. Silva JM, Zhao C, An K-N, Zobitz ME, Amadio PC. Gliding resistance and strength of composite sutures in human flexor digitorum profundus tendon repair: an in vitro biomechanical study. *J Hand Surg Am*. 2009;34(1):87-92. doi:10.1016/j.jhsa.2008.09.020
7. HUMAN. BioDigital Human Visualization Platform. https://human.biodigital.com.
8. Liu RW, Lam PH, Shepherd HM, Murrell GAC. Tape Versus Suture in Arthroscopic Rotator Cuff Repair: Biomechanical Analysis and Assessment of Failure Rates at 6 Months. *Orthop J Sport Med*. 2017;5(4):232596711770121. doi:10.1177/2325967117701212
9. Apostolakos J, Durant TJ, Dwyer CR, et al. The enthesis: a review of the tendon-to-bone insertion. *Muscles Ligaments Tendons J*. 2014;4(3):333.
10. Rothrauff BB, Pauyo T, Debski RE, Rodosky MW, Tuan RS, Musahl V. The Rotator Cuff Organ: Integrating Developmental Biology, Tissue Engineering, and Surgical Considerations to Treat Chronic Massive Rotator Cuff Tears. *Tissue Eng Part B Rev*. 2017;23(4):318-335. doi:10.1089/ten.teb.2016.0446
11. Kastelic J, Galeski A, Baer E, Baer Ohio E. The Multicomposite Structure of Tendon. *Connect Tissue Res*. 1978;6(1):11-23. doi:10.3109/03008207809152283
12. Kjaer M. Role of Extracellular Matrix in Adaptation of Tendon and Skeletal Muscle to Mechanical Loading. 2004. doi:10.1152/physrev.00031.2003
13. Wang JH-C. Mechanobiology of tendon. *J Biomech*. 2006;39(9):1563-1582. doi:10.1016/j.jbiomech.2005.05.011
14. Itoi E, Berglund LJ, Grabowski JJ, et al. Tensile properties of the supraspinatus tendon. *J Orthop Res*. 1995;13(4):578-584. doi:10.1002/jor.1100130413
15. Wilson CL, Duff G. Pathologic study of degeneration and rupture of the supraspinatus tendon. *Arch Surg*. 1943;47(2):121. doi:10.1001/archsurg.1943.01220140003001
16. McCarron JA, Milks RA, Chen X, Iannotti JP, Derwin KA. Improved time-zero

biomechanical properties using poly-L-lactic acid graft augmentation in a cadaveric rotator cuff repair model. *J Shoulder Elb Surg*. 2010;19(5):688-696. doi:10.1016/J.JSE.2009.12.008
17. Kannus P. Structure of the tendon connective tissue. *Scand J Med Sci Sports*. 2000;10(6):312-320.
18. Frantz C, Stewart KM, Weaver VM. The extracellular matrix at a glance. *J Cell Sci*. 2010;123(123):4195-4200. doi:10.1242/jcs.023820
19. Silver FH, Freeman JW, Seehra GP. Collagen self-assembly and the development of tendon mechanical properties. *J Biomech*. 2003;36:1529-1553. doi:10.1016/S0021-9290(03)00135-0
20. Hess GP, Cappiello WL, Poole RM, Hunter SC. Prevention and Treatment of Overuse Tendon Injuries. *Sport Med*. 1989;8(6):371-384. doi:10.2165/00007256-198908060-00005
21. James R, Kesturu G, Balian G, Chhabra A. Tendon: biology, biomechanics, repair, growth factors, and evolving treatment options. *J Hand Surg Am*. 2008;33(1):102-112. doi:10.1016/j.jhsa.2007.09.007
22. Scott A, Backman LJ, Speed C, Update On Pathophysiology T: Tendinopathy: Update on Pathophysiology. *J Orthop Sport Phys Ther* |. 2015;45(11):833. doi:10.2519/jospt.2015.5884
23. Dakin SG, Martinez FO, Yapp C, et al. Inflammation activation and resolution in human tendon disease. *Sci Transl Med*. 2015;7(311):311ra173. doi:10.1126/scitranslmed.aac4269
24. Millar NL, Hueber AJ, Reilly JH, et al. Inflammation is Present in Early Human Tendinopathy. *Am J Sports Med*. 2010;38(10):2085-2091. doi:10.1177/0363546510372613
25. LU Bigliani. The morphology of the acromion and its relationship to rotator cuff tears. *Orthop Trans*. 1986.
26. Harvie P, Ostlere S. Genetic influences in the aetiology of tears of the rotator cuff: sibling risk of a full-thickness tear. *Bone Joint Res*. 2014;86-B(5):696-700. doi:10.1302/0301-620x.86b5.14747
27. Fehringer E V., Sun J, VanOeveren LS, Keller BK, Matsen FA. Full-thickness rotator cuff tear prevalence and correlation with function and co-morbidities in patients sixty-five years and older. *J Shoulder Elb Surg*. 2008;17(6):881-885. doi:10.1016/J.JSE.2008.05.039
28. Ker RF. The implications of the adaptable fatigue quality of tendons for their construction, repair and function. *Comp Biochem Physiol Part A Mol Integr Physiol*. 2002;133(4):987-1000. doi:10.1016/S1095-6433(02)00171-X
29. Kannus P, Józsa L. Histopathological changes preceding spontaneous rupture of a tendon. A controlled study of 891 patients. *J Bone Joint Surg Am*. 1991;73(10):1507-1525. doi:10.2106/00004623-199173100-00009
30. Yamaguchi K, Ditsios K, Middleton WD, Hildebolt CF, Galatz LM, Teefey SA. The demographic and morphological features of rotator cuff disease. A comparison of asymptomatic and symptomatic shoulders. *J Bone Joint Surg Am*. 2006;88(8):1699-1704. doi:10.2106/JBJS.E.00835
31. Minagawa H, Yamamoto N, Abe H, et al. Prevalence of symptomatic and asymptomatic rotator cuff tears in the general population: From mass-screening in one village. *J Orthop*. 2013;10(1):8-12. doi:10.1016/J.JOR.2013.01.008
32. Colvin AC, Egorova N, Harrison AK, Moskowitz A, Flatow EL. National trends in rotator cuff repair. *J Bone Joint Surg Am*. 2012;94(3):227-233. doi:10.2106/JBJS.J.00739
33. Ozaki J, Fujimoto S, Nakagawa Y, Masuhara K, Tamai S. Tears of the rotator cuff

of the shoulder associated with pathological changes in the acromion. A study in cadavera. *J Bone Joint Surg Am*. 1988;70(8):1224-1230. doi:10.2106/00004623-198870080-00015
34. Wu B, Chen J, Rosa T Dela, et al. Cellular response and extracellular matrix breakdown in rotator cuff tendon rupture. *Arch Orthop Trauma Surg*. 2011;131(3):405-411. doi:10.1007/s00402-010-1157-5
35. Riley G. The pathogenesis of tendinopathy. A molecular perspective. *Rheumatology*. 2004;43(2):131-142. doi:10.1093/rheumatology/keg448
36. Brukner P, Khan K. *Clinical Sports Medicine*. 3rd ed. Sydney, Australia: McGraw-Hill; 2006.
37. Galatz LM, Ball CM, Teefey SA, Middleton WD, Yamaguchi K. The outcome and repair integrity of completely arthroscopically repaired large and massive rotator cuff tears. *J Bone Joint Surg Am*. 2004;86-A(2):219-224.
38. Boileau P. Arthroscopic Repair of Full-Thickness Tears of the Supraspinatus: Does the Tendon Really Heal? *J Bone Jt Surg*. 2005;87(6):1229. doi:10.2106/JBJS.D.02035
39. Gazielly DF, Gleyze P, Montagnon C. Functional and anatomical results after rotator cuff repair. *Clin Orthop Relat Res*. 1994;(304):43-53.
40. Thomopoulos S, Parks WC, Rifkin DB, Derwin KA. Mechanisms of tendon injury and repair. *J Orthop Res*. 2015;33(6):832-839. doi:10.1002/jor.22806
41. Fenwick SA, Hazleman BL, Riley GP. The vasculature and its role in the damaged and healing tendon. *Arthritis Res*. 2002;4(4):252. doi:10.1186/ar416
42. Wang JH-C, Guo Q, Li B. Tendon Biomechanics and Mechanobiology—A Minireview of Basic Concepts and Recent Advancements. *J Hand Ther*. 2012;25(2):133-141. doi:10.1016/J.JHT.2011.07.004
43. James R, Kesturu G, Balian G, Chhabra AB. Tendon: Biology, Biomechanics, Repair, Growth Factors, and Evolving Treatment Options. *J Hand Surg Am*. 2008;33(1):102-112. doi:10.1016/J.JHSA.2007.09.007
44. Bassett R, Cofield R. Acute tears of the rotator cuff. The timing of surgical repair. *Clin Orthop Relat Res*. 1983;175:18-24.
45. Itoi E, S T. Conservative treatment of rotator cuff tears. *Clin Orthop Relat Res*. 1992;275:165-173. doi:10.1097%2F00003086-199202000-00024
46. Mikolyzk DK, Wei AS, Tonino P, et al. Effect of Corticosteroids on the Biomechanical Strength of Rat Rotator Cuff Tendon. *J Bone Jt Surgery-American Vol*. 2009;91(5):1172-1180. doi:10.2106/JBJS.H.00191
47. Kapetanos G. The effect of the local corticosteroids on the healing and biomechanical properties of the partially injured tendon. *Clin Orthop Relat Res*. 1982;163:170-179.
48. Kleinman M, Gross A. Achilles tendon rupture following steroid injection. Report of three cases. *J Bone Jt Surg Am*. 1983;65(9):1345-1347.
49. Bartolozzi A, Andreychik D, Ahmad S. Determinants of outcome in the treatment of rotator cuff disease. *Clin Orthop Relat Res*. 1994;308:90-97. doi:10.1097/00003086-199411000- 00015.
50. Millett PJ, Warth RJ. Posterosuperior Rotator Cuff Tears. *J Am Acad Orthop Surg*. 2014;22(8):521-534. doi:10.5435/JAAOS-22-08-521
51. Burkhart SS. A stepwise approach to arthroscopic rotator cuff repair based on biomechanical principles. *Arthrosc J Arthrosc Relat Surg*. 2000;16(1):82-90. doi:10.1016/S0749-8063(00)90133-6
52. Rees JL. The pathogenesis and surgical treatment of tears of the rotator cuff. *J Bone Joint Surg Br*. 2008;90-B(7):827-832. doi:10.1302/0301-620X.90B7.19874
53. Cole B, Kang R, Lewis P, Hayden J, McCarty III L, Alford W. Arthroscopic

rotator cuff repair: prospective functional outcome and repair integrity at minimum 2-year follow-up. *J Shoulder Elb Surg*. 2007;16(5):579-585. doi:10.1016/j.jse.2006.12.011

54. Bedeir YH, Jimenez AE, Grawe BM. Recurrent tears of the rotator cuff: Effect of repair technique and management options. *Orthop Rev (Pavia)*. 2018;10(2):7593. doi:10.4081/or.2018.7593
55. Diduch D, Scanelli J, … MT-J-J of the, 2012 undefined. Tissue anchor use in arthroscopic glenohumeral surgery. *journals.lww.com*. https://journals.lww.com/jaaos/Fulltext/2012/07000/Tissue_Anchor_Use_in_Arthroscopic_Glenohumeral.7.aspx. Accessed April 18, 2019.
56. Park M, clinics SS-H, 2012 undefined. Use of suture anchors and new suture materials in the upper extremity. *hand.theclinics.com*. https://www.hand.theclinics.com/article/S0749-0712(12)00098-4/abstract. Accessed April 18, 2019.
57. Ma R, Chow R, Choi L, Diduch D. Arthroscopic rotator cuff repair: suture anchor properties, modes of failure and technical considerations. *Expert Rev Med Devices*. 2011;8(3):377-387. doi:10.1586/erd.11.4
58. Chaudhry S, Dehne K, Hussain F. A review of suture anchors. *Orthop Trauma*. 2017;33(4):263-270. doi:10.1016/j.mporth.2016.12.001
59. Chu CC. Types and properties of surgical sutures. In: *Biotextiles As Medical Implants*. ; 2013:231-273. doi:10.1533/9780857095602.2.232
60. Srinivasulu K, Dhiraj Kumar N. A review on properties of surgical sutures and applications in medical field. *IMPACT Int J Res Eng Technol*. 2014;2(2):85-96.
61. Muffly TM, Tizzano AP, Walters MD. The history and evolution of sutures in pelvic surgery. *J R Soc Med*. 2011;104(3):107-112. doi:10.1258/jrsm.2010.100243
62. Mackenzie D. The history of sutures. *Med Hist*. 1973;17(2):158-168. doi:10.1017/S0025727300018469
63. Chu C, von Fraunhofer A, Greisler H. *Wound Closure Biomaterials and Devices*. CRC Press; 1996. doi:10.1201/ 9780203733653
64. Barham RE, Butz GW, Ansell JS. Comparison of wound strength in normal, radiated and infected tissues closed with polyglycolic and chromic catgut sutures. *Surg Gynecol Obstet*. 1978;146(6):901-907.
65. Ethicon Inc. Wound Closure Manual. http://www.uphs.upenn.edu/surgery/Education/facilities/measey/Wound_Closure_Manual.pdf. Accessed September 20, 2016.
66. Katz S, Izhar M, Mirelman D. Bacterial adherence to surgical sutures. A possible factor in suture induced infection. *Ann Surg*. 1981;194(1):35-41.
67. St-Jean B, Ménard J, Hinse S, Petit Y, Rouleau D, Beauchamp M. Braided tape suture provides superior bone pull-through strength than wire suture in greater tuberosity of the humerus. *J Orthop*. 2015;12. doi:10.1016/j.jor.2015.01.025
68. Zargar N, Carr A. The regulatory ancestral network of surgical meshes. *PLoS One*. 2018;13(6). doi:10.1371/journal.pone.0197883
69. Heneghan C, Goldacre B, Onakpoya I, et al. Trials of transvaginal mesh devices for pelvic organ prolapse: a systematic database review of the US FDA approval process. *BMJ Open*. 2017;7(12). doi:10.1136/bmjopen-2017-017125
70. Lenzer J. FDA recommends "modernizing" review of devices in wake of global investigation. *BMJ*. 2018;363. doi:10.1136/bmj.k5026
71. Hurwit D, Fanton G, Tella M, Behn A, Hunt KJ. Viscoelastic Properties of Common Suture Material Used for Rotator Cuff Repair and Arthroscopic Procedures. *Arthrosc J Arthrosc Relat Surg*. 2014;30(11):1406-1412. doi:10.1016/J.ARTHRO.2014.05.030

72. Vizesi F, Jones C, Lotz N, Gianoutsos M, Walsh WR. Stress Relaxation and Creep: Viscoelastic Properties of Common Suture Materials Used for Flexor Tendon Repair. *J Hand Surg Am*. 2008;33(2):241-246. doi:10.1016/J.JHSA.2007.10.011
73. Jordan MC, Boelch S, Jansen H, Meffert RH, Hoelscher-Doht S. Does plastic suture deformation induce gapping after tendon repair? A biomechanical comparison of different suture materials. *J Biomech*. 2016;49(13):2607-2612. doi:10.1016/J.JBIOMECH.2016.05.023
74. Wüst DM, Meyer DC, Favre P, Gerber C, Zanzotto E, Ferretti A. Mechanical and Handling Properties of Braided Polyblend Polyethylene Sutures in Comparison to Braided Polyester and Monofilament Polydioxanone Sutures. *Arthrosc J Arthrosc Relat Surg*. 2006;22(11):1146-1153. doi:10.1016/j.arthro.2006.06.013
75. Scherman P, Haddad R, Scougall P, Walsh WR. Cross-Sectional Area and Strength Differences of Fiberwire, Prolene, and Ticron Sutures. *J Hand Surg Am*. 2010;35(5):780-784. doi:10.1016/J.JHSA.2010.02.005
76. Snedeker JG, Foolen J. Tendon injury and repair – A perspective on the basic mechanisms of tendon disease and future clinical therapy. *Acta Biomater*. 2017;63:18-36. doi:10.1016/J.ACTBIO.2017.08.032
77. The Tendon Seed Network - Chan Zuckerberg Initiative. https://chanzuckerberg.com/science/programs-resources/humancellatlas/seednetworks/the-tendon-seed-network/.
78. Koike Y, Trudel G, Curran D, Uhthoff HK. Delay of supraspinatus repair by up to 12 weeks does not impair enthesis formation: A quantitative histologic study in rabbits. *J Orthop Res*. 2006;24(2):202-210. doi:10.1002/jor.20031
79. Adams JE, Zobitz ME, Reach JS, An K-N, Steinmann SP. Rotator Cuff Repair Using an Acellular Dermal Matrix Graft: An In Vivo Study in a Canine Model. *Arthrosc J Arthrosc Relat Surg*. 2006;22(7):700-709. doi:10.1016/J.ARTHRO.2006.03.016
80. Derwin KA, Baker AR, Spragg RK, Leigh DR, Iannotti JP. Commercial Extracellular Matrix Scaffolds for Rotator Cuff Tendon Repair. *J Bone Jt Surg*. 2006;88(12):2665-2672. doi:10.2106/JBJS.E.01307
81. Bourne RB, Bitar H, Andreae PR, Martin LM, Finlay JB, Marquis F. In-vivo comparison of four absorbable sutures: Vicryl, Dexon Plus, Maxon and PDS. *Can J Surg*. 1988;31(1):43-45.
82. Barber FA, Burns JP, Deutsch A, Labbé MR, Litchfield RB. A Prospective, Randomized Evaluation of Acellular Human Dermal Matrix Augmentation for Arthroscopic Rotator Cuff Repair. *Arthrosc J Arthrosc Relat Surg*. 2012;28(1):8-15. doi:10.1016/j.arthro.2011.06.038
83. Holzapfel B, Reichert J, Schantz J, et al. How smart do biomaterials need to be? A translational science and clinical point of view. *Adv Drug Deliv Rev*. 2013;65(581-603). doi:10.1016/j.addr.2012.07.009
84. today FO-M, 2011 undefined. Biomaterials & scaffolds for tissue engineering. *Elsevier*. https://www.sciencedirect.com/science/article/pii/S136970211170058X. Accessed April 18, 2019.
85. Smith RD., Carr A, Dakin S., Snelling S, Yapp C, Hakimi O. The response of tenocytes to commercial scaffolds used for rotator cuff repair. *Eur Cells Mater*. 2016;31:107-118.
86. Shea K, McCarthy M, Ledgard F, Arciero C, Chowaniec D, Mazzocca A. Human tendon cell response to 7 commercially available extracellular matrix materials: an in vitro study. *Arthrosc J Arthrosc Relat Surg*. 2010;26(9):1181-1188.

doi:10.1016/j.arthro.2010.01.020
87. Xu H, Sandor M, Qi S, et al. Implantation of a porcine acellular dermal graft in a primate model of rotator cuff repair. *J Shoulder Elb Surg.* 2012;21(5):580-588. doi:10.1016/j.jse.2011.03.014
88. Lederman E, Toth A, Nicholson G, et al. A prospective, multicenter study to evaluate clinical and radiographic outcomes in primary rotator cuff repair reinforced with a xenograft dermal matrix. *J Shoulder Elb Surg.* 2016;25(12):1961-1970. doi:10.1016/j.jse.2016.02.029
89. Smith R, Zargar N, Brown C, et al. Characterising the macro and micro mechanical properties of scaffolds for rotator cuff repair. *J Shoulder Elb Surg.* 2017;26(11):2038-2046. doi:10.1016/j.jse.2017.06.035
90. Hakimi O, Murphy R, Stachewicz U, Hislop S, Carr AJ. An electrospun polydioxanone patch for the localisation of biological therapies during tendon repair. *Eur Cell Mater.* 2012;24:344-357; discussion 357. http://www.ncbi.nlm.nih.gov/pubmed/23090765. Accessed April 19, 2017.
91. Hakimi O, Mouthuy P-A, Carr A. Synthetic and degradable patches: an emerging solution for rotator cuff repair. *Int J Exp Pathol.* 2013;94(4):287-292. doi:10.1111/iep.12030
92. Zimmer Biomet. BioWick Implant. http://cayennemedical.com/biowick-surelock/. Published 2019.
93. Peyton SR, Ghajar CM, Khatiwala CB, Putnam AJ. The emergence of ECM mechanics and cytoskeletal tension as important regulators of cell function. *Cell Biochem Biophys.* 2007;47(2):300-320. doi:10.1007/s12013-007-0004-y
94. Burdick JA, Mauck RL, Gorman JH, Gorman RC. Acellular biomaterials: an evolving alternative to cell-based therapies. *Sci Transl Med.* 2013;5(176):176ps4. doi:10.1126/scitranslmed.3003997
95. Laurencin C, Nair L. *Nanotechnology and Tissue Engineering.* 1st Editio. CRC Press; 2008. doi:10.1201/9781420051834
96. Frank CB, Hart DA, Shrive NG. Molecular biology and biomechanics of normal and healing ligaments—a review. *Osteoarthr Cartil.* 1999;7(1):130-140. doi:10.1053/joca.1998.0168
97. Waggett AD, Ralphs JR, Kwan APL, Woodnutt D, Benjamin M. Characterization of collagens and proteoglycans at the insertion of the human achilles tendon. *Matrix Biol.* 1998;16(8):457-470. doi:10.1016/S0945-053X(98)90017-8
98. Bosworth LA, Rathbone SR, Bradley RS, Cartmell SH. Dynamic loading of electrospun yarns guides mesenchymal stem cells towards a tendon lineage. *J Mech Behav Biomed Mater.* 2014;39:175-183. doi:10.1016/j.jmbbm.2014.07.009
99. Bhaskar P, Bosworth LA, Wong R, et al. Cell response to sterilized electrospun poly(ε-caprolactone) scaffolds to aid tendon regeneration in vivo. *J Biomed Mater Res A.* 2017;105(2):389-397. doi:10.1002/jbm.a.35911
100. Moraes VY, Lenza M, Tamaoki MJ, Faloppa F, Belloti JC. Platelet-rich therapies for musculoskeletal soft tissue injuries. *Cochrane Database Syst Rev.* 2014;(4). doi:10.1002/14651858.CD010071.pub3
101. Carr AJ, Murphy R, Dakin SG, et al. Platelet-Rich Plasma Injection With Arthroscopic Acromioplasty for Chronic Rotator Cuff Tendinopathy. *Am J Sports Med.* 2015;43(12):2891-2897. doi:10.1177/0363546515608485
102. Guilak F, Cohen DM, Estes BT, Gimble JM, Liedtke W, Chen CS. Control of Stem Cell Fate by Physical Interactions with the Extracellular Matrix. *Cell Stem Cell.* 2009;5(1):17-26. doi:10.1016/J.STEM.2009.06.016
103. Walters NJ, Gentleman E. Evolving insights in cell–matrix interactions: Elucidating how non-soluble properties of the extracellular niche direct stem cell

fate. *Acta Biomater*. 2015;11:3-16. doi:10.1016/J.ACTBIO.2014.09.038
104. García AJ, Vega MD, Boettiger D. Modulation of cell proliferation and differentiation through substrate-dependent changes in fibronectin conformation. *Mol Biol Cell*. 1999;10(3):785-798. doi:10.1091/MBC.10.3.785
105. Woo KM, Chen VJ, Ma PX. Nano-fibrous scaffolding architecture selectively enhances protein adsorption contributing to cell attachment. *J Biomed Mater Res*. 2003;67A(2):531-537. doi:10.1002/jbm.a.10098
106. McCullen SD, Haslauer CM, Loboa EG. Fiber-reinforced scaffolds for tissue engineering and regenerative medicine: use of traditional textile substrates to nanofibrous arrays. *J Mater Chem*. 2010;20(40):8776. doi:10.1039/c0jm01443e
107. Stace E. Electrospun Scaffolds to Promote Tendon Tissue Regeneration in Rotator Cuff Tears. 2018.
108. Erisken C, Zhang X, Moffat K, Levine W, Lu H. Scaffold Fiber Diameter Regulates Human Tendon Fibroblast Growth and Differentiation. *Tissue Eng Part A*. 2012;19(3-4):519-528. doi:10.1089/ten.tea.2012.0072
109. Hopp I, Michelmore A, Smith L, et al. The influence of substrate stiffness gradients on primary human dermal fibroblasts. *Biomaterials*. 2013;34(21):5070-5077. doi:10.1016/j.biomaterials.2013.03.075
110. Discher D, Janmey P, Wang Y. Tissue Cells Feel and Respond to the Stiffness of Their Substrate. *Science (80-)*. 2005;310(5751):1139-1143. doi:10.1126/science.1116995
111. Faucheux N, Schweiss R, Lützow K, Werner C, Groth T. Self-assembled monolayers with different terminating groups as model substrates for cell adhesion studies. *Biomaterials*. 2004;25(14):2721-2730. doi:10.1016/j.biomaterials.2003.09.069
112. Duque Sánchez L, Brack N, Postma A, Pigram PJ, Meagher L. Surface modification of electrospun fibres for biomedical applications: A focus on radical polymerization methods. *Biomaterials*. 2016;106:24-45. doi:10.1016/j.biomaterials.2016.08.011
113. Shuakat MN, Lin T. Recent Developments in Electrospinning of Nanofiber Yarns. *J Nanosci Nanotechnol*. 2014;14(2):1389-1408. doi:10.1166/jnn.2014.9197
114. Kumbar SG, James R, Nukavarapu SP, Laurencin CT. Electrospun nanofiber scaffolds: engineering soft tissues. *Biomed Mater*. 2008;3(3):034002. doi:10.1088/1748-6041/3/3/034002
115. Goonoo N, Jeetah R, Bhaw-Luximon A, Jhurry D. Polydioxanone-based bio-materials for tissue engineering and drug/gene delivery applications. *Eur J Pharm Biopharm*. 2015;97:371-391. doi:10.1016/j.ejpb.2015.05.024
116. Dvir T, Timko B, Kohane D, Langer R. Nanotechnological strategies for engineering complex tissues. *Nat Nanotechnol*. 2011;6:13-22. doi:10.1038/nnano.2010.246
117. Gupta B, Moghe A. Nanofiber structures for medical biotextiles. In: *Biotextiles As Medical Implants*. ; 2013:48-90. doi:10.1533/9780857095602.1.48
118. Bosworth LA, Alam N, Wong JK, Downes S. Investigation of 2D and 3D electrospun scaffolds intended for tendon repair. *J Mater Sci Mater Med*. 2013;24(6):1605-1614. doi:10.1007/s10856-013-4911-8
119. Shang S, Yang F, Cheng X, Walboomers X, Jansen J. The effect of electrospun fibre alignment on the behaviour of rat periodontal ligament cells. *Eur Cells Mater*. 2010;19:180-192. doi:10.22203/eCM.v019a18
120. Sahoo S, Ouyang H, Goh JC-H, Tay TE, Toh SL. Characterization of a novel polymeric scaffold for potential application in tendon/ligament tissue engineering. *Tissue Eng*. 2006;12(1):91-99. doi:10.1089/ten.2006.12.ft-8

121. Teo W, Ramakrishna S. A review on design and nanofibre assemblies. *Nanotechnology*. 2006;17.
122. O'Connor RA, McGuinness GB. Electrospun nanofibre bundles and yarns for tissue engineering applications: A review. *Proc Inst Mech Eng Part H J Eng Med*. 2016;230(11):987-998. doi:10.1177/0954411916656664
123. Ma B, Xie J, Jiang J, Shuler FD, Bartlett DE. Rational design of nanofiber scaffolds for orthopedic tissue repair and regeneration. *Nanomedicine (Lond)*. 2013;8(9):1459-1481. doi:10.2217/nnm.13.132
124. Cai YZ, Zhang GR, Wang LL, Jiang YZ, Ouyang HW, Zou XH. Novel biodegradable three-dimensional macroporous scaffold using aligned electrospun nanofibrous yarns for bone tissue engineering. *J Biomed Mater Res - Part A*. 2012;100 A(5):1187-1194. doi:10.1002/jbm.a.34063
125. Zhu X, Cui W, Li X, Jin Y. Electrospun Fibrous Mats with High Porosity as Potential Scaffolds for Skin Tissue Engineering. *Biomacromolecules*. 2008;9(7):1795-1801. doi:10.1021/bm800476u
126. Rothrauff BB, Lauro BB, Yang G, Debski RE, Musahl V, Tuan RS. Braided and Stacked Electrospun Nanofibrous Scaffolds for Tendon and Ligament Tissue Engineering. *Tissue Eng Part A*. 2017;23(9-10):378-389. doi:10.1089/ten.tea.2016.0319
127. Venugopal J, Ramakrishna S. Applications of polymer nanofibers in biomedicine and biotechnology. *Appl Biochem Biotechnol*. 2005;125(3):147-158. doi:10.1385/ABAB:125:3:147
128. Abhari R, Carr A, Mouthuy P. Multifilament electrospun scaffolds for soft tissue reconstruction. In: Guarino V, Ambrosio L, eds. *Electrofluidodynamic Technologies for Biomaterials and Medical Devices*. Elsevier Limited; 2018:295-328. doi:10.1016/B978-0-08-101745-6.00015-3
129. Mouthuy P, Zargar N, Hakimi O, Lostis E, Carr A. Fabrication of continuous electrospun filaments with potential for use as medical fibres. *Biofabrication*. 2015;7(2):25006. doi:10.1088/1758-5090/7/2/025006
130. Mouthuy P, Somogyi Škoc M, Čipak Gašparović A, Milković L, Carr A, Žarković N. Investigating the use of curcumin-loaded electrospun filaments for soft tissue repair applications. *Int J Nanomedicine*. 2017. doi:10.2147/IJN.S133326
131. Gupta BS. 1 – Manufacture, types and properties of biotextiles for medical applications. In: *Biotextiles As Medical Implants*. ; 2013:3-47. doi:10.1533/9780857095602.1.3
132. Ping Ooi C, Cameron RE. The hydrolytic degradation of polydioxanone (PDSII) sutures. Part I: Morphological aspects. *J Biomed Mater Res*. 2002;63(3):280-290. doi:10.1002/jbm.10180
133. Wu S, Duan B, Liu P, Zhang C, Qin X, Butcher J. Fabrication of aligned nanofiber polymer yarn networks for anisotropic soft tissue scaffolds. *ACS Appl Mater Interfaces*. 2016;8(26):16950-16960. doi:10.1021/acsami.6b05199
134. Tamayol A, Akbari M, Annabi N, Paul A, Khademhosseini A, Juncker D. Fiber-based tissue engineering: Progress, challenges, and opportunities. *Biotechnol Adv*. 2013;31(5):669-687. doi:10.1016/j.biotechadv.2012.11.007
135. *Materials for Bone Disorders*. Elsevier; 2017. doi:10.1016/C2014-0-03361-8
136. Ping Ooi C, Cameron RE. The hydrolytic degradation of polydioxanone (PDSII) sutures. Part I: Morphological aspects. *J Biomed Mater Res*. 2002;63(3):280-290. doi:10.1002/jbm.10180
137. Maurus PB, Kaeding CC. Bioabsorbable implant material review. *Oper Tech Sports Med*. 2004;12(3):158-160. doi:10.1053/J.OTSM.2004.07.015
138. Vieira a. C, Vieira JC, Guedes RM, Marques a. T. Degradation and Viscoelastic

Properties of PLA-PCL, PGA-PCL, PDO and PGA Fibres. *Mater Sci Forum*. 2010;636-637:825-832. doi:10.4028/www.scientific.net/MSF.636-637.825
139. Tan EPS, Lim CT. Effects of annealing on the structural and mechanical properties of electrospun polymeric nanofibres. *Nanotechnology*. 2006;17(10):2649-2654. doi:10.1088/0957-4484/17/10/034
140. Srithep Y, Nealey P, Turng L-S. Effects of annealing time and temperature on the crystallinity and heat resistance behavior of injection-molded poly(lactic acid). *Polym Eng Sci*. 2013;53(3):580-588. doi:10.1002/pen.23304
141. Weir N, Buchanan F, Orr J, Farrar D, Boyd A. Processing, annealing and sterilisation of poly-l-lactide. *Biomaterials*. 2004;25(18):3939-3949. doi:10.1016/j.biomaterials.2003.10.076
142. Fourne F. *Synthetic Fibres: Machines and Equipment Manufacture, Properties*. 1st Editio. Hanser Publications; 1999.
143. Haider S, Al-Zeghayer Y, Ali F, Haider A, A M. Highly aligned narrow diameter chitosan electrospun nanofibers. *J Polym Res*. 2013;20(105). doi:10.1007/s10965-013-0105-9
144. Zong X, Ran S, Fang D, Hsiao BS, Chu B. Control of structure, morphology and property in electrospun poly(glycolide-co-lactide) non-woven membranes via post-draw treatments. *Polymer (Guildf)*. 2003;44(17):4959-4967. doi:10.1016/S0032-3861(03)00464-6
145. Lee C, HJ S, IH C, et al. Nanofiber alignment and direction of mechanical strain affect the ECM production of human ACL fibroblast. *Biomaterials*. 2005;26(11):1261-1270. doi:10.1016/j.biomaterials.2004.04.037
146. Lai C, Zhong G, Yue Z, et al. Investigation of post-spinning stretching process on morphological, structural, and mechanical properties of electrospun polyacrylonitrile copolymer nanofibers. *Polymer (Guildf)*. 2011;52(2):519-528. doi:10.1016/j.polymer.2010.11.044
147. Cho A, Shin D, Jung H, et al. Effect of annealing on the crystallization and properties of electrospun polylatic acid and nylon 6 fibers. *J Appl Polym Sci*. 2011;120(2):752-758. doi:10.1002/app.33262
148. Barber JG, Handorf AM, Allee TJ, Li W-J. Braided nanofibrous scaffold for tendon and ligament tissue engineering. *Tissue Eng Part A*. 2013;19(11-12):1265-1274. doi:10.1089/ten.tea.2010.0538
149. Baji A, Mai Y-W, Wong S-C, Abtahi M, Chen P. Electrospinning of polymer nanofibers: Effects on oriented morphology, structures and tensile properties. *Compos Sci Technol*. 2010;70(5):703-718. doi:10.1016/j.compscitech.2010.01.010
150. Bonnet M, Rogausch K-D, Petermann J. The endothermic "annealing peak" of poly(phenylene sulphide) and poly(ethylene terephthalate). *Colloid Polym Sci*. 1999;277(6):513-518. doi:10.1007/s003960050418
151. Takayama T, Todo M, Tsuji H. Effect of annealing on the mechanical properties of PLA/PCL and PLA/PCL/LTI polymer blends. *J Mech Behav Biomed Mater*. 2011;4(3):255-260. doi:10.1016/j.jmbbm.2010.10.003
152. Yeh G, Hosemann R, Loboda-Cackovic J, Cackovic H. Annealing effects of polymers and their underlying molecular mechanisms. *Polymer (Guildf)*. 1976;17(4):309-318. doi:10.1016/0032-3861(76)90187-7
153. Abhari RE, Mouthuy P-A, Zargar N, Brown C, Carr A. Effect of annealing on the mechanical properties and the degradation of electrospun polydioxanone filaments. *J Mech Behav Biomed Mater*. 2017;67. doi:10.1016/j.jmbbm.2016.11.023
154. Ali S a M, Zhong SP, Doherty PJ, Williams DF. Mechanisms of polymer degradation in implantable devices. I. Poly(caprolactone). *Biomaterials*. 1993;14(9):648-656. doi:10.1016/0142-9612(93)90063-8

155. Aibibu D, Hild M, Cherif C. *Advances in Braiding Technology: Specialized Techniques and Applications*. (Kyosev Y, ed.). Woodhead Publishing Series in Textiles; 2016. doi:10.1016/C2014-0-03190-5
156. Marui Textile Machinery Co. Ltd. Mini Twister AMT-2S. http://www.marusans.com/e/products/products_00.html.
157. August Herzog Maschinenfabrik. Rope braiding machine SENG 1/32-160. http://www.herzog-online.com/_rubric/index.php?rubric=Products+Rope-braiding-machines+EN.
158. Jakob Müller AG. Narrow Fabric Loom NH2 53 4/66. https://www.mueller-frick.com/fileadmin/user_upload/domain1/Leaflets/WE/NH2_53/NH2_53_61140_en_10_15.pdf.
159. Lotus A, Bhargava S, Bender E, et al. Electrospinning route for the fabrication of p-n junction using nanofiber yarns. *J Appl Phys*. 2009;106(1):014303. doi:10.1063/1.3157206
160. Fennessey SF, Farris RJ. Fabrication of aligned and molecularly oriented electrospun polyacrylonitrile nanofibers and the mechanical behavior of their twisted yarns. *Polymer (Guildf)*. 2004;45(12):4217-4225. doi:10.1016/j.polymer.2004.04.001
161. Ali U, Zhou Y, Wang X, Lin T. Direct electrospinning of highly twisted, continuous nanofiber yarns. *J Text Inst*. 2012;103(1):80-88. doi:10.1080/00405000.2011.552254
162. Freeman JW, Woods MD, Laurencin CT. Tissue engineering of the anterior cruciate ligament using a braid–twist scaffold design. *J Biomech*. 2007;40:2029-2036. doi:10.1016/j.jbiomech.2006.09.025
163. Czaplewski SK, Tsai T-L, Duenwald-Kuehl SE, Vanderby R, Li W-J. Tenogenic differentiation of human induced pluripotent stem cell-derived mesenchymal stem cells dictated by properties of braided submicron fibrous scaffolds. *Biomaterials*. 2014;35(25):6907-6917. doi:10.1016/j.biomaterials.2014.05.006
164. Hu W, Huang Z-M, Liu X-Y. Development of braided drug-loaded nanofiber sutures. *Nanotechnology*. 2010;21(31):315104. doi:10.1088/0957-4484/21/31/315104
165. Hu W, Huang Z-M, Meng S-Y, He C. Fabrication and characterization of chitosan coated braided PLLA wire using aligned electrospun fibers. *J Mater Sci Mater Med*. 2009;20(11):2275-2284. doi:10.1007/s10856-009-3797-y
166. Xie J, Ma B, Michael PL. Fabrication of novel 3D nanofiber scaffolds with anisotropic property and regular pores and their potential applications. *Adv Healthc Mater*. 2012;1(5):674-678. doi:10.1002/adhm.201200100
167. Khil M-S, Bhattarai SR, Kim H-Y, Kim S-Z, Lee K-H. Novel fabricated matrix via electrospinning for tissue engineering. *J Biomed Mater Res*. 2005;72B(1):117-124. doi:10.1002/jbm.b.30122
168. Hajiani F, Jeddi A a a, Gharehaghaji a. a. An investigation on the effects of twist on geometry of the electrospinning triangle and polyamide 66 nanofiber yarn strength. *Fibers Polym*. 2012;13(2):244-252. doi:10.1007/s12221-012-0244-3
169. Cooper JA, Lu HH, Ko FK, Freeman JW, Laurencin CT. Fiber-based tissue-engineered scaffold for ligament replacement: design considerations and in vitro evaluation. *Biomaterials*. 2005;26(13):1523-1532. doi:10.1016/j.biomaterials.2004.05.014
170. Hu B, Gao DJ, Yu FH, Wang TT, Pan YM, Yang XM. Endoscopic stenting for post-transplant biliary stricture: Usefulness of a novel removable covered metal stent. 2011;18(5):640-645. doi:10.1007/s00534-011-0408-3
171. Su C-I, Liu Y-S, Lu C-H, Lin C-W, Wu S-P. Effect of Twist and Draw on

Morphology and Tensile Property of Electrospun Nanofibrous Yarns. *Polym Plast Technol Eng*. 2015;54(11):1106-1112. doi:10.1080/03602559.2014.986803
172. Zhou Y, Fang J, Wang X, Lin T. Strip twisted electrospun nanofiber yarns: Structural effects on tensile properties. *J Mater Res*. 2012;27(03):537-544. doi:10.1557/jmr.2011.295
173. Latifi M, Yousefzadeh M, Teo W-E, Amani-Tehran M, Ramakrishna S. Continuous twisted yarn from well-aligned nanofibers by a water vortex. *Soc Plast Res*. 2011. doi:10.1002/spepro.003599
174. Rao Y, Farris R. A modeling and experimental study of the influence of twist on the mechanical properties of high-performance fiber yarns. *J Appl Polym Sci*. 2000;77(9):1938-1949. doi:10.1002/1097-4628(20000829)77:9<1938::AID-APP9>3.0.CO;2-D
175. Zhong S, Zhang Y, Lim CT. Fabrication of large pores in electrospun nanofibrous scaffolds for cellular infiltration: a review. *Tissue Eng Part B Rev*. 2012;18(2):77-87. doi:10.1089/ten.TEB.2011.0390
176. Wu J, Huang C, Liu W, et al. Cell Infiltration and Vascularization in Porous Nanoyarn Scaffolds Prepared by Dynamic Liquid Electrospinning. *J Biomed Nanotechnol*. 2014;10(4):603-614. doi:10.1166/jbn.2014.1733
177. Yang J, Shi G, Bei J, et al. Fabrication and surface modification of macroporous poly(L-lactic acid) and poly(L-lactic-co-glycolic acid) (70/30) cell scaffolds for human skin fibroblast cell culture. *J Biomed Mater Res*. 2002;62(3):438-446. doi:10.1002/jbm.10318
178. Grier WK, Iyoha EM, Harley BAC. The influence of pore size and stiffness on tenocyte bioactivity and transcriptomic stability in collagen-GAG scaffolds. *J Mech Behav Biomed Mater*. 2017;65:295-305. doi:10.1016/J.JMBBM.2016.08.034
179. Butler SL, Kohles SS, Thielke RJ, Chen C, Vanderby R. Interstitial fluid flow in tendons or ligaments: A porous medium finite element simulation. *Med Biol Eng Comput*. 1997;35(6):742-746. doi:10.1007/BF02510987
180. Rnjak-Kovacina J, Wise SG, Li Z, et al. Tailoring the porosity and pore size of electrospun synthetic human elastin scaffolds for dermal tissue engineering. *Biomaterials*. 2011;32(28):6729-6736. doi:10.1016/j.biomaterials.2011.05.065
181. Gu BK, Park SJ, Kim MS, Kang CM, Kim J-I, Kim C-H. Fabrication of sonicated chitosan nanofiber mat with enlarged porosity for use as hemostatic materials. *Carbohydr Polym*. 2013;97(1):65-73. doi:10.1016/J.CARBPOL.2013.04.060
182. Horan RL, Collette AL, Lee C, Antle K, Chen J, Altman GH. Yarn design for functional tissue engineering. *J Biomech*. 2006;39(12):2232-2240. doi:10.1016/j.jbiomech.2005.07.007
183. He CL, Huang ZM, Han XJ. Fabrication of drug-loaded electrospun aligned fibrous threads for suture applications. *J Biomed Mater Res - Part A*. 2009;89(1):80-95. doi:10.1002/jbm.a.32004
184. News MP. Defining the standard for medical grade polymers. https://www.medicalplasticsnews.com/news/opinion/what-is-a-medical-grade-polymer/.
185. Martins J, Lach A, Morris H, Carr A, Mouthuy P. Polydioxanone implants: a systematic review on safety and performance in patients. *Unpubl under Rev*. 2019.
186. Hakimi O, Murphy R, Stachewicz U, Hislop S, Carr A. An electrospun polydioxanone patch for the localisation of biological therapies during tendon repair. *Eur Cells Mater*. 2012;24:344-357. doi:10.22203/eCM.v024a25
187. Slivka MA, Chu CC, Zhang YL. Laser confocal microscopic study of pH profiles of synthetic absorbable fibers upon in vitro hydrolytic degradation. *J Mater Sci Mater Med*. 2001;12(3):241-247. doi:10.1023/a:1008963132565

188. Boland ED, Coleman BD, Barnes CP, Simpson DG, Wnek GE, Bowlin GL. Electrospinning polydioxanone for biomedical applications. *Acta Biomater*. 2005;1(1):115-123. doi:10.1016/j.actbio.2004.09.003
189. Pillai CKS, Sharma CP. Review paper: absorbable polymeric surgical sutures: chemistry, production, properties, biodegradability, and performance. *J Biomater Appl*. 2010;25(4):291-366. doi:10.1177/0885328210384890
190. Abhari R, Martins J, Morris H, PA M, Carr A. Synthetic sutures: Clinical evaluation and future developments. *J Biomater Appl*. 2017;0(0):1-12. doi:10.1177/0885328217720641
191. Hakimi O, Chaudhury S, Murphy R, Carr A. Differential growth on sutures of tendon cells derived from torn human rotator cuff. *J Biomed Mater Res Part B Appl Biomater*. 2012;100B(3):685-692. doi:10.1002/jbm.b.31993
192. ISO 13485 Medical devices. https://www.iso.org/iso-13485-medical-devices.html.
193. Vaquette C, Cooper-White JJ. Increasing electrospun scaffold pore size with tailored collectors for improved cell penetration. *Acta Biomater*. 2011;7(6):2544-2557. doi:10.1016/j.actbio.2011.02.036
194. Eichhorn SJ, Sampson WW. Statistical geometry of pores and statistics of porous nanofibrous assemblies. *J R Soc Interface*. 2005;2(4):309-318. doi:10.1098/rsif.2005.0039
195. Charousset C, Grimberg J, Duranthon LD, Bellaïche L, Petrover D, Kalra K. The Time for Functional Recovery After Arthroscopic Rotator Cuff Repair: Correlation With Tendon Healing Controlled by Computed Tomography Arthrography. *Arthrosc J Arthrosc Relat Surg*. 2008;24(1):25-33. doi:10.1016/J.ARTHRO.2007.07.023
196. Rashid M. Augmentation Strategies in Rotator Cuff Repair. 2019.
197. *VERSALOK ® Suture Anchor for Rotator Cuff Repair*. http://synthes.vo.llnwd.net/o16/LLNWMB8/US Mobile/Synthes North America/Product Support Materials/Technique Guides/DSUSMTK12160881-Mitek Versalok.pdf.
198. Miller T, Feinblatt J, Craw J, Litsky A, Flanigan D. Evaluation of high-strength orthopedic sutures: a head-to-head comparison. *Orthopaedics*. 2010;33(9):674. doi:10.3928/01477447-20100722-08
199. Halder A, Zobitz M, Schultz F, An K. Mechanical properties of the posterior rotator cuff. *Clin Biomech (Bristol, Avon)*. 2000;15(6):456-462. doi:10.1016/S0268-0033(99)00095-9
200. Weldon CB, Tsui JH, Shankarappa SA, et al. Electrospun drug-eluting sutures for local anesthesia. *J Control Release*. 2012;161(3):903-909. doi:10.1016/j.jconrel.2012.05.021
201. Padmakumar S, Joseph J, Harsha Neppalli M, et al. Electrospun Polymeric Core−sheath Yarns as Drug Eluting Surgical Sutures. 2016. doi:10.1021/acsami.6b00874
202. Reneker DH, Yarin AL. Electrospinning jets and polymer nanofibers. *Polymer (Guildf)*. 2008;49(10):2387-2425. doi:10.1016/j.polymer.2008.02.002
203. Bashur CA, Dahlgren LA, Goldstein AS. Effect of fiber diameter and orientation on fibroblast morphology and proliferation on electrospun poly(d,l-lactic-co-glycolic acid) meshes. *Biomaterials*. 2006;27(33):5681-5688. doi:10.1016/j.biomaterials.2006.07.005
204. Luo CJ, Stoyanov SD, Stride E, Pelan E, Edirisinghe M. Electrospinning versus fibre production methods: from specifics to technological convergence. *Chem Soc Rev Chem Soc Rev*. 2012;41(41):4708-4735. doi:10.1039/c2cs35083a

205. Vrieze S De, Clerck K De. 80 Years of Electrospinning. *Int Conf Latest Adv High-Tech Text Text Mater Proc*. 2009:60-63. https://biblio.ugent.be/publication/767594/file/767596.pdf. Accessed June 26, 2017.
206. Baldwin M, Snelling S, Dakin S, Carr A. Augmenting endogenous repair of soft tissues with nanofibre scaffolds. *J R Soc Interface*. 2018;15(141):20180019. doi:10.1098/rsif.2018.0019
207. Keun Kwon I, Kidoaki S, Matsuda T. Electrospun nano- to microfiber fabrics made of biodegradable copolyesters: structural characteristics, mechanical properties and cell adhesion potential. *Biomaterials*. 2005;26(18):3929-3939. doi:10.1016/j.biomaterials.2004.10.007
208. Klumpp D, Rudisile M, Kühnle RI, et al. Three-dimensional vascularization of electrospun PCL/collagen-blend nanofibrous scaffolds in vivo. *J Biomed Mater Res Part A*. 2012;100A(9):n/a-n/a. doi:10.1002/jbm.a.34172
209. Pu J, Yuan F, Li S, Komvopoulos K. Electrospun bilayer fibrous scaffolds for enhanced cell infiltration and vascularization in vivo. *Acta Biomater*. 2015;13:131-141. doi:10.1016/j.actbio.2014.11.014
210. Lach AA, Morris HL, Martins JA, Stace ET, Carr AJ, Mouthuy P-A. Pyridine as an additive to improve the deposition of continuous electrospun filaments. H Ribeiro M, ed. *PLoS One*. 2019;14(4):e0214419. doi:10.1371/journal.pone.0214419
211. ISO 14644-1:2015 - Cleanrooms and associated controlled environments — Part 1: Classification of air cleanliness by particle concentration. https://www.iso.org/standard/53394.html.
212. ADMET. Rope and Thread. http://www.admet.com/products/test-fixtures-and-accessories/test-fixtures/rope-and-thread/.
213. Liu X, Zheng S, Dan W, Dan N. Ultrasound-mediated Preparation and Evaluation of a Collagen/PVP-PCL Micro-and Nanofiber Scaffold Electrospun from Chloroform/Ethanol Mixture. *Fibers Polym*. 2016;17(8):1186-1197. doi:10.1007/s12221-016-6400-4
214. Koncar V, Koncar V. Structural health monitoring of processes related to composite manufacturing. *Smart Text Situ Monit Compos*. January 2019:295-381. doi:10.1016/B978-0-08-102308-2.00004-8
215. ISO 2062:2009 - Textiles. Yarns from packages. Determination of single-end breaking force and elongation at break using constant rate of extension (CRE) tester. https://www.iso.org/standard/45642.html.
216. Širc J, Hobzová R, Kostina N, et al. Morphological characterization of nanofibers: methods and application in practice. *J Nanomater*. 2012. doi:10.1155/2012/327369
217. Ritter H, Analytical LD-I& EC, 1945 undefined. Pressure porosimeter and determination of complete macropore-size distributions. Pressure porosimeter and determination of complete macropore-size distributions. *ACS Publ*. https://pubs.acs.org/doi/pdf/10.1021/i560148a013. Accessed June 12, 2019.
218. Washburn EW. Note on a Method of Determining the Distribution of Pore Sizes in a Porous Material. *Proc Natl Acad Sci U S A*. 1921;7(4):115-116. doi:10.1073/pnas.7.4.115
219. Micromeritics Instrument Corporation. Mercury Intrusion Porosimetry Theory. https://www.micromeritics.com/Repository/Files/Mercury_Porosemitry_Theory_poster_.pdf. Accessed June 12, 2019.
220. Ping Ooi C, Cameron RE. The hydrolytic degradation of polydioxanone (PDSII) sutures. Part II: Micromechanisms of deformation. *J Biomed Mater Res*. 2002;63(3):291-298. doi:10.1002/jbm.10181
221. Boland ED, Coleman BD, Barnes CP, Simpson DG, Wnek GE, Bowlin GL.

Electrospinning polydioxanone for biomedical applications. *Acta Biomater*. 2005;1(1):115-123. doi:10.1016/j.actbio.2004.09.003
222. Ishikiriyama K, Pyda M, Zhang G, Forschner T, Grebowicz J, Wunderlich B. Heat capacity of poly-p-dioxanone. *J Macromol Sci Part B*. 1998;37(1):27-44. doi:10.1080/00222349808220453
223. Lin T, Wang H, Wang H, Wangt X. Effects of polymer concentration and cationic surfactant on the morphology of electrospun polyacrylonitrile nanofibres. *J Mater Sci techonology*. 2005;21(1):1-4.
224. Athira KS, Sanpui P, Chatterjee K. Fabrication of Poly(Caprolactone) Nanofibers by Electrospinning. *J Polym Biopolym Phys Chem*. 2014;2(4):62-66. doi:10.12691/jpbpc-2-4-1
225. Xie J, Li X, Xia Y. Putting Electrospun Nanofibers to Work for Biomedical Research. *Macromol Rapid Commun*. 2008;29(22):1775-1792. doi:10.1002/marc.200800381
226. Srithep Y, Javadi A, Pilla S, et al. Processing and characterization of recycled poly(ethylene terephthalate) blends with chain extenders, thermoplastic elastomer, and/or poly(butylene adipate-co-terephthalate). *Polym Eng Sci*. 2011;51(6):1023-1032. doi:10.1002/pen.21916
227. Hoffman JD, Lauritzen JI, Passaglia E, Ross GS, Frolen LJ, Weeks JJ. Kinetics of polymer crystallization from solution and the melt. *Kolloid-Zeitschrift und Zeitschrift für Polym*. 1969;231(1-2):564-592. doi:10.1007/BF01500015
228. Nixon A, Watts A, Schnabel L. Cell- and gene-based approaches to tendon regeneration. *J Shoulder Elb Surg*. 2012;21(2):278-294. doi:10.1016/j.jse.2011.11.015
229. Zhang J, Jones S, Wang D, et al. Influence of thermal annealing on mechanical properties and in vitro degradation of poly(p-dioxanone). *Polym Eng Sci*. 2019;59(8):1701-1709. doi:10.1002/pen.25169
230. Ethicon Product Guide. *PDS Flexible Plates*.; 2004. http://www.medicommers.hu/katalogus/134-145.pdf.
231. Cobra Braiding Machinery Ltd, UK. http://www.cobrabraids.com/.
232. MB Medical Braiding Machines. http://medbraider.com/.
233. HERZOG Braiding Machines. https://herzog-online.com/en/home/.
234. Bhardwaj N, Kundu SC. Electrospinning: A fascinating fiber fabrication technique. *Biotechnol Adv*. 2010;28(3):325-347. doi:10.1016/j.biotechadv.2010.01.004
235. Phipps MC, Clem WC, Grunda JM, Clines GA, Bellis SL. Increasing the pore sizes of bone-mimetic electrospun scaffolds comprised of polycaprolactone, collagen I and hydroxyapatite to enhance cell infiltration. *Biomaterials*. 2012;33(2):524-534. doi:10.1016/j.biomaterials.2011.09.080
236. Khorshidi S, Solouk A, Mirzadeh H, et al. A review of key challenges of electrospun scaffolds for tissue-engineering applications. *J Tissue Eng Regen Med*. 2016;10(9):715-738. doi:10.1002/term.1978
237. Feng Z, Ishibashi M, Nomura Y, Kitajima T, Nakamura T. Constraint Stress, Microstructural Characteristics, and Enhanced Mechanical Properties of a Special Fibroblast-embedded Collagen Construct. *Artif Organs*. 2006;30(11):870-877. doi:10.1111/j.1525-1594.2006.00314.x
238. Sawaguchi N, Majima T, Funakoshi T, et al. Effect of cyclic three-dimensional strain on cell proliferation and collagen synthesis of fibroblast-seeded chitosan-hyaluronan hybrid polymer fiber. *J Orthop Sci*. 2010;15(4):569-577. doi:10.1007/s00776-010-1488-7
239. Akbari M, Tamayol A, Bagherifard S, et al. Textile Technologies and Tissue Engineering: A Path Toward Organ Weaving. *Adv Healthc Mater*. 2016;5:751-766.

doi:10.1002/adhm.201500517
240. Vuornos K, Björninen M, Talvitie E, et al. Human Adipose Stem Cells Differentiated on Braided Polylactide Scaffolds Is a Potential Approach for Tendon Tissue Engineering. *Tissue Eng Part A*. 2016;22(5-6):513-523. doi:10.1089/ten.tea.2015.0276
241. Lu HH, Cooper JA, Manuel S, et al. Anterior cruciate ligament regeneration using braided biodegradable scaffolds: in vitro optimization studies. *Biomaterials*. 2005;26(23):4805-4816. doi:10.1016/j.biomaterials.2004.11.050
242. Pham Q, Sharma U, Mikos A. Electrospun Poly(ε-caprolactone) Microfiber and Multilayer Nanofiber/Microfiber Scaffolds: Characterization of Scaffolds and Measurement of Cellular Infiltration. *Biomacromolecules*. 2006;7(10):2796-2805. doi:10.1021/BM060680J
243. Yan E, Fan Y, Sun Z, et al. Biocompatible core–shell electrospun nanofibers as potential application for chemotherapy against ovary cancer. *Mater Sci Eng C*. 2014;41:217-223. doi:10.1016/j.msec.2014.04.053
244. Qian W, Yu D-G, Li Y, Liao Y-Z, Wang X, Wang L. Dual Drug Release Electrospun Core-Shell Nanofibers with Tunable Dose in the Second Phase. *Int J Mol Sci*. 2014;15(1):774-786. doi:10.3390/ijms15010774
245. Woodhead Publishing Series in Textiles. In: *Biotextiles As Medical Implants*. ; 2013:xxi-xxvi. doi:10.1016/B978-1-84569-439-5.50025-9
246. Omeroglu S. The effect of braiding parameters on the mechanical properties of braided ropes. *Fibres Text East Eur*. 2006. http://www.fibtex.lodz.pl/2006/4/53.pdf. Accessed August 29, 2016.
247. Hollister SJ. Porous scaffold design for tissue engineering. *Nat Mater*. 2005;4(7):518-524. doi:10.1038/nmat1421
248. Lin CY, Kikuchi N, Hollister SJ. A novel method for biomaterial scaffold internal architecture design to match bone elastic properties with desired porosity. *J Biomech*. 2004;37(5):623-636. doi:10.1016/j.jbiomech.2003.09.029
249. Hollister SJ, Maddox RD, Taboas JM. Optimal design and fabrication of scaffolds to mimic tissue properties and satisfy biological constraints. *Biomaterials*. 2002;23(20):4095-4103. doi:10.1016/S0142-9612(02)00148-5
250. Derwin K, Badylak S, Steinmann S, Iannotti J. Extracellular matrix scaffold devices for rotator cuff repair. *J Shoulder Elb Surg*. 2010;19(3):467-476. doi:10.1016/j.jse.2009.10.020
251. Chu C, Kizil Z. Quantitative evaluation of stiffness of commercial suture materials. *Surg Gynecol Obstet*. 1989;168(3):233-238.
252. Lindblom K. On Pathogenesis of Ruptures of the Tendon Aponeurosis of the Shoulder Joint. *Acta radiol*. 1939;(6):563-577. doi:10.1177/028418513902000604
253. Lo C-M, Wang H-B, Dembo M, Wang Y. Cell Movement Is Guided by the Rigidity of the Substrate. *Biophys J*. 2000;79(1):144-152. doi:10.1016/S0006-3495(00)76279-5
254. Gray DS, Tien J, Chen CS. Repositioning of cells by mechanotaxis on surfaces with micropatterned Young's modulus. *J Biomed Mater Res*. 2003;66A(3):605-614. doi:10.1002/jbm.a.10585
255. Badylak S, Gilbert T. Immune Response to Biologic Scaffold Materials. *Semin Immunol*. 2008;20(2):109-116. doi:10.1016/j.smim.2007.11.003
256. Wu J, Hong Y. Enhancing cell infiltration of electrospun fibrous scaffolds in tissue regeneration. *Bioact Mater*. 2016;1(1):56-64. doi:10.1016/j.bioactmat.2016.07.001
257. Kennedy K, Bhaw-Luximon A, Jhurry D. Cell-matrix mechanical interaction in electrospun polymeric scaffolds for tissue engineering: Implications for scaffold

design and performance. *Acta Biomater*. 2017;50:41-55. doi:10.1016/j.actbio.2016.12.034
258. Wilson CJ, Clegg RE, Leavesley DI, Pearcy MJ. Mediation of Biomaterial–Cell Interactions by Adsorbed Proteins: A Review. *Tissue Eng*. 2005;11(1-2):1-18. doi:10.1089/ten.2005.11.1
259. Othman Z, Cillero Pastor B, van Rijt S, Habibovic P. Understanding interactions between biomaterials and biological systems using proteomics. *Biomaterials*. 2018;167:191-204. doi:10.1016/jbiomaterials.2018.03.020
260. Bellis SL. Advantages of RGD peptides for directing cell association with biomaterials. *Biomaterials*. 2011;32(18):4205-4210. doi:10.1016/J.BIOMATERIALS.2011.02.029
261. Rahmany MB, Van Dyke M. Biomimetic approaches to modulate cellular adhesion in biomaterials: A review. *Acta Biomater*. 2013;9(3):5431-5437. doi:10.1016/J.ACTBIO.2012.11.019
262. Yang D, Lü X, Hong Y, Xi T, Zhang D. The molecular mechanism of mediation of adsorbed serum proteins to endothelial cells adhesion and growth on biomaterials. *Biomaterials*. 2013;34(23):5747-5758. doi:10.1016/J.BIOMATERIALS.2013.04.028
263. Kim SH, Ha HJ, Ko YK, et al. Correlation of proliferation, morphology and biological responses of fibroblasts on LDPE with different surface wettability. *J Biomater Sci Polym Ed*. 2007;18(5):609-622. doi:10.1163/156856207780852514
264. Wan Y, Qu X, Lu J, et al. Characterization of surface property of poly (lactide-co-glycolide) after oxygen plasma treatment. *Biomaterials*. 2004;25(19):4777-4783. doi:10.1016/j.biomaterials.2003.11.051
265. Hamdan M, Blanco L, Khraisat A, Tresguerres IF. Influence of Titanium Surface Charge on Fibroblast Adhesion. *Clin Implant Dent Relat Res*. 2006;8(1):32-38. doi:10.2310/j.6480.2005.00028.x
266. Schneider G, English A, Abraham M, Zaharias R, Stanford C, Keller J. The effect of hydrogel charge density on cell attachment. *Biomaterials*. 2004;25(15):3023-3028. doi:10.1016/j.biomaterials.2003.09.084
267. Engler A, Richert L, Wong J, Picart C, Discher D. Surface probe measurements of the elasticity of sectioned tissue, thin gels and polyelectrolyte multilayer films: Correlations between substrate stiffness and cell adhesion. *Surf Sci*. 2004;570(1-2):142-154. doi:10.1016/j.susc.2004.06.179
268. Folkman J, Moscona A. Role of cell shape in growth control. *Nature*. 1978;273(5661):345-349. doi:10.1038/273345a0
269. Ben-Ze'ev A, Farmer SR, Penman S. Protein synthesis requires cell-surface contact while nuclear events respond to cell shape in anchorage-dependent fibroblasts. *Cell*. 1980;21(2):365-372. doi:10.1016/0092-8674(80)90473-0
270. Singhvi R, Kumar A, Lopez G, et al. Engineering cell shape and function. *Science (80-)*. 1994;264(5159):696-698. doi:10.1126/science.8171320
271. Kendal A, Snelling S, Dakin S, Stace E, Mouthuy P. Resorbable electrospun polydioxanone fibres modify the behaviour of cells from both healthy and diseased human tendons. *Eur Cells Mater*. 2017;33:169-182. doi:10.22203/eCM.v033a13
272. Yin Z, Chen X, Song H, et al. Electrospun scaffolds for multiple tissues regeneration in vivo through topography dependent induction of lineage specific differentiation. *Biomaterials*. 2015;44:173-185. doi:10.1016/j.biomaterials.2014.12.027
273. Zhang C, Yuan H, Liu H, et al. Well-aligned chitosan-based ultrafine fibers committed teno-lineage differentiation of human induced pluripotent stem cells

for Achilles tendon regeneration. *Biomaterials*. 2015;53:716-730. doi:10.1016/j.biomaterials.2015.02.051
274. Hakimi O, Mouthuy P a., Zargar N, Lostis E, Morrey M, Carr A. A layered electrospun and woven surgical scaffold to enhance endogenous tendon repair. *Acta Biomater*. 2015;26:124-135. doi:10.1016/j.actbio.2015.08.007
275. Gilchrist CL, Ruch DS, Little D, Guilak F. Micro-scale and meso-scale architectural cues cooperate and compete to direct aligned tissue formation. *Biomaterials*. 2014;35(38):10015-10024. doi:10.1016/j.biomaterials.2014.08.047
276. Yao L, Bestwick CS, Bestwick LA, Maffulli N, Aspden RM. Phenotypic Drift in Human Tenocyte Culture. *Tissue Eng*. 2006;12(7):1843-1849. doi:10.1089/ten.2006.12.1843
277. Tyanova S, Temu T, Sinitcyn P, et al. The Perseus computational platform for comprehensive analysis of (prote)omics data. *Nat Methods*. 2016;13(9):731-740. doi:10.1038/nmeth.3901
278. Mi H, Muruganujan A, Ebert D, Huang X, Thomas PD. PANTHER version 14: more genomes, a new PANTHER GO-slim and improvements in enrichment analysis tools. *Nucleic Acids Res*. 2019;47(D1):D419-D426. doi:10.1093/nar/gky1038
279. Thomas PD, Campbell MJ, Kejariwal A, et al. PANTHER: a library of protein families and subfamilies indexed by function. *Genome Res*. 2003;13(9):2129-2141. doi:10.1101/gr.772403
280. Norde W. Adsorption of proteins from solution at the solid-liquid interface. *Adv Colloid Interface Sci*. 1986;25:267-340. doi:10.1016/0001-8686(86)80012-4
281. Horbett T. Proteins: structure, properties, and adsorption to surfaces. In: *Biomaterials Science: An Introduction to Materials in Medicine*. Academic Press, New York; 1996:133-141.
282. Llopis-Hernández V, Rico P, Ballester-Beltrán J, Moratal D, Salmerón-Sánchez M. Role of Surface Chemistry in Protein Remodeling at the Cell-Material Interface. Chin W-C, ed. *PLoS One*. 2011;6(5):e19610. doi:10.1371/journal.pone.0019610
283. Webb K, Hlady V, Tresco PA. Relative importance of surface wettability and charged functional groups on NIH 3T3 fibroblast attachment, spreading, and cytoskeletal organization. *J Biomed Mater Res*. 1998;41(3):422-430. doi:10.1002/(SICI)1097-4636(19980905)41:3<422::AID-JBM12>3.0.CO;2-K
284. Chen S, Liu L, Zhou J, Jiang S. Controlling Antibody Orientation on Charged Self-Assembled Monolayers. *Langmuir*. 2003;19(7):2859-2864. doi:10.1021/LA026498V
285. Wang H, Castner D, Ratner B, Jiang S. Probing the Orientation of Surface-Immobilized Immunoglobulin G by Time-of-Flight Secondary Ion Mass Spectrometry. *Langmuir*. 2004;20(5):1877-1887. doi:10.1021/LA035376F
286. Washington R, Entrekin R. Process for hot stretching braided ligatures. 2001.
287. Pokropinski Jr H, Scalzo H, Fischer J. Process for making sutures having improved knot tensile strength. April 2005.
288. Banes A, Horesovsky G, Larson C, et al. Mechanical load stimulates expression of novel genesin vivoandin vitroin avian flexor tendon cells. *Osteoarthr Cartil*. 1999;7(1):141-153. doi:10.1053/joca.1998.0169
289. Chiquet M, Gelman L, Lutz R, Maier S. From mechanotransduction to extracellular matrix gene expression in fibroblasts. *Biochim Biophys Acta - Mol Cell Res*. 2009;1793(5):911-920. doi:10.1016/j.bbamcr.2009.01.012
290. Bosworth LA, Gibb A, Downes S. Gamma irradiation of electrospun poly(ε-caprolactone) fibers affects material properties but not cell response. *J Polym Sci Part B Polym Phys*. 2012;50(12):870-876. doi:10.1002/polb.23072

291. Subramony SD, Dargis BR, Castillo M, et al. The guidance of stem cell differentiation by substrate alignment and mechanical stimulation. *Biomaterials*. 2013;34(8):1942-1953. doi:10.1016/j.biomaterials.2012.11.012
292. Badami A, Kreke M, Thompson M, Riffle J, Goldstein A. Effect of fiber diameter on spreading, proliferation, and differentiation of osteoblastic cells on electrospun poly(lactic acid) substrates. *Biomaterials*. 2006;27(4):596-606. doi:10.1016/j.biomaterials.2005.05.084
293. Chen M, Patra PK, Warner SB, Bhowmick S. Role of Fiber Diameter in Adhesion and Proliferation of NIH 3T3 Fibroblast on Electrospun Polycaprolactone Scaffolds. *Tissue Eng*. 2007;13(3):579-587. doi:10.1089/ten.2006.0205
294. Solon J, Levental I, Sengupta K, Georges PC, Janmey PA. Fibroblast Adaptation and Stiffness Matching to Soft Elastic Substrates. *Biophys J*. 2007;93(12):4453-4461. doi:10.1529/biophysj.106.101386
295. Taylor SE, Vaughan-Thomas A, Clements DN, et al. Gene expression markers of tendon fibroblasts in normal and diseased tissue compared to monolayer and three dimensional culture systems. *BMC Musculoskelet Disord*. 2009;10(1):27. doi:10.1186/1471-2474-10-27
296. Murphy CM, Haugh MG, O'Brien FJ. The effect of mean pore size on cell attachment, proliferation and migration in collagen–glycosaminoglycan scaffolds for bone tissue engineering. *Biomaterials*. 2010;31(3):461-466. doi:10.1016/j.biomaterials.2009.09.063
297. Wong JKF, Cerovac S, Ferguson MWJ, McGrouther DA. The Cellular Effect of a Single Interrupted Suture on Tendon. *J Hand Surg Am*. 2006;31(4):358-367. doi:10.1016/j.jhsb.2006.03.162
298. Wong J, Alyouha S, Kadler K, Ferguson M, McGrouther D. The cell biology of suturing tendons. *Matrix Biol*. 2010;29(6):525-536. doi:10.1016/j.matbio.2010.06.002
299. Wang X, Ding B, Li B. Biomimetic electrospun nanofibrous structures for tissue engineering. *Mater Today*. 2013;16(6):229-241. doi:10.1016/j.mattod.2013.06.005
300. Lee I, Kwon O, Meng W, Kang I, Ito Y. *Nanofabrication of Microbial Polyester by Electrospinning Promotes Cell Attachment*. Vol 12.; 2004. doi:10.1007/BF03218414
301. Tsugawa AJ, Verstraete FJM. Suture materials and biomaterials. *Oral Maxillofac Surg Dogs Cats*. January 2012:69-78. doi:10.1016/B978-0-7020-4618-6.00007-5
302. Downing TL, Soto J, Houssin T, et al. Biophysical regulation of epigenetic state and cell reprogramming. *Nat Mater*. 2013;12:1154-1162. doi:10.1038/nmat3777
303. Hwang CM, Park Y, Park JY, et al. Controlled cellular orientation on PLGA microfibers with defined diameters. *Biomed Microdevices*. 2009;11(4):739-746. doi:10.1007/s10544-009-9287-7
304. Zhang X, Bogdanowicz D, Erisken C, Lee NM, Lu HH. Biomimetic scaffold design for functional and integrative tendon repair. *J Shoulder Elb Surg*. 2012;21(2):266-277. doi:10.1016/j.jse.2011.11.016
305. Leong MF, Rasheed MZ, Lim TC, Chian KS. In vitro cell infiltration and in vivo cell infiltration and vascularization in a fibrous, highly porous poly(D,L-lactide) scaffold fabricated by cryogenic electrospinning technique. *J Biomed Mater Res Part A*. 2009;91A(1):231-240. doi:10.1002/jbm.a.32208
306. Nam J, Huang Y, Agarwal S, Lannutti J. Improved Cellular Infiltration in Electrospun Fiber via Engineered Porosity. *Tissue Eng*. 2007;13(9):2249-2257. doi:10.1089/ten.2006.0306
307. Silva MMCG, Cyster LA, Barry JJA, et al. The effect of anisotropic architecture on cell and tissue infiltration into tissue engineering scaffolds. *Biomaterials*. 2006;27(35):5909-5917. doi:10.1016/j.biomaterials.2006.08.010

308. Baker BM, Gee AO, Metter RB, et al. The potential to improve cell infiltration in composite fiber-aligned electrospun scaffolds by the selective removal of sacrificial fibers. *Biomaterials*. 2008;29(15):2348-2358. doi:10.1016/J.BIOMATERIALS.2008.01.032
309. Lee JB, Jeong SI, Bae MS, et al. Highly Porous Electrospun Nanofibers Enhanced by Ultrasonication for Improved Cellular Infiltration. *Tissue Eng Part A*. 2011;17(21-22):2695-2702. doi:10.1089/ten.tea.2010.0709
310. Dean BJF, Franklin SL, Carr AJ. A systematic review of the histological and molecular changes in rotator cuff disease. *Bone Joint Res*. 2012;1(7):158-166. doi:10.1302/2046-3758.17.2000115
311. Kawamura S, Ying L, Kim H-J, Dynybil C, Rodeo SA. Macrophages accumulate in the early phase of tendon–bone healing. *J Orthop Res*. 2005;23(6):1425-1432. doi:10.1016/j.orthres.2005.01.014.1100230627
312. Nerurkar NL, Sen S, Baker BM, Elliott DM, Mauck RL. Dynamic culture enhances stem cell infiltration and modulates extracellular matrix production on aligned electrospun nanofibrous scaffolds. *Acta Biomater*. 2011;7(2):485-491. doi:10.1016/J.ACTBIO.2010.08.011
313. Cardwell RD, Dahlgren LA, Goldstein AS. Electrospun fibre diameter, not alignment, affects mesenchymal stem cell differentiation into the tendon/ligament lineage. *J Tissue Eng Regen Med*. 2014;8(12):937-945. doi:10.1002/term.1589
314. Trafton A. Natural polyester makes new sutures stronger, safer. MIT news. http://news.mit.edu/2007/sutures. Published 2007.
315. Newer polyethylene suture designs show greater strength over earlier suture types. Healio. https://www.healio.com/orthopedics/arthroscopy/news/online/%7Bb1767cff-11db-4ca7-a632-169ea88d3b21%7D/newer-polyethylene-suture-designs-show-greater-strength-over-earlier-suture-types. Published 2006.
316. Dudley L, Gamble C, Preston J, et al. What Difference Does Patient and Public Involvement Make and What Are Its Pathways to Impact? Qualitative Study of Patients and Researchers from a Cohort of Randomised Clinical Trials. *PLoS One*. 2015;10(6):e0128817. doi:10.1371/journal.pone.0128817
317. Yock, Zenios, Makower. *Biodesign: The Process of Innovating Medical Technologies*. 2nd ed. Cambridge University Press; 2015.
318. Pauly H, Sathy B, Olvera D, et al. Hierarchically Structured Electrospun Scaffolds with Chemically Conjugated Growth Factor for Ligament Tissue Engineering. *Tissue Eng Part A*. 2017;23(15-16). doi:10.1089/ten.tea.2016.0480
319. Hayes T, Hosie I. Turning Nanofibres into Products: Electrospinning from a Manufacturer's Perspective. In: *Electrospinning for High Performance Sensors*. Springer, Cham; 2015:305-329. doi:10.1007/978-3-319-14406-1_13
320. Hast MW, Zuskov A, Soslowsky LJ. The role of animal models in tendon research. *Bone Joint Res*. 2014;3(6):193-202. doi:10.1302/2046-3758.36.2000281
321. Curfman GD, Redberg RF. Medical Devices — Balancing Regulation and Innovation. *N Engl J Med*. 2011;365(11):975-977. doi:10.1056/NEJMp1109094
322. *EU Regulation 2017/745 on Medical Devices*. Vol 60.; 2017.
323. The Electrospinning Company. https://www.electrospinning.co.uk/.
324. IME Medical Electrospinning. https://www.ime-electrospinning.com/.
325. Stace E, Mouthuy P, AJ C, Ye H. Biomaterials: Electrospinning. In: *Comprehensive Biotechnology*. Elsevier; 2019:424-441. doi:10.1016/B978-0-444-64046-8.00273-1
326. Nexplanon (Etonogestrel Implant). Merck & Co., Inc. https://www.nexplanon.com/.
327. Bistolfi A, Massazza G, Verné E, Massè A. Antibiotic-loaded cement in

orthopedic surgery: a review. *ISRN*. 2011. http://downloads.hindawi.com/journals/isrn.orthopedics/2011/290851.pdf. Accessed December 15, 2016.

328. Xience: Everolimus Eluting Coronary Stent System. Abbott (Vascular). https://www.vascular.abbott/int/products/coronary-intervention/xience-xpedition-drug-eluting-stent.html?8di80r.
329. Dumanian G, Tulaimat A, Dumanian Z. Experimental study of the characteristics of a novel mesh suture. *Br J Surg*. 2015;102(10):1285-1292. doi:10.1002/bjs.9853
330. Staat M, Trenz E, Lohmann P, et al. New measurements to compare soft tissue anchoring systems in pelvic floor surgery. *J Biomed Mater Res Part B Appl Biomater*. 2012;100B(4):924-933. doi:10.1002/jbm.b.32654
331. Subramanian A, Vu D, Larsen G, Lin H. Preparation and evaluation of the electrospun chitosan/PEO fibers for potential applications in cartilage tissue engineering. *J Biomater Sci Polym Ed*. 2005;16(7):861-873. doi:10.1163/1568562054255682

Chapter 8

Appendices

Appendix A: Additional information for Chapter 2

Table A.1: USP size classification for synthetic absorbable sutures.

USP designation	Suture diameter (mm)
8-0	0.04-0.049
7-0	0.05-0.069
6-0	0.07-0.099
5-0	0.1-0.149
4-0	0.15-0.199
3-0	0.2-0.249
2-0	0.3-0.339
0	0.35-0.399
1	0.4-0.499
2	0.5-0.599
3	0.6-0.699
4	0.6-0.699
5	0.7-0.799
6	0.8-0.899
7	0.9-0.999

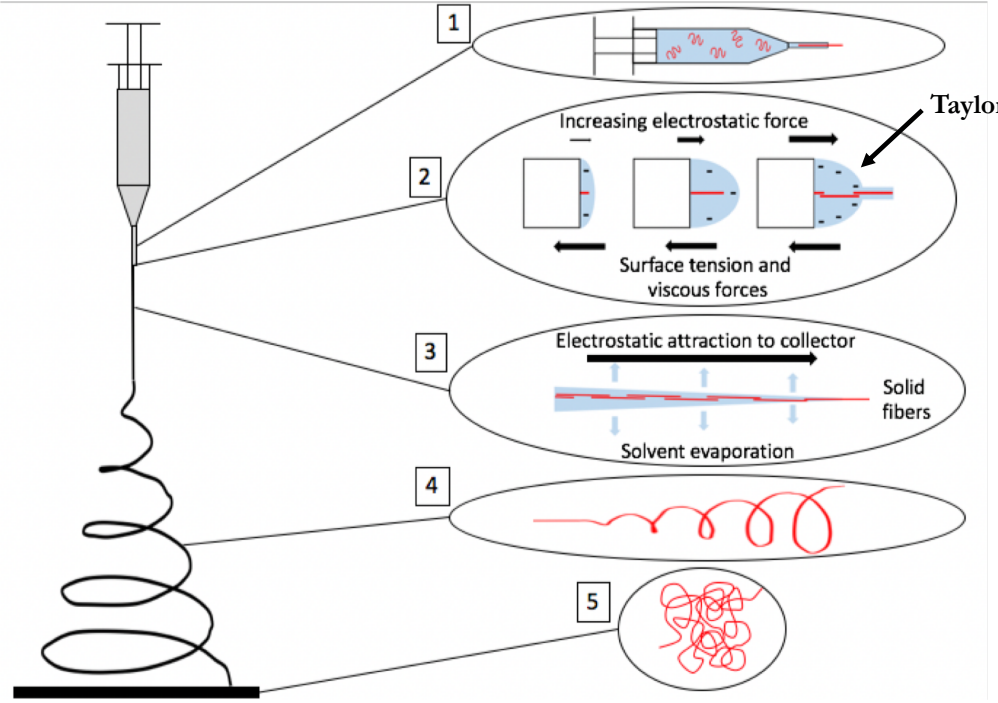


Figure A.1: Stages of the electrospinning process. (1) Polymer chains are randomly dispersed throughout the solution, but elongate when subjected to shear stress as they approch the nozzle and are pumped into the electric field of the electrospinning chamber. (2) Application of the electrostatic force builds up charge separation. When the charge separation is sufficient to overcome the surface tension and viscous forces of the solution, a Taylor cone is formed. (3) Charge repulsions induce whipping and instability, which stretches polymer chains. Throughout this time, the volatile solvent is evaporating. (4) Polymer chains are held together through intermolecular interactions. (5) Randomly orientated fibres are deposited on the grounded collector. Figure modified from Stace et al.[107]

Appendix B: Additional information for Chapter 3

Table B.1: PDO manufacturers and concentrations tested for optimal electrospinning.

PDO variables	Range tested	Methods and reported outcomes
Manufacturer	Evonik Industries, Riverpoint Medical, Poly-med Inc.	A 9% solution was used to electrospin filaments. 35 filaments were twisted into a yarn (5 filaments S twist, 7 bundles Z twist). Yarns were tested to failure with a Zwick tensile testing machine with a 5kN load cell at rate of 0.5mm until failure. Force at break (N) and strain at break (%) were reported. N=5 for each condition.
Concentration	6%, 7%, 9%, 11%	A range of filaments were electrospun using different Riverpoint PDO concentrations. Filaments were imaged using SEM at 5000x magnification. Fibre diameter was measured using ImageJ. Filaments were also tested with a Deben Stage tensile testing machine with a 20N load cell until failure. N=10 for each condition.

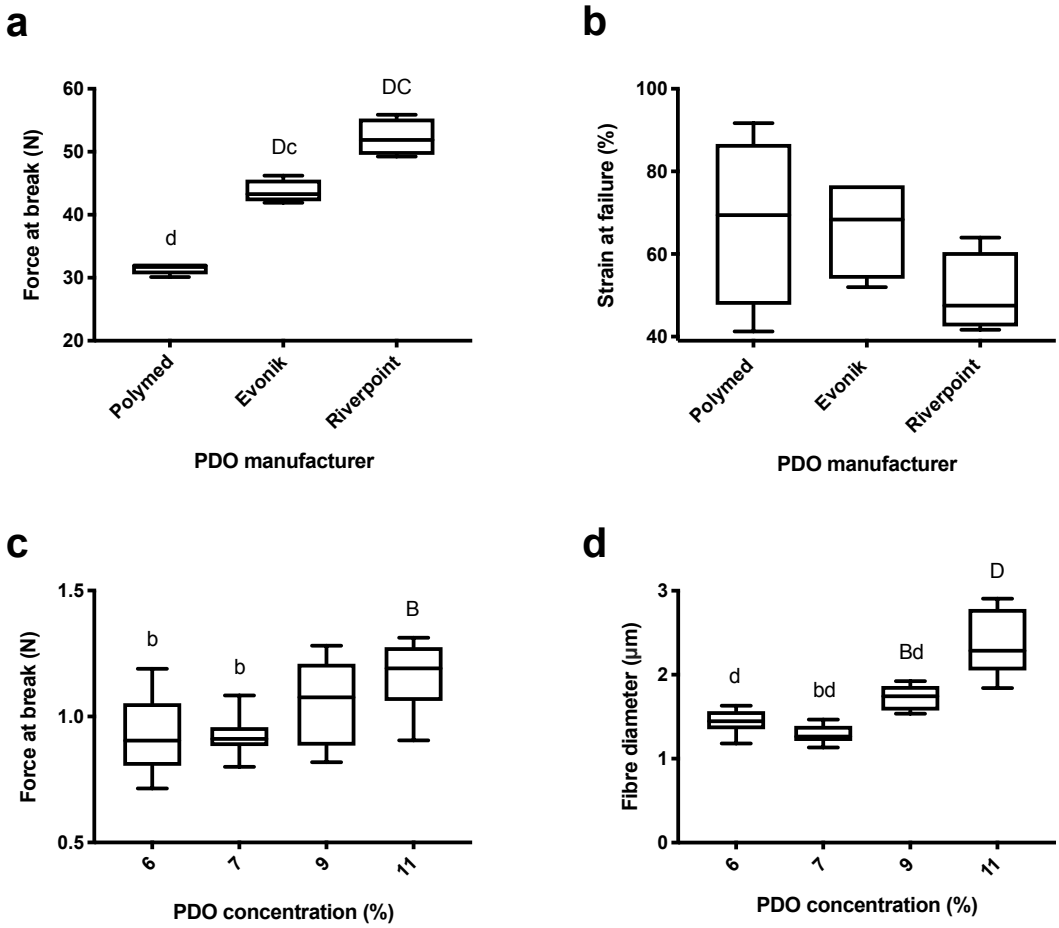


Figure B.1: Influence of PDO manufacturer and concentration on electrospun filament properties. (a,b) Influence of PDO manufacturer (Polymed, Evonik, Riverpoint) on multifilament electrospun yarn mechanical properties. (a) Force at break (N) was significantly higher for yarns spun with Riverpoint compared to Evonik ($p=0.0007$) or Polymer ($p<0.0001$). Strain at break (%) was not significant between the manufacturers tested. (c,d) Influence of PDO concentration on filament force at break and fibre dimeter. (c) Electrospinning with a 11% PDO solution resulted in a higher force at break, compared to spinning at 6% ($p=0.0033$) or 7% ($p=0.0027$). (d) Fibre diameter was significantly higher using an 11% solution, compared to all other concentrations ($p<0.0001$). Electrospinning with a 9% solution also led to a higher concentration compared to a 7% solution ($p=0.0026$). Error bars represent standard deviations; n=5 for the PDO manufacturer experiments and n=10 for the PDO concentration experiment.

Appendix B.2: Annealing electrospun filaments.

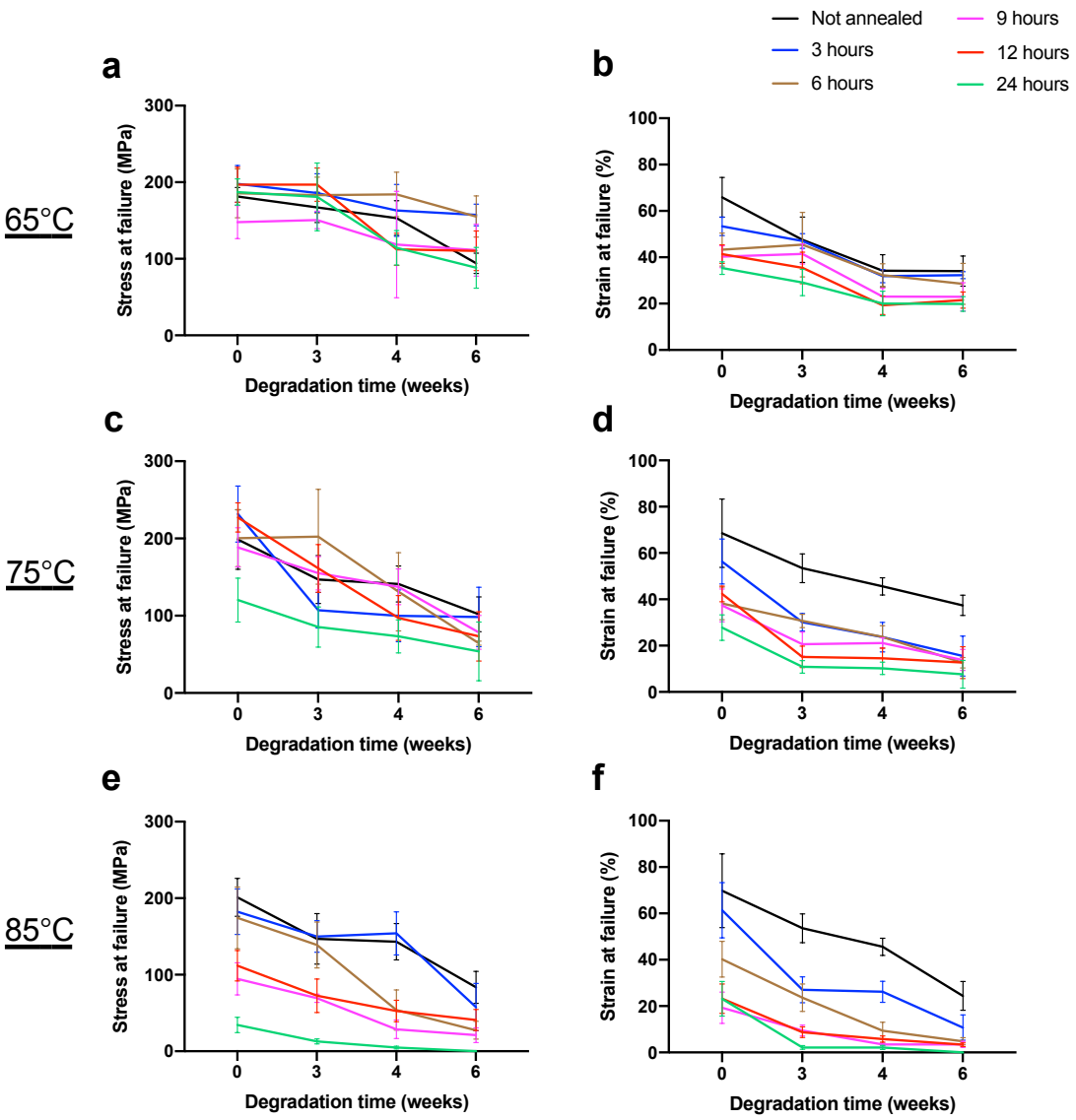


Figure B.2: Changes in mechanical properties of electrospun filaments annealed for various times at 65°C, 75°C, and 85°C, over a 6-week degradation period. Stress at failure (MPa) and strain at failure (%) shown as a function of annealing time and degradation time for samples annealed at (a,b) 65°C, (c,d) 75°C, and (e,f) 85°C. Error bars represent standard deviations; n=10 for each condition.

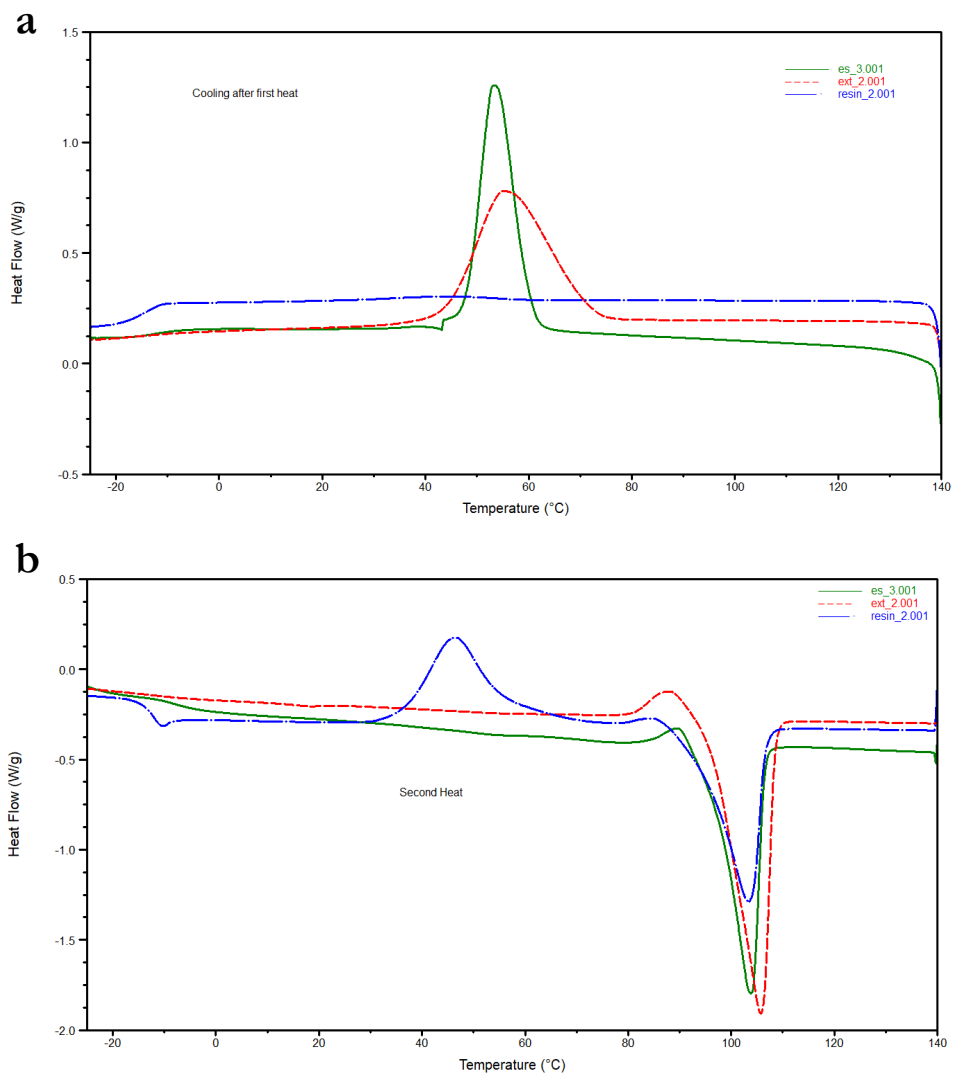


Figure B.3: Representative thermal data comparing PDO electrospun filament, melt-extruded yarn, and raw resin. (a) Cooling after the first heat shows a rapid recrystallisation over a narrow temperature range for the electrospun filament (es), a broader crystallisation over a wide temperature range for the extruded yarn (ext), and a smaller recrystallisation over the lowest temperature range for the resin (resin). All samples exhibited a glass transition. These results suggest that the raw resin is more amorphous than the electrospun or extruded materials; (b) The second heat indicated that the electrospun and resin exhibit glass transitions in the region of -20-10°C. The resin also exhibits a cold crystallisation between 25-75°C. Finally, all three materials exhibit crystallisation just prior to the main melting peak.

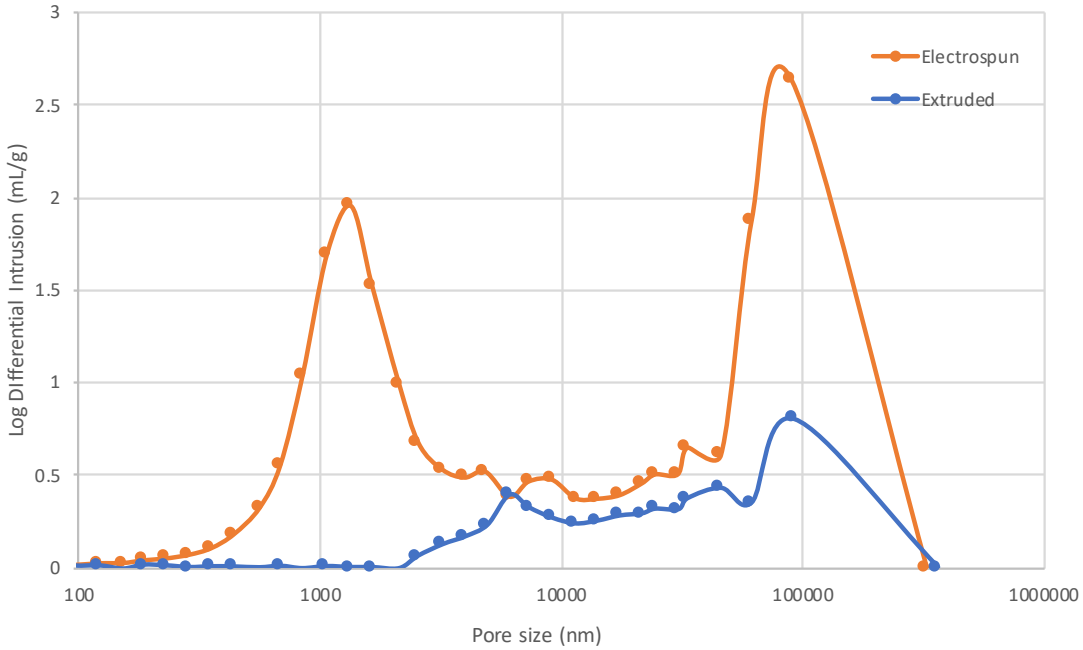


Figure B.4: Representative pore size distribution of electrospun filaments and extruded yarns, measured by Hg porosimetry. The local maxima of the curves represent the most frequent pore diameters. The electrospun intrusion curve showed two broad peaks: one around 1µm and the other between 50-100µm. The intrusion curve from the melt-extruded yarns showed a similar range of pore sizes, but with less intrusion. The local maxima were around 7µm and the other between 50-100µm.

Appendix C: Additional information for Chapter 4

Appendix C.1: Pilot hand-braiding and twisting electrospun filaments into sutures

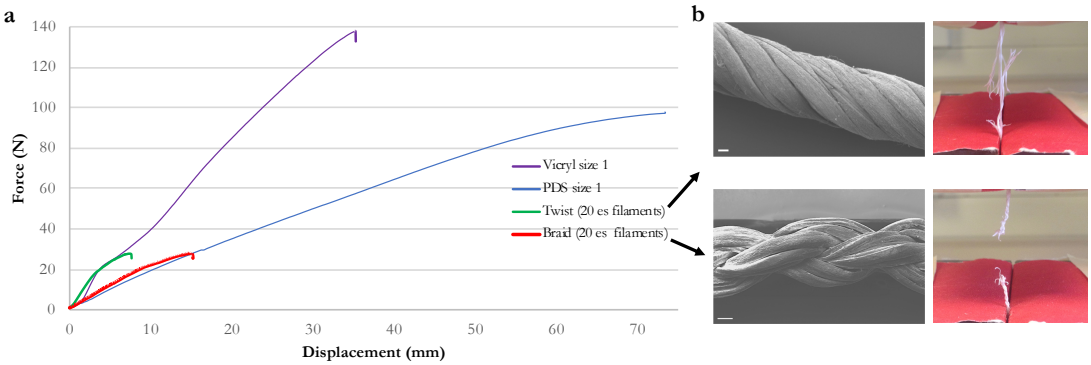


Figure C.1: Pilot data comparing hand-braiding and hand-twisting electrospun filaments to surgical PDS and Vicryl sutures. (a) Force-displacement graph comparing hand-twisted and hand-braided sutures compared to similarly sized PDS and Vicryl sutures. Hand-made sutures have 5-6 times lower force at failure compared to surgical

sutures; (b) SEM images of hand-made sutures (left panel) and images of the suture after mechanical failure (right panel). Twisted sutures exhibit much more fraying compared to braided sutures. Scale bars represent 200μm.

Appendix C.2: Pull through testing

Methods:

The pull through properties between electrospun braided sutures and control sutures were compared. Gelatine was used to mimic a uniform soft tissue surrogate and was prepared by dissolving 80ml gelatine (Knox Unflavoured Gelatine, Kraft Foods, Northfield, IL, USA) in 350ml of boiling water and pouring the mixture into a square mould (23.5cm × 23.5cm × 4cm).[329,330] The mould was left in a 4°C fridge for 24 hours to solidify. The resulting gel was cut into rectangles (4cm × 3cm × 1.2cm). Sutures were cut into 15cm pieces and soaked in PBS (Sigma-Aldrich, USA) for 5 min prior to testing. A suture needle (Sterilseal SN1326, Aspen Medical, UK) was attached to the electrospun sutures and used to pass the suture through the whole gel at 1cm from the edge of the gel. A Zwick tensile testing machine with a 5 kN load cell (Zwick Roell Group, USA) was used to mechanically test each sample. The gel was placed into a small mould and mounted in to lower stationary grip of the machine. The suture was left untied and clamped to the upper grip. Two different pull through tests were performed to mimic different physiological loading conditions.[329–331] First, the upper grip moved at a rate of 2 mm/min until the suture pulled through the material. For the second test, the upper grip moved at a rate of 500 mm/min to mimic an abrupt force.[329,330] Electrospun and control sutures were used for each pull through test (n=5) and the maximum force at pull out (N), strain at pull through (%), and work done until failure (Nmm) was recorded.

Results:

Electrospun and surgical sutures were pulled through a ballistics gel, in order to mimic the

moving of a suture through a uniform soft tissue surrogate. Under both pull through loading conditions (2mm/min and 500mm/min), the electrospun sutures displayed a larger force-displacement curve compared with Vicryl and PDS controls. In all cases, there was no failure of the suture and failure occurred by pull through of the gel. The mechanical pull through results are given in Appendix C.2.

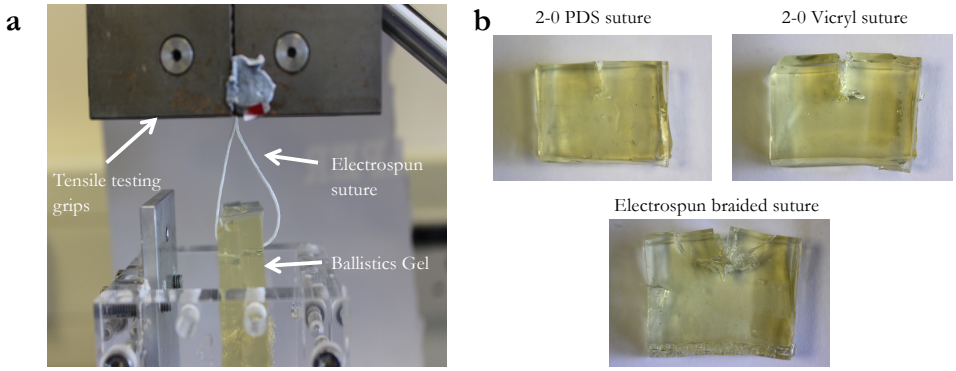


Figure C.2: Pull through testing of braided electrospun sutures compared to surgical sutures PDS and Vicryl. (a) Custom testing setup used for suture pull through a ballistics gel; (b) Ballistic gel after pull through at 2 mm/min of 2-0 PDS (top left), 2-0 Vicryl (top right), and electrospun suture (bottom), resulting in a different fracture profile of the gel between the sutures tested.

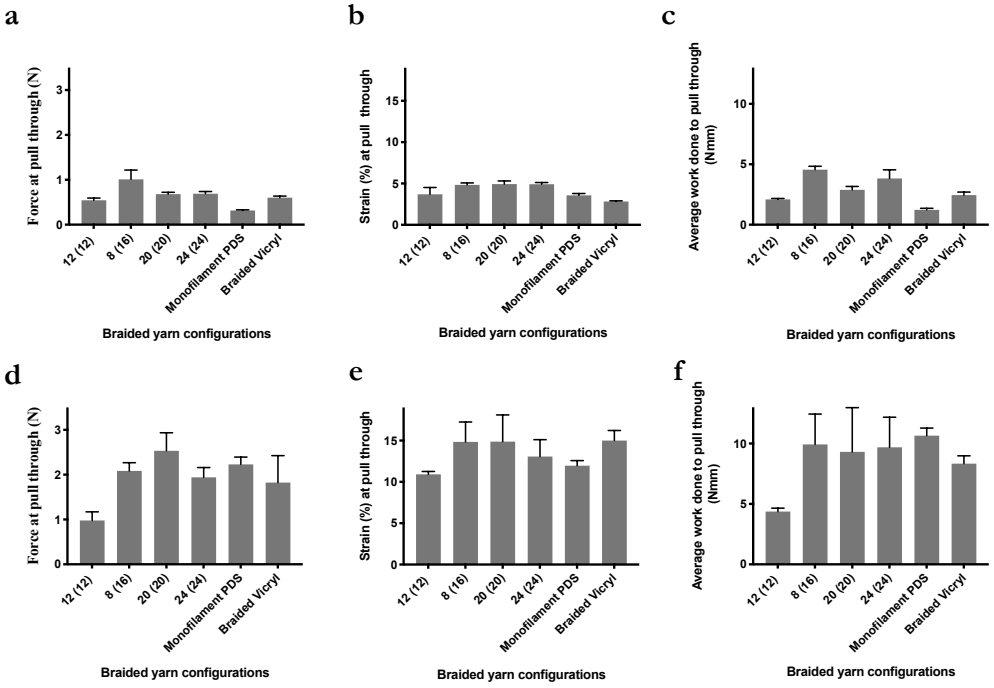


Figure C.3: Mechanical pull through properties of braided electrospun sutures compared to surgical sutures PDS and Vicryl. (a-c) Pull through of all sutures at 2mm/min. (a) Force at pull through (N); (b) strain at pull through (%); (c) Average work done to pull through (Nmm). (d-f) Pull through of all sutures at 500mm/min. (d) Force at pull through (N); (e) strain at pull through (%); (f) Average work done to pull through (Nmm). N=3 for each condition.

Appendix C.3: Mercury porosimetry of the hybrid suture components

Differences in porosity between the sheath (electrospun filaments braided without a core), the core (melt-extruded yarns used as core material), and the final hybrid suture (electrospun sheath with melt-extruded core) were measured by Hg porosimeter and are presented in Figure C.2. The overall porosity was 60±7% for the electrospun sheath, 53±6% for the melt-extruded core, and 40±4% for the hybrid suture. The difference in overall porosity between the electrospun sheath and the hybrid suture was statistically significant (p=0.0116). The average pore diameter was 387±86nm for the electrospun sheath, 451±149nm for the melt-extruded core, and 198±17nm for the hybrid suture. The difference in porosity between the melt-extruded core and hybrid suture was statistically significant (p=0.0474).

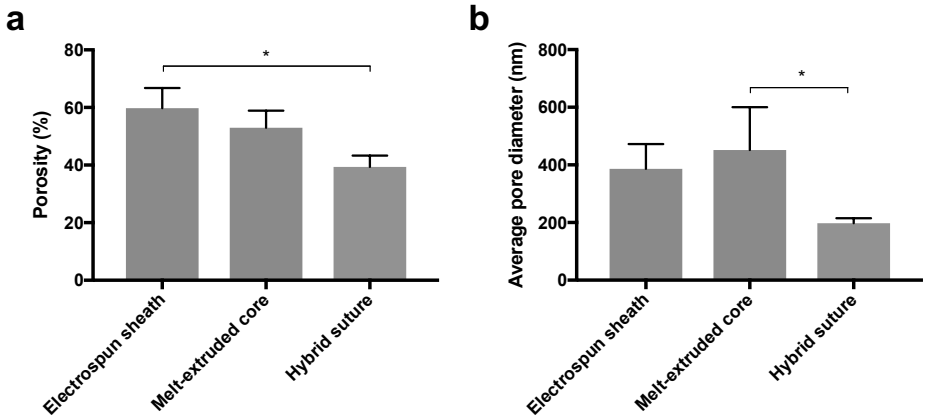


Figure C.4: Hg porosimetry data comparing the electrospun sheath, melt-extruded cores, and hybrid braided sutures. The electrospun sheath was made up 12 filaments, the melt-extruded core was made up of 4 yarns, and the hybrid suture was a combination of these materials. (a) Overall porosity (%) was significantly higher for the electrospun sheath compared to the hybrid suture (p=0.0116); (b) Average pore diameter (nm) was significant higher for the melt-extruded core compared to the hybrid suture (p=0.0474). Statistical significance was determined at *p<0.05, **p<0.01, ***p<0.001, ****p<0.0001.

Error bars represent standard deviations; n=3 for all conditions.

Appendix C.4: Study protocol for a pilot usability study

This study protocol was developed with input from clinical trials managers, research nurses, and orthopaedic surgeons at the NOC. The subjects for this study will be orthopaedic surgeons who specialise in shoulder rotator cuff tear in the UK. Initially, surgeons that have been previously involved in the clinical trials CSAW and UKUFF will be recruited. The usability test is made up of seven steps. Consent will be taken to videotape the performance tasks. Surgeons will initially fill out a background questionnaire, indicating their surgical preferences and views about rotator cuff operations. They will then perform two tasks. First, they will load the novel hybrid suture onto a Versalok suture anchor. Then, they will perform a simulated double row repair of the hybrid suture with a rotator cuff model. Following this, they will fill out two questionnaires evaluating the material properties of the hybrid suture and its usability for the operation. Data will be analysed by compiling questionnaire data, as well as evaluating the qualitative state of the repair from the video and the quantitative state of repair from a pull out test (following methods in Chapter 4.4.7).

Table C.1: Materials needed for usability testing.

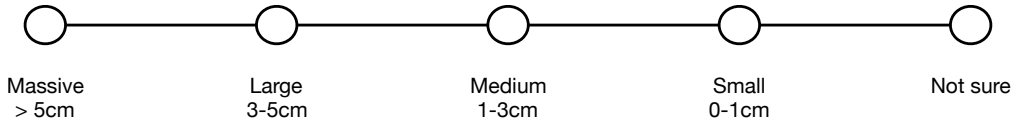
Materials needed
Rotator cuff Sawbones model (+spare)
Base unit for rotator cuff model
Suture anchor (Versalok)
Suture passer
G clamps to clamp model to table
Hammer
Tensioning gun
PDF of instructions of anchor system
BioYarn (+spare)
Video camera

Hybrid Suture - Usability Study Questionnaires

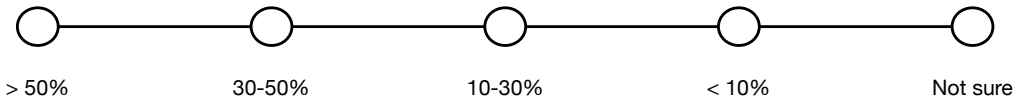
Name: _____

Part 1: Background questions (please tick ALL that apply)

What size rotator cuff tears do you repair?



What is your current re-tear rate?



Which implants do you use to augment torn rotator cuffs?

e.g. Anchor, Suture, Patch etc

_____

How do you assess a successful outcome?

Patient reported

Patient scores

MRI images

Ultrasound images

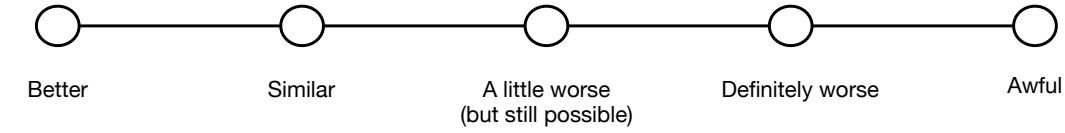
Other: _____

Why do you think patients re-tear?

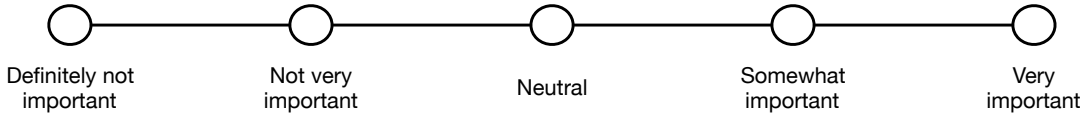
_____

Part 2: Material Properties (please tick ONE of the below)

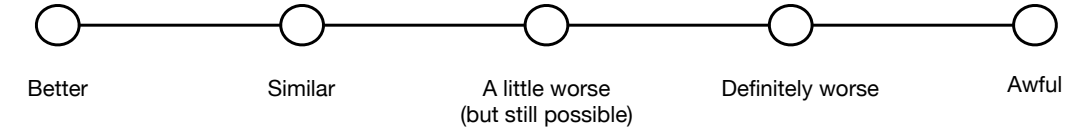
1a. Your impression of the **strength** of this device compared to your preferred suture?



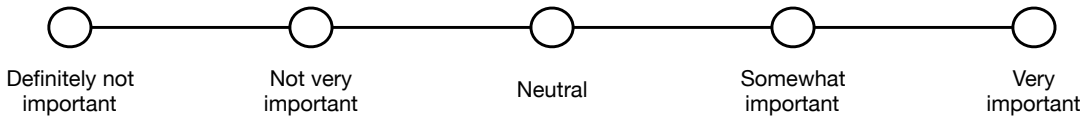
1b. How important is **suture strength** for this application?



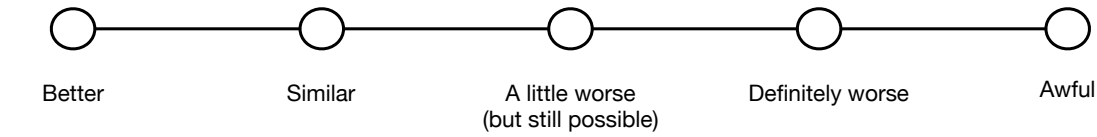
2a. Your impression on the **strain** ('stretchiness') of this device compared to your preferred suture?



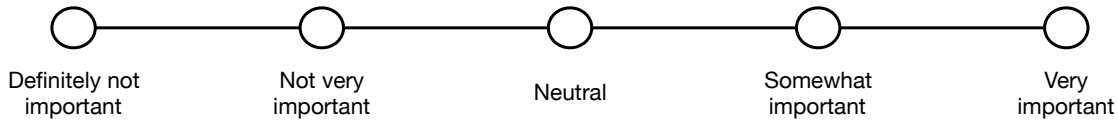
2b. How important is controlling **suture strain** ('stretchiness') for this application?



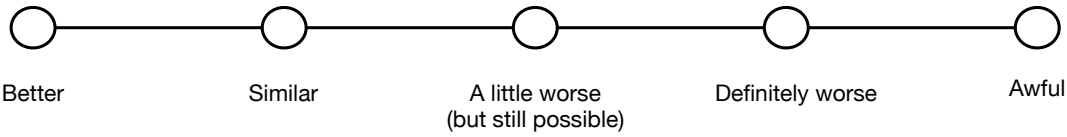
3a. Your impression on the **fraying** of this device compared to your preferred suture?



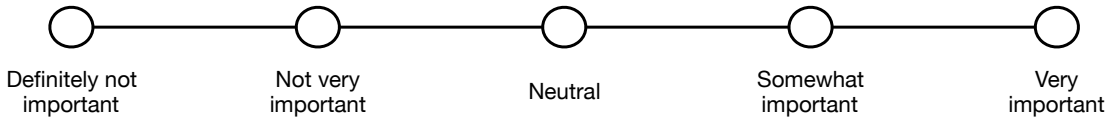
3b. How important is reducing fraying for this application?



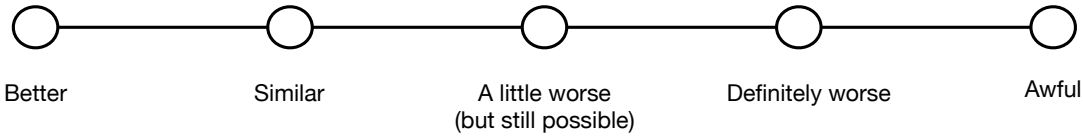
4a. Your impression of the **memory** of this device compared to your preferred suture?



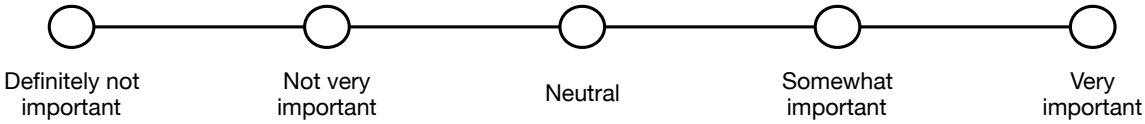
4b. How important is suture **memory** for this application?



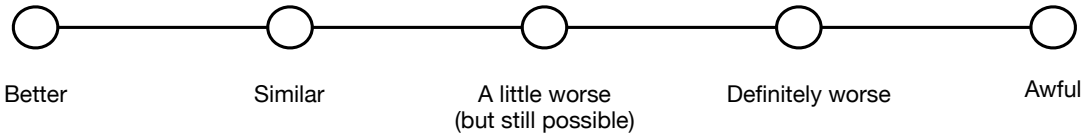
5a. Your impression of the **size (diameter)** of this device compared to your preferred suture?



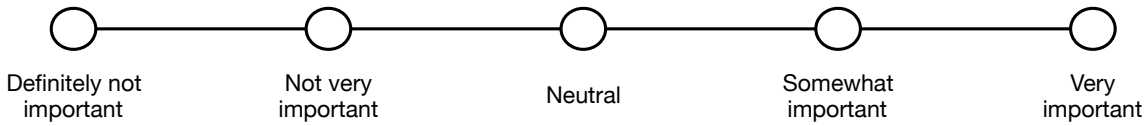
5b. How important is **suture size (diameter)** for this application?



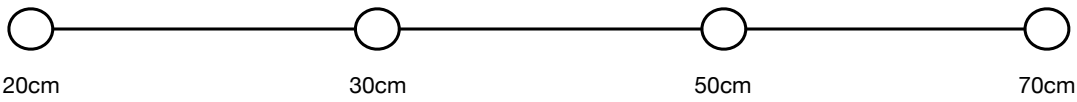
6a. Your impression of the **length** of this device compared to your preferred suture for this application?



6b. How important is **suture length** for this application?



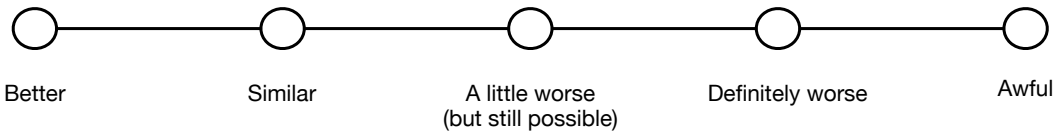
6c. What is the minimum length with which you could comfortably use for this application?



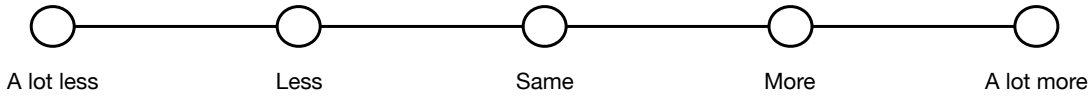
Part 3: Usability and Potential Improvements (please tick ONE of the below)

Given that this suture behaves differently to your preferred suture, please give some indication about your threshold to use it.

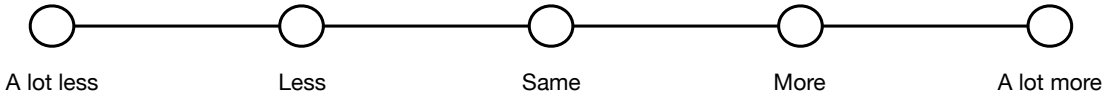
How usable was this suture for this specific application, compared to your preferred suture?



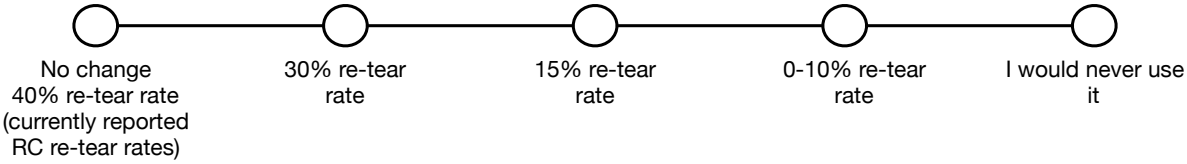
Compared to a suture, how much would you pay for this product?



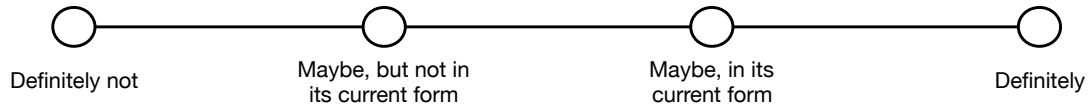
Compared to a patch/scaffold, how much would you pay for this product?



What change in re-tear rate would encourage you to use this product?



Would you consider this product (or a variant) for other applications?



If you answered anything other than 'Definitely not' in the question above, please elaborate

_____

Any other feedback about the design or use of this product that you would like to share?

_____

End of Questionnaire.

Appendix D: Additional information for Chapter 5

Appendix D.1: Supplementary information for protein corona composition analysis

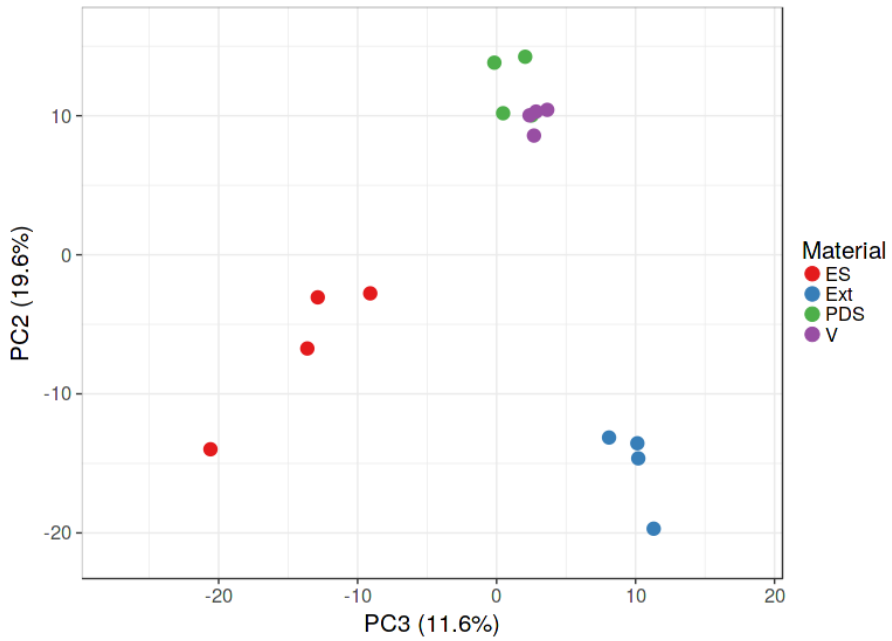


Figure D.1: Principal component analysis (PC2/PC3) of protein coronas formed on electrospun filaments (Es), and melt-extruded yarns (Ext), as well as on surgical sutures PDS (PDS) and Vicryl (V). The four materials were incubated in human serum for 1 hour before undergoing mass spectrometry to analyse the adsorbed protein coronas. PCA separates the coronas based on material type. In contrast to PCA analysis in the first two components, when adding the third component, the control sutures cluster together and there is separation between electrospun filaments and melt-extruded yarns.

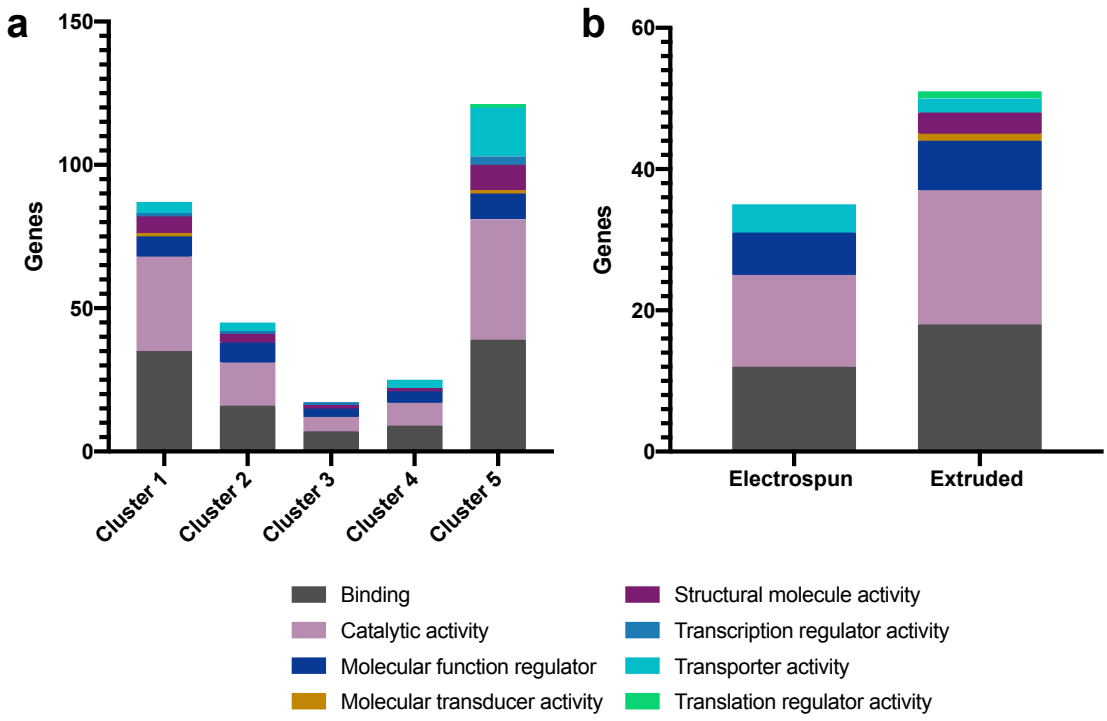


Figure D.2: Functional pathways of detected proteins. (a) Differentially expressed proteins in the coronas of PDS sutures, electrospun filaments, and melt-extruded yarns formed five main clusters; (b) Differentially expressed proteins in the coronas of electrospun filaments and melt-extruded yarns.

Table D.1: Full list of differentially expressed proteins in the coronas of electrospun and melt-extruded yarns. There were two different clusters of bound proteins detected, totalling 102 different proteins. 41 proteins were enriched with electrospun filaments (Up in ES) and 61 proteins were enriched with extruded yarns (Down in ES).

Up in ES	Apolipoprotein A-II	APOA2
	Kallistatin	SERPINA4
	Splicing factor, proline- and glutamine-rich	SFPQ
	Isoform 4 of Protein WWC2	WWC2
	Gelsolin	GSN
	Carboxypeptidase N subunit 2	CPN2
	Immunoglobulin heavy variable 3-15	IGHV3-15
	Isoform 2 of Glial fibrillary acidic protein	GFAP
	Isoform 3 of Plasminogen activator inhibitor 1 RNA-binding protein	SERBP1
	Keratin, type I cytoskeletal 14	KRT14
	Polymeric immunoglobulin receptor	PIGR
	Opiorphin prepropeptide	OPRPN
	Isoform 2 of Serpin B12	SERPINB12
	Lipocalin-1	LCN1
	Keratin, type I cytoskeletal 20	KRT20
	Dermcidin	DCD
	Isoform 1B of Desmocollin-1	DSC1
	Serum paraoxonase/arylesterase 1	PON1
	Transthyretin	TTR
	Ceruloplasmin	CP
	APOC4-APOC2 readthrough (NMD candidate)	APOC4-APOC2
	NADH dehydrogenase [ubiquinone] 1 alpha subcomplex subunit 6	NDUFA6
	Isoform 2 of TBC1 domain family member 30	TBC1D30
	Uncharacterized protein C3orf85	C3orf85
	Keratinocyte differentiation-associated protein	KRTDAP
	Plasma alpha-L-fucosidase	FUCA2
	Out at first protein homolog	OAF
	Keratin, type II cytoskeletal 6B	KRT6B
	Histidine-rich glycoprotein	HRG
	Apolipoprotein C-III variant 1	APOC3
	Keratin, type II cytoskeletal 6A	KRT6A
	Voltage-dependent anion-selective channel protein 1	VDAC1
	Apolipoprotein M	APOM
	Apolipoprotein F	APOF
	Isoform 2 of Eukaryotic translation initiation factor 4B	EIF4B
	NADH dehydrogenase [ubiquinone] 1 alpha subcomplex subunit 12	NDUFA12
	Biotinidase	BTD
	Isoform 1 of Protein POF1B	POF1B
	Fetuin-B	FETUB
	Obscurin	OBSCN
	Phosphatidylcholine-sterol acyltransferase	LCAT

Down in ES	Fibrinogen beta chain	FGB
	Trifunctional enzyme subunit alpha, mitochondrial	HADHA
	Prenylcysteine oxidase 1	PCYOX1
	Immunoglobulin heavy constant mu (Fragment)	IGHM
	Keratin, type I cytoskeletal 16	KRT16
	Lupus La protein	SSB
	Immunoglobulin lambda constant 7	IGLC7
	Immunoglobulin lambda-like polypeptide 5	IGLL5
	Alpha-actinin-3	ACTN3
	Antithrombin-III	SERPINC1
	Protein AMBP	AMBP
	Alpha-actinin-4	ACTN4
	Protein S100-A12	S100A12
	Collagen alpha-3(VI) chain	COL6A3
	Heat shock protein HSP 90-beta	HSP90AB1
	Complement C1q subcomponent subunit A (Fragment)	C1QA
	Inter-alpha-trypsin inhibitor heavy chain H3	ITIH3
	Isoform 2 of Pregnancy zone protein	PZP
	Coagulation factor VIII	F8
	Isoform 2 of Insulin-like growth factor-binding protein complex acid lab	IGFALS
	Complement C5	C5
	Immunoglobulin heavy constant gamma 2	IGHG2
	Vitamin D-binding protein	GC
	Serum albumin	ALB
	Mannan-binding lectin serine protease 2	MASP2
	Trypsin-1	PRSS1
	Immunoglobulin heavy variable 3-30	IGHV3-30
	CD5 antigen-like	CD5L
	Isoform 4 of Heat shock protein 105 kDa	HSPH1
	Isoform 2 of Alpha-actinin-1	ACTN1
	Leucine-, glutamate- and lysine-rich protein 1	LEKR1
	Serpin I2	SERPINI2
	ADP/ATP translocase 2	SLC25A5
	Plakophilin-1	PKP1
	Isoform 2 of Thrombospondin-3	THBS3
	Immunoglobulin kappa constant	IGKC
	Galectin-3-binding protein	LGALS3BP
	Myosin-9	MYH9
	Peroxiredoxin-4	PRDX4
	Isoform 12 of Titin	TTN
	ADP/ATP translocase 4	SLC25A31
	Apolipoprotein B-100	APOB
	Isoform 2 of Multimerin-1	MMRN1
	Keratin, type I cytoskeletal 17 (Fragment)	KRT17
	Lipopolysaccharide-binding protein	LBP
	Divergent protein kinase domain 2A	DIPK2A
	Multimerin-1	MMRN1
	Beta-2-microglobulin	B2M
	Neuron navigator 3	NAV3
	Coagulation factor XIII A chain	F13A1
	Complement C1s subcomponent	C1S
	Heat shock 70 kDa protein 6	HSPA6
	Histidine ammonia-lyase	HAL
	Isoform 5 of Hyaluronidase-1	HYAL1
	Keratin, type II cytoskeletal 1b	KRT77
	Receptor-type tyrosine-protein phosphatase F (Fragment)	PTPRF
	Myosin-7B	MYH7B
	Apolipoprotein A-V	APOA5
	Coagulation factor X	F10
	General transcription factor 3C polypeptide 4	GTF3C4
	Isoform 2 of CDK5 regulatory subunit-associated protein 2	CDK5RAP2

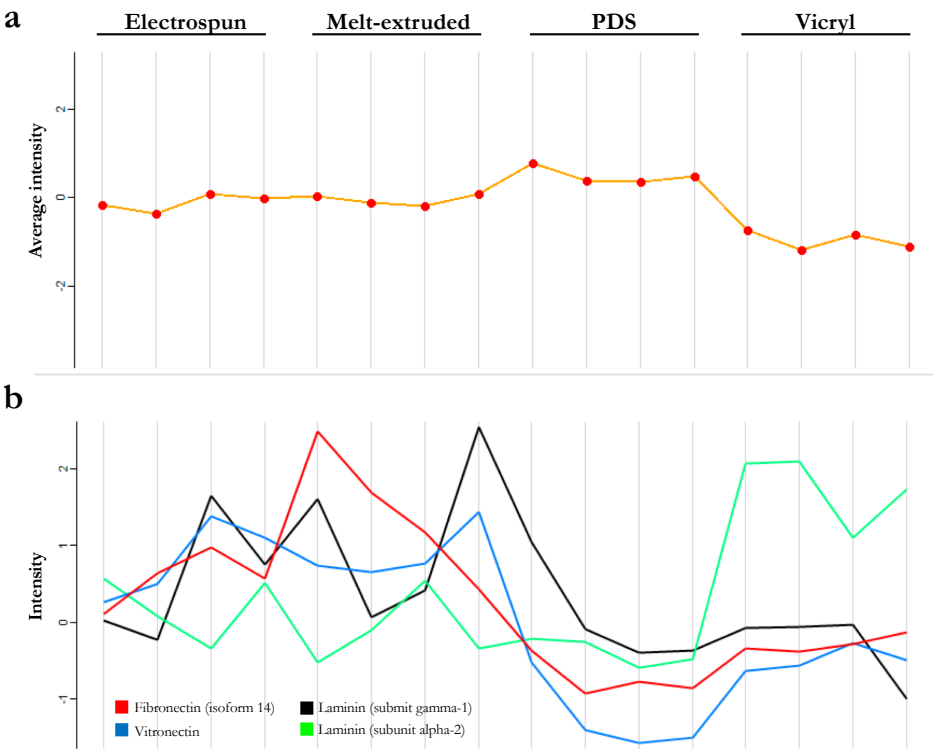


Figure D.3: Differential expression of binding proteins in the coronas of electrospun filaments, melt-extruded yarns, PDS, and Vicryl. (a) Binding protein abundance calculated by averaging the intensity of all binding proteins for each material; (b) Abundance of specific binding proteins fibronectin, vitronectin, and laminin, that are thought to be important in mediating cell attachment. Each vertical line intersects one sample, i.e. n=4 per material tested.

Appendix E: List of equipment and suppliers

5kN tensile stage	Zwick Roell, Herefordshire, UK
10cm dishes	Griener, Frickenhausen, Germany
24-well plate	Corning Inc, Corning, NY, USA
AFDh 80 fine yarn carriers	Herzog Braiding Machines, Germany
AutoPore IV 9500 Mercury Porosimetry	Micromeritics Instruments, GA ,USA
PrestoBlue	Invitrogen, Paisley, UK
Aluminium stubs	Agar Scientific, Essex, UK
Carbon tape	Agar Scientific, Essex, UK
Cell crowns (24-well)	Scaffdex, Tampere, Finland
CT20 20N in situ tensile stage	Deben UK Ltd, Suffolk, UK
DMEM F-12	Lonza, Slough, UK
EVO LS15 Scanning Electron Microscope	Zeiss, Oberkochen, Germany
Fetal Bovine Serum	Labtech, Uckfield, UK
FluoStar Optima microplate reader	BMG Labtech, Ortenberg, Germany
HFIP	Apollo Scientific Ltd, Cheshire, UK
Knox unflavoured gelatine	Kraft foods, Northfield, USA
Lo Bind Eppendorfs	Eppendorf AG, Hamburg, Germany
LS-7010MR optical micrometre laser	Keyence, Milton Keynes, UK
Melt-Extrusion Spinning Line	Fibre Extrusion Technologies, Leeds, UK
MFP-3D Atomic Force Microscope	Asylum Research, High Wycombe, UK
Penicillin-streptomycin	ThermoFisher Scientific, MA, USA
PDO (Evonik)	Evonik Nutrition and Care, Germany
PDO (Polymed)	Poly-Med Medical Devices, SC, USA
PDO (Riverpoint)	Riverpoint Medical, Portland, OR, USA
PDO (Sigma)	Sigma Aldrich, Dorset, UK
PDS suture	Johnson & Johnson Devices, USA
Phosphate Buffered Saline	Sigma Aldrich, Dorset, UK
Pyridine	Sigma Aldrich, Dorset, UK
Q2000-1275Differential Scanning Calorimeter	TA Instruments, Hertfordshire, UK
SC7620 Mini Sputter Coater	Quorum Technologies, Laughton, UK
SkyScan 1172 microCT scanner	Bruker, Kontich, Belgium
SN1326 Steriseal suture needle	Aspen Medical, London, UK

Trizol	Invitrogen, Paisley, UK
TZero aluminium pans	TA Instruments, Hertfordshire, UK
UF750 drying oven	Memert, Germany
USB2-micro-250X optical digital microscope	Plugable, Redmond, WA, USA
VF 1/(4-32) Variation Braiding Machine	Herzog Braiding Machines, Germany
Vicryl coated suture	Johnson & Johnson Devices, USA
Vystat 2264	Vickers Oils, Leeds, UK